In compliance with the
Canadian Privacy Legislation
some supporting forms
may have been removed from
this dissertation.

While these forms may be included
in the document page count,
their removal does not represent
any loss of content from the dissertation.

University of Alberta

Intermediate Field Mixing of Wastewater Effluent in the North Saskatchewan River at Edmonton, Alberta

by

Karen Dow

A thesis submitted to the Faculty of Graduate Studies and Research in partial fulfillment of the

requirements for the degree of Master of Science

in

Water Resources Engineering

Department of Civil and Environmental Engineering

Edmonton, Alberta

Fall, 2003

National Library
of Canada

Acquisitions and
Bibliographic Services

395 Wellington Street
Ottawa ON K1A 0N4
Canada

Bibliothèque nationale
du Canada

Acquisisitons et
services bibliographiques

395, rue Wellington
Ottawa ON K1A 0N4
Canada

Your file Votre référence
ISBN: 0-612-87751-5
Our file Notre référence
ISBN: 0-612-87751-5

The author has granted a non-exclusive licence allowing the National Library of Canada to reproduce, loan, distribute or sell copies of this thesis in microform, paper or electronic formats.

The author retains ownership of the copyright in this thesis. Neither the thesis nor substantial extracts from it may be printed or otherwise reproduced without the author's permission.

L'auteur a accordé une licence non exclusive permettant à la Bibliothèque nationale du Canada de reproduire, prêter, distribuer ou vendre des copies de cette thèse sous la forme de microfiche/film, de reproduction sur papier ou sur format électronique.

L'auteur conserve la propriété du droit d'auteur qui protège cette thèse. Ni la thèse ni des extraits substantiels de celle-ci ne doivent être imprimés ou aturement reproduits sans son autorisation.

Canada

University of Alberta

Library Release Form

Name of Author: Karen Dow

Title of Thesis: Intermediate Field Mixing of Wastewater Effluent in the North Saskatchewan River at Edmonton, Alberta

Degree: Master of Science

Year this Degree Granted: 2003

Permission is hereby granted to the University of Alberta Library to reproduce single copies of this thesis and to lend or sell such copies for private, scholarly or scientific research purposes only.

The author reserves all other publication and other rights in association with the copyright in the thesis, and except as herein before provided, neither the thesis nor any substantial portion thereof may be printed or otherwise reproduced in any material form whatever without the author's prior written permission.

September 30/03

University of Alberta

Faculty of Graduate Studies and Research

The undersigned certify that they have read, and recommend to the Faculty of Graduate Studies and Research for acceptance, a thesis entitled **Intermediate Field Mixing of Wastewater Effluent in the North Saskatchewan River at Edmonton, Alberta** submitted by **Karen Dow** in partial fulfillment of the requirements for the degree of **Master of Science in Water Resources Engineering.**

ABSTRACT

The intermediate field mixing characteristics of the Gold Bar Wastewater Treatment Plant outfall into the North Saskatchewan River at Edmonton were evaluated. The intermediate field mixing is important for the initial dilution of wastewater effluent; furthermore, a good understanding of the intermediate field mixing characteristics is needed in the event of future retrofitting of the outfall structure. An extensive field study was conducted to delineate the bathymetry of the study area and evaluate the mixing characteristics by means of a steady state dye test. The topographic and limited velocity results of the field study were used to create and validate a depth averaged hydrodynamic model of the study reach in order to extract streamtube information which was then used to evaluate the mixing characteristics of the study reach. From the analysis it is evident that the distribution of effective transverse mixing coefficient can be qualitatively related to local river conditions.

ACKNOWLEDGEMENTS

First, I would like to acknowledge my supervisors Dr. Peter Steffler and Dr. David Zhu for their knowledge and support. Special thanks to Dr. Peter Steffler for your guidance and patience that pushed me to achieve more than I ever thought possible. Thank you to my examining committee, Dr. John Wilson and Dr. Rajaratnam, for your efforts and valuable suggestions.

Thanks to Sheldon Lovell and Perry Fedun, technicians in the water resources engineering group. Without you guys I would have no data and no computer to analyze my data with!

Many people were part of the extensive field work that was carried out in this study. A huge thank you to Dan Healy! I certainly could not have completed the field survey without your knowledge, precision and friendship that made the time pass quickly. To all those that assisted with the dye test, a huge thanks! Canhua Zhao, Hesham Fouli, Zahiraniza Mustaffa, Ken Van Der Vinne, Twyla Kowalcyzk, Ahmed Moawad, and Stephen Edwini-Bonsu: this would not have been possible without your time and effort in the freezing weather. A big thank you to Andrew Burrows, who assisted in the two dimensional hydrodynamic modeling. Your hard work and diligence is greatly appreciated. This would not be possible without your long hours when I needed them most.

I would like to acknowledge the following people who provided data and support during this research: Chandra Mahabir and Patricia Stevenson of Alberta Environment, Jay Kinoshita of Butler Survey Supplies, Abdul Mohammed, Lakshaman Samarasinghe, Vince Corkery and Fernando Sacluti of Gold Bar Wastewater Treatment Plant, Lyndon Gyurek and Taion Siu of the City of Edmonton.

I'd like to thank the following organizations for their financial support during my studies:

Natural Sciences and Engineering Research Council of Canada
PGS-A
Informatics Circle of Research Excellence
Graduate Student Award
University of Alberta
Walter H. Johns Graduate Fellowship
City of Edmonton
Funding for field studies

A heartfelt thank you to my parents and my sister, Diane, for their continued love and support throughout my studies and for helping me reach my dreams and goals. To my all family and friends, thanks for your encouragement and many phone calls.

Last, but definitely not least thanks to Erick for your love, inspiration, encouragement, patience, and support. This would not have been possible without you there by my side pushing me to achieve my goals and reminding me to enjoy life.

TABLE OF CONTENTS

CHAPTER 1 INTRODUCTION 1

1.1 NORTH SASKATCHEWAN RIVER AT EDMONTON 2

1.1.1 Effects of Ammonia 4

1.1.2 Previous Mixing Studies in the North Saskatchewan River at Edmonton 5

1.1.3 Study Area 6

1.2 RESEARCH OVERVIEW 7

1.3 RESEARCH OBJECTIVES 9

CHAPTER 2 BATHYMETRIC SURVEY 16

2.1 BANK SURVEY AND CONTROL POINTS 16

2.1.1 Data Correction 17

2.2 BOAT SURVEY 18

2.3 UTM COORDINATES 20

2.3.1 GPS Technology 20

2.3.2 GPS Survey 22

2.3.3 Transformation of Coordinates 23

2.4 VELOCITY MEASUREMENTS 24

2.5 RESULTS 25

2.5.1 Bed Program 25

2.5.2 Topography Observations 26

2.6 WATER SURFACE ELEVATIONS FOR HYDRODYNAMIC MODELS 27

CHAPTER 3 HYDRODYNAMIC MODELING 44

3.1 1-D FLOW ANALYSIS 44

3.1.1 Calibration of Model 45

3.1.1.1 Known Water Surface Elevations for Calibration 45

3.1.1.2 Cross Section Data 45

3.1.1.3 Unsteady Flow Profile for Flow Selection 46

3.1.1.4 Calibration of Steady State Model 47

3.1.2 Boundary Conditions for Two-Dimensional Model 47

3.2 TWO DIMENSIONAL HYDRODYNAMIC MODELING 49

3.2.1 Mesh Program 49

3.2.2 River2D Calibration 50

3.2.2.1 Known Water Surface Elevations for Calibration 51

3.2.2.2 Calibration of Water Surface Profile 51

3.2.2.3 Velocity Profiles 52

3.2.2.4 Velocity Field and Cumulative Discharge Distribution Observations 54

CHAPTER 4 BACKGROUND INFORMATION FOR MIXING STUDY 81

4.1 RIVER MIXING THEORY 81

4.1.1 Physical Processes 81

4.1.2 Mixing Regimes 83

4.1.3 Three Dimensional Mixing 84

4.1.4 Two Dimensional Mixing 84

4.1.4.1 Transverse Mixing Coefficient 87

4.1.4.1.1 Method of Moments 88

4.2 FLUORESCENCE THEORY 90

4.2.1 Rhodamine WT 91

4.2.1.1 Rhodamine WT Losses 91

4.2.1.2 Rhodamine WT as a Tracer 94

CHAPTER 5 MIXING STUDY 95

5.1 DYE TEST 95

5.1.1 Input Location and Dye Test Timing 95

5.1.2 Preparation of Input Dye Solution 96

5.1.3 Preliminary Plume Estimate and Sampling Locations 97

5.1.4 Dye Test 99

5.1.4.1 Sample Collection 99

5.1.5 Effluent Flow 100

5.2 SAMPLE ANALYSIS 101

5.2.1 Fluorometer 101

5.2.2 Calibration Procedure 101

5.2.3 Cuvet Selection 103

5.2.4 Sample Analysis 104

5.2.5 Input Dye Concentration 106

5.2.6 Recovery Ratio 106

5.3 RESULTS 110

5.3.1 October 29, 2002 Concentration Profiles 110

5.3.2 November 7, 2002 Concentration Profiles 111

5.4 TRANSVERSE MIXING COEFFICIENT 112

5.5 SENSITIVITY ANALYSIS 116

CHAPTER 6 CONCLUSIONS AND RECOMMENDATIONS 170

6.1 SUMMARY 170

6.2 CONCLUSIONS 172

6.3 RECOMMENDATIONS 173

CHAPTER 7 REFERENCES 174

APPENDIX: RHODAMINE WT AS A TRACER 178

LIST OF TABLES

TABLE 2.1: TRANSFORMATION PARAMETERS FOR CORRECTION OF SURVEY DATA. 32
TABLE 2.2: TRANSFORMATION OF ELEVATION. 35
TABLE 2.3: CALCULATED TRANSFORMATION PARAMETERS USING THE SURVEYED POINTS. 35
TABLE 2.4: CALCULATED ERROR ASSOCIATED WITH THE TRANSFORMATION PARAMETERS. 36
TABLE 2.5: FINAL TRANSFORMATION PARAMETERS. 36
TABLE 2.6: CALCULATED ERROR ASSOCIATED WITH FINAL TRANSFORMATION PARAMETERS FOR EACH POINT. 36
TABLE 2.7: SUMMARY OF VELOCITY, pH, AND TEMPERATURE MEASUREMENTS TAKEN OCTOBER 29, 2002 AND NOVEMBER 7, 2002 38
TABLE 3.1: COMPARISON OF THE EFFECT OF INCLUDING BRIDGE PIERS ON WATER SURFACE PROFILES IN HEC-RAS 61
TABLE 3.2: COMPARISON OF OBSERVED CHANGE IN WATER SURFACE ELEVATIONS TO COMPUTED CHANGE IN WATER SURFACE ELEVATIONS FOR DYE TEST DAYS. 65
TABLE 3.3: BOUNDARY CONDITIONS FOR WATERS EDGE CALIBRATION ESTIMATED FROM HEC-RAS. 68
TABLE 3.4: SUMMARY OF FINAL VELOCITY COMPARISONS 75
TABLE 5.1: SUMMARY OF CALIBRATION CURVE INVESTIGATION 124
TABLE 5.2: CALIBRATION STANDARDS USED FOR SAMPLE ANALYSIS. 125
TABLE 5.3: ERROR FROM CUVET SELECTION PROCEDURE. 126
TABLE 5.4: ACCURACY CHECK 128
TABLE 5.5: BLANK SAMPLES. 128
TABLE 5.6: EFFLUENT SAMPLES. 129
TABLE 5.7: RIVER SAMPLES COLLECTED OCTOBER 29, 2002. 130
TABLE 5.8: RIVER SAMPLES COLLECTED NOVEMBER 7, 2002. 131
TABLE 5.9: DILUTION SET ONE. 132
TABLE 5.10: DILUTION SET TWO. 132
TABLE 5.11: RECOVERY RATIO SUMMARY. 133
TABLE 5.12: RIVER WATER RECOVERY CHECK. 134
TABLE 5.13: 2500 PPT STANDARD RECOVERY RATIO COMBINATIONS 134
TABLE 5.14: OCTOBER 29, 2002 RECOVERY RATIO CORRECTED DEPTH AVERAGED SAMPLES. 136
TABLE 5.15: OCTOBER 29, 2002 RECOVERY RATIO CORRECTED SURFACE SAMPLES. 137
TABLE 5.16: NOVEMBER 7, 2002 RECOVERY RATIO CORRECTED DEPTH AVERAGED SAMPLES. 139
TABLE 5.17: NOVEMBER 7, 2002 RECOVERY RATIO CORRECTED SURFACE SAMPLES. 140
TABLE 5.18: CUMULATIVE DISCHARGE SUMMARY FOR OCTOBER 29, 2002. 149
TABLE 5.19: CUMULATIVE DISCHARGE SUMMARY FOR NOVEMBER 7, 2002. 151

TABLE 5.20: SUMMARY OF CALCULATED MASS FLUX. 152
TABLE 5.21: SUMMARY OF CALCULATED VARIANCES BASED ON SCALED ADJUSTED C-Q PROFILES. 153
TABLE 5.22: CALCULATED TRANSVERSE FACTOR OF DIFFUSION AND TRANSVERSE MIXING COEFFICIENTS. 154
TABLE 5.23: ROUGHNESS DEFINITION FOR SENSITIVITY ANALYSIS. 155
TABLE 5.24: SENSITIVITY ANALYSIS: ABSOLUTE ERROR IN MODELED VELOCITIES. 158
TABLE 5.25: SENSITIVITY ANALYSIS: SUMMARY OF MODELED VELOCITY ERROR, CALCULATED MASS FLUX, AND CALCULATED VARIANCE. 164
TABLE 5.26: SENSITIVITY ANALYSIS: CALCULATED TRANSVERSE FACTORS OF DIFFUSION AND MIXING COEFFICIENTS FOR SECTION BETWEEN STATION 320 AND 1000. 167
TABLE 5.27: SENSITIVITY ANALYSIS: CALCULATED TRANSVERSE FACTORS OF DIFFUSION AND MIXING COEFFICIENTS FOR SECTION BETWEEN STATION 1000 AND THE END. 168

LIST OF FIGURES

FIGURE 1.1: MAP OF NORTH SASKATCHEWAN RIVER AT EDMONTON, ALBERTA. 10

FIGURE 1.2: STEEP SIDE WALLS OF RIVER TAKEN FROM GOLD BAR PEDESTRIAN BRIDGE LOOKING UPSTREAM. 10

FIGURE 1.3: MAP OF STUDY AREA. 11

FIGURE 1.4: PLAN AND PROFILE OF GBWWTP OUTFALL STRUCTURE. 12

FIGURE 1.5: GBWWTP OUTFALL STRUCTURE. 13

FIGURE 1.6: GBWWTP OUTFALL STRUCTURE FROM DOWNSTREAM. 13

FIGURE 1.7: GBWWTP OUTFALL STRUCTURE CHUTE WITH HYDRAULIC JUMP. 14

FIGURE 1.8: IMMEDIATELY UPSTREAM OF GBWWTP OUTFALL. 14

FIGURE 1.9: GBWWTP OUTFALL STRUCTURE. 15

FIGURE 1.10: GBWWTP OUTFALL STRUCTURE LOOKING DOWNSTREAM. 15

FIGURE 2.1: 360° PRISM USED IN SURVEYS. 29

FIGURE 2.2: BENCHMARK LOCATIONS AND BANK SURVEY IN LOCAL COORDINATE SYSTEM. 30

FIGURE 2.3: ORIGINAL BANK SURVEY BEFORE CORRECTIONS. 31

FIGURE 2.4: GEOMETRY OF COORDINATE TRANSFORMATION. 32

FIGURE 2.5: SETUP OF PRISM AND TRANSDUCER. 33

FIGURE 2.6: LINES TRAVERSED BY BOAT WITHIN BANKS IN LOCAL COORDINATE SYSTEM. 34

FIGURE 2.7: CLOSE UP OF LINES TRAVERSED BY BOAT IN THE FIRST SECTION NEAR THE 50TH STREET PEDESTRIAN BRIDGE. 35

FIGURE 2.8: FINAL PLOT OF TRANSFORMED COORDINATES. 37

FIGURE 2.9: LOCATION OF VELOCITY MEASUREMENTS TAKEN OCTOBER 29, 2002 AND NOVEMBER 7, 2002. 38

FIGURE 2.10: FINAL BED TOPOGRAPHY WITH 0.5 METRE CONTOURS. 40

FIGURE 2.11: CLOSE UP OF TOPOGRAPHY AT OUTFALL WITH 0.5 METRE CONTOURS. 41

FIGURE 2.12: MAP OF BOAT LINES CHOSEN FOR CALIBRATION OF HEC-RAS. 42

FIGURE 2.13: CLOSE UP OF FIRST BOAT SECTION WITH CHOSEN LINE. 42

FIGURE 2.14: DIFFERENCE IN WATER SURFACE ELEVATION OF TRAVELING UPSTREAM AND TRAVELING DOWNSTREAM BOAT LINES. 43

FIGURE 3.1 MAP OF CROSS SECTION LOCATIONS OBTAINED FROM ALBERTA ENVIRONMENT. 57

FIGURE 3.2: WATER SURFACE ELEVATIONS USED FOR CALIBRATION OF HEC-RAS. 58

FIGURE 3.3: EFFECT OF BOUNDARY CONDITIONS ON STUDY AREA WHEN REACH EXTENDED TO STATION 55. 58

FIGURE 3.4: ORIGINAL (A) AND FINAL (B) HEC-RAS PLAN OF CROSS SECTIONS IN GEOMETRY FILE. 59

FIGURE 3.5: EFFECT OF BRIDGE PIERS ON WATER SURFACE PROFILE IN HEC-RAS. 60

FIGURE 3.6: TRAVEL TIME FROM LOW LEVEL BRIDGE TO STUDY AREA BASED ON UNSTEADY FLOW HYDROGRAPHS. 62

FIGURE 3.7: FINAL HEC-RAS CALIBRATION WATER SURFACE PROFILES. 63

FIGURE 3.8: BED ROUGHNESS FROM FINAL HEC-RAS CALIBRATION. 64
FIGURE 3.9: FINAL COMPUTATIONAL MESH GENERATED IN RIVER2D. 66
FIGURE 3.10: CLOSE UP OF FINAL MESH AT OUTFALL STRUCTURE 67
FIGURE 3.11: FINAL CALIBRATED WATER SURFACE PROFILE IN RIVER2D. 68
FIGURE 3.12: BED ROUGHNESS FROM WATER SURFACE CALIBRATION. 69
FIGURE 3.13: STAGE DISCHARGE CURVE FOR OUTFLOW BOUNDARY OF STUDY AREA DEVELOPED FROM WATER SURFACE CALIBRATION 70
FIGURE 3.14: FINAL BED ROUGHNESS FROM VELOCITY CALIBRATION OF RIVER2D. 71
FIGURE 3.15: VELOCITY COMPARISON OCTOBER 29, 2002 AT STATION -30 72
FIGURE 3.16: VELOCITY COMPARISON NOVEMBER 7, 2002 AT STATION 80. 72
FIGURE 3.17: VELOCITY COMPARISON NOVEMBER 7, 2002 AT STATION 320. 73
FIGURE 3.18: VELOCITY COMPARISON NOVEMBER 7, 2002 AT STATION 1000. 73
FIGURE 3.19: VELOCITY COMPARISON NOVEMBER 7, 2002 AT STATION 1500. 74
FIGURE 3.20: VELOCITY COMPARISON NOVEMBER 7, 2002 AT STATION END. 74
FIGURE 3.21: CLOSE UP OF VELOCITY FIELD AT OUTFALL STRUCTURE OCTOBER 29, 2002. 77
FIGURE 3.22: CLOSE UP OF VELOCITY FIELD AT OUTFALL STRUCTURE NOVEMBER 7, 2002. 77
FIGURE 3.23: CLOSE UP OF VELOCITY FIELD AT OUTFALL FOR A DISCHARGE OF 90 M^3/S. 78
FIGURE 3.24: CLOSE UP OF VELOCITY FIELD AT OUTFALL FOR A DISCHARGE OF 300 M^3/S. 78
FIGURE 3.25: VELOCITY FIELD AT ALLUVIAL DEPOSIT OCTOBER 29, 2002 79
FIGURE 3.26: VELOCITY FIELD AT ALLUVIAL DEPOSIT NOVEMBER 7, 2002 79
FIGURE 3.27: CUMULATIVE DISCHARGE DISTRIBUTION NOVEMBER 7, 2002. 80
FIGURE 5.1: INPUT LOCATION IN PLAN VIEW. 120
FIGURE 5.2: TYPICAL EFFLUENT FLOW FOR WEEKDAY IN OCTOBER 121
FIGURE 5.3: PRELIMINARY PLUME ESTIMATES. 121
FIGURE 5.4: DYE INJECTION SET UP. 122
FIGURE 5.5: LOCATIONS OF SAMPLES COLLECTED OCTOBER 29 AND NOVEMBER 7, 2002. 122
FIGURE 5.6: EFFLUENT FLOW ON TEST DAYS. 123
FIGURE 5.7: EFFLUENT FLOW DURING DYE TESTS 123
FIGURE 5.8: ERROR OF CALIBRATION CURVES. 124
FIGURE 5.9: CUVET SELECTION 127
FIGURE 5.10: DECREASING FLUORESCENCE WITH CONSECUTIVE READINGS 127
FIGURE 5.11: DECREASING FLUORESCENCE WITH SUBSEQUENT SETS 128
FIGURE 5.12: EFFLUENT SAMPLES COLLECTED THROUGHOUT DYE TESTS. 129
FIGURE 5.13: EXPECTED AVERAGE EFFLUENT CONCENTRATION WITH MEASURED EFFLUENT CONCENTRATIONS 133
FIGURE 5.14: RECOVERY RATIO PLOT. 135
FIGURE 5.15: RECOVERY RATIO WITH THIRD ORDER POLYNOMIAL FIT 135

FIGURE 5.16: CONCENTRATION PLOTS FOR CROSS SECTIONS TAKEN OCTOBER 29, 2002. 142
FIGURE 5.17: CONCENTRATION PLOTS FOR CROSS SECTIONS TAKEN NOVEMBER 7, 2002. 144
FIGURE 5.18: ORIGINAL C-Q DISTRIBUTIONS FOR OCTOBER 29, 2002. 146
FIGURE 5.19: ORIGINAL C-Q DISTRIBUTIONS FOR NOVEMBER 7, 2002. 146
FIGURE 5.20: ADJUSTED C-Q DISTRIBUTIONS FOR OCTOBER 29, 2002. 147
FIGURE 5.21: ADJUSTED C-Q DISTRIBUTIONS FOR NOVEMBER 7, 2002. 147
FIGURE 5.22: SCALED ADJUSTED C-Q DISTRIBUTIONS FOR OCTOBER 29, 2002. 148
FIGURE 5.23: SCALED ADJUSTED C-Q DISTRIBUTIONS FOR NOVEMBER 7, 2002. 148
FIGURE 5.24: VARIANCE OF SCALED ADJUSTED C-Q DISTRIBUTIONS. 153
FIGURE 5.25: LINEAR TRENDLINES FIT TO VARIANCE DISTRIBUTION. 154
FIGURE 5.26: SENSITIVITY ANALYSIS OF VELOCITY PROFILE: STATION 80, NOVEMBER 7, 2002. 155
FIGURE 5.27: SENSITIVITY ANALYSIS OF VELOCITY PROFILE: STATION 320, NOVEMBER 7, 2002. 156
FIGURE 5.28: SENSITIVITY ANALYSIS OF VELOCITY PROFILE: STATION 1000, NOVEMBER 7, 2002. 156
FIGURE 5.29: SENSITIVITY ANALYSIS OF VELOCITY PROFILE: STATION 1500, NOVEMBER 7, 2002. 157
FIGURE 5.30: SENSITIVITY ANALYSIS OF VELOCITY PROFILE: STATION END, NOVEMBER 7, 2002. 157
FIGURE 5.31: SENSITIVITY ANALYSIS: CONCENTRATION – CUMULATIVE DISCHARGE DISTRIBUTION, STATION 80, NOVEMBER 7, 2002 160
FIGURE 5.32: SENSITIVITY ANALYSIS: CONCENTRATION – CUMULATIVE DISCHARGE DISTRIBUTION, STATION 320, NOVEMBER 7, 2002 160
FIGURE 5.33: SENSITIVITY ANALYSIS: CONCENTRATION – CUMULATIVE DISCHARGE DISTRIBUTION, STATION 640, NOVEMBER 7, 2002 161
FIGURE 5.34: SENSITIVITY ANALYSIS: CONCENTRATION – CUMULATIVE DISCHARGE DISTRIBUTION, STATION 1000, NOVEMBER 7, 2002 161
FIGURE 5.35: SENSITIVITY ANALYSIS: CONCENTRATION – CUMULATIVE DISCHARGE DISTRIBUTION, STATION 1500, NOVEMBER 7, 2002 162
FIGURE 5.36: SENSITIVITY ANALYSIS: CONCENTRATION – CUMULATIVE DISCHARGE DISTRIBUTION, STATION END, NOVEMBER 7, 2002 162
FIGURE 5.37: SENSITIVITY ANALYSIS: RANKING BASED ON SPREAD OF C-Q DISTRIBUTION COMPARED WITH THE AVERAGE MODELED VELOCITY ERROR OF STATIONS. 163
FIGURE 5.38: SENSITIVITY ANALYSIS: MASS FLUX FROM C-Q DISTRIBUTION COMPARED WITH THE AVERAGE MODELED VELOCITY ERROR 163
FIGURE 5.39: SENSITIVITY ANALYSIS: CALCULATED MASS FLUX COMPARED WITH CALCULATED VARIANCE. 165
FIGURE 5.40: VARIANCE OF CASES ALONG THE STUDY AREA. 165
FIGURE 5.41: LINEAR TRENDLINES FIT TO VARIANCES BETWEEN STATIONS 320 AND 1000. 166
FIGURE 5.42: LINEAR TRENDLINES FIT TO VARIANCES BETWEEN STATIONS 1000 AND THE END. 166

FIGURE 5.43: COMPARISON OF ERROR IN VELOCITY PROFILES WITH CALCULATED TRANSVERSE MIXING COEFFICIENT FOR STATIONS 320 TO 1000. 169
FIGURE 5.44: COMPARISON OF ERROR IN VELOCITY PROFILES WITH CALCULATED TRANSVERSE MIXING COEFFICIENT FOR STATIONS 1000 TO END. 169

LIST OF SYMBOLS

C = Concentration of the substance

D = transverse factor of diffusion

D_m = coefficient of molecular diffusion

e = dispersion coefficient

E = easterly coordinate

E_x, E_z = mixing coefficients that include the effects of depth averaged turbulent diffusion and differential advection

F, F_1, F_o = fluorescence

g = gravitational acceleration

h = depth of flow

k = the fluorescent decay coefficient

k_s = roughness height

K = first order decay rate

m_x, m_z = metric coefficients have been introduced to account for the variation in distances from one surface to the next due to river curvature and/or the variation of width along the river

M = mass of dye per unit of time or mass flux

n = direction perpendicular to the unit area

n = -0.0027/°C for Rhodamine WT

N = northerly coordinate

ppb = parts per billion

ppm = parts per million

ppt = parts per trillion

q = cumulative discharge

$\bar{q}$ = value for the cumulative discharge at the bank where the discharge is located

s = scaling factor

S = the slope of the channel

t = time

T = temperature

T_{ad} = advective transport per unit area per unit time

T_{disp} = dispersive transport

T_m = transport by molecular diffusion per unit area per unit time

T_t = turbulent diffusive transport

T_x = translation x factor

T_y = translation y factor

u = the local depth averaged velocity

u^* = the local shear velocity

U = time-averaged velocity component in the x direction

$\bar{u}$ = cross sectional mean velocity

$\overline{uc}$ = time averaged turbulent fluxes

V = time-averaged velocity component in the y direction

V_A = volume of sample

W = time-averaged velocity component in the z direction

x = longitudinal coordinate

x_e = the ratio of the volume of effluent water in the sample

X' = scaled local x coordinate

Y' = scaled local y coordinate

y = transverse coordinate

y_r = recovery ratio

α = angle from state plane coordinate system used to calculate rotation factor

β = angle from local coordinate system used to calculate rotation factor

ε_x = turbulent diffusion coefficient

ε_t =transverse mixing coefficient

σ_q^2 = variance of the concentration distribution with cumulative discharge

θ = rotation factor

θ_T = temperature correction factor

CHAPTER 1 INTRODUCTION

Demands on water bodies are increasing as populations in major centers are increasing. There is more need for waste disposal, water supply and leisure all of which take its toll on the water bodies. There is an increasing need to understand how the river bodies are reacting to these increasing loads. The mixing characteristics of the receiving water body are of great importance to a wastewater treatment plant. Often plants rely on the dilution of the effluent in the receiving water bodies in order to meet water quality standards. The knowledge of the mixing characteristics of the receiving water body is necessary to determine acceptable levels of effluent input and to determine the impact from accidental releases of toxic substances.

A river becomes vertically fully mixed within a short distance of being loaded due to the high width to depth ratio of rivers. This region is critical for the initial dilution of the effluent plume entering the river. After this point, transverse mixing is dominant or the spreading of the plume across a channel. There is only a small body of published research on transverse mixing especially regarding how natural channel characteristics affect transverse mixing coefficients. These mixing coefficients are necessary to understand how quickly pollutants are being mixed across a receiving river body in order to assess matters such as fish passage. The intermediate field can be considered the region that is far enough downstream of the outfall where the jet effects of the effluent discharge are no longer the dominant forces, but not far enough downstream of the discharge to be able to average channel characteristics

A field mixing test can be used to evaluate site specific mixing coefficients. The objective of the mixing test is to measure the capacity of the river to dilute and transport a neutral substance. A continuous dye test where a fluorescent dye is injected at a constant rate establishes a steady plume for which the distribution of concentration can be measured. Spatial changes can then be evaluated to establish general mixing characteristics of the region of interest. In order to evaluate these mixing characteristics, a

good knowledge of the velocity field of the receiving water body is required. Typically field velocity measurements are made concurrently with sampling during a dye test. Field velocity measurements are both time consuming and error prone so it would be of great use to engineers to be able to use the results of a hydrodynamic model in order to evaluate mixing coefficients rather than having to rely on field velocity measurements.

The intermediate field mixing characteristics of the Gold Bar Wastewater Treatment Plant (GBWWTP) outfall into the North Saskatchewan River at Edmonton were evaluated. GBWWTP is specifically concerned about the initial dilution of ammonia in the receiving river, especially given Environment Canada's new, more stringent regulation on ammonia. Effective June 1, 2005 new limits for ammonia nitrogen will be as follows: 10 mg/L in winter and 5 mg/L in summer. A good understanding of the mixing characteristics of the North Saskatchewan River would assist GBWWTP in the event of future retrofitting of the outfall structure.

1.1 NORTH SASKATCHEWAN RIVER AT EDMONTON

The North Saskatchewan River originates in the meltwaters of the Saskatchewan Glacier, one of six major glaciers in the Columbia Icefields of the Rocky Mountains. The Columbia Icefields is one of the largest non-polar ice and snow accumulations with an area of approximately 325 square kilometers and a depth of 365 meters. It flows 1287 kilometers across Alberta through to the center of Saskatchewan where it joins the South Saskatchewan River to create the Saskatchewan River. From here it flows across the prairies into Manitoba emptying into Lake Winnipeg where it is transported via the Nelson River to Hudson Bay. The North Saskatchewan River drains an area of 122 800 square kilometers.

It has been a regulated river since 1961 when the Brazeau hydroelectric development began operation and was further regulated in August 1962 with the Bighorn development. The construction of the dams assured winter flows that were four or five

times the minimum that occurred in the past. Mean monthly discharges range from 113 m^3/s in January to 339 m^3/s in August (Milne et al., 1993). Discharges have diurnal fluctuations of about 30% around the mean discharge due to the operation of the hydroelectric plants.

At Edmonton, the North Saskatchewan River has a drainage area of 28 000 km^2. The river meanders irregularly through the city as shown in Figure 1.1 with a total length of 60 kilometres within the city boundaries. The river through the city is a single channel entrenched in a valley about 50 meters deep with steep side walls pictured in Figure 1.2. It is approximately 150 to 200 m wide and 1.5 to 4.5 metres deep with frequent point and side bars (Cochrane Engineering Inc., 1997). Bed materials consist primarily of quartzite gravel with a mean particle size of 0.24 mm and modal size of 16 mm (Milne et al., 1993). Manning's roughness has been found to vary between 0.025 to 0.053 (Van der Vinne, 1991).

At Edmonton, the water is used for both consumptive and non consumptive uses and is subjected to contamination from natural and man-made sources. Overall the water quality in the North Saskatchewan River is generally rated as good. Mercury had been identified as a critical pollutant in the 1970s and had damaging effects because mercury accumulates in the food chain (Bouthillier, 1984). Today the primary source of annual loading of BOD, phosphorus, nitrogen and fecal coliforms is the Gold Bar waste water treatment plant.

The most common fish species found in the North Saskatchewan River at Edmonton include riverine cool water game fish species such as pike, walleye and goldeye. Others that are occasionally noted are yellow perch, mooneye, sauger and lake sturgeon and coldwater salmonids such as mountain whitefish and bulltrout (Allan, 1984). The North Saskatchewan River cintains the westernmost population of lake sturgeon in North America. The lake sturgeon population in the North Saskatchewan River is currently less than 2000 fish of which approximately 200 are mature enough to spawn which may be too low to guarantee long term sustainability. Municipal and

domestic effluents have a negative effect on aquatic populations which causes a reduction in prey for the sturgeon. Juvenile sturgeon are particularly sensitive to chemical pollution (http://greatcanadianrivers.com).

1.1.1 Effects of Ammonia

Ammonia enters aquatic environments from sewage effluent, deposition of human wastes without treatment, industrial discharges, and runoff from animal culture and agricultural operations. Fish are the critical organism when determining ammonia limitations in aquatic environments as fish cannot tolerate a large concentration of ammonia because it reduces the oxygen carrying capacity of the blood which can lead to suffocation. Acutely toxic concentrations in fish can cause a loss of equilibrium, hyper excitability, increased breathing, cardiac output, oxygen uptake, and in extreme cases convulsions, coma and death. At lower concentrations, effects include a reduction in egg hatching success, reduction in growth rate and morphological development, and pathological changes in the tissue of the gills, liver and kidney. Percidae and Salmoidae are the most sensitive families to ammonia toxicity with Walleye and Rainbow trout being the most sensitive species within these families (WHO, 1986).

Ammonia present in wastewater effluents is in ionized (NH_4^+) and nonionized (NH_3) forms. It is the nonionized form of ammonia that is potentially toxic to fish. Factors that can modify the toxicity of ammonia to fish include dissolved oxygen concentration, temperature, pH, previous acclimatization of the fish to ammonia, fluctuating exposures, carbon dioxide concentration, salinity, and the presence of other toxic substances. The acute toxicity of NH_3 has been shown to increase when pH decreases while there are indications that NH_3 toxicity is greater at low temperatures < 10°C (WHO, 1986).

Unlike dye, ammonia can undergo chemical transforms (nitrification) and biological uptake. When modeling ammonia, it is important to account for the fact that ammonia follows a first order decay rate, κ_{av}, which generally ranges between 1×10^{-6} to 2.3×10^{-5}

per second at 20 °C at base e (Gowda, 1984a). Golder (1995) found an ammonia loss of 1.0/day fit best to all transects modeled. Decay rates of ammonia are dependent on temperature and must be adjusted according to a modified Van't Hoff-Arrhenius relationship:

$$K_{T2} = K_{T1}\theta_T^{T2-T1} \qquad 1.1$$

where θ_T = temperature correction factor = 1.106 for ammonia. (Gowda, 1984b)

1.1.2 Previous Mixing Studies in the North Saskatchewan River at Edmonton

There have been a few mixing studies initiated on the North Saskatchewan River in the past, the majority of which focused on longitudinal dispersion using a slug injection test. In recent years, a few notable near field and transverse mixing studies have been conducted.

Milne et al (1993) examined residual chlorine decay in the North Saskatchewan River at Edmonton. They conducted a steady state dye test at the water treatment plants and used the results to calibrate a steady state river mixing and pollutant transport model to derive transverse mixing coefficients. They found the transverse mixing coefficient, ε_t, to vary between 0.016 and 0.893 m^2/s along the study reach that extended 4500 meters downstream of the Rossdale water treatment plant.

Golder Associates Ltd. (1994) used Milne et al. tracer data to calibrate the WASP water quality model from the City of Edmonton to the Saskatchewan border. They found $\varepsilon_t = 0.63$ m^2/s between Rossdale water treatment plant and GBWWTP and $\varepsilon_t = 0.1$ m^2/s between GBWWTP and Capital Wastewater treatment plant.

Golder Associates Ltd. (1995) in a report "*Joint Industry- Municipal North Saskatchewan River Study*" determined that currently the effluent discharge from

GBWWTP creates an ammonia plume that is easily detectable almost 20 kilometres downstream. They conducted a steady state dye test at GBWWTP outfall structure, but complete mixing of the dye into the effluent was not achieved. This report identified GBWWTP effluent discharge as being the principal cause of environmental degradation in the North Saskatchewan River in the 60 kilometer stretch that was examined. They recommend that field studies should be undertaken to describe the mixing of discharge effluent in the river in support of mathematical simulation modeling.

Cochrane Engineering and Trillium Engineering produced a report entitled "*Near Field Mixing of Outfall Discharges in the North Saskatchewan River*" in February 1997. This report indicated a need for more field data collection, specifically that field measurements of concentration profiles downstream of the GBWWTP effluent outfall are needed as well as a more detailed description of river geometry and velocities in the vicinity of the outfall.

1.1.3 Study Area

The study area spanned the North Saskatchewan River in Edmonton from a point roughly 0.5 kilometres upstream of the GBWWTP outfall to a point approximately 2 kilometres downstream of the outfall structure. The region is accessible via a boat launch located at the end of 50th Street just downstream of the 50th Street Pedestrian Bridge. A map highlighting the area can be seen in Figure 1.3.

The GBWWTP, opened in 1956, serves about 650 000 Edmonton City residents and treats non hazardous wastewater from industry. Typically 100 000 megalitres are treated annually at the plant. Pre-screening and grit removal occurs first with the removal of rags, gravel and stones from the flow. Primary treatment then removes approximately 50% of the solids via mechanical screening and gravity settling. These settled solids, also known as sludge, are treated by anaerobic digestion before being spread on farmland as a soil conditioner. The flow moves on to secondary treatment where the wastewater is

aerated to stimulate the multiplication of micro-organisms in the wastewater that feed on the organic matter. The activated sludge produced in this stage is then settled out in secondary clarifiers. Approximately 90% of the activated sludge is returned to the secondary treatment stage to replenish the microbial populations and the remaining 10% is sent to thicken before being treated by anaerobic digestion. The final stage of tertiary treatment involves nutrient removal and effluent disinfection. Ultra-violet technology is already in place for the disinfection of the effluent, but GBWWTP is expected to be operating at full tertiary treatment standards by 2005.

After the final ultra-violet treatment, the effluent flows through a channel to the outfall structure into the North Saskatchewan River at an average rate of 3.13 m^3/s (Golder, 1995). The outfall structure is located on the south bank of the river and consists of a steep chute, 4.572 meters wide and 32.9 meters long, illustrated in Figure 1.4. Flow is conveyed down the chute into a deepened pool-like area on the edge of the river formed by a riprap blanket that slopes up from the edge of the chute to the natural river bed. A submerged hydraulic jump is formed within the chute. Figures 1.5 through to 1.10 illustrate the outfall structure as well as the effluent plume in the near field region. It is noticed in Figure 1.8 through 1.10 that the rip rap remains exposed and a portion of the effluent is being directed upstream around the rip rap

1.2 RESEARCH OVERVIEW

In order to evaluate the mixing characteristics, a detailed field study was initiated to cover the study area described above. The field studies conducted complemented a recently initiated research program directed at investigating the effect of local conditions on near field effluent mixing. The studies also satisfied some of the recommendations that have been made in a previous report produced by Cochrane Engineering and Trillium Engineering in February 1997. The ultimate goal of this research was to establish computational modeling criteria for location specific intermediate field mixing. The objective of the field study was to obtain a detailed bathymetric map of the region and a

good idea of the mixing characteristics of the river during low flow conditions which are the most critical for ammonia concentrations.

A detailed bathymetry survey was conducted with the banks being surveyed using a total station over October 1 to 4, 2002 and October 11, 2002. The main portion of the channel was surveyed using a robotic total station synchronized with a sonic depth sounder on October 7 to 9, 2002.

In order to evaluate the mixing characteristics of the study area, a steady state dye test was conducted on October 29, 2002 and November 7, 2002. Depth averaged and surface samples were collected at 10 cross sections beginning at the outfall structure and ending at a point approximately two kilometres downstream of the outfall structure. Approximately 10 samples per cross section were collected and brought back to the lab for analysis. During the dye test, velocity measurements were made at six cross sections along with temperature and pH measurements.

The measured topography and limited velocity and water surface data were used to create and validate a depth averaged hydrodynamic model of the study reach. The results of the calibrated model were then used to extract cumulative discharge information in order to analyze the collected concentration profiles. The mixing characteristics of the reach were analyzed and compared to the local hydraulic conditions of the study area. A sensitivity analysis was performed to evaluate the sensitivity of the mixing characteristics to the accuracy of the velocity field.

1.3 RESEARCH OBJECTIVES

The work reported upon herein had the following site specific objectives:

1. Develop a detailed bathymetry map of an area of the North Saskatchewan River that covers from a point 0.5 kilometres upstream of the GBWWTP outfall structure to a point 2 kilometres downstream of the GBWWTP outfall structure.

2. Obtain information regarding the mixing characteristics of the study area by conducting a steady state dye test during a low flow period in the North Saskatchewan River which is the most critical time in terms of pollution.

3. Create a two dimensional hydrodynamic model of the study reach using the field data.

4. Evaluate the mixing characteristics of the study reach using the results of the hydrodynamic model in combination with the dye test results.

The work reported upon herein had the following general research contributions:

1. Indicate the sensitivity of the mixing coefficients to the accuracy of the hydrodynamic model.

2. Suggest whether local hydraulic characteristics affect mixing conditions.

3. Indicate how detailed field velocity measurements need to be in order to appropriately evaluate mixing conditions.

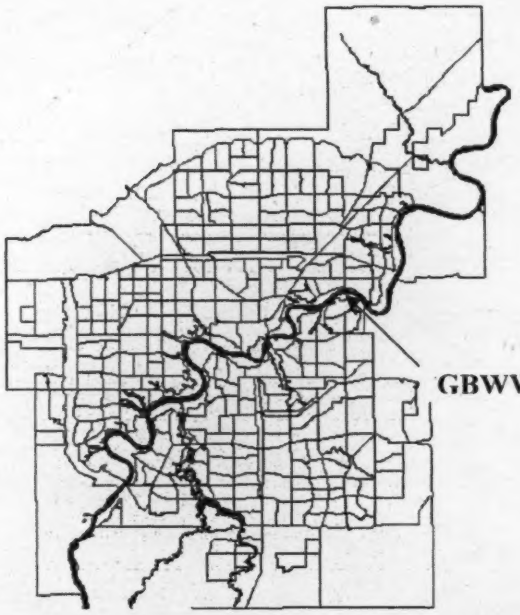

Figure 1.1: Map of North Saskatchewan River at Edmonton, Alberta.

Adapted from: http://maps.gov.edmonton.ab.ca/.

Figure 1.2: Steep side walls of river taken from Gold Bar Pedestrian Bridge looking upstream.

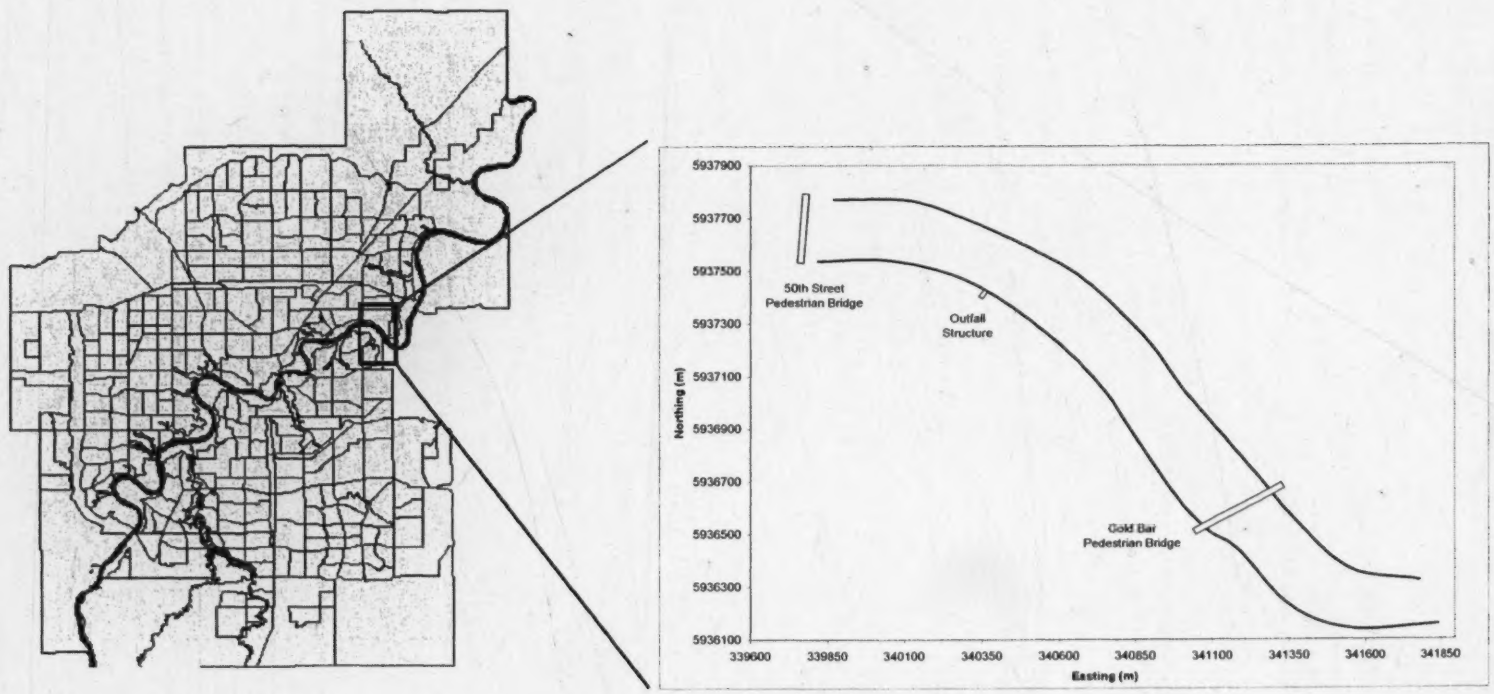

Figure 1.3: Map of study area.

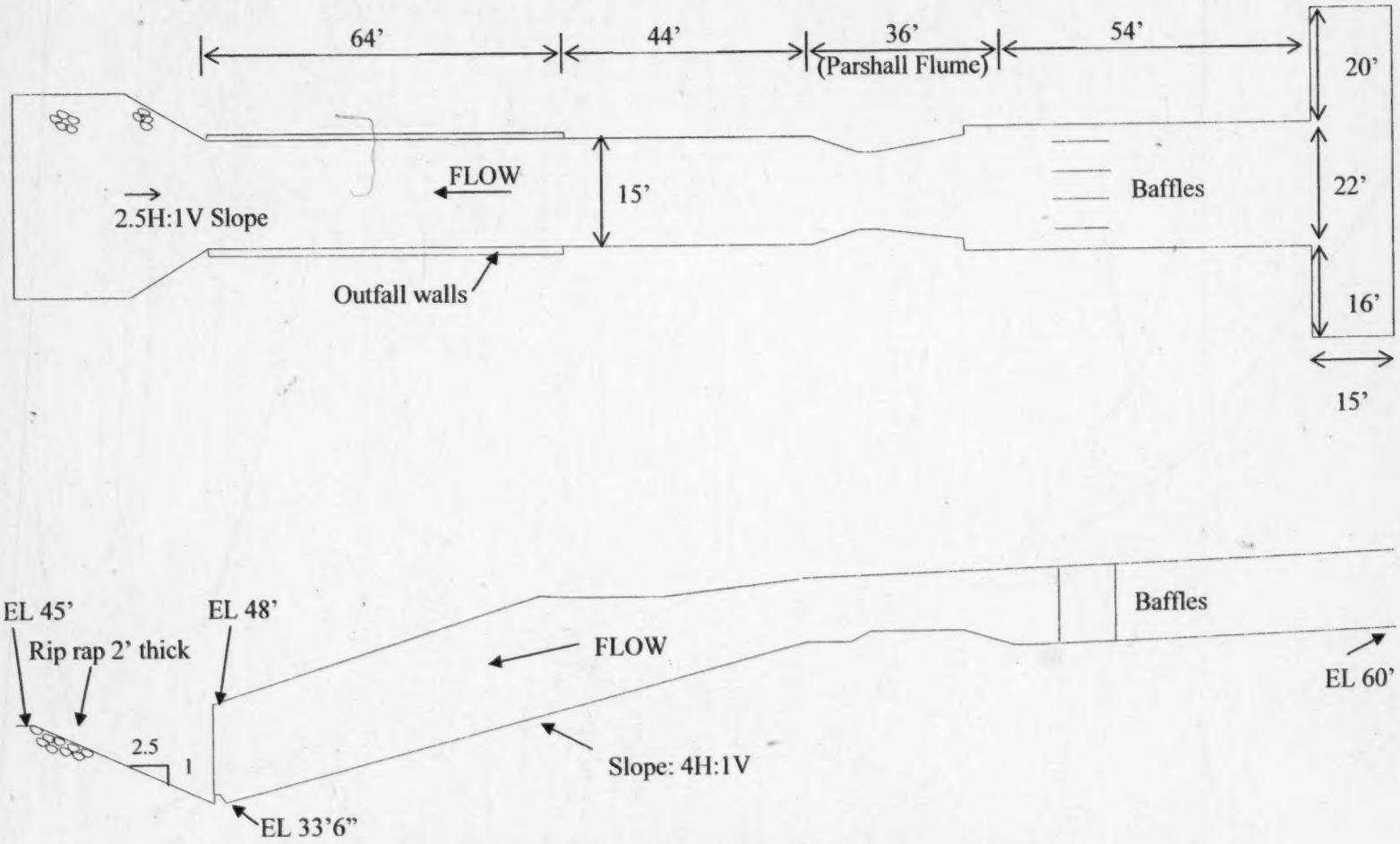

Figure 1.4: Plan and profile of GBWWTP outfall structure.

Note: Approximately to scale. Figure adapted from plans obtained from GBWWTP.

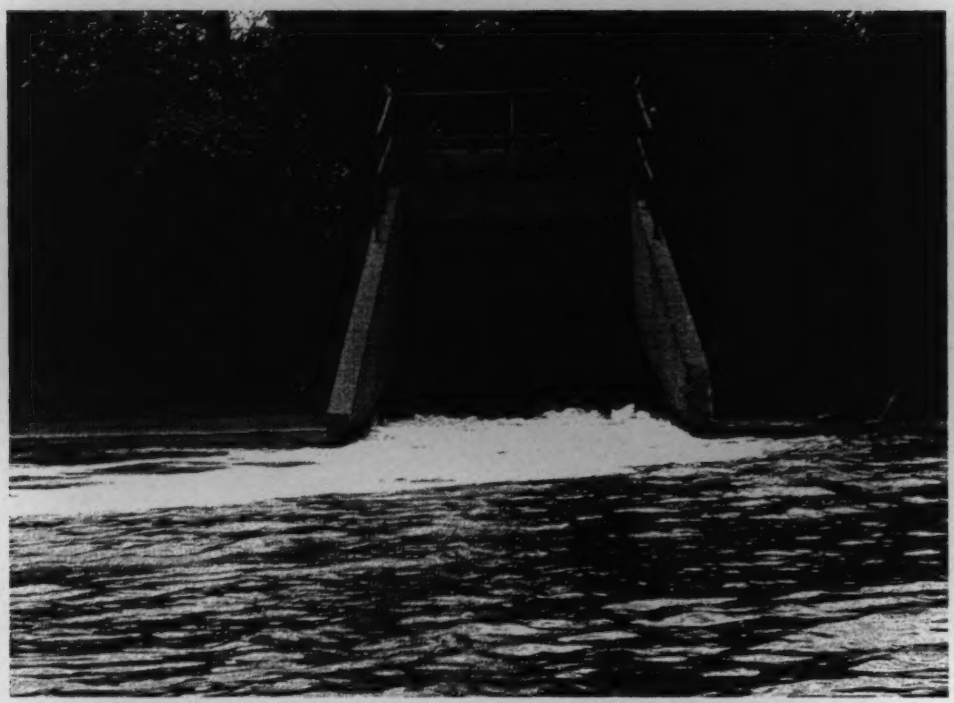

Figure 1.5: GBWWTP Outfall Structure.

Figure 1.6: GBWWTP Outfall Structure from downstream.

Figure 1.7: GBWWTP Outfall Structure chute with hydraulic jump.

Figure 1.8: Immediately upstream of GBWWTP outfall.

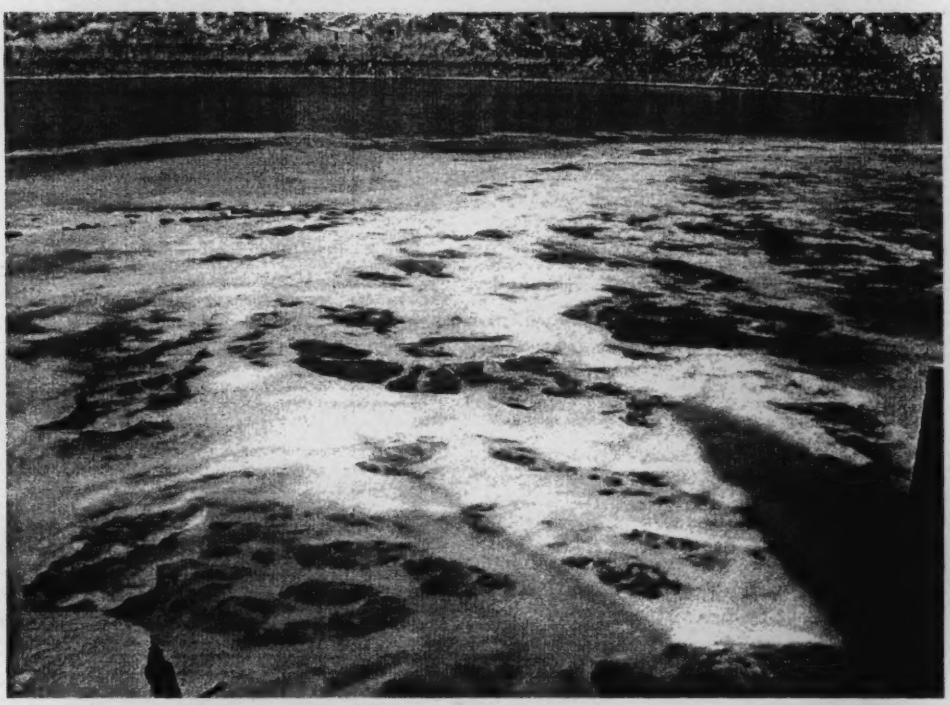

Figure 1.9: GBWWTP Outfall Structure.

Figure 1.10: GBWWTP Outfall Structure looking downstream.

CHAPTER 2 BATHYMETRIC SURVEY

The bathymetry of the river was mapped from a point roughly 0.5 km upstream of the GBWWTP outfall structure to a point approximately 2 km downstream of the outfall structure. A Leica TCRA1103plus Robotic Total Station was used for the entire survey. A 360° prism, illustrated in Figure 2.1, was used for all the surveying which under average atmospheric conditions has a range of 1500 meters. Under standard measurement mode, the total station has a standard deviation of 2 mm + 2 ppm and under rapid tracking mode a standard deviation of 10 mm + 2 ppm. The longer the measurement the greater the error so the expected vertical error on a 1 km observation would be 10 mm plus 2 ppm of 1000 m for a total of 12 mm.

2.1 Bank Survey and Control Points

An initial control point was established on a solid rock at the boat launch, designated as (1000, 1000, 500) metres North, East and Elevation respectively. Unfortunately, survey control marker information was not available prior to the survey so the survey was conducted under a local coordinate system and transformed at a later date. A light post located at the boat launch was designated as True North, or zero azimuth, that all other points were referenced to. Additional control points (benchmarks) were established along the length of the river as the survey progressed downstream. When available, objects such as large rocks were used as control points; otherwise a short stake was pounded into the desired location. All benchmarks on the south side of the river were designated "BMS_" and the numbers were incremented from 0 to 19. The staked benchmarks were located as close to the riverbank as possible, but were considered temporary as there was a concern of movement. Water level fluctuations at the study site were significant and resulted in submerged benchmarks on occasion.

The topographic study began with surveying the south river banks. The banks were surveyed using a "feature-line" principle which meant that rather than having a grid pattern of points, breaks in topography and visible features were mapped out using lines.

Generally speaking a feature-line was run at the top of the river bank (if it was accessible; if not the slope and height was estimated), at the bottom of the river bank, the edge of the water, and a single feature-line in the water approximately 0.5 metres deep. In addition any unique features, such as gravel bars, that were within wading proximity were picked up using feature-lines.

The north river banks are quite steep so rather than establishing benchmarks along that bank, the total station was set up on the south bank and the rod-person was boated across the river. It was surveyed in a similar manner to the south bank, however it was found that fewer feature-lines were necessary due to the steepness of the slope. Figure 2.2 presents the bank surveys along with the benchmark locations in the local coordinate system.

2.1.1 Data Correction

At a point in the bank survey, an error occurred in the setup of the total station and data downstream of BMS11 was affected as shown in Figure 2.3. There were four corrections that had to be made. In order to correct the data, a transformation of coordinates was used. All benchmarks were re-surveyed beginning at benchmark BMS5 in order to determine transformation parameters. There are three steps involved in a coordinate transformation: rotation, scaling, and translation (Wolf & Brinker, 1994). The geometry of the coordinate transformation is illustrated in Figure 2.4. The rotation angle is calculated as follows:

$$\theta = \alpha - \beta \tag{2.1}$$

where:

$$\alpha = \tan^{-1}\left[\frac{E_B - E_A}{N_B - N_A}\right] \tag{2.2}$$

$$\beta = \tan^{-1}\left[\frac{X_B - X_A}{Y_B - Y_A}\right] \tag{2.3}$$

where X-Y represents the local assumed coordinate system and E-N is a state plane coordinate system and A and B designate two points for which the coordinates are known in both coordinate systems.

The scaling factor can be calculated as follows:

$$s = \frac{\sqrt{(E_B - E_A)^2 + (N_B - N_A)^2}}{\sqrt{(X_B - X_A)^2 + (Y_B - Y_A)^2}} \quad \textbf{2.4}$$

If the scale factor is unity then it can be ignored as both coordinate systems are of equal scale. From the scale factor and rotation factor, the X' and Y' coordinates can be calculated as:

$$X'_A = sX_A \cos\theta - sY_A \sin\theta \quad \textbf{2.5}$$

$$Y'_A = sX_A \sin\theta + sY_A \cos\theta \quad \textbf{2.6}$$

Translation factors to shift the origin of the X'-Y' coordinate system to the E-N system are calculated as:

$$T_x = E_A - X'_A \quad \textbf{2.7}$$

$$T_y = N_A - Y'_A \quad \textbf{2.8}$$

From these parameters the coordinates can be transformed as:

$$E = sX \cos\theta - sY \sin\theta + T_x \quad \textbf{2.9}$$

$$N = sX \sin\theta + sY \cos\theta + T_y \quad \textbf{2.10}$$

The correction parameters derived are summarized in Table 2.1.

2.2 Boat Survey

To survey the main portion of the river channel, a SonarLite Portable Echo Sounder synchronized with a robotic total station system was utilized to measure the depths of the river. The SonarLite is a single beam echo sounder specifically designed for use by surveyors. It is accurate to ± 0.02 meters within a depth range of 0.30 to 90 meters with a beam pattern of 5 to 10 degrees. The transducer of the sounder was mounted to the stern of the boat with a 360° prism mounted directly above the transducer at a measured

offset of 1.375 meters illustrated in Figure 2.5. In this manner the total station would be constantly recording the position of the sonar transducer. The SonarLite stores time stamped depth data internally at a rate of one ping per second. The sonar was run continuously throughout the surveys.

The robotic total station was equipped with a rapid tracking program, FastRecord. FastRecord utilizes the Lock ATR Mode of the total station which finds, locks-on and follows the prism. It also utilizes the Rapid Track Mode which sets the instruments EDM to measure a distance constantly. After locking on, FastRecord continually measures and records point data in an ASCII file stored in the data format below:

point, north, east, elevation, date, time

A position is recorded approximately every 0.3 seconds. The total station was started and stopped for each new line so one file was generated for each line traversed. The total station under ATR lock mode using a 360-degree prism has a range of approximately 600 metres under average atmospheric conditions.

Benchmarks were established on the 50th Street Pedestrian Bridge (BMP50 and BMP51) and the Gold Bar Pedestrian Bridge (BMP100 and BMP101) as they provided excellent viewing points of the river reach. The study area was broken down into five sections, First section, Outfall Section, Upstream Bridge section, Under Bridge section, and Downstream Bridge section, due to visibility and range issues as shown in Figure 2.6. The main sections were surveyed over two days: October 7 and October 8, 2002 and areas that were missed were picked up on October 9, 2002. The clocks in the total station and the sonar were manually synchronized immediately prior to the survey of each section. The boat drove approximately 10 lines longitudinally up and down a river section as well as a zigzag line across each section as shown in a close up of the first section in Figure 2.7. It was difficult to maintain a lock on the prism under sunny conditions due to the reflection off the water, but the speed of the boat was not an issue. The total station could easily maintain a lock on the prism at a pace equivalent to that of a brisk walk. Over the entire study area, a total of 48,973 points were taken.

From the two sets of data, the bed elevation was calculated by matching the time stamps of the ASCII files generated. The total station data was then matched to the sonar data utilizing the VLOOKUP function in excel. This function searches for a value, in this case the time stamp, in the leftmost column of a table returning a value in the same row from a column you specify in the table. If VLOOKUP can't find the value, it uses the largest value that is less than the lookup value. In this manner the position of each depth value was matched and the bed elevation was calculated as the elevation of the sonar transducer less the depth recorded by the sonar at that position. Occasionally the sonar would generate two depths for the same time stamp. In these cases the first point was chosen and the second discarded. Since the sonar was run continuously and the total station was run intermittently, the sonar would occasionally match the same position from the total station data to different depths because of how the VLOOKUP function executes. In these cases the first point matched would be kept and the remaining discarded. A total of 11,402 points were matched.

2.3 UTM Coordinates

Because the survey was conducted in a local coordinate system, the data had to be transformed into a conventional coordinate system. In order to do this, three of the established benchmarks were surveyed precisely using Ashtech Locus GPS units and an Alberta Survey Control Marker (ASCM).

2.3.1 GPS Technology

Information in this section has been modified from course notes from 53.373, Garmin GPS Guide for Beginners and Trimble Tutorial.

GPS, global positioning system, utilizes a system of 24 satellites: 21 navigational and 3 active spares. The satellites orbit the earth in 12 hour orbits at an altitude such that the satellites repeat the same track and configuration over any point approximately every 24 hours (4 minutes earlier each day). The satellites transmit low power radio signals on

several frequencies that can pass through clouds, glass and plastic, but not solid objects such as buildings and mountains. The transmitted code is called "pseudo-random code" because it looks like a noise signal.

There is a control segment that consists of tracking stations located around the world and the master control facility located at the Falcon Air Force Base in Colorado. The control segment measures signals from the satellites and incorporates them into orbital models. These models compute precise orbital data (ephemeris data) and clock corrections for each satellite. The control segment then uploads the information to the satellites.

GPS receivers convert satellite signals into position, velocity, and time estimates. The receiver calculates the exact location on the basis of triangulation so in order to calculate a receiver's position in 3D at least four satellite signals are required. The receiver generates the same pseudo-random code that the satellite is generating and compares the two codes to determine how much delay is required to match the two. The delay between the two codes is then multiplied by the speed of light to get the distance to the satellite. Parallel multi channel receivers are the most common nowadays and typically have five to twelve receiver circuits each devoted to one particular satellite signal. This way a satellite lock can be maintained at all times.

GPS errors are a combination of noise, bias, and blunders. Noise is the combined effect of code noise and noise within the receiver and can result in errors of a couple of meters. Bias errors result from Selective Availability: the intentional degradation of the satellite signals by the U.S. Department of Defense (this was turned off May 2000). Blunders are due to control segment mistakes due to computer or human error, user mistakes, and receiver errors from software or hardware failure. Blunders can result in up to hundreds of kilometers of error.

Specific sources of error include ionosphere and troposphere delays, signal multi-path, receiver clock errors, orbital errors, the number of satellites visible, and the satellite

geometry. Ionosphere and troposphere delays occur because the speed of light is only constant in a vacuum. The charged particles in the ionosphere and the water vapor of the troposphere slow down the satellite signals. Receivers use a built-in model to calculate an average delay, but it is not exact. A dual frequency receiver is much more exact in correcting for delays because it compares the relative speeds of two different signals. Signal multi-path error occurs when the satellite signals are reflected off objects, for example tall buildings, which increases the time of travel of the signal and introduces errors. Good receivers use sophisticated signal rejection techniques to minimize multi-path errors. Receiver clock errors occur because it is far too expensive to put precise atomic clocks into receivers so as a result distance measurements need to be corrected. Orbital errors are due to inaccuracies in the satellites reported location since they can't be monitored every second; however they only account for a very small portion of the total error. Error from satellite geometry is based on the "Geometric Dilution of Precision" (GDOP). If a receiver chooses satellites that are located at wide angles relative to each other, the error region is minimized and therefore the GDOP is low. A good receiver will choose satellites that give the lowest GDOP.

2.3.2 GPS Survey

There are two types of surveys using GPS units: static and kinematic. This survey was carried out in static survey mode which yields a horizontal accuracy of 5 mm + 1 ppm (rms) and vertical accuracy of 10 mm + 2 ppm (rms) with an occupation time of 15 to 60 minutes depending on distance between the Locus Receivers. RMS indicates that 68% of data points would fall within this range and the first number refers to the base error while the second ppm is distance dependent. In static mode two Locus units are used with one placed on each end of a baseline and left to gather data for a period of time. Static surveys provide the highest level of reliability and accuracy as a large amount of data is collected at each point. The two units must collect data simultaneously over the same period of time in order for data to be usable. The maximum distance of the baseline is 20 km.

The survey was conducted over two days: November 18 and 19, 2002. ASCM 107383 was used located on Hardisty Drive. This static survey was conducted with one Locus receiver unit set up over the ASCM and the other unit set up over a benchmark. Benchmarks BMSR, BMS0, BMP50 and BMP51 were all occupied. The rock and the bridge benchmarks were considered to be relatively permanent so little to no shift was anticipated on those benchmarks, but the BMS0 was a stake and movement was suspected. Only three benchmarks were required for the transformation so if movement was observed on BMS0 it would simply be discarded. They were turned on to simultaneously collect data until the receivers indicated that enough data had been collected for a baseline within 5 km. Typically this was around 25 minutes. Then both receivers were turned off and a new session was started once the rover receiver was set up on a new benchmark.

The data were downloaded via infrared cables and processed using the Locus Project Manager Software. In processing, a control point remains fixed in the software (in this case the ASCM) and the information is used to adjust the other occupations accordingly.

2.3.3 Transformation of Coordinates

First the elevations of the points were adjusted from the local coordinate system to the global coordinate system. Table 2.2 summarizes the differences for each of the occupations. An average correction of 111.968 metres was added to transform all the data to UTM coordinates.

Transformation parameters were calculated between the BMSR (A) and BMP50 (B), BMSR (A) and BMP51 (C), and BMSR (A) and BMS0 (D) and are summarized in Table 2.3. The parameters are identical for the first two pairs, however there is a significant difference in the parameters calculated using BMS0. A check can be performed on the parameters by calculating the E-N coordinates of the benchmarks not used in the calculation. The error associated with the transformation parameters is

summarized in Table 2.4. Using the transformation parameters calculated from BMSO, error greater than 100 metres is found for the transformation of the two bridge benchmarks. Using the transformation parameters calculated from the bridge parameters, error on the order of 1 metre is found for the transformation of BMS0.

It is evident that the data collected over benchmark BMS0 is suspect and as such the information was discarded. An average of the transformation parameters between the bridge benchmarks and BMSR, summarized in Table 2.5, was used to convert all data points to UTM coordinates. A final check was performed using the average transformation parameters to compare to the three valid data points and found the error to be within approximately 5 mm as shown in Table 2.6.

A final plot of the transformed survey is shown in Figure 2.8.

2.4 VELOCITY MEASUREMENTS

Velocity measurements were taken during the dye tests on October 29, 2002 and November 7, 2002. A Marsh McBirney flow meter was used to measure the velocity. The depth was roughly estimated using tape markings equally spaced along the cord. If the depth was less than 75 cm a single reading was taken at 0.6 of the depth, and if the depth was greater than 75 cm two readings were taken at 0.2 and 0.8 of the depth. At each location that a velocity measurement was made, a pH reading and temperature reading was taken using a Hanna pH Checker and a Fisher Scientific Traceable Digital Thermometer. Each location was recorded using the total station.

A cross section 30 metres upstream of the outfall was chosen to do a detailed velocity cross section with approximately 20 points completed. This took a considerable amount of time and was the only cross section that was completed on October 29. On November 7, approximately 10 measurements were made across stations 80, 320, 1000, and 1500 as well as five measurements were made across the station at the end of the

study area. Locations of all velocity measurements are illustrated in Figure 2.9. Table 2.7 summarizes all the measurements taken.

2.5 RESULTS

The topographic information was imported into the bed program of the River2D model in order to derive a digital elevation model of the study area.

2.5.1 Bed Program

Actual representation of the physical features of the river channel bed is crucial for accurate modeling of the river flow. The topographic information collected from the bathymetry survey was imported into the bed program of River2D as a series of nodes and breaklines. The model is based on Triangulated Irregular Network (TIN) methodology for interpolation of nodal parameters. Breaklines are used to define feature-lines which tell the model to interpolate elevations along a breakline.

The data was triangulated and adjusted until a logical representation of the bed topography was reached. Adjustments are necessary in order to ensure the triangulation of the data achieves a reasonable representation of the bed surface topography. Areas that are susceptible to misrepresentation include areas that have gaps in data nodal points, areas with large changes in topography such as bank areas that may have material added due to triangulation leaving artificial outcrops, ridges, etc. Adjustments are made by adding nodes or breaklines and involve the judgment of the model user. The general procedure is to zoom in at a close resolution and pan around the bed comparing areas to upstream and downstream in order to notice any apparent discrepancy in bed topography and to decide whether the feature is real or artificial. A good knowledge of the study area assists in this process.

A few nodes were added around the study area at a higher elevation. These points describe high ground outside the river channel. Between these added nodes and the nodes of the study area, boundary nodes were added. This procedure is important to make sure that there are topographic points outside of the computational boundary to allow for interpolation at the boundary. It is also important that the computational boundary be outside of the required model area (ie. in a dry area).

During the survey, it was difficult to survey the bridge piers and the outfall structure itself. Plans for the Gold Bar Pedestrian Bridge were obtained from Alberta Environment. The centerline point of each of the four piers had been surveyed. Using this information and the pier dimensions from the bridge plans, nodes were added into the bed file. The piers were treated as internal no flow boundaries. The outfall structure was added in a similar manner. The tops of the outfall structure walls had been surveyed and the plans of the outfall structure were obtained from GBWWTP. The outfall structure was defined as an inflow boundary. The final bathymetry file is illustrated in Figure 2.10 with bed contours every 0.5 metres. A close up of the outfall section is shown in Figure 2.11 to illustrate the detail achieved from the bathymetric survey.

2.5.2 Topography Observations

Referring to Figure 2.10 some interesting topography features are noticed. Color contours are plotted along with contour lines every 0.5 metre. At the outfall structure, the deepest portion of the channel is about mid-channel on the opposite side of the rip rap blanket. There would be a tendency for the majority of the flow to be carried in this deep area. From here moving downstream extending to a point a few hundred metres upstream of the Gold Bar Pedestrian Bridge, it is noticed that the south bank is quite shallow with a mild transverse slope. Through this section the deepest portion of the channel tends to be closer to the north bank, which is quite steep indicated by the tight contour lines.

From this point to the pedestrian bridge, the south bank becomes steeper and the deepest portion of the channel occurs in the bank areas with the shallow point occurring in mid-channel. Immediately downstream of the bridge piers on the south bank, an alluvial fan like deposit is noticed. This causes a narrowing of the river channel with the deepest portion of the channel at the north bank. Immediately downstream of the alluvial deposit, the south bank tends to be quite shallow with several gravel deposits. Coming into the bend, the deepest portion of the channel switches from the north bank to the south bank. The south bank becomes steeper while the north bank flattens out.

2.6 Water Surface Elevations for Hydrodynamic Models

The data from the boat survey was used for water surface elevations over the study area. With the prism mounted to the boat a known distance above the depth sounder, the elevation of the depth sounder was recorded at all points. It was assumed that as the boat traverses the river it remains plane to the water surface and therefore the depth sounder is maintained at the water surface. The error in this assumption is estimated to be approximately a few centimeters and would have a tendency, if the boat did not remain plane, to read an elevation that was below the actual water surface.

The survey data was plotted for each section and a single line was chosen to represent that section's water surface elevation. Figure 2.12 shows the boat lines that were chosen for the water surface calibration. Figure 2.13 illustrates the first section with the chosen line highlighted. The line was chosen based on proximity to banks as a midpoint line would be ideal, whether the line remained relatively straight, and the fluctuation in the surveyed water surface elevation (if for instance another boat passed while surveying, waves were observed in the surveyed water surface elevation which are not representative of the actual water elevation). The under bridge section was not used for any calibration of the water surface.

It was realized that the boat survey points had a significant amount of oscillation within the data (±5 cm). Another problem, shown in Figure 2.14, was a difference of 6

cm noticed between lines that were traveled upstream versus downstream, the upstream lines being lower than the downstream, which suggested that the assumption of the sounder transducer remaining on the water surface was false. Downstream boat lines had been used for the calibration of the 1-D model which were considered a better approximation of the actual water surface. Using these points to calibrate the 1-D model was adequate considering the accuracy expected, but for the 2-D model it was decided to use more accurate waters edge points from the bank surveys.

Figure 2.1: 360° prism used in surveys.

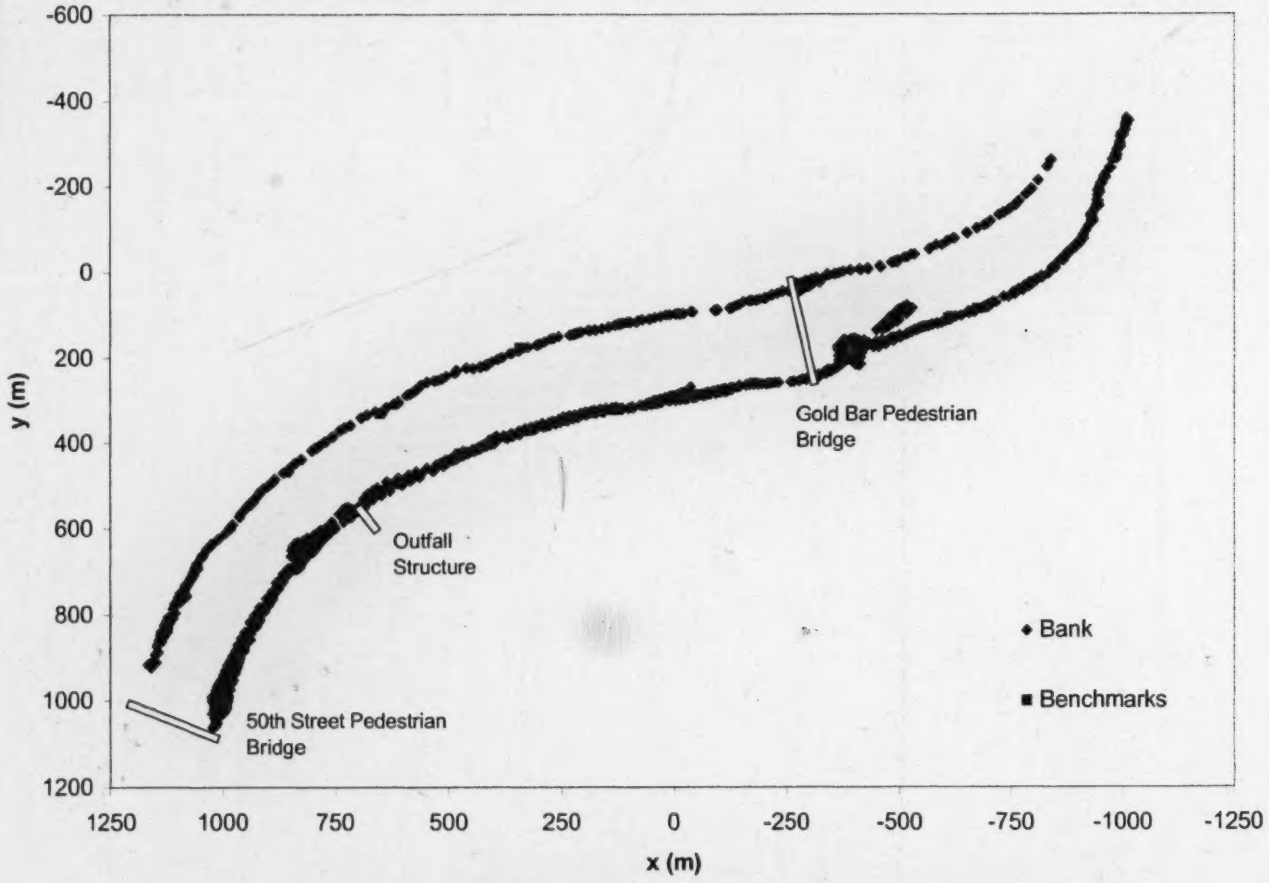

Figure 2.2: Benchmark locations and bank survey in local coordinate system.

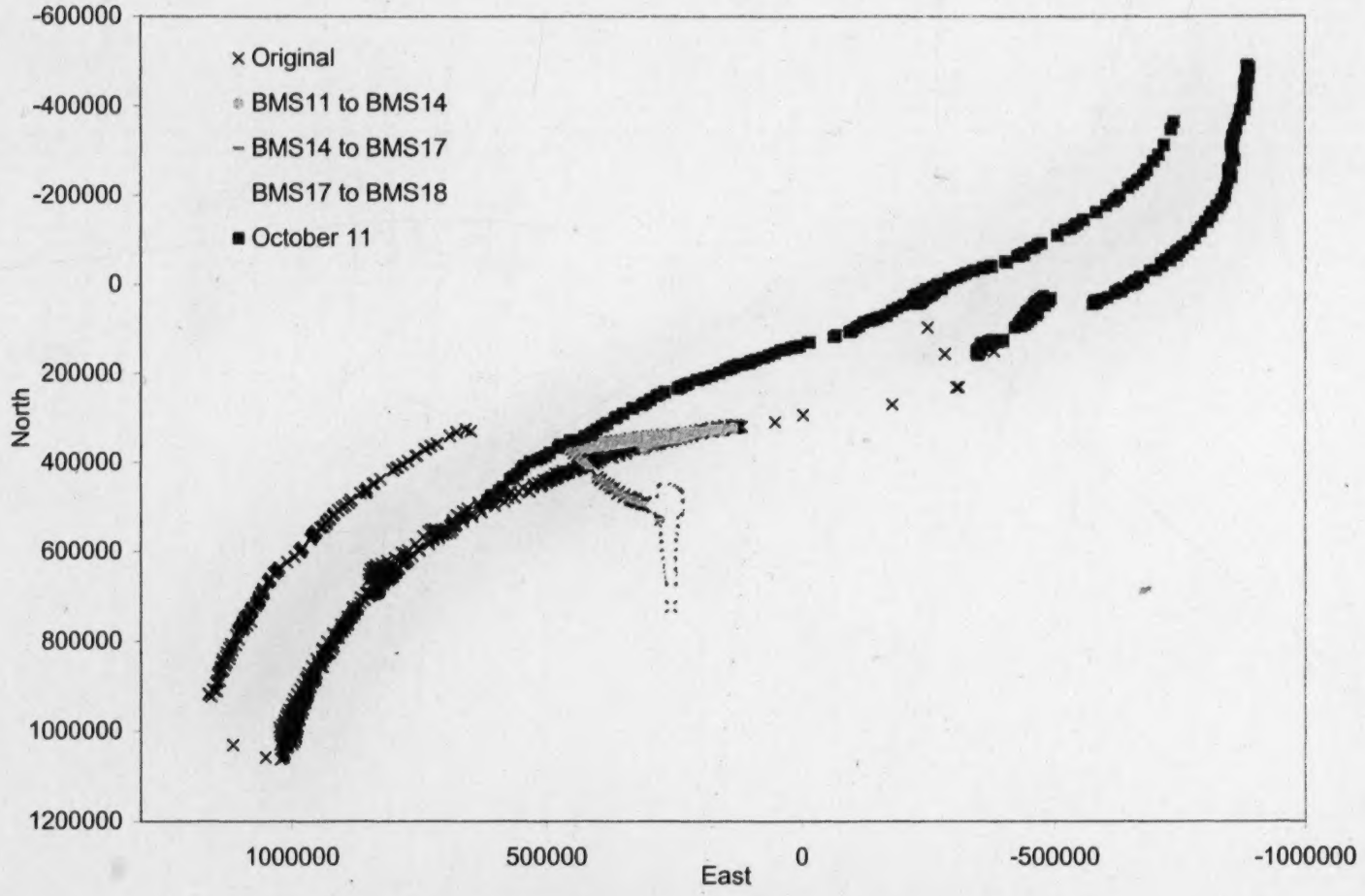

Figure 2.3: Original bank survey before corrections.

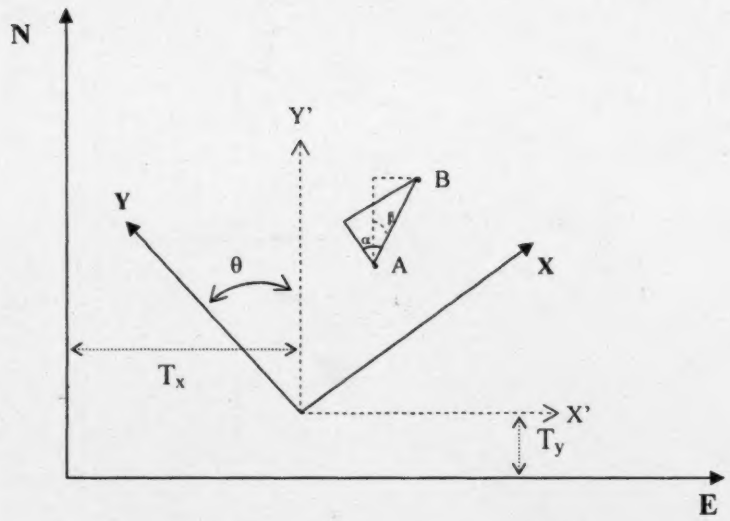

Figure 2.4: Geometry of coordinate transformation.

Table 2.1: Transformation parameters for correction of survey data.

Data that was transformed	Rotation around	θ
BMS11 to BMS14	BMS11	0.0435
BMS14 to BMS17	BMS14	-2.222
BMS17 to BMS18	BMS17	-1.232
October 11 Data	BMS17	-0.1842

Figure 2.5: Setup of prism and transducer.

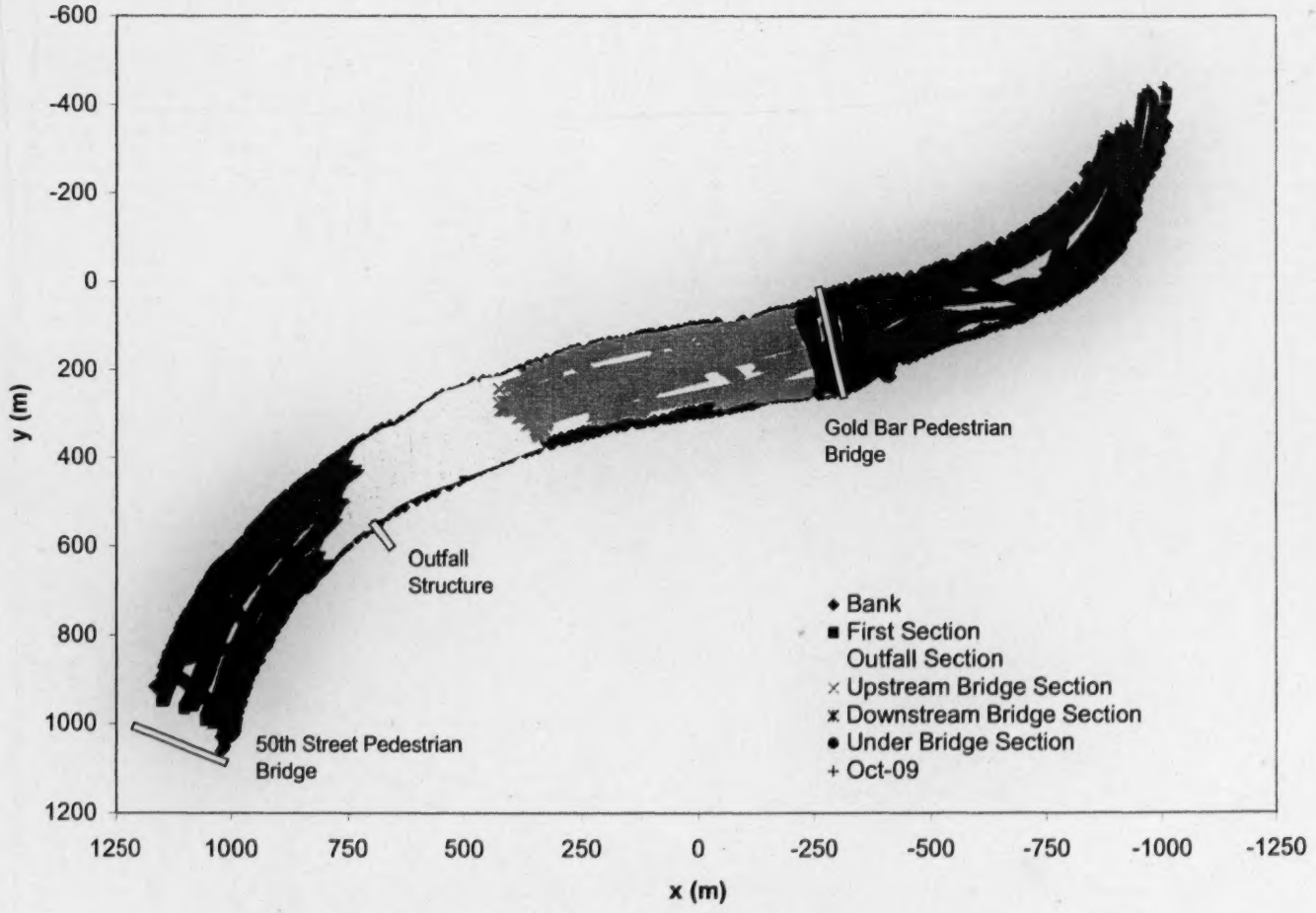

Figure 2.6: Lines traversed by boat within banks in local coordinate system.

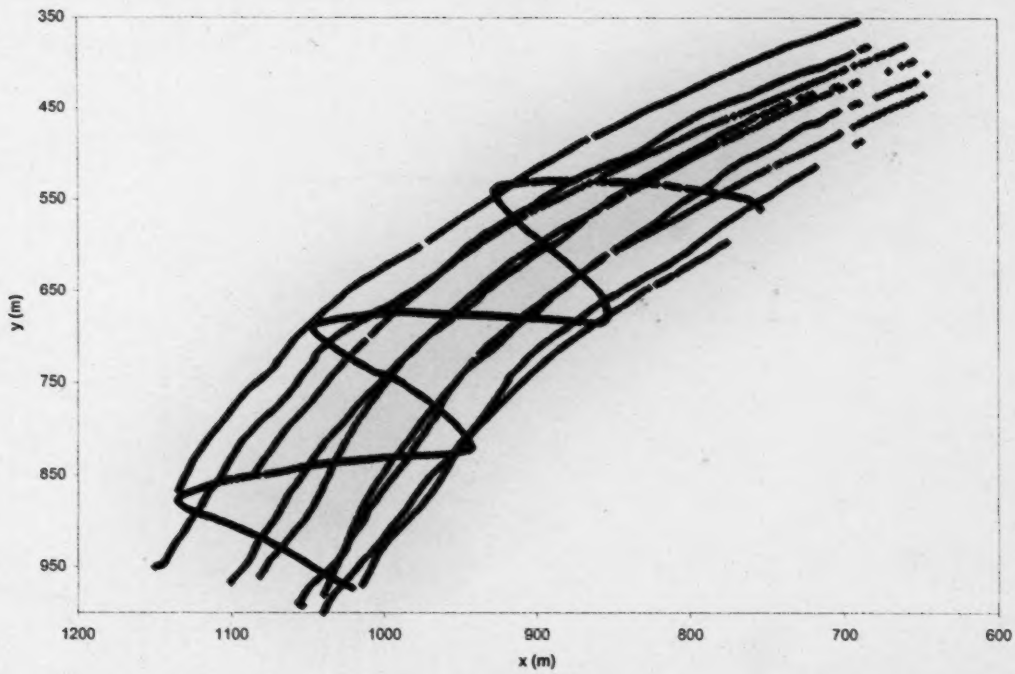

Figure 2.7: Close up of lines traversed by boat in the first section near the 50th Street Pedestrian Bridge.

Table 2.2: Transformation of elevation.

Benchmark	Difference in elevation (m)
BMSR	111.96
BP51	111.969
BP50	111.971
BMS0	111.97
AVERAGE	**111.968**

Table 2.3: Calculated Transformation Parameters using the surveyed points.

	A & B	A & C	A & D
θ	1.938	1.938	-1.193
T_x	341141.944	341141.992	338551.166
T_y	5936991.406	5936991.514	5938126.150

Table 2.4: Calculated error associated with the transformation parameters.

	A & B	A & C	A & D
ΔE of B (m)		0.011	146.988
ΔN of B (m)		-0.011	-53.780
ΔE of C (m)	0.013		-212.430
ΔN of C (m)	0.000		-6.778
ΔE of D (m)	0.027	0.027	
ΔN of D (m)	-1.124	-1.115	

Table 2.5: Final transformation parameters.

θ	1.938
T_x	341141.964
T_y	5936991.463

Table 2.6: Calculated error associated with final transformation parameters for each point.

	Difference (m)
ΔE of A	-0.004
ΔN of A	0.003
ΔE of B	0.007
ΔN of B	-0.005
ΔE of C	0.004
ΔN of C	0.000

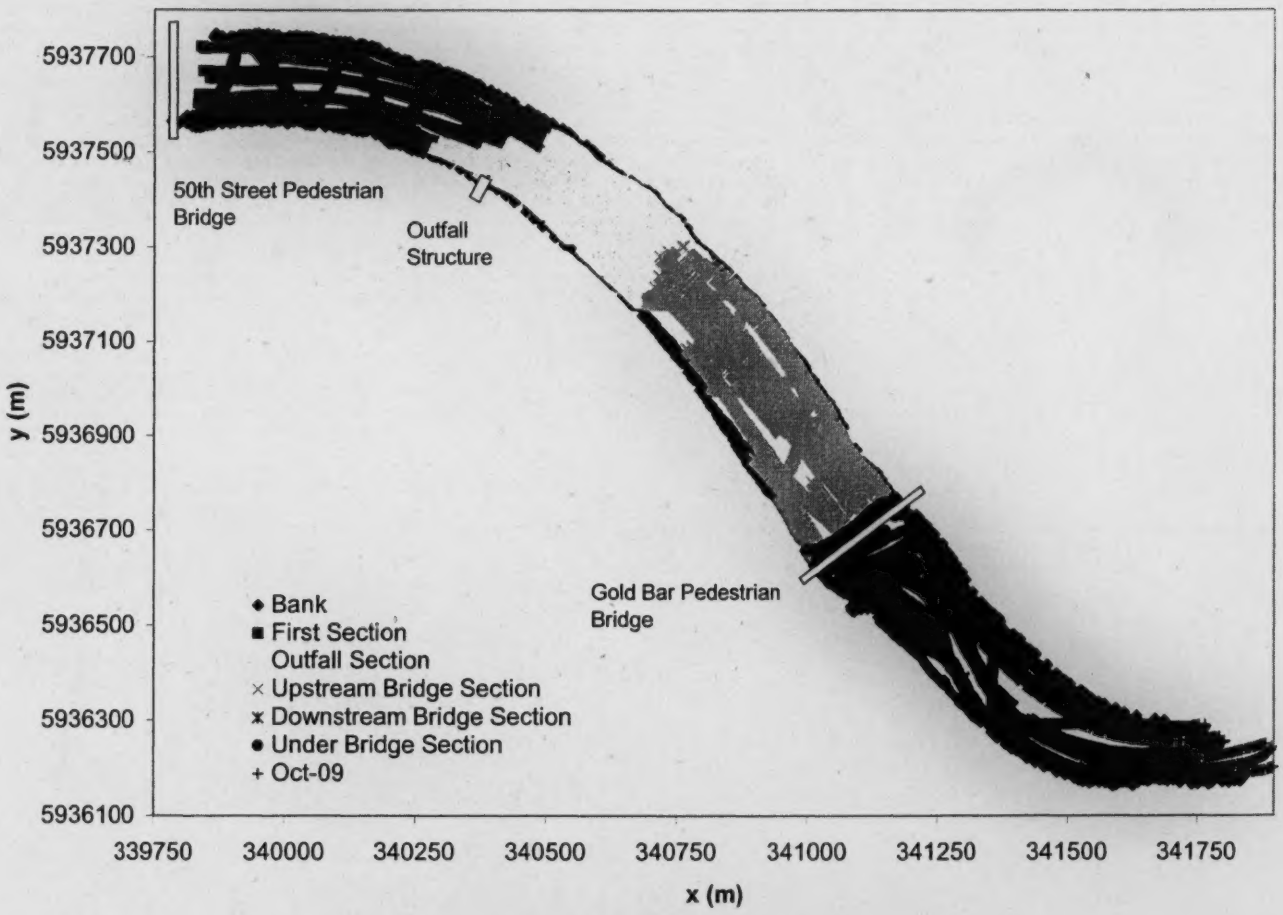

Figure 2.8: Final plot of transformed coordinates.

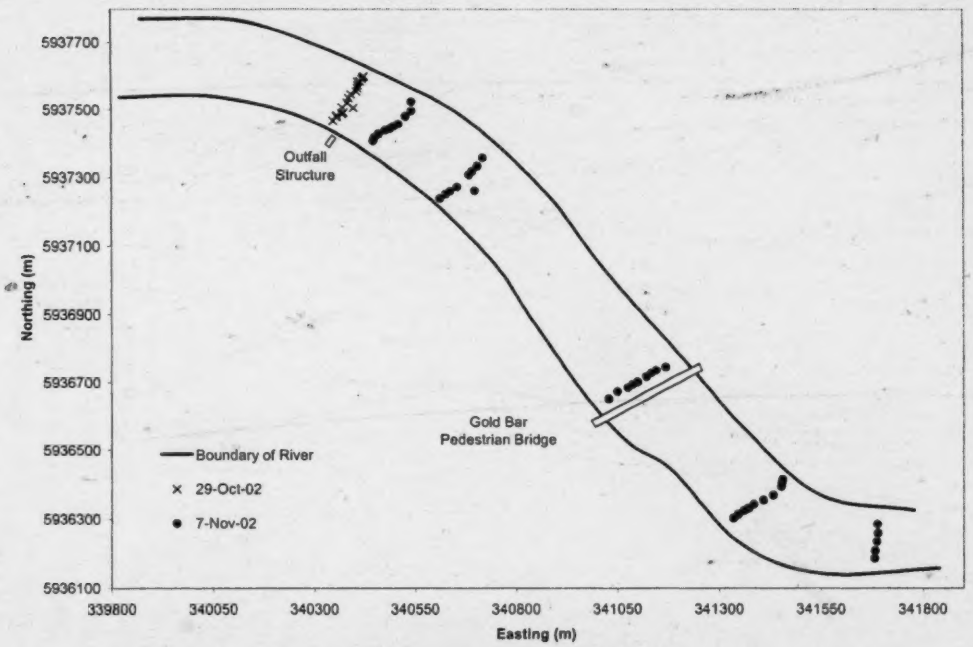

Figure 2.9: Location of velocity measurements taken October 29, 2002 and November 7, 2002.

Table 2.7: Summary of velocity, pH, and temperature measurements taken October 29, 2002 and November 7, 2002.

Point	East	North	Velocity (m/s)			Temperature (°C)	pH
			0.2D	0.6D	0.8D		
Station -30							
V-30-1	340348.584	5937469.069		0.01		0.36	8.92
V-30-2	340356.757	5937480.840		0.1		0.32	8.51
V-30-3	340370.156	5937489.682	0.48		0.26	0.38	8.56
V-30-4	340374.945	5937492.615	0.51		0.57	0.52	8.1
V-30-5	340371.415	5937507.855	0.81		0.5	0.54	8.17
V-30-6	340399.891	5937506.219	0.53		0.64	0.59	8.45
V-30-7	340384.634	5937521.652	0.53		0.63	0.6	8.52
V-30-8	340386.991	5937535.708	0.52		0.73	0.61	8.56
V-30-9	340393.246	5937546.803	0.54		0.58	0.63	8.63
V-30-10	340407.364	5937555.282	0.37		0.38	0.64	8.7
V-30-11	340409.747	5937564.820	0.25		0.32	0.68	8.7
V-30-12	340410.354	5937574.291	0.3		0.4	0.73	8.68
V-30-13	340410.442	5937583.696	0.41		0.41	0.77	8.95
V-30-14	340416.498	5937584.896		0.23		0.77	8.95
V-30-15	340420.915	5937591.397		0.3		0.81	8.87
V-30-16	340423.177	5937597.696	0.2		0.21	0.82	8.91
V-30-17	340425.975	5937600.071		0.14		0.81	8.86
V-30-18	340357.873	5937484.120		0.18		0.42	8.9

Point	East	North	Velocity (m/s)			Temperature (°C)	pH
			0.2D	0.6D	0.8D		
Station 80							
V80-1	340542.839	5937525.069		0.17		2.68	8.34
V80-2	340542.985	5937497.854	0.35		0.45	0.53	8.34
V80-3	340527.728	5937482.166	0.36		0.52	0.25	8.39
V80-04	340510.992	5937458.642	0.68		0.83	0.26	8.5
V80-05	340498.411	5937451.624	0.66		0.81	0.25	8.59
V80-07	340489.647	5937445.211	0.53		0.81	0.27	8.77
V80-08	340461.898	5937429.269	0.45		0.5	0.8	8.79
V80-09	340450.694	5937418.284	0.08		0.14	12.2	8.39
V80-10	340447.659	5937407.603		0.15		10.61	8.09
Station 320							
V320-01	340612.025	5937239.163		0.19		11.4	8.45
V320-02	340627.067	5937252.378		0.33		6.3	4.62
V320-03	340637.503	5937261.101	0.44		0.66	2.1	7.72
V320-04	340655.251	5937273.193	0.58		0.72	1.96	7.72
V320-05	340698.832	5937261.989	0.44		0.8	4.05	7.79
V320-06	340684.712	5937308.250	0.52		0.65	3.14	7.76
V320-07	340692.381	5937318.482	0.36		0.52	0.44	7.93
V320-8	340705.711	5937333.835	0.47		0.51	0.45	7.82
V320-09	340718.488	5937358.187	0.37		0.56	0.56	7.82
Station 1000							
V1000-2	341029.942	5936652.018	0.45		0.72	0.62	7.35
V1000-3	341050.343	5936673.202		0.56		0.55	7.58
V1000-4	341076.112	5936684.242	0.58		0.77	0.55	7.55
V1000-5	341088.028	5936693.433	0.59		0.79	0.56	6.81
V1000-6	341100.736	5936701.147	0.48		0.88	0.56	7.61
V1000-7	341121.930	5936716.821	0.53		0.88	0.55	7.62
V1000-8	341134.725	5936727.802	0.59		0.89	0.56	7.7
V1000-9	341146.250	5936735.228	0.65		0.93	0.58	7.35
V1000-10	341169.252	5936744.703		0.78		0.7	7.65
Station 1500							
V1500-1	341335.822	5936303.104		0.12		16.6	6.92
V1500-2	341347.033	5936313.314		0.28		5.82	5.92
V1500-3	341361.672	5936324.114		0.33		4.42	4.97
V1500-4	341373.060	5936330.706	0.5		0.58	1.8	4.93
V1500-5	341385.866	5936342.422	0.52		0.91	0.59	6.98
V1500-6	341409.471	5936354.163	0.57		0.93	0.58	6.76
V1500-7	341433.221	5936368.078	0.67		0.95	0.59	6.35
V1500-8	341452.875	5936392.847	0.48		0.69	0.71	5.4
V1500-9	341454.074	5936402.707	0.5		0.71	0.71	5.55
V1500-10	341456.274	5936413.226	0.07		0.72	0.72	5.94
Station END							
VE-1	341681.066	5936184.986	0.5		0.65	1.63	6.95
VE-2	341682.318	5936207.546	0.31		0.71	0.56	7.6
VE-3	341686.737	5936233.891	0.55		0.66	0.59	6.55
VE-4	341689.547	5936258.449	0.49		0.6	0.6	5.2
VE-5	341688.209	5936284.526	0.18		0.29	0.69	5.55

Note: A tributary exists just upstream of Station 1500 which accounts for the increased temperature at that location.

Figure 2.10: Final bed topography with 0.5 metre contours.

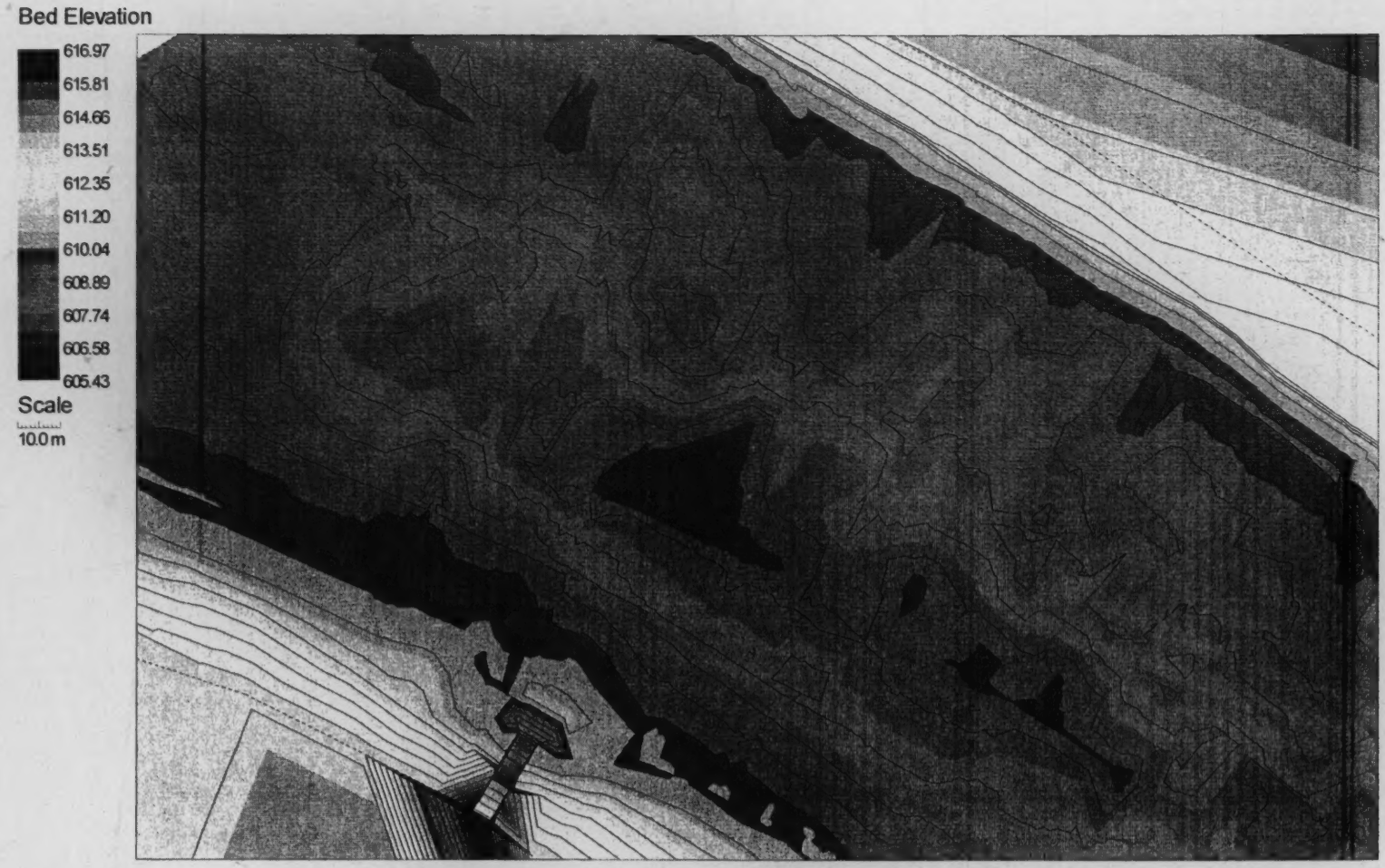

Figure 2.11: Close up of topography at outfall with 0.5 metre contours.

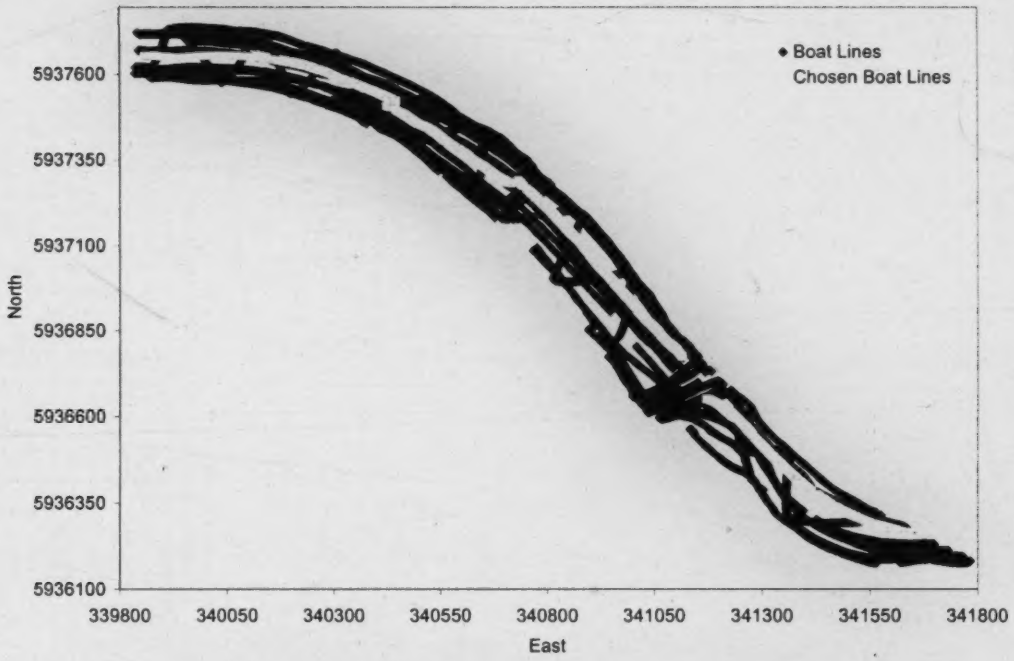

Figure 2.12: Map of boat lines chosen for calibration of HEC-RAS.

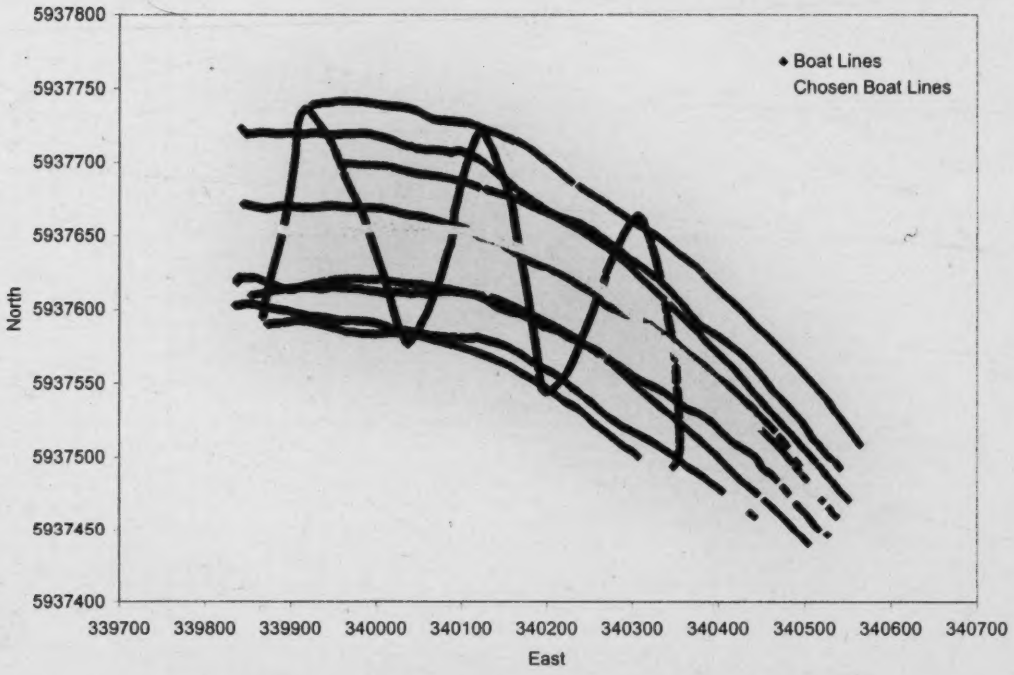

Figure 2.13: Close up of first boat section with chosen line.

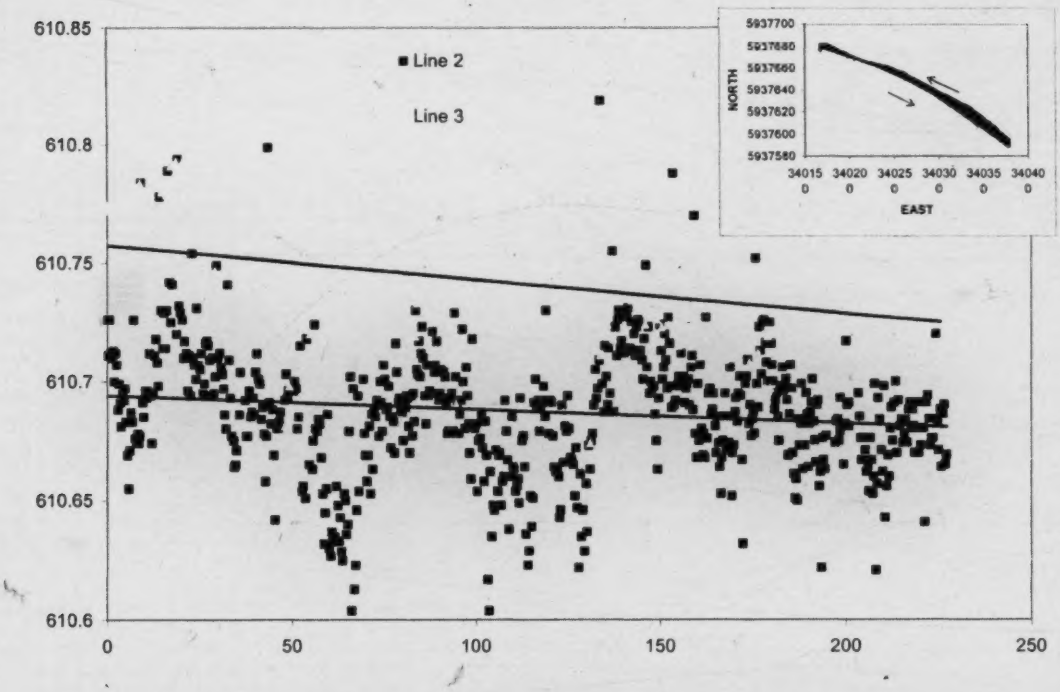

Figure 2.14: Difference in water surface elevation of traveling upstream and traveling downstream boat lines.

CHAPTER 3 HYDRODYNAMIC MODELING

3.1 1-D FLOW ANALYSIS

A one dimensional flow analysis was necessary in order to determine appropriate boundary conditions for the two dimensional model and to estimate travel time from the gauge location to the study area. The Water Survey Canada gauge from which flow data was obtained is located at the Low Level Bridge, approximately 6.8 kilometres upstream of the beginning of the study area. As the flow and water level fluctuate significantly throughout the day mainly due to upstream hydropower regulation, a one dimensional streamwise model is necessary in order to determine flow and stage information at the study area for the times in question.

Half hourly flow data at the Low Level Bridge was obtained from Alberta Environment Flow Forecasting Unit for the months of October and November 2002. Cross section information from the Low Level Bridge to a point 15.5 km downstream of the study area was also obtained from Alberta Environment River Engineering and Water Monitoring Section in HEC-2 format. Figure 3.1 illustrates the locations of the cross sections obtained.

HEC-RAS, Hydrologic Engineering Center's River Analysis System, was developed at the Hydrologic Engineering Center (HEC) a division of the Institute for Water Resources (IWR) in the U.S. Army Corps of Engineers. HEC-RAS was developed to perform one-dimensional steady and unsteady flow hydraulics. It is software that is available to the public and may be freely downloaded from: http://www.hec.usace.army.mil/default.html. For further information about the theory behind HEC-RAS the reader is instructed to consult the Hydraulic Reference Manual.

3.1.1 Calibration of Model

Observed water surface elevations are necessary in order to calibrate the one-dimensional model. The bed roughness, Manning's n, is the parameter that is calibrated in order to match the computed water surface profile of HEC-RAS to an observed water surface profile.

3.1.1.1 Known Water Surface Elevations for Calibration

From the boat lines chosen in the Section 2.6, the points had to be referenced to the Low Level Bridge in order to compare to the modeled water surface profile. The distance from the Low Level Bridge gauging station to the upstream side of the Gold Bar Pedestrian Bridge is known to be 8537.36 metres from information obtained from Alberta Environment. During the boat survey, the upstream sides of the Gold Bar Pedestrian bridge piers were surveyed. These were taken as the upstream boundary of the bridge at 8537.36 metres. The boat survey data could then be easily referenced to this location. Figure 3.2 shows the final water surface profile for the boat lines chosen. The surveys took place over two days and as such each section was surveyed during different flow rates.

3.1.1.2 Cross Section Data

The cross section information obtained from Alberta Environment was in HEC-2 format and had to be imported into HEC-RAS. HEC-RAS supersedes HEC-2 and consequently there are computational differences between the two programs. There are a few problems associated with importing HEC-2 data into HEC-RAS especially when importing bridge data. Bridge piers in HEC-2 are treated as a single pier so care must be taken to ensure that bridge data is imported properly.

The cross section data obtained, extended upstream from the eastern City Limits at Fort Saskatchewan to the High Level Bridge in central Edmonton. These cross sections were used in a flood risk mapping study and as such were concerned with high flow and stage situations. The geometry file was modified so that the upstream side of the Low Level Bridge was the upstream boundary and the downstream boundary was chosen far enough downstream of the Gold Bar study area so that any boundary condition assumptions did not affect water levels in the study area. The new geometry file extended from station 79.2 to station 45. Initially station 55 was chosen as the downstream boundary, but it was found that water level assumptions at this location affected the Gold Bar study area as shown in Figure 3.3. This prompted the extension of the geometry file to station 45 in order to ensure no affects on the study area would be noticed. A total of 44 cross sections spanned this reach so additional cross-sections were interpolated in order to compute a representative water surface profile. Figure 3.4 illustrates the plan view of the original HEC-RAS geometry file and the final geometry file showing the additional cross sections.

One of the difficulties in importing HEC-2 data is the treatment of bridges as mentioned above. It was suspected that at the low flow rates in question, the head loss at the bridges would be minimal. It was decided to run the uncalibrated model with bridges and without to see if they dramatically affected the water surface profile. Two representative flow rates were chosen to test the omission of the bridges and the difference in water surface elevation between the two profiles for both flow rates were considered to be minimal considering the accuracy at which the water surface was measured as shown in Figure 3.5 and summarized in Table 3.1.

3.1.1.3 Unsteady Flow Profile for Flow Selection

The unsteady flow model was run for October 7 and October 8, 2002 using the uncalibrated model without bridges to get an idea of the travel time from the low level bridge to the study area in order to use the appropriate flow data for the calibration of the

steady state model. The beginning of the study area is approximately 6775 metres downstream of the Low Level Bridge and the end of the study area is approximately 9250 metres downstream of the Low Level Bridge. The travel time was estimated by calculating the time difference between the hydrographs as illustrated in Figure 3.6. It was found that on average the travel time to the beginning of the study area was 2 hours and to the end of the study area, 2.75 hours. Based on this information, the input steady flow was determined by calculating the average flow at the gauge location over the time duration of the boat survey approximately 2 to 2.5 hours earlier than the survey took place.

3.1.1.4 Calibration of Steady State Model

The steady state model was first run with the existing Manning's n values obtained from the flood risk mapping study. Four profiles were necessary as each section of the boat survey was done at a different discharge. It was discovered that the predicted water levels were well below the observed water levels indicating a higher roughness was needed. Several runs were attempted in order to derive a suitable match between the observed and computed water surface profiles. As there were no available observed water surface elevations outside of the study reach, a blanket Manning's n was applied upstream of the study area and downstream of the study area in order to match water levels within the study area. The calibration matched water surface elevations to within ± 5 cm, as shown in Figure 3.7, which was considered adequate given the error in the measurements. Figure 3.8 illustrates the final calibrated bed roughness with the corresponding stations.

3.1.2 Boundary Conditions for Two-Dimensional Model

The calibrated geometry file was used to run an unsteady flow profile for the two dye test days: October 29 and November 7, 2002. The flow hydrograph for both days was input from 0000 to 2330.

The predicted change in water surface elevation over the dye test period was compared to the change in water surface elevation observed at the outfall. HEC-RAS predicted a change in elevation for October 29 at river station 66 of 0.04 metres which matches the change in water surface elevation observed as shown in Table 3.2. However for November 7, HEC-RAS predicted an increase in water surface elevation of 0.05 metres while a decrease of 0.02 metres was observed. This can be explained by the presence of ice on the river on November 7. Border ice was present in the beginning of the day and as the flow increased, the stage increased lifting the border ice off the banks. As the flow was increasing, it was being held back slightly by the border ice and stage was building up. When the border ice finally lifted, it sent a wave surge down the river that traveled faster than the one-dimensional model would have predicted since the ice effects can not be added to HEC-RAS. This means that HEC-RAS is predicting that the flow in the study area is on the raising limb of the hydrograph when in reality it should be in the falling limb because of the wave surge that would have passed through the area quickly.

The calibrated geometry file was also used to run a steady flow profile for boundary conditions for the calibration of the two dimensional model. It was noticed that there was little difference between profiles 1 and 2 and between profiles 3 and 4 during the calibration of the one-dimensional model. Instead of running the two dimensional model with four flow rates and boundary conditions, two flow rates would be adequate. An average of the gauge flows over the entire duration of the first two surveys yielded a flow of 196.29 m^3/s and for the second two surveys a flow of 153.04 m^3/s which corresponded to a water elevation at the downstream boundary of the study area of 610.26 m and 610.51 m respectively.

3.2 TWO DIMENSIONAL HYDRODYNAMIC MODELING

River2D, developed at the University of Alberta, was used to model the study area. It is a depth averaged two-dimensional finite element hydrodynamic model. Details of the formulation of this model may be found in Ghanem et al. (1995). The model has four programs which include R2D_Bed, R2D_Mesh, R2D_Ice and River2D. The modeling procedure is to import surveyed field data into R2D_Bed in order to edit and refine the data into a logical representation of the bed topography. The finalized .bed file is then used in R2D_Mesh to build a mesh and specify boundary conditions for the problem. An input file for River2D is then created in R2D_Mesh and the problem is run in the hydrodynamic program River2D. R2D_Ice is only required if modeling flow under ice cover.

3.2.1 Mesh Program

A computational mesh was designed on top of the bed topography. The basic procedure is to input the final bed topography file into the mesh program. The boundary is first delineated and discretized by adding boundary nodes. Mesh nodes are added to the interior of the modeled region and are triangulated. The mesh nodes take the bed elevation and roughness by interpolating from the underlying bed topography file. The mesh is smoothed after triangulating which adjusts the nodal positions to regularize the triangle shapes. A QI value is displayed (a mesh quality index) which represents the minimum triangle quality of the mesh. An ideal mesh would have a QI of 1.0 which corresponds to equilateral triangles however typical acceptable QI values are in the order of 0.15 to 0.5. The mesh developed should be refined to a point where further mesh refinement produces little change in the simulated results. Typically a fine mesh should be used in regions where simulated water surface elevations are unrealistic, where large topographic changes or lateral boundaries are encountered, and on water edges.

The mesh was created though a number of steps. Initially a boundary node spacing of 13 metres and a uniform node spacing of 13 metres was applied with a

regional node spacing of 5 metres applied around the bridge piers. Further refinement was necessary around the bridge piers and outfall structure in order to achieve an acceptable QI value of 0.2. At this stage approximately 5000 nodes were present.

After the program had converged to within 10%, the bank area was refined using the auto refine option which added a node in the middle of the existing triangle where the depth was less than 0.5 metres. This increased the nodes to 6500. The auto refine command was then used again to refine the mesh everywhere with a positive depth. This increased the nodes to approximately 15000. The banks were then refined three more times and the entire flow area was refined once more. The final mesh, illustrated in Figure 3.9, was completed with a total 63 424 nodes and 126808 elements. The smallest element had sides of approximately 10 cm while the largest element had sides of approximately 7.5 metres.. Figure 3.10 illustrates a close up of the outfall area which shows the strategy of fine refinement along the bank areas and heavy refinement at the outfall where large changes in topography are encountered.

3.2.2 River2D Calibration

The model was calibrated by changing the bed roughness in order to match known water surface elevations. Estimates of bed roughness, k_s, had been made in the field by visual inspection of the bed surface. In general, the roughness was relatively consistent throughout the study reach comprised of primarily quartzite gravels. As a general rule the bed roughness, k_s, can be estimated as 3.5 times the diameter of rock that has 84% of the material finer than this diameter (Montes, 1998). This would suggest that a reasonable range of bed roughness for this reach would be between 0.05 and 0.3. The roughness was kept constant across the channel, but was allowed to vary along the channel.

3.2.2.1 Known Water Surface Elevations for Calibration

Waters edge point were used to calibrate the two dimensional hydrodynamic model. These points were surveyed over October 1-3, 2002 at four different inflow rates: 148.73, 108.56, 174.75, and 158.06 m^3/s. The flow rate was determined by taking an average of the flow at the gauge over the period of the survey shifted two to two and half hours before to account for travel time. The flow over the survey times was generally steady. The calibrated HEC-RAS geometry file was used to run a steady flow profile in order to obtain boundary conditions for October 1-3, 2002. The corresponding outflow elevations are summarized in Table 3.3.

3.2.2.2 Calibration of Water Surface Profile

The roughness was assumed to stay constant regardless of discharge. The effluent inflow rate for all days was relatively consistent so an average effluent flow rate of 3.33 m^3/s was used for all days. Initially the inflow boundary was assumed to be at the top of the outfall structure chute. This created modeling problems because the flow was supercritical at the inflow boundary. In order to alleviate this problem, a deepened pool was introduced just upstream of the top of the chute so that the inflow would be subcritical. In doing so, the hydraulic jump in the outfall chute was modeled, but there was difficulty in achieving a uniform velocity profile. In the end the inflow boundary was designated at the base of the outfall chute, where the flow was subcritical.

Initially a rough calibration was achieved by matching the water surface profile to the downstream boat lines. The calibration was further refined by matching the water surface profile to the waters edge points until a satisfactory match was achieved. A sensitivity analysis was performed on the assumed downstream boundary elevation. In doing so, it was found that the area was heavily backwater affected. The upstream water surface profile was highly correlated with the assumed downstream boundary water surface elevation. The approach was then to calibrate the model by first changing the bed

roughness in order to match the slope of the water surface profile and then increasing the downstream boundary water surface elevation until a match between the measured waters edge values and the modeled profile was reached. As can be seen in Figure 3.11, the modeled results for the four different discharges matched the surveyed values to within ± 5 cm, which is well within the scatter of the measurements. The final calibrated bed roughness values ranged between 0.05 at the downstream boundary to 0.35 at the upstream boundary, as shown in Figure 3.12, which fell within the range of acceptable roughness values based on the field observations. In order to obtain the appropriate downstream boundary water surface elevations for other discharges, a rating curve was developed from the results of the calibration. Figure 3.13 illustrates the determined stage-discharge relationship with a linear relationship between points assumed. The discharge for the dye test days fell within the curve so points were interpolated in order to get the downstream boundary elevations.

3.2.2.3 Velocity Profiles

As a final check, the modeled velocities were compared to the measured velocities taken during the dye tests on October 29 and November 7 at flow rates of 112.95 m^3/s and 148.797 m^3/s respectively. The discharge during the dye test was relatively constant so averaging was considered appropriate. A constant roughness was again assumed for all discharges.

The results of the modeled velocities matched the measured velocities satisfactorily. In general the pattern of the velocity profile was matched, but the model underestimated the velocity with the greatest discrepancy at the waters edge. Possible reasons for this include:

1. Water levels are being modeled too high
2. Discharge is too low
3. The current meter used measures velocities that are too high.

In order to improve the solution the following were adjusted:

1. Keep the same downstream boundary elevation, but increase the discharge. This scenario is unlikely because it suggests that there is a problem with the Water Survey of Canada gauge at the Low Level Bridge, which according to Alberta Environment is one of the best gauges in the region.
2. Increase the number of mesh nodes at the banks.
3. Alter the roughness at the banks. A blanket roughness was initially applied and was not allowed to vary across the channel. It is conceivable that a lower roughness at the banks exists.

The first step of increasing the discharge while keeping the downstream boundary elevation the same produced uncertain results. It seemed to improve the solution in some areas, but deteriorated it in others so overall the improvement was questionable.

It was found that further refinement along the water's edge improved the solution so the mesh was refined to a point where further refinement had little affect on the modeled solution as described in the mesh section above.

The final step was to alter the roughness at the banks in order to improve the solution illustrated in Figure 3.14. The bed roughness values are summarized in Section 5.5. A higher roughness along the south banks from the outfall to a point approximately 100 metres downstream was used. In this region, there were tall weeds that covered the entire flow depth. From this point the roughness was reduced at the south banks to the end of the study reach. Generally, it had been observed that the bed near the banks was very clay like with few rocks or gravels. The majority of the gravels were observed in the main channel. A lower roughness was also used along the north bank from a point approximately 850 metres downstream of the outfall to the end of the study area. In this region the north bank is flattening out as it becomes the inside of a bend and tended to be comprised of more clay than gravels.

Figures 3.15 through 3.20 illustrate the final velocity profiles with a summary of the data in Table 3.4. On average, the profiles matched to within an average absolute error of 23.6 % which is considered adequate considering the error involved in measuring the velocity field.

3.2.2.4 Velocity Field and Cumulative Discharge Distribution Observations

Some interesting results came from the modeled velocity field and cumulative discharge distributions which can be extracted from the River2D model. The cumulative discharge represents the discharge that passes between the bank and some point out from the bank where q = 0 at the right bank and q = Q at the left bank. Figure 3.21 displays the modeled velocity field from October 29 in the vicinity of the outfall with the cumulative discharge between 0 and 3.33 m^3/s displayed which is the magnitude of effluent flow. Right beside the outfall walls circulation zones exist and the top of the rip rap blanket is exposed. Approximately one third of the effluent flow turns downstream with a portion of this turning around becoming trapped behind the exposed rip rap in a relatively stagnant area. The remaining two thirds of the effluent flow hits the rip rap slope and is redirected upstream around the exposed rip rap before turning and moving downstream. Figure 3.22 displays the modeled velocity field from November 7 in the vicinity of the outfall with the cumulative discharge between 0 and 3.33 m^3/s. A different flow pattern is noticed in this case as the total inflow is much higher, approximately 152 m^3/s compared to 116 m^3/s from October 29. The circulation zones beside the outfall walls are still present and the rip rap still remains exposed, although it is more submerged than it was on October 29. About 30% more of the effluent flow is being directed downstream which is due to the higher ambient velocity of the river water. It is more difficult for the effluent outflow to overcome the ambient velocity with the higher discharge so less of the effluent flow is being directed upstream by the rip rap slope. The effluent flow is still turning around becoming trapped in a circulation zone behind the exposed rip rap.

In order to examine the flow patterns at the outfall a lower discharge of 90 m^3/s and higher discharge of 300 m^3/s were run assuming a constant effluent flow of 3.33 m^3/s. At the lower discharge, shown in Figure 3.23, about 25% of the effluent flow is directed downstream while 75% of the effluent flow is directed upstream. The effluent flow reaches farther upstream than the flow of October 29 as it has a greater ability to overcome the ambient velocity. More of the rip rap is exposed and the zone behind the rip rap is more stagnant. Conversely with the higher discharge shown in Figure 3.24, none of the rip rap is exposed and all of the effluent flow is directed immediately downstream out of the outfall structure. In both cases, circulation zones still exist beside the outfall structure walls.

Another interesting location for velocity field exists at the alluvial deposit described above. Figure 3.25 illustrates the velocity field with the cumulative discharge between 0 and 25 m^3/s for October 29 at a flow rate of 116.29 m^3/s. The flow tightens just before the bridge piers, then hits the alluvial deposit and is directed around it. There is a circulation zone at the top of the deposit. The flow then continues and expands as it travels downstream. Part of the gravel remains exposed at this low flow which is where the river bed had a very mild slope and a tendency for gravel bars to occur. This location is an excellent one for mixing as a great amount of turbulence and eddies to form and hence a good mixing location. Figure 3.26 illustrates the velocity field at the same location for November 7. A very similar pattern is observed for both days; however none of the gravel remains exposed on November 7.

From the final hydrodynamic model, the cumulative discharge can be computed and the distribution examined. For illustration purposes, the cumulative discharge is plotted between 0 and 25 m^3/s for November 7 in Figure 3.27. The cumulative discharge expands slightly over the first 100 metres or so downstream of the outfall structure. From this point to a point a few hundred metres upstream of the pedestrian bridge the cumulative discharge stays relatively constant. Through this section it is noticed that 16.5% of the flow covers about 1/3 of the river width. The majority of the flow is carried by the north side of the channel. This is the section where the south bank remains quite

shallow with a mild slope. From this point there is a contraction in the cumulative discharge distribution before hitting the alluvial deposit. The flow curves around the deposit and expands to cover just about half the flow width. At this point 16.5% of the flow is being carried by half the river width. Again this location it is quite shallow at the south bank as discussed above with a lot of gravel bars. The flow then tightens up as it heads into the bend where the south bank deepens at the outside of the bend. The October 29 cumulative discharge distribution exhibits similar patterns indicating that the overall flow pattern does not change significantly with discharge, at least for relatively low flows.

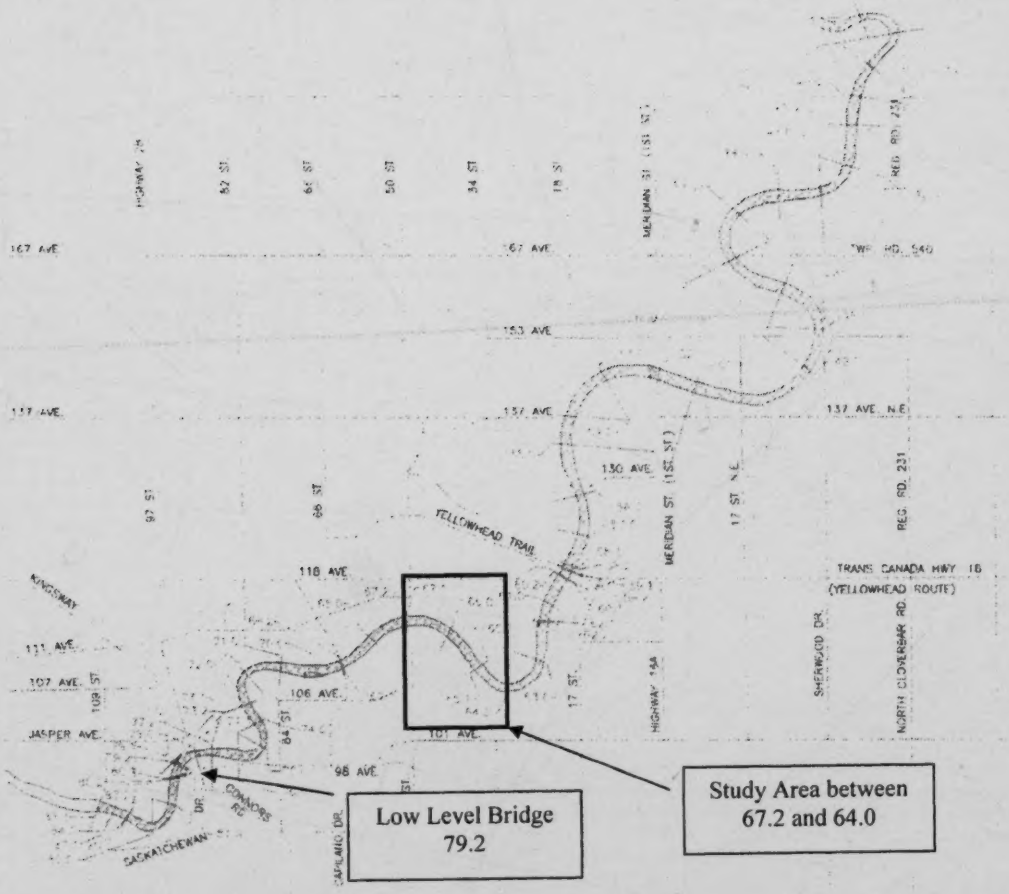

Figure 3.1 Map of cross section locations obtained from Alberta Environment.

Adapted from figure obtained from North Saskatchewan River at Edmonton Flood Risk Mapping Study submitted to Alberta Environmental Protection by Philips Planning & Engineering Limited.

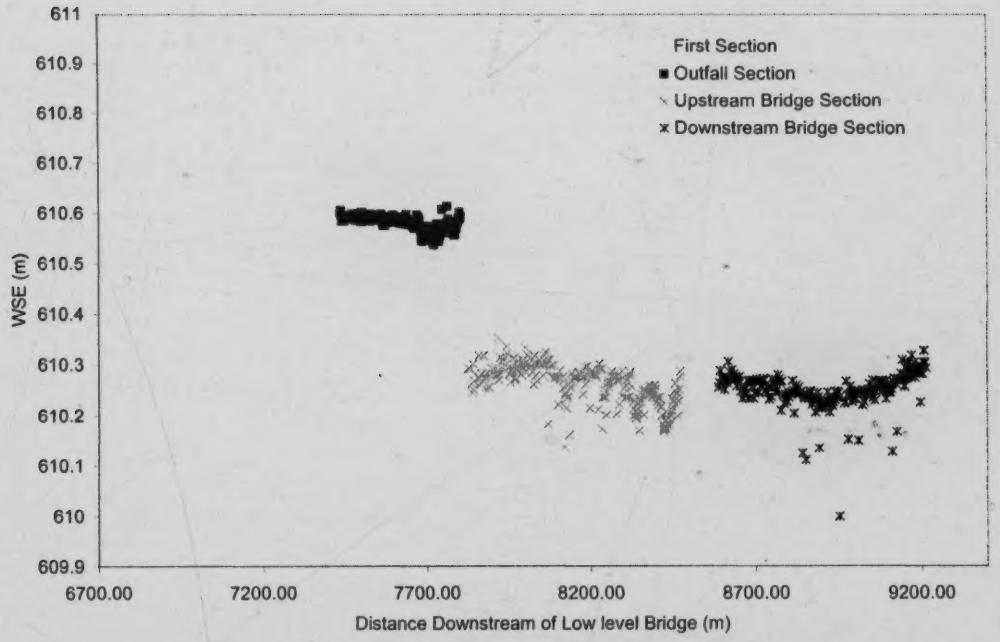

Figure 3.2: Water surface elevations used for calibration of HEC-RAS.

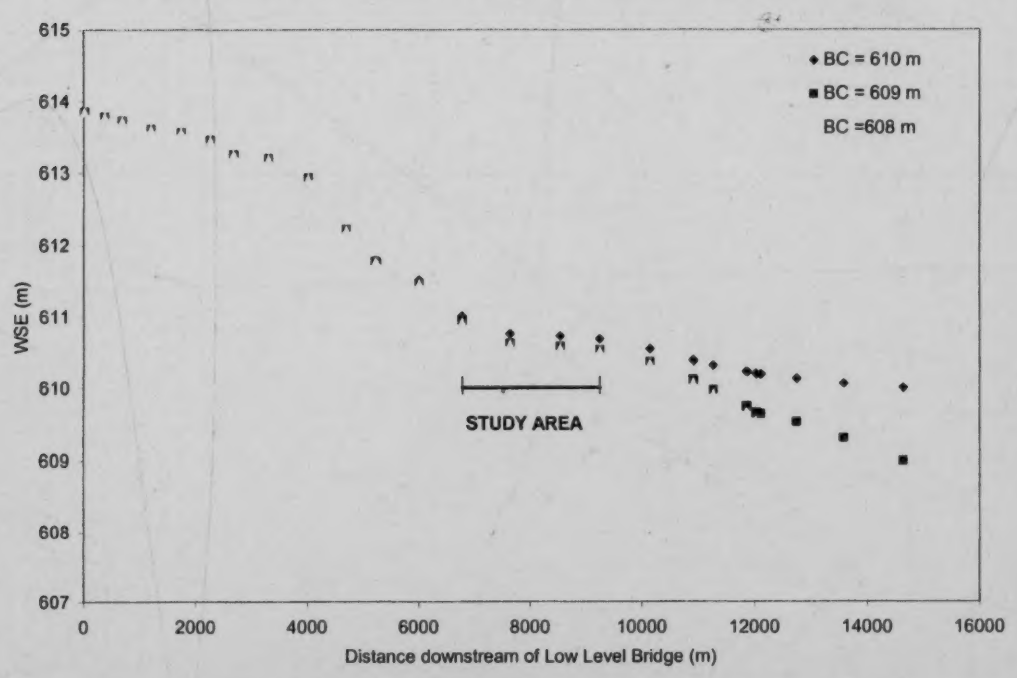

Figure 3.3: Effect of boundary conditions on study area when reach extended to station 55.

(a)

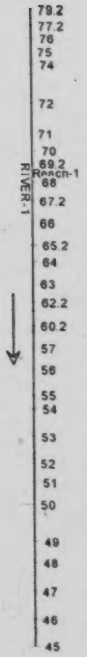

(b)

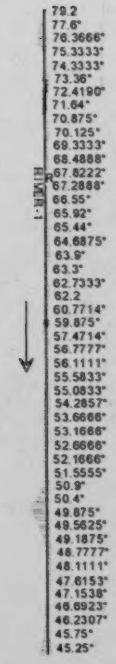

Figure 3.4: Original (a) and final (b) HEC-RAS plan of cross sections in geometry file.

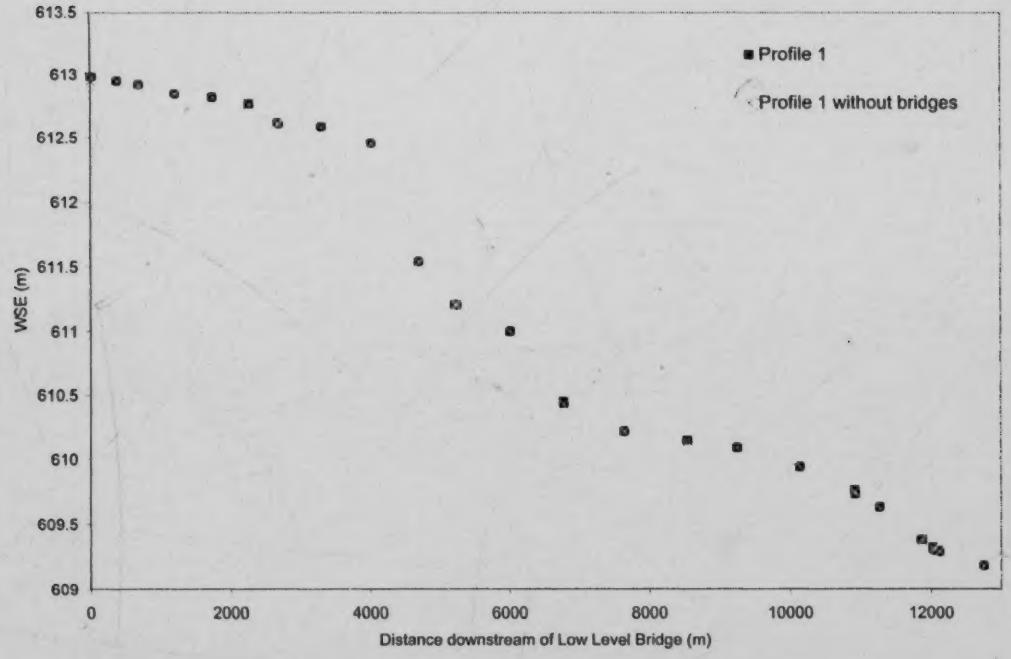

Figure 3.5: Effect of bridge piers on water surface profile in HEC-RAS.

Table 3.1: Comparison of the effect of including bridge piers on water surface profiles in HEC-RAS.

River Station	Thalweg (m)	Distance from Low Level Bridge (m)	Water Surface Elevation (m)	Water Surface Elevation no bridges (m)	Difference in elevation (m)
79.2	610.46	0	612.98	612.95	0.03
79.14999		0.1	Bridge		
79.1	609.65	21.76	612.98	612.98	0
78	607.61	378.8	612.95	612.95	0
77.2	608.95	687.04	612.92	612.92	0
77.14999		687.14	Bridge		
77.1	608.95	691.91	612.92	612.91	0.01
76	609.77	1206.23	612.85	612.85	0
75	607.03	1744.35	612.82	612.82	0
74	610.37	2266.83	612.77	612.76	0.01
73.2	610.45	2678.31	612.62	612.62	0
73.14999		2678.41	Bridge		
73.1	610.25	2691.05	612.61	612.61	0
72	606.16	3304	612.59	612.59	0
71	610.66	4017.2	612.46	612.46	0
70	609.84	4698.34	611.54	611.54	0
69.2	608.8	5218.33	611.21	611.21	0
69.14999		5218.43	Bridge		
69.1	608.76	5247.8	611.21	611.21	0
68	608.51	6009.75	611	611	0
67.2	608.84	6774.82	610.45	610.43	0.02
67.14999		6774.92	Bridge		
67.1	608.6	6779.69	610.44	610.43	0.01
66	606.96	7641.36	610.22	610.22	0
65.2	607.22	8537.36	610.15	610.14	0.01
65.14999		8537.46	Bridge		
65.1	607.44	8542.22	610.15	610.14	0.01
64	605.63	9247.8	610.09	610.09	0
63	606.85	10143.4	609.94	609.94	0
62.2	606.82	10914.8	609.76	609.75	0.01
62.15		10914.9	Bridge		
62.1	607.46	10920.48	609.73	609.73	0
61	607.57	11265.85	609.63	609.63	0
60.2	607.68	11858.74	609.38	609.38	0
60.15		11858.84	Bridge		
60.1	607.5	11878.09	609.38	609.37	0.01
59.2	607.36	12025.7	609.32	609.31	0.01
59.15		12025.8	Bridge		
59.1	607.26	12036.69	609.3	609.3	0
58.2	606.7	12111.06	609.29	609.29	0
58.15		12111.16	Bridge		
58.1	607.08	12116.7	609.29	609.29	0
57	607.06	12750.71	609.18	609.18	0
56	606.45	13584.14	608.99	608.99	0
55	606.77	14638.82	607.85	607.85	0

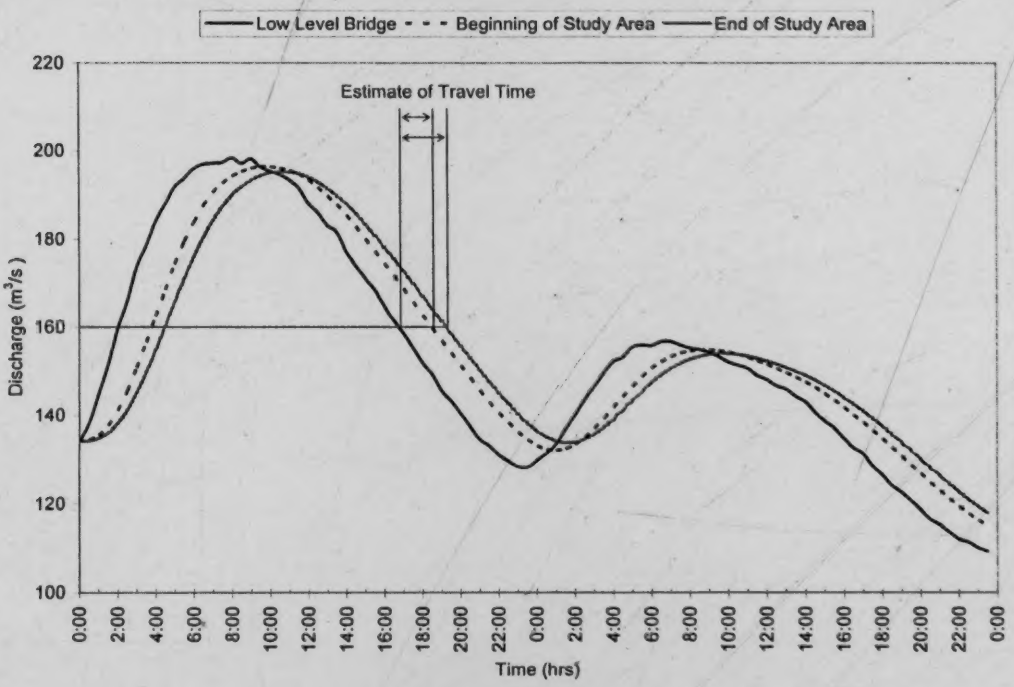

Figure 3.6: Travel time from low level bridge to study area based on unsteady flow hydrographs.

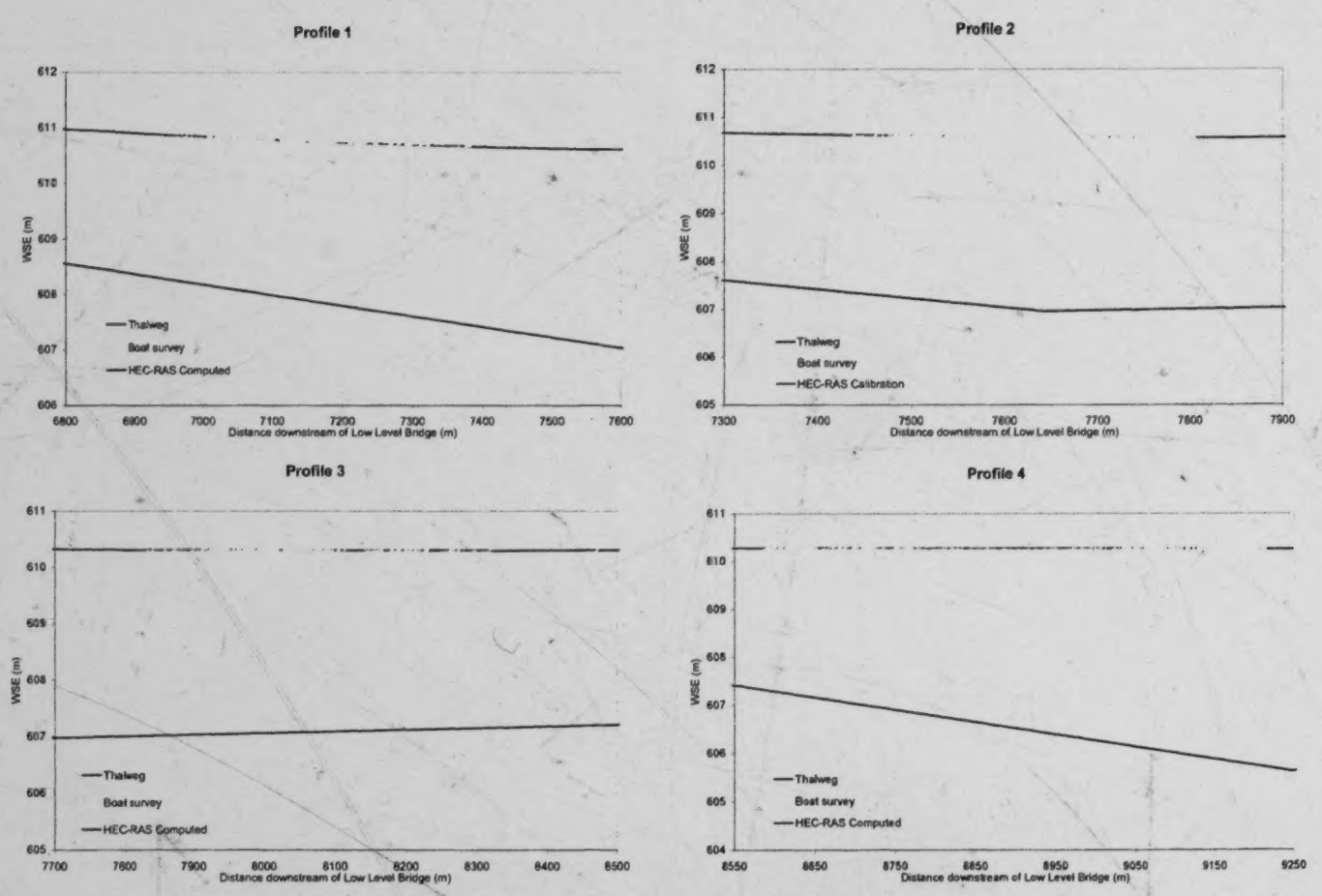

Figure 3.7: Final HEC-RAS calibration water surface profiles.

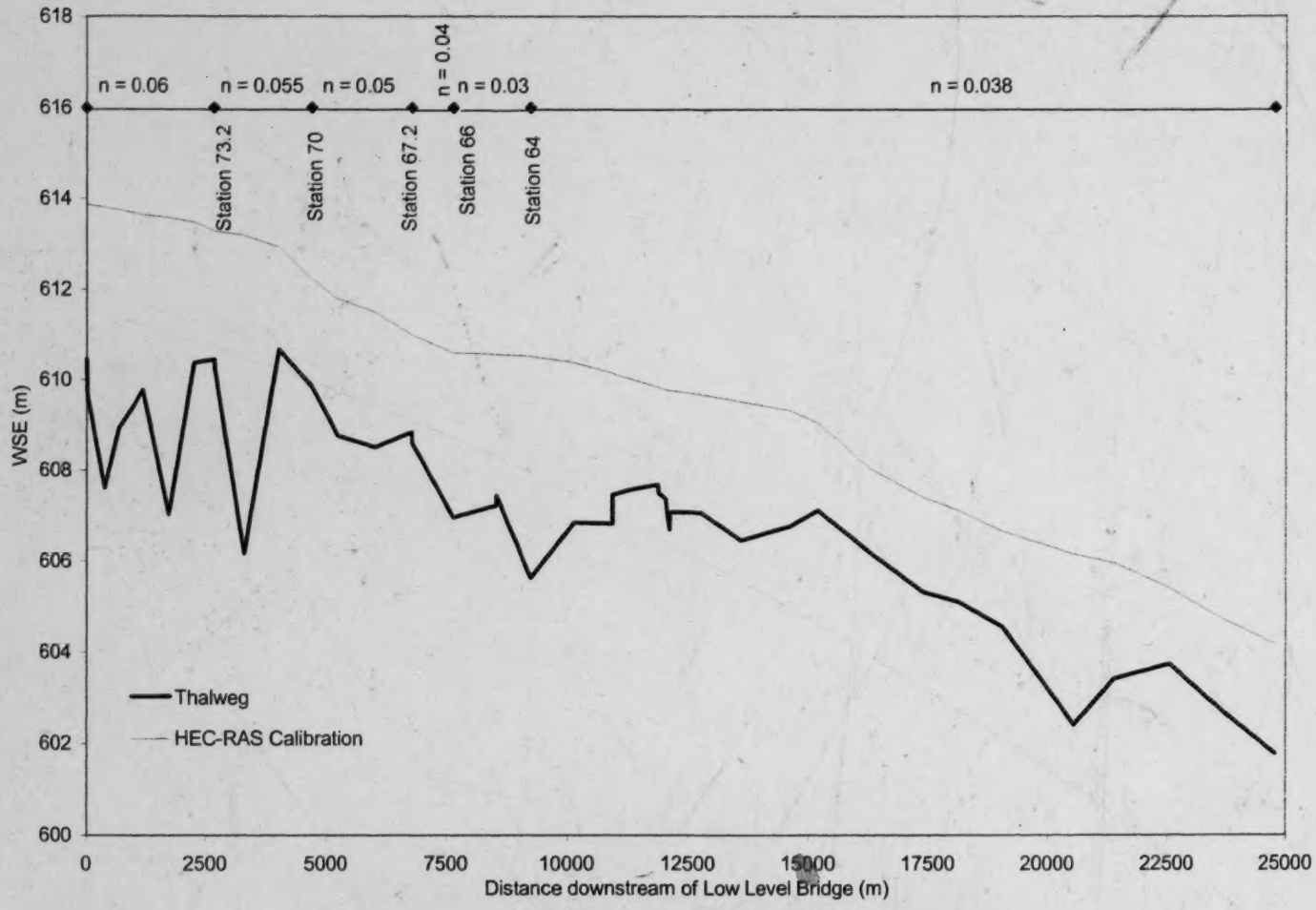

Figure 3.8: Bed roughness from final HEC-RAS calibration.

Table 3.2: Comparison of observed change in water surface elevations to computed change in water surface elevations for dye test days.

Date	RS: 66 Stage (m)	Monitor Stage (m)	Date	RS: 66 Stage (m)	Monitor Stage (m)
29/10/2002 13:30	610.02	3.97	07Nov2002 1310	610.22	4.56
29/10/2002 14:00	610.01	3.97	07Nov2002 1340	610.24	4.56
29/10/2002 14:30	610.01	3.955	07Nov2002 1410	610.25	4.56
29/10/2002 15:00	610	3.95	07Nov2002 1440	610.26	4.56
29/10/2002 15:30	610	3.94	07Nov2002 1520	610.27	4.55
29/10/2002 16:00	609.99	3.94	07Nov2002 1600	610.27	4.55
29/10/2002 16:30	609.98	3.935	07Nov2002 1630	610.27	4.54
Change	**- 0.04**	**- 0.035**	**Change**	**0.05**	**- 0.02**

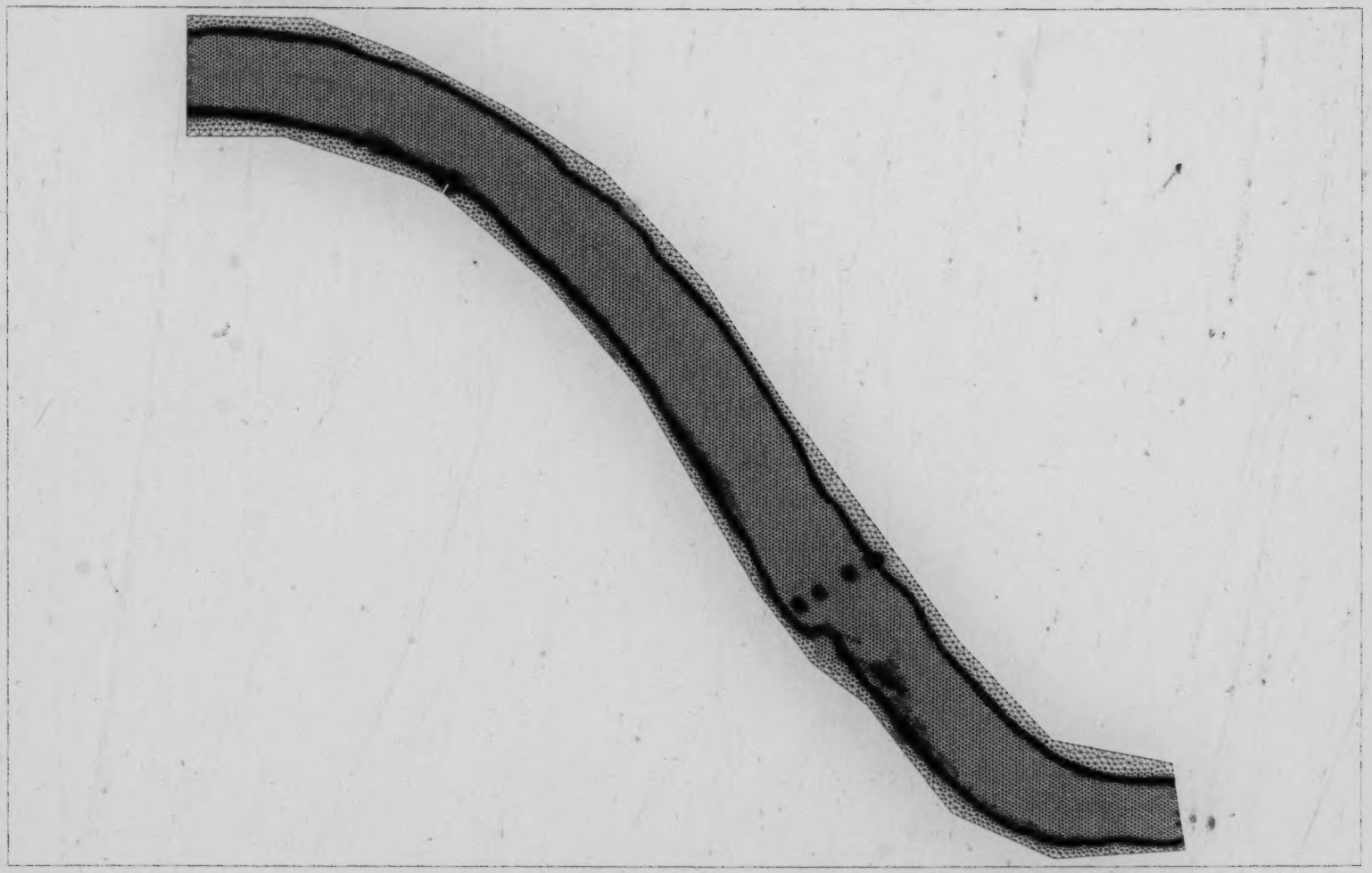

Figure 3.9: Final computational mesh generated in River2D.

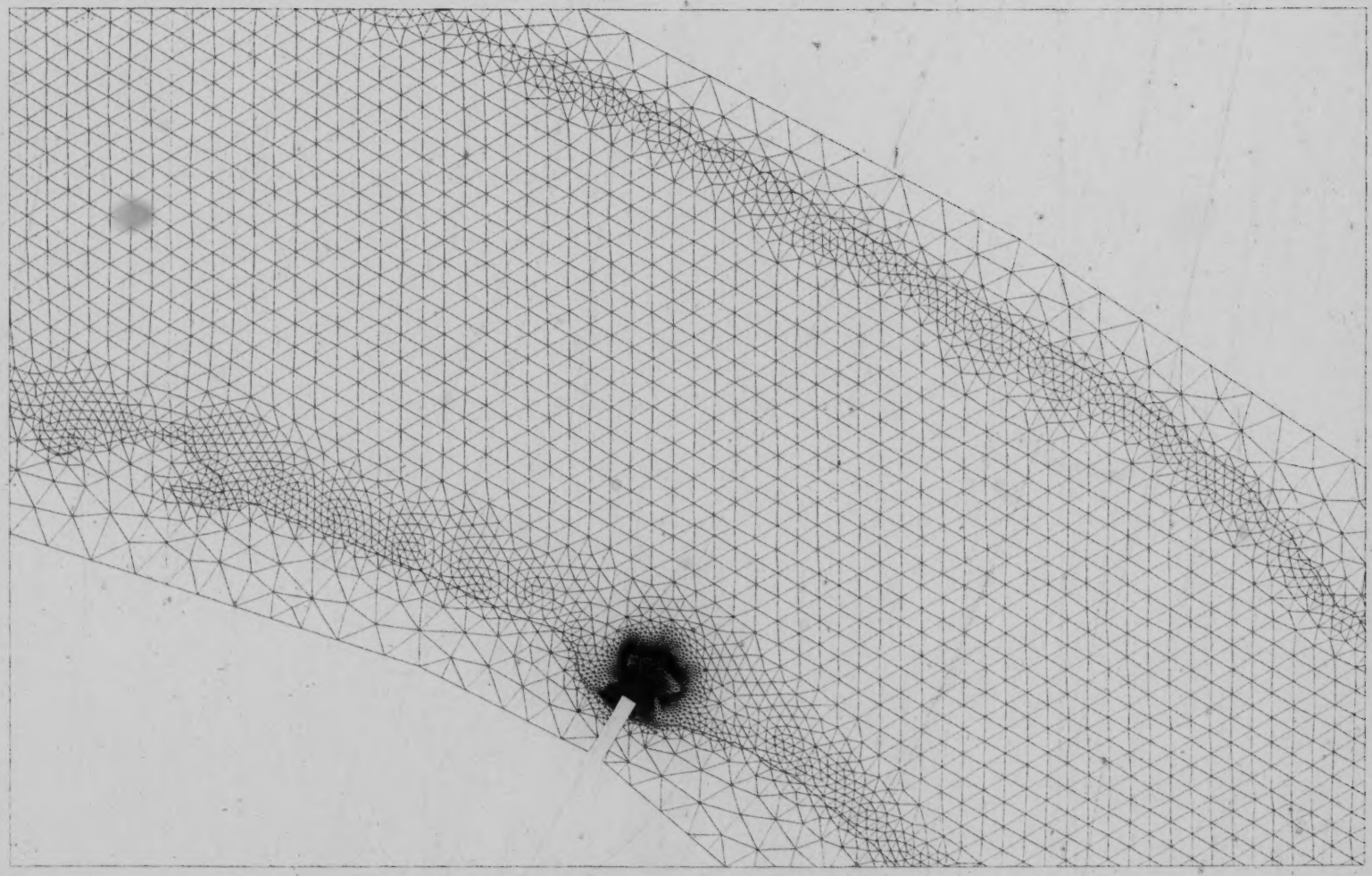

Figure 3.10: Close up of final mesh at outfall structure.

Table 3.3: Boundary conditions for waters edge calibration estimated from HEC-RAS.

Date	Discharge (m^3/s)	Downstream Water Surface Elevation from HEC-RAS (m)
October 1, 2002	148.73	610.23
October 2, 2002	108.56	609.93
October 3, 2002-AM	174.75	610.39
October 3, 2002-PM	158.06	610.3

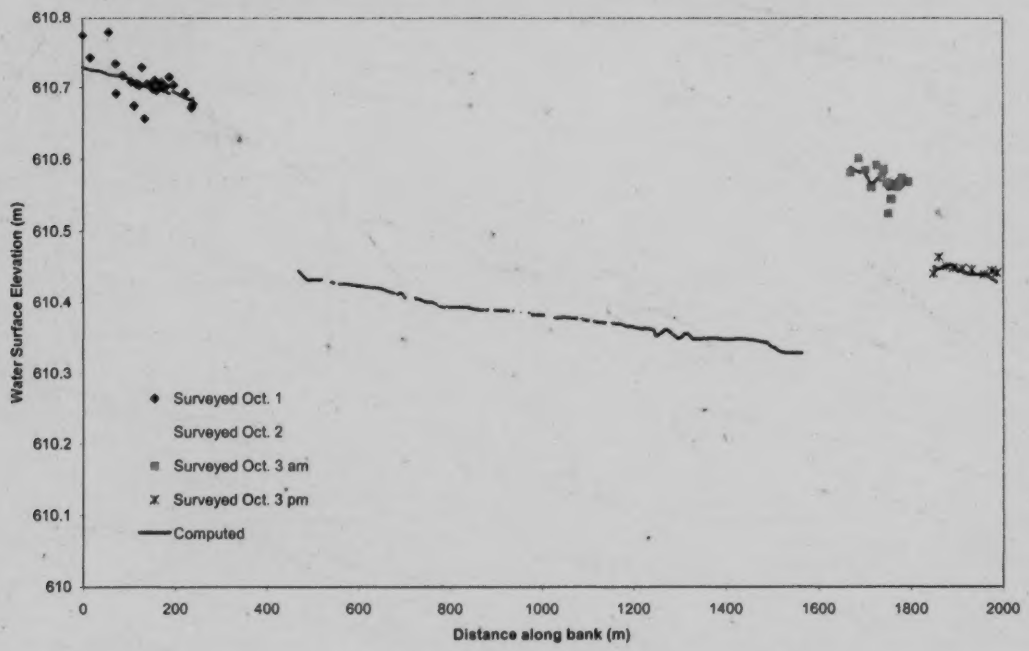

Figure 3.11: Final calibrated water surface profile in River2D.

Figure 3.12: Bed roughness from water surface calibration.

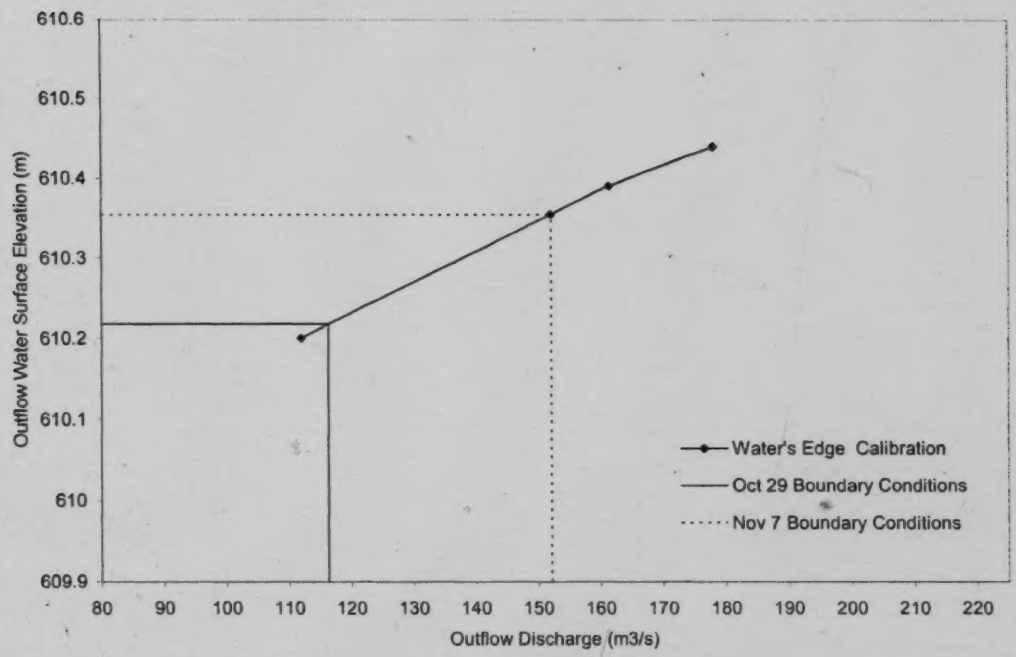

Figure 3.13: Stage discharge curve for outflow boundary of study area developed from water surface calibration.

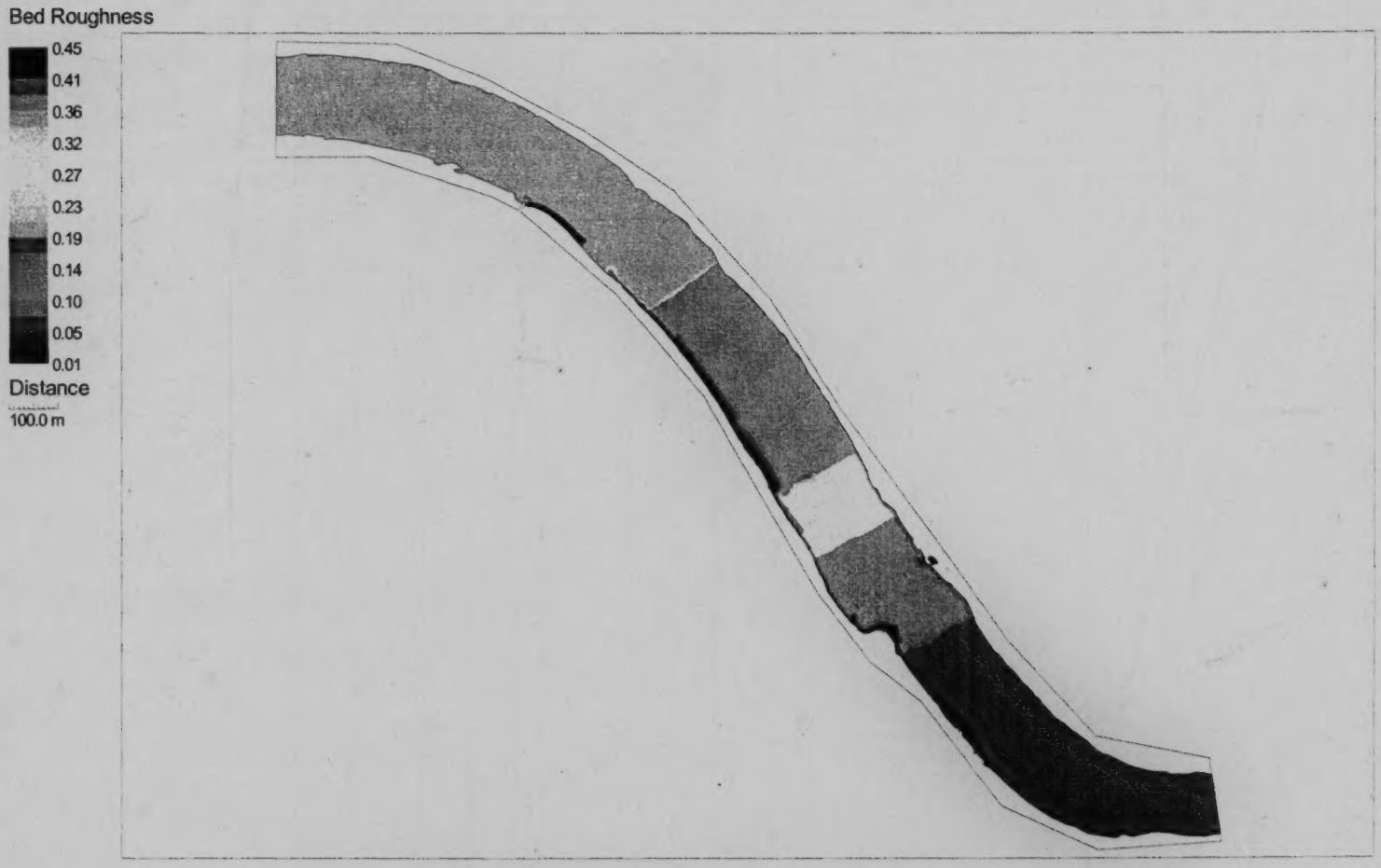

Figure 3.14: Final bed roughness from velocity calibration of River2D.

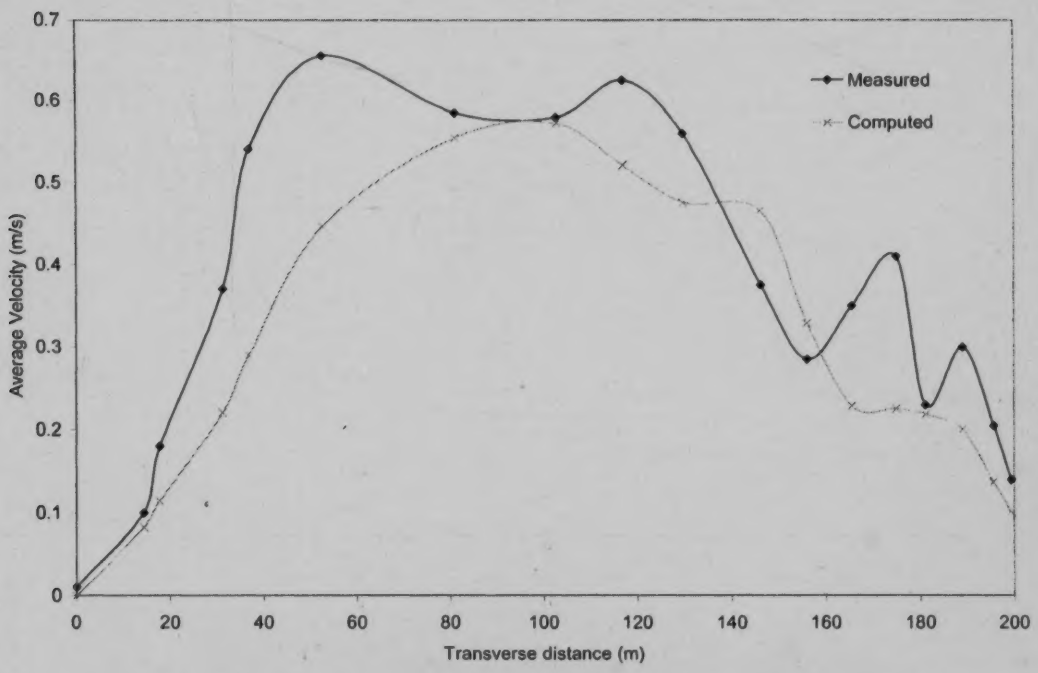

Figure 3.15: Velocity comparison October 29, 2002 at Station -30.

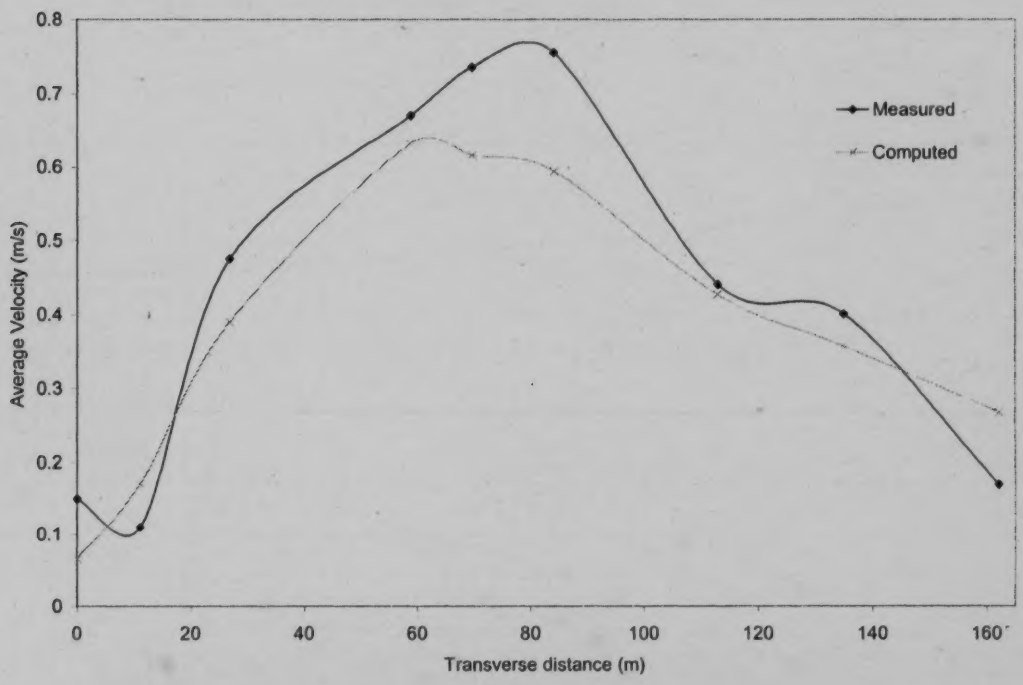

Figure 3.16: Velocity comparison November 7, 2002 at Station 80.

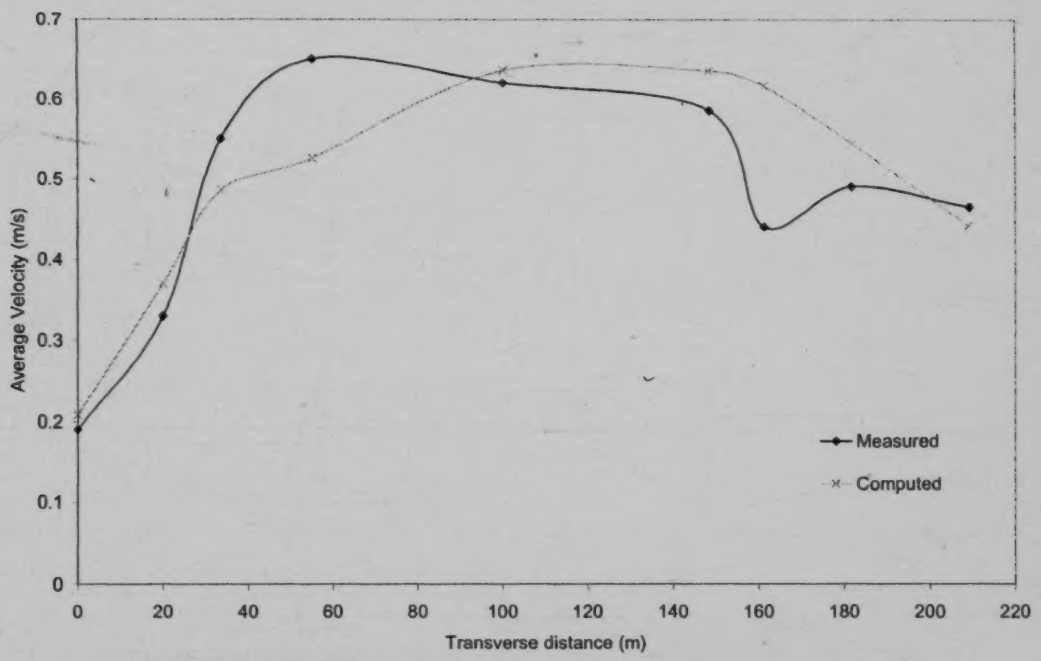

Figure 3.17: Velocity comparison November 7, 2002 at Station 320.

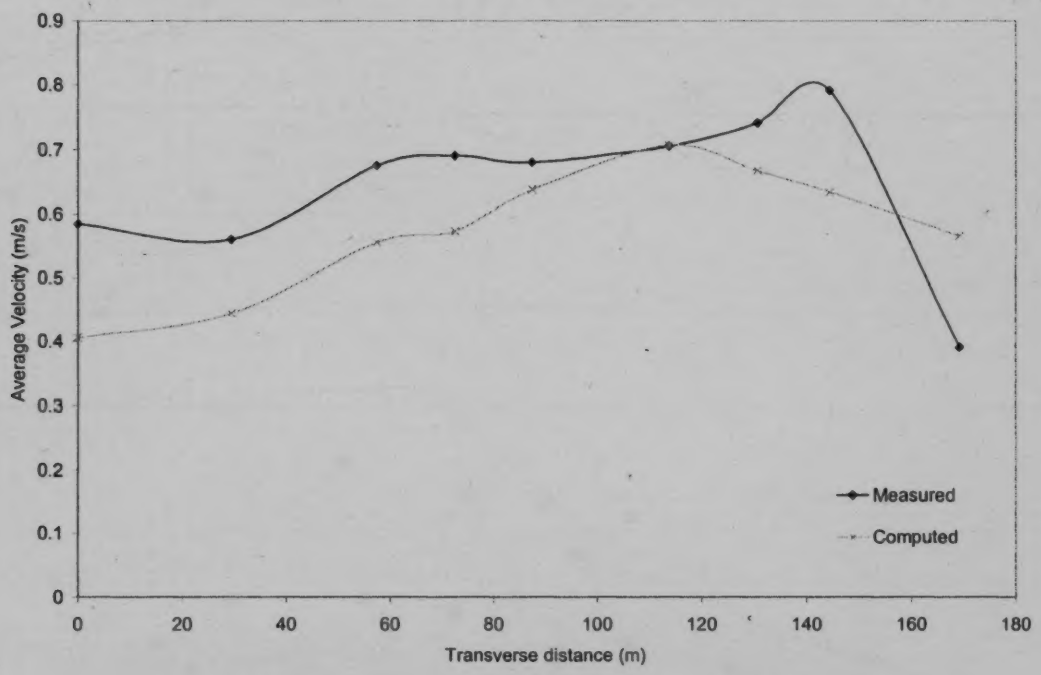

Figure 3.18: Velocity comparison November 7, 2002 at Station 1000.

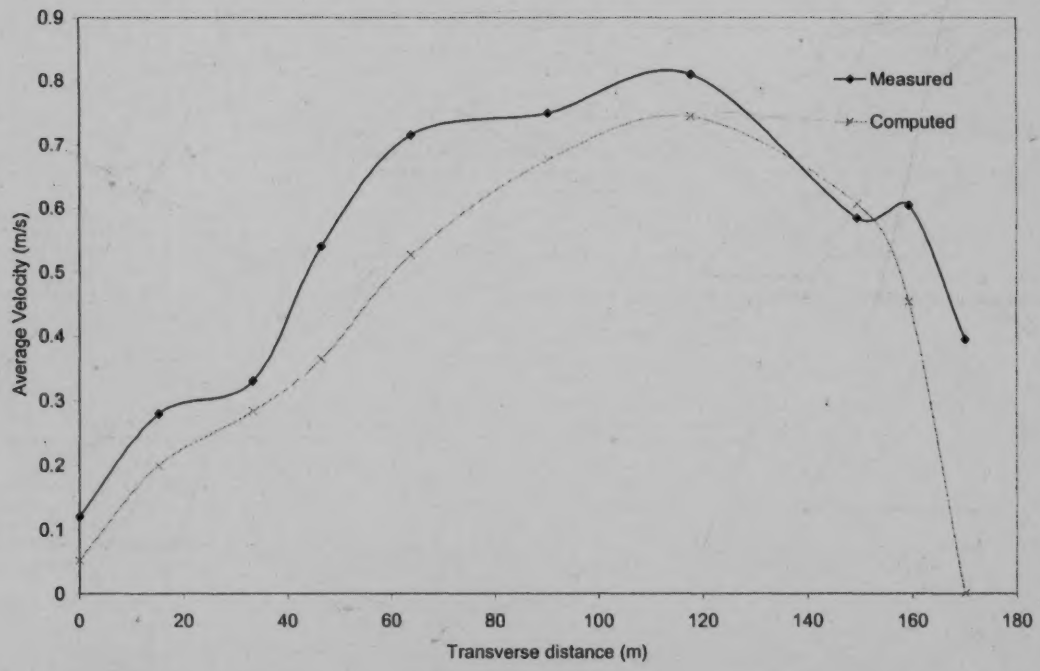

Figure 3.19: Velocity comparison November 7, 2002 at Station 1500.

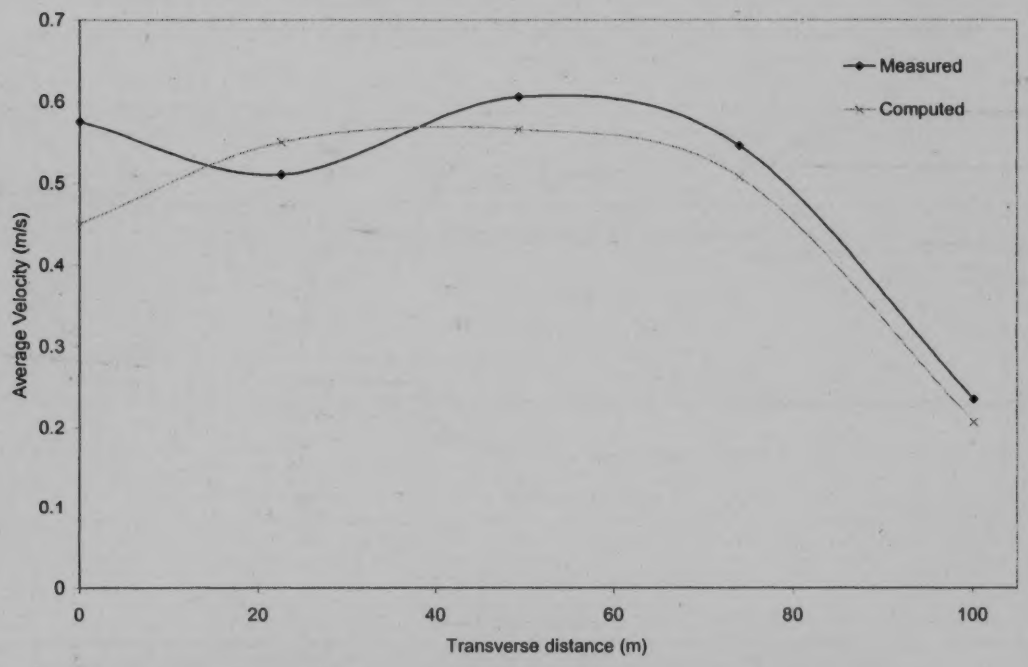

Figure 3.20: Velocity comparison November 7, 2002 at Station End.

Table 3.4: Summary of final velocity comparisons.

POINT ID	East	North	Transverse Distance (m)	Average Velocity (m/s)	Modeled Velocity (m/s)	Difference
V-30-1	340348.584	5937469.069	0.000	0.01	0	-100%
V-30-2	340356.757	5937480.840	14.331	0.1	0.0826	-17%
V-30-18	340357.873	5937484.120	17.796	0.18	0.1146	-36%
V-30-3	340370.156	5937489.682	31.279	0.37	0.22	-41%
V-30-4	340374.945	5937492.615	36.895	0.54	0.29	-46%
V-30-5	340371.415	5937507.855	52.539	0.655	0.4455	-32%
V-30-6	340399.891	5937506.219	81.061	0.585	0.5547	-5%
V-30-7	340384.634	5937521.652	102.763	0.58	0.5724	-1%
V-30-8	340386.991	5937535.708	117.015	0.625	0.5205	-17%
V-30-9	340393.246	5937546.803	129.751	0.56	0.4758	-15%
V-30-10	340407.364	5937555.282	146.220	0.375	0.4652	24%
V-30-11	340409.747	5937564.820	156.050	0.285	0.3293	16%
V-30-12	340410.354	5937574.291	165.541	0.35	0.229	-35%
V-30-13	340410.442	5937583.696	174.946	0.41	0.2253	-45%
V-30-14	340416.498	5937584.896	181.120	0.23	0.2194	-5%
V-30-15	340420.915	5937591.397	188.979	0.3	0.2003	-33%
V-30-16	340423.177	5937597.696	195.673	0.205	0.1368	-33%
V-30-17	340425.975	5937600.071	199.342	0.14	0.1015	-28%
Average Absolute Error for Section						**29%**
V80-1	340542.839	5937525.069	162.032	0.17	0.2682	58%
V80-2	340542.985	5937497.854	134.817	0.4	0.3572	-11%
V80-3	340527.728	5937482.166	112.933	0.44	0.4258	-3%
V80-04	340510.992	5937458.642	84.063	0.755	0.5945	-21%
V80-05	340498.411	5937451.624	69.657	0.735	0.6161	-16%
V80-07	340489.647	5937445.211	58.797	0.67	0.6321	-6%
V80-08	340461.898	5937429.269	26.795	0.475	0.3895	-18%
V80-09	340450.694	5937418.284	11.104	0.11	0.1703	55%
V80-10	340447.659	5937407.603	0.000	0.15	0.0659	-56%
Average Absolute Error for Section						**27%**
V320-01	340612.025	5937239.163	0.000	0.19	0.2086	10%
V320-02	340627.067	5937252.378	20.022	0.33	0.3702	12%
V320-03	340637.503	5937261.101	33.624	0.55	0.4865	-12%
V320-04	340655.251	5937273.193	55.099	0.65	0.5265	-19%
V320-05	340698.832	5937261.989	100.097	0.62	0.636	3%
V320-06	340684.712	5937308.250	148.465	0.585	0.6354	9%
V320-07	340692.381	5937318.482	161.252	0.44	0.6163	40%
V320-8	340705.711	5937333.835	181.584	0.49	0.5448	11%
V320-09	340718.488	5937358.187	209.085	0.465	0.4418	-5%
Average Absolute Error for Section						**13%**
V1000-2	341029.942	5936652.018	0.000	0.585	0.4057	-31%
V1000-3	341050.343	5936673.202	29.410	0.56	0.4439	-21%
V1000-4	341076.112	5936684.242	57.444	0.675	0.5564	-18%
V1000-5	341088.028	5936693.433	72.493	0.69	0.5741	-17%
V1000-6	341100.736	5936701.147	87.359	0.68	0.6382	-6%
V1000-7	341121.930	5936716.821	113.719	0.705	0.7067	0%
V1000-8	341134.725	5936727.802	130.581	0.74	0.6667	-10%
V1000-9	341146.250	5936735.228	144.290	0.79	0.6345	-20%
V1000-10	341169.252	5936744.703	169.167	0.39	0.5655	45%
Average Absolute Error for Section						**19%**

POINT ID	East	North	Transverse Distance (m)	Average Velocity (m/s)	Modeled Velocity (m/s)	Difference
V1500-1	341335.822	5936303.104	0.000	0.12	0.0527	-56%
V1500-2	341347.033	5936313.314	15.164	0.28	0.2003	-28%
V1500-3	341361.672	5936324.114	33.355	0.33	0.2837	-14%
V1500-4	341373.060	5936330.706	46.514	0.54	0.3636	-33%
V1500-5	341385.866	5936342.422	63.870	0.715	0.5272	-26%
V1500-6	341409.471	5936354.163	90.235	0.75	0.6768	-10%
V1500-7	341433.221	5936368.078	117.760	0.81	0.7448	-8%
V1500-8	341452.875	5936392.847	149.379	0.585	0.6076	4%
V1500-9	341454.074	5936402.707	159.313	0.605	0.4538	-25%
V1500-10	341456.274	5936413.226	170.060	0.395	0	-100%
Average Absolute Error for Section						**30%**
VE-1	341681.066	5936184.986	0.000	0.575	0.4501	-22%
VE-2	341682.318	5936207.546	22.594	0.51	0.5496	8%
VE-3	341686.737	5936233.891	49.307	0.605	0.5653	-7%
VE-4	341689.547	5936258.449	74.025	0.545	0.5075	-7%
VE-5	341688.209	5936284.526	100.136	0.235	0.2071	-12%
Average Absolute Error for Section						**11%**
Overall average absolute error						**23.6%**

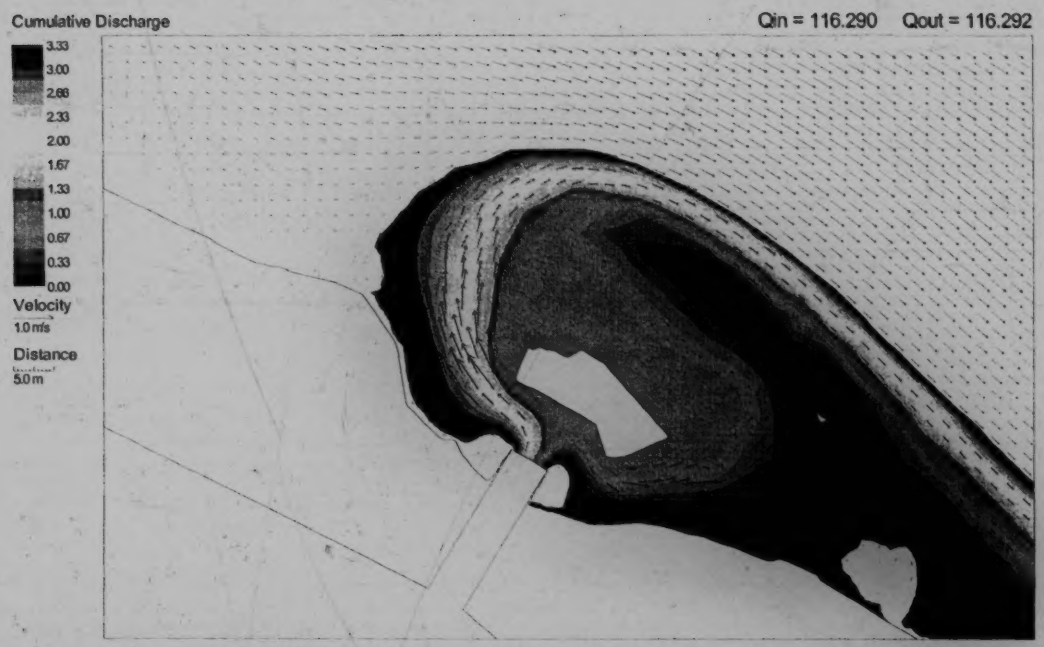

Figure 3.21: Close up of velocity field at outfall structure October 29, 2002.

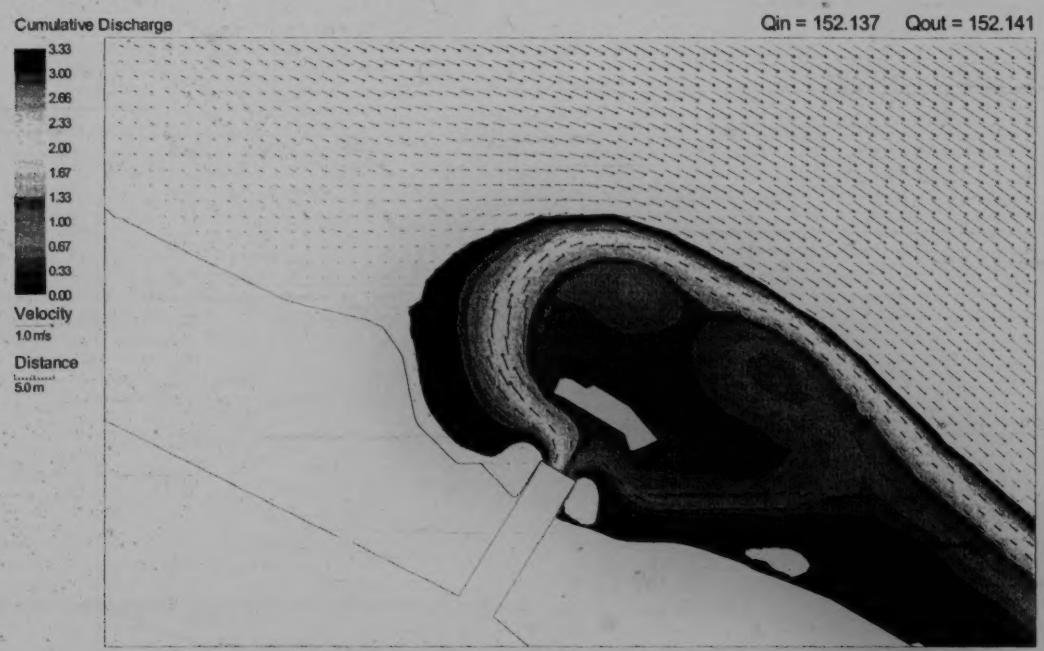

Figure 3.22: Close up of velocity field at outfall structure November 7, 2002.

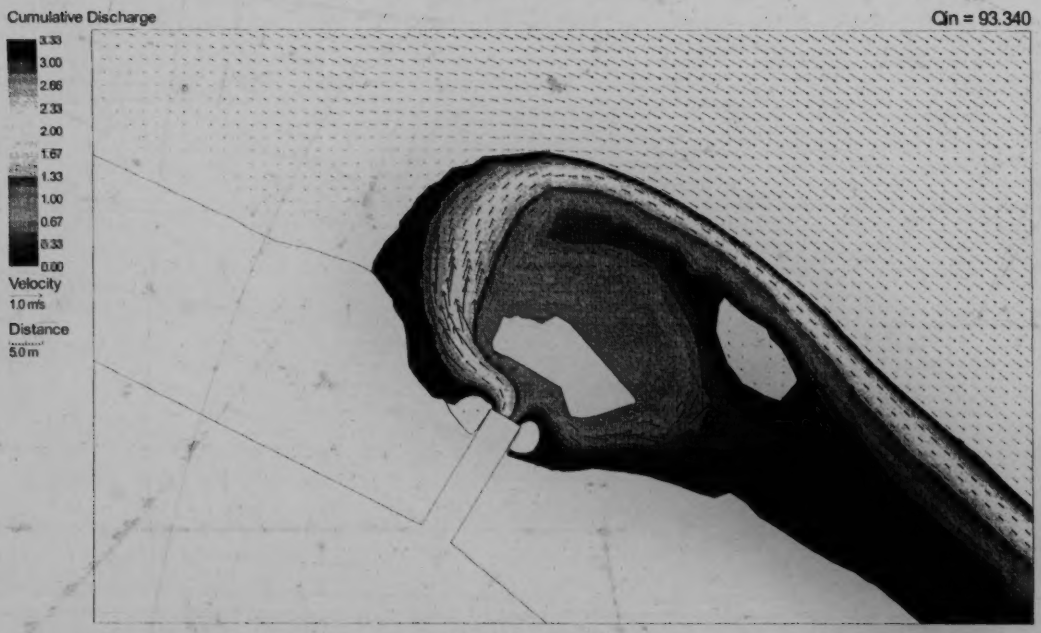

Figure 3.23: Close up of velocity field at outfall for a discharge of 90 m^3/s.

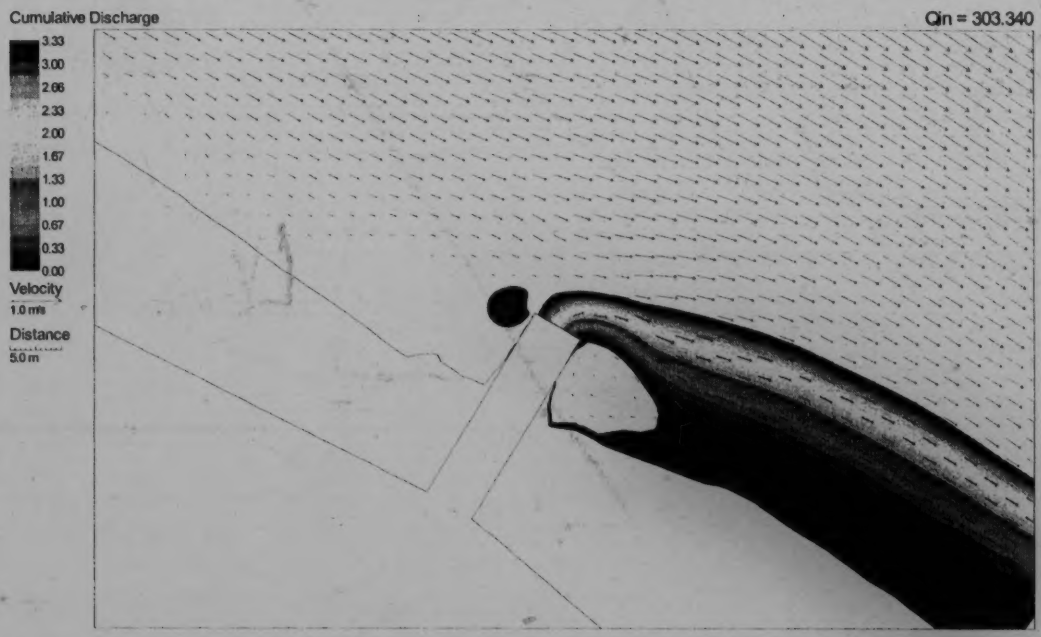

Figure 3.24: Close up of velocity field at outfall for a discharge of 300 m^3/s.

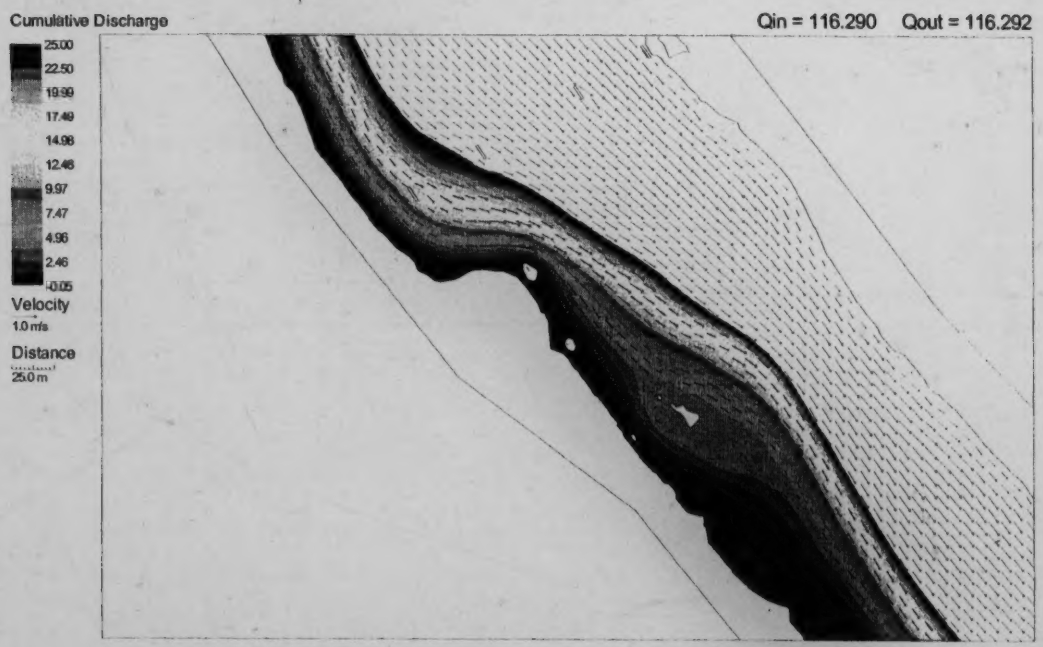

Figure 3.25: Velocity field at alluvial deposit October 29, 2002.

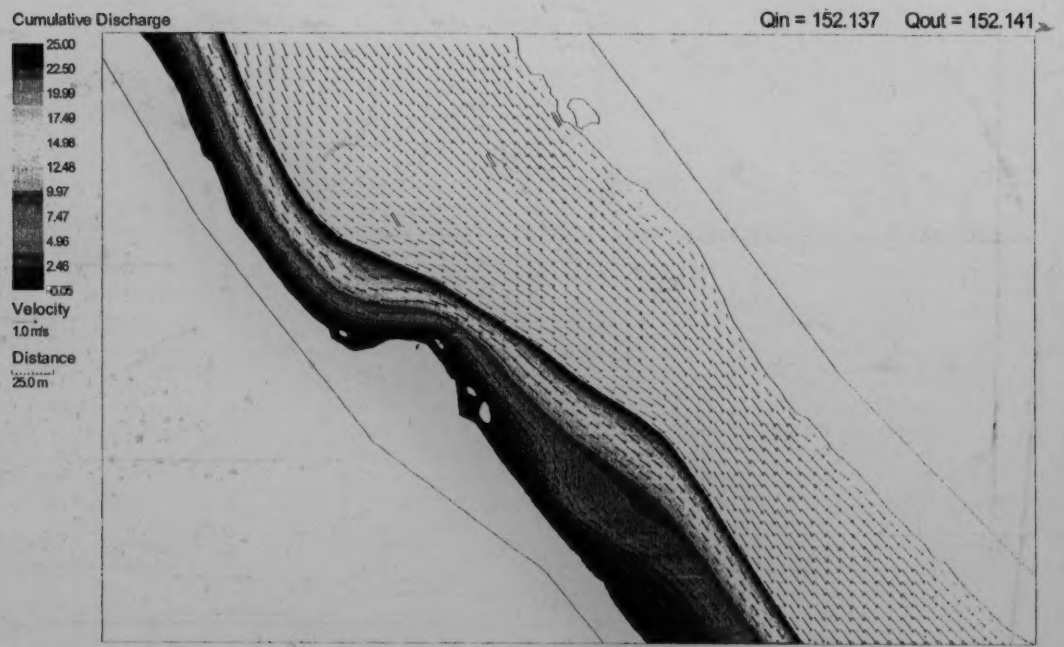

Figure 3.26: Velocity field at alluvial deposit November 7, 2002.

Figure 3.27: Cumulative discharge distribution November 7, 2002.

CHAPTER 4 BACKGROUND INFORMATION FOR MIXING STUDY

4.1 RIVER MIXING THEORY

4.1.1 Physical Processes

There are a number of dominant physical processes in river mixing of which some are more important than others are depending on what area of the river is of interest. Advection, molecular diffusion, turbulent diffusion, dispersion, secondary circulation, and non-neutral substances all play a role in the mixing of a river.

Advection involves the movement of a substance by action of the river current. The direction of transport is the same direction as that of the current and the amount of material that is transported can be expressed as the product of the velocity and concentration (Elhadi et al., 1984),

$$T_{ad} = UC \qquad 4.1$$

where T_{ad} = advective transport per unit area per unit time, U = velocity perpendicular to the unit area, and C = Concentration of the substance transported.

Molecular diffusion involves the spreading of molecules from areas of higher concentration to areas of lower concentration. It is due to the motion of the molecules and can be described by Fick's law of diffusion from Fischer (1979) as:

$$T_m = -D_m \frac{\partial C}{\partial \mathrm{n}} \qquad 4.2$$

in which T_m = transport by molecular diffusion per unit area per unit time, n = direction perpendicular to the unit area and D_m = coefficient of molecular diffusion. D_m is a property of the solvent and solute and is therefore a constant. It is typically of the order 10^{-9} m^2/s. In turbulent flows, the molecular diffusion is negligible compared to the turbulent diffusion. Fluid motions in the environment are almost always turbulent.

Turbulent diffusion is the transport of a substance due to the fluctuating component of the instantaneous velocity and enhanced molecular diffusion. Turbulent eddies erode the edges of the effluent plume which causes increased concentration gradients which enhances molecular diffusion. Fischer (1979) describes Taylor's analysis which showed after some start-up time a turbulent mixing coefficient can be defined analogous to the molecular diffusion coefficient. Enough time must have elapsed for a particle to forget its initial velocity. After this time, the variance of the effluent plume increases linearly with time and the turbulent diffusion can be expressed in the same form as molecular diffusion:

$$T_t = \overline{uc} = -\varepsilon \frac{\partial C}{\partial \mathsf{n}} \qquad \textbf{4.3}$$

where T_t = turbulent diffusive transport $\overline{uc}$ = time averaged turbulent fluxes, and ε = turbulent diffusion coefficient. ε is a property of the flow and is of the order 10^{-3} m^2/s.

Dispersion is caused by the differential advection that exists in river flow. The velocity gradient causes different parts of the plume to be advected at different rates. This in turn causes a concentration gradient, which leads to enhanced diffusion. Dispersion is generally lumped together with the diffusive transport as:

$$T_{disp} + T_t = -e \frac{\partial C}{\partial \mathsf{n}} \qquad \textbf{4.4}$$

where T_{disp} = dispersive transport and e = dispersion coefficient. The dispersion coefficient includes the effects of turbulent diffusion and differential advection (Elhadi et al., 1984).

Secondary circulation can be caused by the fact that turbulence is not identical in all directions or by channel curvature. This does not produce any net flow, but can contribute to mass transport as dispersive transport is induced due to differential advection if the concentration is not uniform across a cross section. Secondary circulation therefore has the effect of increasing the dispersion coefficient, e, when it is present (Elhadi et al., 1984).

Non-neutral substances introduce other physical mechanisms that must be considered when modeling river mixing. If the density of the effluent is different than that of the receiving waters, buoyancy effects must be considered. If a river contains fine sediments, it is likely that pollutants will coat the sediments and the transport of the pollutant will have to be considered as the transport of sediments. These processes will not be discussed in detail here.

4.1.2 Mixing Regimes

Downstream of a wastewater or cooling water discharge, the mixing of the river takes place in three different regimes. The first regime, often referred to as the near field, mixing is dominated by the jet effects of the effluent discharge into the river. The initial momentum and the buoyancy of the effluent must be considered, as these are the dominant forces in river mixing in this regime. The regime extends to the point where vertical mixing has been completed. The amount of time and distance for the first regime to take place is rather small in comparison to the second and third regimes and often a large dilution is achieved at this stage. The second regime is one in which the river mixing is dominated by turbulent transverse mixing. The third regime extends after the point where a transverse mixing has been complete and only longitudinal temperature or

concentration gradients remain (Demetracopoulos and Stefan, 1983). The second and third regimes are commonly referred to as the far field, the point at which disturbances in the velocity profile caused by the effluent discharge have subsided and the river is vertically fully mixed (Webel and Schatzmann, 1984). The intermediate field can be considered the region that is far enough downstream of the outfall where the jet effects of the effluent discharge are no longer the dominant forces, but not far enough downstream of the discharge to be able to average channel characteristics.

4.1.3 Three Dimensional Mixing

Three dimensional mixing in rivers is governed by the principle of conservation of mass. This yields the following equation:

$$\frac{\partial C}{\partial t} + \underbrace{U\frac{\partial C}{\partial x} + V\frac{\partial C}{\partial y} + W\frac{\partial C}{\partial z}}_{ADVECTIVE\ \ TERMS} = \underbrace{\frac{\partial}{\partial x}(\varepsilon_x \frac{\partial C}{\partial x}) + \frac{\partial}{\partial y}(\varepsilon_y \frac{\partial C}{\partial y}) + \frac{\partial}{\partial z}(\varepsilon_z \frac{\partial C}{\partial z})}_{DIFFUSIVE\ \ TERMS} \qquad 4.5$$

where C = concentration, U, V, and W are the time-averaged velocity components in the x, y, and z directions respectively and ε_x, ε_y, and ε_z are the turbulent diffusion coefficients (Elhadi et al., 1984). In meandering channels a curvilinear coordinate system is often used. The application of this equation typically requires the use of the momentum equations, as much more data is required than usually available to define the flow field. Application of the above equation is only important when examining mixing in the near field regime of the river where momentum and buoyancy effects are dominant.

4.1.4 Two Dimensional Mixing

There has been a substantial amount of research into the modeling of two dimensional river mixing. This occurs in the second regime after the river becomes fully

vertically mixed, which is a relatively short distance compared to the distance that it takes the flow to become fully mixed in the transverse direction. Natural streams typically have a large width to depth ratio and will therefore mix rapidly in the vertical direction in comparison to the transverse and longitudinal directions. Usually a natural stream can be considered vertically fully mixed 50 to 100 river depths downstream of the pollutant source (Yotsukura & Sayre, 1976).

The three dimensional mass conservation equation above can be integrated over the depth of flow, h, to produce:

$$\frac{\partial(\langle hC\rangle)}{\partial t}+\frac{\partial(h\langle UC\rangle)}{\partial x}+\frac{\partial(h\langle WC\rangle)}{\partial z}=\frac{\partial}{\partial x}(hE_x\frac{\partial\langle C\rangle}{\partial x})+\frac{\partial}{\partial z}(hE_z\frac{\partial\langle C\rangle}{\partial z}) \qquad 4.6$$

where the E_x and E_z are the mixing coefficients that include the effects of depth averaged turbulent diffusion and differential advection defined as:

$$E_x=\langle\varepsilon_x\rangle+e_x \qquad 4.7$$

where the angle brackets denote an average taken over the depth and e_x is an advective dispersion coefficient (Yotsukura & Sayre, 1976). For the remainder of this section U, W, and C represent to the depth averaged values.

Analytical solutions for this equation exist for steady state conditions and the continuous release of pollutants. This equation is described in Cartesian coordinates and can be transformed into natural curvilinear coordinates using a streamtube approach.

The Cartesian coordinate system is not convenient for use in natural rivers because the river plan and width changes along the length. Yotsukura and Sayre (1976) introduced a "natural" coordinate system that is more suitable for natural river geometries. The coordinate system is an orthogonal one with the longitudinal, horizontal, and vertical planes all perpendicular to each other. The z axis is measured from the right

bank (looking downstream) to the left bank, is perpendicular to the y axis which is measured from the bed upwards and is perpendicular to the x-axis which runs along the downstream direction. The mass conservation equation in this coordinate system can be expressed as:

$$m_x m_z \frac{\partial}{\partial t}(hC) + \frac{\partial}{\partial x}(m_z hUC) + \frac{\partial}{\partial z}(m_x hWC) = \frac{\partial}{\partial x}(\frac{m_z}{m_x} hE_x \frac{\partial C}{\partial x}) + \frac{\partial}{\partial z}(\frac{m_x}{m_z} hE_z \frac{\partial C}{\partial z}) \quad \textbf{4.8}$$

where metric coefficients m_x and m_z have been introduced to account for the variation in distances from one surface to the next due to river curvature and/or the variation of width along the river. The metric coefficients m_x and m_z may vary from point to point, but m_x=1 on the x axis and m_z = 1 on the z axis. If $m_x = m_z = 1$ everywhere then the coordinate system reduces to a rectangular Cartesian coordinate system. Fischer (1979) states for practical purposes the introduction of metrics is not important.

For the continuous release of a tracer into steady state river flow (or flow that mildly fluctuates about a mean value), the above equation can be simplified. As it is steady state, the concentration is no longer time dependent so the first term vanishes. The dispersive transport in the longitudinal direction is also much smaller than that in the transverse direction and can be neglected reducing the equation to:

$$\frac{\partial}{\partial x}(m_z hUC) + \frac{\partial}{\partial z}(m_x hWC) = \frac{\partial}{\partial z}(\frac{m_x}{m_z} hE_z \frac{\partial C}{\partial z}) \quad \textbf{4.9}$$

This equation can be further simplified if the concept of cumulative discharge, or streamtubes, is introduced. The cumulative discharge can be defined as:

$$q = \int_0^z m_z hU dz \quad \textbf{4.10}$$

represents the discharge that passes between the bank and some distance z out from the bank where q = 0 at z = 0 (right bank) and q = Q at z = left bank. Yotsukura and Sayre (1976) obtained the following equation for steady state two dimensional mixing based on the cumulative discharge:

$$\frac{\partial C}{\partial x} = \frac{\partial}{\partial q}\left(Uh^2 m_x E_z \frac{\partial C}{\partial q}\right) \qquad 4.11$$

The product $Uh^2 m_x E_z$ is referred to as the transverse factor of diffusion, D, and is analogous to a diffusion coefficient. This then reduces to the classical Fickian diffusion equation:

$$\frac{\partial C}{\partial x} = D\frac{\partial^2 C}{\partial q^2} \qquad 4.12$$

Elhadi et al. (1984) suggested that for one to predict concentration distributions using numerical solutions, the following must be known:

- Plan view of stretch with location of the injection point
- Depth average longitudinal velocity component and local depth at various locations across and along the stream
- An initial concentration distribution downstream of the injection point
- Boundary conditions at the banks of the stream
- Transverse dispersion coefficient

They suggest that the most difficult thing to estimate is the transverse dispersion coefficient. The common approach is to conduct a dye test in the river and determine the transverse mixing coefficient either using the method of moments or the simulation method.

4.1.4.1 Transverse Mixing Coefficient

At present, there is no reliable theoretical means of evaluating transverse mixing coefficients. The three methods of determining transverse mixing coefficients include the method of moments (discussed below); simulation methods where a trial and error approach is used to fit simulated concentration profiles to measured concentration

profiles, and empirical methods based on experimental and field experiments are available. A discussion of field and experimental results can be found in Beltaos (1979). Overall it has been found that the transverse mixing coefficient determined for real rivers is considerably higher than those found for straight, rectangular laboratory flumes. It has been hypothesized that there are a number of different factors contributing to this phenomenon including secondary circulation in rivers due to bends, irregular cross sections, and dead zones. The transverse mixing coefficient is therefore a very site-specific parameter that must be determined for each case separately.

The most accurate way to evaluate transverse mixing coefficients, although costly, is to use a continuous point source of tracer so that concentrations are steady and can be measured in the river. From these results, the method of moments can be used to evaluate transverse mixing coefficients.

4.1.4.1.1 Method of Moments

The generalized method of moments developed for steady tracer input by Holley et al (1972) applied to the streamtube model developed by Yotsukura and Sayre (1976) is the most common method used to analyze transverse mixing coefficients. When concentration distributions are examined as a function of the transverse distance, there is a tendency for the distributions to be skewed to one side shifting back and forth from one side to another. When concentration distributions are examined as a function of cumulative discharge however, the distributions tend to be more symmetrical resembling Gaussian distribution curves because the cumulative discharge takes into account the tendency for the flow to meander back and forth. The peak of the concentration distribution as a function of cumulative discharge exists at the injection point.

For a continuous injection with steady state conditions, the mass flux at each cross section must be constant and equal to the input mass flux rate. This can be calculated at each cross section as:

$$M = \int_{q=0}^{Q} Cdq \qquad 4.13$$

Once this requirement is met, from Rutherford (1994), the transverse factor of diffusion can be calculated from the relationship between the concentration distribution and cumulative discharge. For a bank discharge, where the plume has not reached the opposite bank the transverse factor of diffusion can be evaluated as:

$$D = \frac{1}{2}\frac{d\sigma_q^2}{dx} \qquad 4.14$$

where x is the longitudinal coordinate and σ_q^2 is the variance of the concentration distribution with cumulative discharge. The variance can be evaluated as:

$$\sigma_q^2 = \frac{\int_{q=0}^{Q} (q-\bar{q})^2 Cdq}{\int_{q=0}^{Q} Cdq} \qquad 4.15$$

where $\bar{q}$ is the value for the cumulative discharge at the bank where the discharge is located (either zero or Q).

The transverse factor of diffusion is typically transformed to a transverse mixing coefficient, as the factor of diffusion is difficult to compare to other rivers with different spatial and discharge characteristics. Fischer (1979) suggests D can be transformed into the transverse mixing coefficient as:

$$\varepsilon_t = \frac{D}{uh^2} \qquad 4.16$$

where u is the local depth averaged velocity and h is the local depth of flow. This transverse mixing coefficient is then reported in a dimensionless form for ease of comparison between study reaches. From Fischer (1979), it is converted to a nondimensional transverse mixing coefficient as:

$$\frac{\varepsilon_t}{hu^*} \qquad \textbf{4.17}$$

where u^* is the local shear velocity defined as:

$$u^* = \sqrt{ghS} \qquad \textbf{4.18}$$

and S is the slope of the channel.

Rutherford (1994) summarized reported transverse dispersion coefficients and suggests that in straight channels:

$$0.15 < \frac{\varepsilon_t}{hu^*} < 0.30$$

for irregular but gently meandering channels:

$$0.3 < \frac{\varepsilon_t}{hu^*} < 0.90$$

and for curved channels:

$$1 < \frac{\varepsilon_t}{hu^*} < 3$$

4.2 FLUORESCENCE THEORY

A fluorescent substance is one that absorbs light of one wavelength or color and emits light of another wavelength or color. A fluorescent substance will first absorb energy from an outside source such as the sun or an ultra-violet lamp. This absorbed energy will excite some electrons resulting in enlarged electron orbits known as the "excited state" of electrons. The electrons will emit energy in the form of photons (light) as excited electrons return to "ground state" or normal state. Typically emitted energy is at a lower frequency and longer wavelength. The most strongly fluorescent materials fluoresce in the ultraviolet to green part of the spectrum. (Wilson et al., 1986). Fluorescent substances have well defined excitation and emission spectra, which allows for analysis of the material.

4.2.1 Rhodamine WT

Rhodamine WT is a non-toxic, highly fluorescent dye that is commonly used in tracer studies. Known for its unique ability to absorb green light and emit red light, a fluorometer is easily configured to read the concentration of Rhodamine WT dye present in a sample. Since this is a unique property, interference from other compounds is rare (Turner Designs, Fluorescent Tracer Studies). Rhodamine WT was developed to overcome Rhodamine B's drawback of absorption to suspended sediments and typically comes in a 20% active solution with a specific gravity of 1.19. It is very dark red in color and quite viscous. Everts & Kanwar (1994) summarized some of the physical and chemical properties of Rhodamine WT as follows:

Generic name	C.I. Acid Red 388
Dye type	Xanthene
Molecular Weight	567 g/mole
Compositional formula	$C_{29}H_{29}N_2O_5Na_2Cl$
Toxicity (rat LD_{50} oral)	> 25g/kg
Excitation wavelength	555 nm
Emission wavelength	580 nm
Minimum detectability	0.013 μg/L

4.2.1.1 Rhodamine WT Losses

There are a few things that affect the fluorescence of Rhodamine WT dye: photodecomposition, chemical degradation, loss by adsorption onto suspended sediments and on the bed, turbidity, pH, and temperature.

Photochemical decay is dependent on the light intensity and wavelength and can be described by the relationship:

$$F = F_1 \exp(-kt) \qquad 4.19$$

where F_1 is the initial fluorescence, F is the fluorescence at time t, and k is the decay coefficient (Smart & Laidlaw, 1977). If samples are stored out of the sunlight, the

fluorescence will not degrade and will remain stable for years. Buchanan (1964) noted that field samples that were stored in the dark showed no change after six months. Photochemical decay in a field study is not a concern unless the study is carried out over several days (Turner Designs, Practical guide to flow measurement).

Chemical degradation is not likely to occur, but the most likely compound to affect Rhodamine WT is chlorine. Chlorine has been shown to destroy Rhodamine WT within a few minutes at all pH levels, however Deaner (1973) has proven that a residual chlorine level in considerable excess of that found in drinking water or wastewater had no affect on the fluorescence of the Rhodamine WT dye.

In general, loss of dye due to sorption is considered negligible with Rhodamine WT dye, but it can be checked. Adsorption is the adhesion to the surfaces of solid bodies or liquids with which they are in contact. Smart & Laidlaw (1977) found a decrease in the percentage of dye loss with an increase in initial dye concentration. They also found that organic sediments adsorb far more dye than inorganic sediments. Everts and Kanswar (1994) claim that initial dye concentration and pH affect the amount of adsorption of Rhodamine WT with organic matter. They found that clay content influenced the amount of Rhodamine WT adsorption, but the greatest single influence on the amount of Rhodamine WT adsorption was organic carbon content. Turner Designs (Flow Measurements…) claimed they had never seen a case where solids adsorbed the dye, but it could happen if, for example, the solids contained activated charcoal. Bencala et al. (1983) performed studies of Rhodamine WT losses in a mountain stream environment and showed in their lab studies very substantial uptake of Rhodamine WT by relatively small amounts of sediment. Sabatini & Austin (1991) found the background ions affected the level of Rhodamine WT adsorption. Kasnavia et al (1999) furthered this study, finding that fluorescent dyes are large organic molecules that are water soluble because of ionic functional groups. These groups, however, can interact with oppositely charged surface sites increasing dye sorption due to ion exchange. Organic matter typically has both positive and negative sites associated with it. They concluded that "the dual cationic and anionic charges on Rhodamine dyes suggest that they will sorb onto almost all

mineral surfaces (i.e. any charged surface) making them less attractive as conservative tracers". Smart & Laidlaw (1977) found that if sediment concentrations are below 1000 mg/L adsorption effects will be negligible unless the sediment is extremely fine or organic in nature. Loss due to adsorption can be corrected by making a dilution of dye in natural water and in distilled water at a concentration close to that expected in the study as dye loss is dependent on initial dye concentration. A correction factor of the ratio of the reading of the distilled water sample to that of the natural water can by applied to all sample readings.

In terms of turbidity, it has been found that it generally takes a large amount of turbidity to affect the fluorescence of Rhodamine WT, but it can easily be corrected for if need be since the effect of turbidity is a proportional one. For example, if 10% of the light is blocked the reading will be reduced by 10%. There are three methods to correct for turbidity. If the turbidity is constant, the standards used to calibrate the fluorometer should be made with the natural turbid water. This automatically corrects for turbidity as the amount of light blocked in the standards will be the same as for the samples. The second method is to remove the suspended sediment through filtration or settling. In most cases if the suspended sediments are allowed to settle for 10 to 20 hours, the decanted sample can be measured accurately. The final method is dilution of the sample using distilled water to reduce the concentration of the suspended sediments to a level that's negligible (Turner Designs, Flow Measurements…).

The pH of the sample needs to be within the range of 4.5 to 10.5 otherwise the fluorescence will drop rapidly. Smart & Laidlaw (1977) suggested that the fluorescence of Rhodamine WT is significantly affected below a pH of 5.0. The pH of a sample can be corrected by adding baking soda if the pH is low and some dilute acid if the pH is high.

The temperature of the sample also has a tremendous impact on the fluorescence and must be taken account of. It has been shown that the fluorescence of Rhodamine WT has a temperature coefficient of -2.7% per degree centigrade so the sample and the standard must be at the same temperature or a correction must be applied as:

$$F = F_o \exp[n(T - T_o)] \qquad 4.20$$

where F is the calculated fluorescence at the temperature T, F_o is the observed fluorescence at the observed temperature T_o and n = -0.027/°C for Rhodamine WT (Smart & Laidlaw, 1977).

4.2.1.2 Rhodamine WT as a Tracer

Rhodamine WT is commonly used as a water tracer as recommended by Smart and Laidlaw (1977). It is considered to be a safe tracer with minimal impact on the environment at low concentrations, it is stable as long as certain precautions are taken, and is very soluble in water, which makes it an ideal water tracer. It can easily be detected at low concentration levels and is fluorescent in a part of the spectrum not common to materials generally found in water and is relatively inexpensive. Additional information regarding the use of Rhodamine WT as a tracer can be found in Appendix A.

CHAPTER 5 MIXING STUDY

5.1 DYE TEST

5.1.1 Input Location and Dye Test Timing

The input location for the dye solution is crucial as complete mixing of the dye with the effluent must occur in order to ensure that an accurate depiction of the effluent plume is measured. It was decided that the dye would be injected into sample ports located in the Ultra-Violet treatment building located in Figure 5.1. The ports are positioned after the final treatment of the effluent so degradation of the dye due to the ultra violet light treatment would not be a concern. After the sample port, the effluent flows into a channel through a set of baffles before hitting the steep slope of the outfall structure. Complete mixing would be likely from this injection point, but samples of effluent at the outfall were taken at regular intervals during the dye test to check for complete mixing.

The effluent flow is not constant throughout the day so it was desired to conduct the test during a relatively constant period in order to achieve near steady state conditions in the river. Typical weekday effluent flow for October was obtained from GBWWTP illustrated in Figure 5.2. The test had to be completed during daylight hours so a period of 900 to 1700 was available for the test. Over this period, the effluent flow increases rapidly over the morning hitting the peak around noon then decreasing at a slower rate over the afternoon. The early afternoon period exhibits somewhat of a plateau so it was decided to carry out the dye test during this period. This extended the dye test over two afternoons rather than one day in order to collect the desired number of samples.

5.1.2 Preparation of Input Dye Solution

The dye had to be prepared as a solution to be injected into the effluent. From previous studies it was known that the minimum reliable concentration the fluorometer would be able to read was 50 ppt which is equivalent to 0.05 µg/L while the maximum reliable concentration was suggested to be around 5000 ppt. The discharge in the North Saskatchewan River was estimated to be roughly 150 m^3/s so if complete mixing is assumed to occur, the minimum dose rate could be calculated as:

$$0.05\frac{\mu g}{L} * 150\frac{m^3}{s} * 1000\frac{L}{m^3} = 7500\,\mu g/s$$

One of the conditions of the dye test was to ensure that the dye remained invisible. The maximum concentration expected would occur in the outfall and if a dry weather effluent flow was assumed this would produce the highest possible estimate for the maximum concentration. From Near Field Mixing of Outfall Discharges, a dry weather effluent flow can be assumed to be 1.45 m^3/s. From this the maximum concentration expected in the outfall is:

$$Maximum\ Concentration = \frac{Dose\ rate}{Effluent\ Flow} = \frac{7500}{1.45 * 1000} = 5.172\,\mu g/L = 5.172\ ppb$$

Rhodamine WT becomes visible at 10 ppb in large volumes of water (Turner Designs, Bulletin 104) so this would be well below the visible limit as well as within the range of the fluorometer.

The peristaltic pump to be used in the dye test, a VWR Scientific Variable Speed Pump (Medium Flow) 54856-075 set at slow and a dial speed of 10, was calibrated and was determined that the dye input flow rate would be 14.9 mL/minute. Knowing the pump rate and the desired dosage rate, the desired input concentration could be calculated as:

$$C_{input} = \frac{Dose\ rate}{Pump\ rate} = \frac{7500}{14.9/60} = 30.20\ g/L$$

From this it was known that the dye test would take place over two days so enough solution had to be mixed in order to pump over that period. A minimum of 12 hours was anticipated which translates to a minimum volume of solution of approximately 10.7 L.

A Nalgene 20 L container was to be used to mix the input dye solution which, following Turner Designs recommendation to left 20% air space in the container to facilitate complete mixing, left 16 L available for solution. The mixture was not precisely measured, as the exact concentration would be determined later by diluting the input dye solution to read in the fluorometer. Approximately 2.3 L of Rhodamine WT and 13 L of distilled water were mixed which would yield a concentration in the range of 30 g/L. The container was thoroughly mixed by swirling the container using a rotary motion, inverting the container swirling again and repeating this procedure 10 times. The container was stored in a dark garbage bag to protect the solution from sunlight during transport to the injection point.

5.1.3 Preliminary Plume Estimate and Sampling Locations

A preliminary estimate of the dye plume was made assuming that the river was vertically fully mixed and could be approximated as a rectangular channel of depth h. For a bank discharge at z = 0, an image source must be included at z = 0 to account for reflection off the banks to yield an equation derived from Fischer (1979) as:

$$C(x,z) = \frac{M/h}{\bar{u}\sqrt{4\pi\varepsilon_t \, x/\bar{u}}}\left[\exp\left(-\frac{z^2}{4\varepsilon_t \, x/\bar{u}}\right) + \exp\left(-\frac{z^2}{4\varepsilon_t \, x/\bar{u}}\right)\right] \qquad 5.1$$

where M = mass of dye per unit of time, ε_t = transverse mixing coefficient, $\bar{u}$ = cross sectional mean velocity, z = transverse coordinate, and x = longitudinal coordinate.

An estimate of the mass flow rate of dye is known from above to be M = 7500 μg/s = 7500 m^3/s ppt. From Milne et al (1993), at the Rossdale Water Treatment Plant (which is upstream of the GBWWTP) mean hydraulic properties are $\bar{u}$ = 0.828 m^3/s and h = 1.63 m. The transverse mixing coefficients in the literature vary quite a bit so three different values were used to estimate the plume spread. From Golder (1995), ε_t = 0.63 m^2/s from Rossdale Water Treatment Plant to GBWWTP and ε_t = 0.1 m^2/s from GBWWTP to Capital Region Wastewater Treatment Plant. From Milne et al. the maximum value of transverse mixing coefficient used was ε_t = 0.893 m^2/s. These values were all tested in the above equation to get an estimate of the plume spread in the channel. Two intermediate values of transverse mixing coefficient were also tested, ε_t = 0.25 m^2/s and ε_t = 0.50 m^2/s. The edge of the plume was taken at a point when the concentration dropped below 5% of the maximum concentration at that cross section. As can be seen in Figure 5.3, the maximum predicted distance from the bank that the plume would spread is 160 metres. A higher transverse mixing coefficient caused the plume to spread more, it is likely that the transverse mixing coefficient for this area is in the range of ε_t = 0.1 m^2/s from Golder (1995) values so the edge of the plume at a point 2000 metres downstream of the outfall would be within 50 metres from the bank.

It was decided that sampling 10 cross sections would be ideal with approximately 10 points per cross section to yield about 100 points total. Since the region near the outfall is the most critical and interesting, it was decided that the spacing between cross sections near the outfall be small, gradually increasing as the end of the study area was reached. It was decided that cross sections at 0, 10, 20, 40, 80, 160, 320, 640, 1000, 1500, and 2000 metres downstream of the outfall be sampled. Prior to the dye test, stakes were placed at each cross section location for easy location during the test.

5.1.4 Dye Test

The dye test was carried out over two days, October 29 and November 7, 2002. On both days the pump was setup around 12:00 and sampling began around 14:00 on October 29 and 13:00 on November 7; the delay was to ensure that steady state conditions were met in the river before sampling began. The original plan was to complete the second portion of the dye test on October 30, however the temperature had dropped so much that frazil ice formed in the river. It took a few days for all the frazil pans to wash out of the system so the earliest possible date to complete the dye test was November 7. Even on this date, there was border ice in the morning that lifted as the day progressed and the flow increased. The ice sheets did not interfere too much with the sampling procedure and was decided that the presence would have little effect on the mixing characteristics in the area of interest. From the one dimensional modeling from section 3.1, it was noted that the ice may have had an effect on the discharge in the North Saskatchewan River. Two cross sections (80 and 320) were repeated on November 7 in order for there to be some overlap between the two days. The dye was pumped through Tygon tubing into the sample port shown in Figure 5.4. Prior to dye injection, random river and effluent samples were collected to determine the background concentrations as well as the dye recovery properties of the river and effluent water.

5.1.4.1 Sample Collection

Two sampling crews were active; one crew in a boat and the other wading in the water. At each sampling cross section, the wading crew walked out from the south bank into the river and began sampling at that location working their way back towards the bank. The boat crew began sampling beside the wading crew, and worked their way towards the middle of the river. Approximately 10 samples per cross section were collected; the sample locations are illustrated in Figure 5.5.

At each sample location, a depth averaged sample and a surface sample were collected using 125 mL Nalgene polyethylene bottles with polypropylene screw closures.

All sample bottles were pre-labeled with either a number beginning with "D" to designate a depth averaged sample or "S" to indicate a surface sample. The sample number was recorded in the total station along with the position coordinate in order to match the data after the samples were analyzed. Initially a DH48 sampler was used for the depth averaged sample. The sampler was lowered to the bed and raised above the water at a slow, constant rate with the nozzle pointing into the flow. If not enough water was present in the bottle or if the bottle was full, the process was repeated as a truly depth averaged sample would not have been collected. The DH48 sampler is fitted with one pint bottles from which the collected sample was poured off into the 125 mL bottles. At one point, one of the DH48 samplers was lost in the river so a specially constructed device was outfitted into which the 125 mL Nalgene bottles were secured in an upright position. A similar procedure was used for these samplers to collect a depth averaged sample. The surface sample at each location was simply collected with the 125 mL bottles. All the filled bottles were stored in coolers to protect the samples from the sunlight.

Throughout the dye test, effluent samples were collected from the outfall structure every half hour for the duration of the dye tests. These samples were to verify that complete mixing of the dye with the effluent had occurred before the effluent reached the river. Samples were collected at a point just downstream of where the submerged hydraulic jump occurred in the chute.

5.1.5 Effluent Flow

The effluent flow was provided in ML/day every two minutes for the dye test days by GBWWTP. As shown in Figure 5.6, the effluent flow for both test days was very similar. When comparing the effluent flow during the dye test period, as shown in Figure 5.7, the average effluent flow for October 29 was 3.33 m^3/s while the average effluent flow for November 7 was 3.34 m^3/s.

5.2 SAMPLE ANALYSIS

5.2.1 Fluorometer

The fluorometer used to analyze the samples was a Turner Quantech Digital Filter Fluorometer, Model FM109525 manufactured by Barnstead Thermolyne. Excitation energy in this fluorometer is provided by a quartz-halogen lamp with a wavelength range of 340-750 nanometres (nm). Excitation filters are used to allow only light of a specific wavelength to pass through the sample to excite a particular molecule. For this a narrow band filter is used, which are designated by the center wavelength and have a 10 nm nominal band pass curve. For Rhodamine a NB540 excitation filter is used. Detection of the emission light is provided by a high gain, low noise photomultiplier tube. Emission filters are used to allow emitted light above a specific wavelength to pass into the photomultiplier tube. These are Sharp Cut filters which are designated by the wavelength at which they exhibit a transmission of 37%. Typically transmission is less than 1% at a wavelength 10 nm less than the rate wavelength. For Rhodamine an SC585 emission filter is used. The fluorometer has a concentration range of 0.00 – 9999.99 units selected by the user.

5.2.2 Calibration Procedure

The fluorometer must be calibrated using standards of known concentration within the concentration range that will be tested. Because of the linear response of Rhodamine fluorescence, only two standards are required to calibrate the fluorometer plus a blank sample. It is recommended by Turner Designs to use distilled water for the preparation of standards and for the blank in order to achieve a definite record of the magnitude of the system background fluorescence and to ensure negative values will never be encountered.

Standards were prepared following the guide by Turner Designs and were referred to in terms of active ingredient of Rhodamine WT. A Nichiryo Nichipet EX Autoclavable Digital Pipetter with disposable tips was used with a fully adjustable volume range of

100-1000 µL for all pipetting. Initially, a 100 ppb standard was prepared by weighing 5 grams of dye on a Denver Instrument Company analytical balance and diluting it in a 500 mL volumetric flask with distilled water. This produced a 2 g/L solution. Next, 5 grams of dilution #1 was diluted with distilled water in another 500 mL volumetric flask following the same procedure of #1 to yield a 20 mg/L (or ppm) solution. Finally, 2.5 grams of dilution #2 was diluted with distilled water in a 500 mL volumetric flask to yield a 100 ppb solution. This standard became the basis for the remaining of the standards prepared using the analytical balance following the relationship:

$$C_B = \frac{V_A}{V_B} C_A = \frac{M_A}{M_B} C_A \qquad \textbf{5.2}$$

where V represents the volume of the samples and M represents the mass of the samples. Initially, a first set of standards were prepared to understand the fluorometer and to select appropriate cuvets covering that range of 50 to 5000 ppt. The first set of standards were made precisely, but were not recorded exactly as: 5000, 2500, 1000, 750, 500, 250, 100, and 50 ppt.

The number of calibration standards required to create the most accurate calibration curve was investigated. A 5 point, 3 point, and 2 point calibration curve was investigated thoroughly. The results are summarized in Table 5.1. Figure 5.8 illustrates that the five point calibration curve produced the greatest overall error with significant error at lower concentrations. The two point calibration curve using the 5000 ppt, 100 ppt and blank standards produced the most accurate and consistent results, even at lower concentrations. This calibration curve was used for all sample analysis.

Prior to the analysis of the samples, a second set of calibration standards were precisely created and recorded as shown in Table 5.2. This set of calibration standards was used for a two point calibration curve of the fluorometer for the analysis of the samples and to perform accuracy checks each time the fluorometer was used.

5.2.3 Cuvet Selection

Cuvets can affect the results and so the appropriate cuvets must be chosen in order to ensure the most accurate readings. Two different types of cuvets were chosen for comparison: standard cuvets and cuvets with four clear sides. Both were Fisherbrand disposable polystyrene of dimensions 12.5L x 12.5W x 45H mm with a capacity of 4.5 mL. Polystyrene cuvets should be chosen for analysis in the visible spectral range (340-750 nm). Fisher Scientific claims that the four-clear-sided cuvets are ideal for fluorimetry. Standard cuvets have two slightly frosted sides and two clear sides with molded in arrows to indicate the direction of transmission on one of the clear sides. The standard cuvets also have a mold impression number assuring precision between samples. Cuvets must be handled very carefully. Scratches, fingerprints, dust, air bubbles, etc. can all affect the fluorescence readings by scattering the light. Great care must be taken to minimize these affects. Cuvets must be filled at least 2/3 full in order to achieve accurate readings.

Several comparisons were done between the two cuvet types at two different calibration curves. It was found that the readings for the clear cuvets gave inconsistent readings and considerable error at lower concentrations as seen in Table 5.3. Figure 5.9 illustrates that at lower concentrations the clear cuvets had very high error at both calibration curves. Negative values were read for the lower concentrations using the clear cuvets. Since the standard cuvets gave more consistent readings and overall greater accuracy, they were chosen for the sample analysis.

Two interesting trends were noted while this work was being carried out. The first of which was that the fluorescence readings of the same cuvets decreased over time if they were read consecutively as illustrated in Figure 5.10. When the cuvets were left overnight, the readings were identical to the first set of measurements of the previous day. This demonstrated the sensitivity of the fluorescence to the temperature of the sample. As the cuvet is read, the intense light warms the cuvet; as the temperature of the sample increases, the fluorescence decreases which is consistent with what was seen here.

It is therefore imperative that the samples remain at the exact temperature of the calibration standards and that each sample be read once, quickly in order to avoid any temperature affects.

The second trend that was noted was a decrease in fluorescence for each subsequent set of cuvets drawn from the same standard vials as shown in Figure 5.11. This indicated that over time fluorescence was being lost in the vials that held the calibration standards. The initial set of cuvets was used for all sample analysis in order to avoid this problem.

5.2.4 Sample Analysis

Samples collected were brought back to the lab and stored in a fridge in order to minimize the biological activity that may occur in the effluent. Samples were allowed to settle before analysis so that turbidity would not be an issue. Extreme caution was taken when handling samples for fear of contamination. Disposable gloves were worn when handling samples and a new pair was used to handle each sample bottle. The sample was drawn off the top of the bottle using the pipette and 20 mL was transferred to a scintillation vial and 3.5 mL was transferred to a standard cuvet. The scintillation vial was for safe keeping in case future readings of the sample would be desired. The cuvets were filled approximately 24 hours prior to measurement.

For precise measurements the samples and standards must be at the same temperature. It was found that even air temperature fluctuations were enough to produce inconsistent results. In order to alleviate this problem, cuvets were placed in a cuvet rack in a pan of water at room temperature with the water level in the pan covering at least the bottom ¾ of the cuvet. Cuvets were left in the water bath for at least 30 minutes before any measurements were made. The water bath temperature was taken at the beginning of the measurements and at the end to ensure consistency. If fluctuations of more than 0.5 ^{o}C were observed, the fluorometer would have been recalibrated. This never happened.

Cuvets were wiped off carefully using KimWips before being placed in the fluorometer for measurement. Measurement of the cuvets were made rapidly. If the cuvet was in the fluorometer for longer than 45 seconds, it was removed to be read at a later time. Cuvets that were read were not placed back in the water bath to avoid temperature fluctuations of the water. All samples were read on the same calibration curve for consistency between readings and were all read on the same day.

Standards that were not used for the calibration of the fluorometer were used as an accuracy check before the samples were read in the fluorometer. As seen in Table 5.4 the average absolute error was less than 5% with fairly consistent results.

A number of blank river and effluent samples had been collected at random locations prior to the dye test in order to establish the background fluorescence of the system. Two cuvets were tested in order to average the readings. As shown in Table 5.5, the background fluorescence of the blank river samples was on average about 33 ppt. The background fluorescence of the blank effluent samples were quite high around 535 ppt on average.

Samples of effluent had been collected approximately every half hour for the duration of the dye test, the results of which are summarized in Table 5.6. On average the fluorescence on November 7 was slightly higher than October 29, but all values were within the same range as shown in Figure 5.12. There is a bit of fluctuation throughout the dye test in concentration, but this is attributed to the variable effluent flow.

Table 5.7 and 5.8 summarize the sample data collected on October 29 and November 7. A total of 106 depth averaged samples and 116 surface samples were analyzed.

5.2.5 Input Dye Concentration

The input dye concentration is required to understand whether complete mixing occurred prior to entering the river and to know the mass input for the dye test. It was expected that the dye concentration would be around 30 g/L so it was known that dilution of the mixture was necessary in order to bring the input sample within the range of the fluorometer. Samples of the input dye mixture were taken on both dye test days which were diluted with distilled water using the scale. Two sets of dilutions were made in different ways and are summarized in Tables 5.9 and 5.10. The first dilution calculated an input of 28.51 g/L and the second dilution calculated an input of 29.03 g/L. Taking an average of the two input concentration, the expected concentration in the outfall would be approximately 2739 ppt including the background concentration.

From the actual effluent concentration measurements taken, the average outfall concentration (subtracting the background concentration of the effluent) for October 29 dye test was 2642 ppt (± 100 ppt) while the average for November 7 was 2833 ppt (± 175 ppt). The average of all the samples taken on both dye test days is 2737 ppt which agrees very well with the expected concentration of 2739 ppt which indicates that complete mixing likely occurred before the effluent entered the river as shown in Figure 5.13. In this figure, the effluent flow is shown for both days on the left y axis, while the measured and expected concentration is plotted using the right y axis. The effluent flow is not constant throughout the dye test period and fluctuations in the measured concentration are noticed. It is conceivable that the peaks in the measured concentration coincide with the dips in effluent flow as they are within 5 minutes of each other. The time of the effluent samples were not recorded precisely.

5.2.6 Recovery Ratio

A recovery ratio test is needed to ensure that the physical and chemical properties of the study water don't interfere with the measurement of fluorescence of the Rhodamine WT. In order to calculate the recovery ratio, two standards of the same

concentration must be made in the range of the expected sample concentrations: one with study water and the other with distilled water. Then, the recovery ratio is calculated as follows:

1. Prepare standard using distilled water
2. Prepare identical standard using study water
3. Read background fluorescence of study water
4. Calculate recovery ratio as 2-3 divided by 1

The recovery standards were prepared according to the approach suggested by Turner Designs. A 100 ppm dilution using distilled water was prepared, and this was further diluted with distilled water and study water for comparison. Initially, two sets of recovery standards were created: one using a random sample of river water and one using a sample of effluent water taken from the outfall spillway. Three concentrations were tested with two cuvet readings per concentration in order to average them: 2500, 1000, and 500 ppt. The results are summarized in Table 5.11.

As can be seen in the table, the recovery ratio for river water hovered around 67% while the recovery ratio for effluent water is around 100%. It was decided to repeat the recovery ratio test in river water to make sure that it was not a laboratory error and was in fact a low recovery ratio. Two additional 2500 ppt river water standards and one 1000 ppt river water standard were created following the procedure described above using the same 100 ppm distilled water standard from before. An additional 2500 ppt river water standard was created from scratch using the original dye rather than the 100 ppm distilled water standard to confirm that using the 100 ppm standard was not the cause of the low recovery ratio. The results are summarized in Table 5.12.

The recovery ratio in river water was consistently in the region of 70% (± 2%) regardless of river water sample used and whether or not the recovery standard was created using the 100 ppm distilled water standard or from scratch using pure Rhodamine

WT dye. Conversely, it was found that 100% (± 2%) of the dye was being recovered in effluent water.

It was decided to investigate this phenomenon further by creating recovery standards using portions of river water mixed with effluent water summarized in Table 5.13. To begin with, three different combinations were tested; 75% river water, 50% river water, and 25% river water. A mixture of effluent water and river water was prepared and then the recovery standard was created following the procedure outlined above. The recovery ratio appeared to rise rapidly to 75% river water and then remains close to 100% recovery as shown in Figure 5.14. It was questioned whether the curve accurately represented solutions with a large percentage of river water so two additional recovery standards were prepared: 95% river water and 87.5% river water. These fell right on the curve. Similar combinations of river water and distilled water were prepared to determine whether it was the dilution of the river water that increased the recovery ratio or whether it was a property of the effluent water that increased the recovery ratio. Three combinations of river water and distilled water were tested: 75%, 50% and 25% river water. The distilled water curve appears to mirror the effluent water curve which would suggest that it is a property of the effluent water that removes or abates the recovery properties of the river water. The cause of this was explored; however no satisfactory explanation was attained.

It was further questioned whether the order in which the standards were mixed would affect the recovery ratio. In all the above tests, the river water was mixed with the effluent or distilled water first and then was used to dilute the 100 ppm distilled water standard. In the field study, dye was first mixed with effluent water and then diluted with river water so it is important to know whether this would affect the recovery ratio. Two 2500 ppt recovery standards were prepared. The first was prepared by mixing river water with the 100 ppm distilled water solution and then further diluted by adding effluent water. The second was prepared by mixing effluent water with the 100 ppm distilled water solution and further diluted by adding river water. Both standards were made to 2500 ppt with a ratio of 95% river water and 5% effluent water. The results of this test

proved to be inconclusive as seen in Figure 5.14. As usual, two cuvets were prepared with both solutions in order to average the values to obtain a concentration reading. The cuvets of effluent water added to the river water solution were approximately the same reading on average 1715.38 ppt which yields a 67.16% recovery. This falls below the expected recovery, but is within the range of values previously recorded. However, the cuvets of river water added to the effluent water solution read 1732.99 ppt and 2449.95 ppt yielding 67.87% and 96.64% recoveries respectively. The first cuvet is similar to the effluent water added to river solution results, which would suggest that the order of mixing does not affect the river recovery. The second cuvet with a recovery of 96.64% would suggest the opposite: that the order of mixing does affect the river recovery and that if dye is mixed with effluent prior to dilution with river water the recovery can be assumed to be 100%. Further studies are required in order to solve this issue, unfortunately due to a lack of time and water samples these results remain inconclusive.

In order to correct all the measured sample data, a third order polynomial was fitted to the effluent mixture recovery curve constraining the recovery ratio to a maximum of 100% as shown in Figure 5.15. This yielded the following equation:

$$y_r = 0.6814x_e^3 - 1.5601x_e^2 + 1.1571x_e + 0.7217 \quad 5.3$$

where y_r = recovery ratio and x_e = the ratio of the volume of effluent water in the sample to the total volume of the sample. The observed concentration is related to the actual concentration as:

$$C_{observed} = y_r C_{actual} \quad 5.4$$

and the actual concentration is related to the concentration of the effluent inflow as:

$$C_{actual} = x_e C_{effluent} \quad 5.5$$

Combining the above equations, the actual concentration at each sample location was calculated after first subtracting the river background concentration from all values.

5.3 RESULTS

The location of the sample numbers had been recorded in the total station so the concentrations were matched to the locations and the recovery ratio corrected values were calculated. The results are tabulated in Tables 5.14 to 5.17 and shown in Figures 5.16 and 5.17.

5.3.1 October 29, 2002 Concentration Profiles

Station 0 exhibits a slight discrepancy between the depth-averaged sample and surface sample concentrations. It shows that dye is present approximately 35 metres from the south bank. A portion of the effluent flowed upstream of Station 0 around the rip rap, however no measurements were made in this area. The maximum concentration at Station 0 is approximately 2800 ppt.

Station 10 shows a minimal discrepancy between the surface and depth averaged sample concentrations. This rapid mixing is likely due to the initial momentum from the effluent that causes the cross section to appear vertically fully mixed. The concentration remains consistent around 2600 ppt until a point roughly 20 metres from the bank.

Station 20 shows that near the south bank the river is vertically fully mixed until a point approximately 10 metres from the bank. At this point the river becomes stratified with the depth-averaged sample being lower than the surface sample. The surface sample shows a high consistent concentration until 20 metres from the bank, roughly the same as cross section 10.

Station 40 shows a lessening of the difference between the surface and depth averaged samples. The concentration is constant which shows little decay of the plume to a point 20 metres from the bank similar to cross sections 10 and 20.

Station 80 exhibits stratification, as the depth-averaged sample becomes lower than the surface sample again. This suggests that buoyancy effects are dominant. The initial momentum of the effluent flow would quickly mix the effluent in the river as evident at station 40. Then the buoyancy effects would begin to come into play and stratification would occur as the effluent flow is at a much higher temperature than the ambient river flow which would tend to sink to the bottom which in turn would lead to a lower depth averaged sample. There is evidence of the beginning of decay in the plume. The maximum concentration at this cross section is approximately 2700 ppt, which indicates little dilution from the outfall.

Station 160 shows that the flow is now vertically fully mixed and the concentration distribution follows a typical distribution for a bank discharge. The maximum concentration at this section is approximately 2400 ppt.

Station 320 remains vertically fully mixed and the peak concentration is about 2200 ppt. This is a dilution of the maximum concentration of only 75% over 320 metres. The plume extends approximately 40 metres from the south bank.

5.3.2 November 7, 2002 Concentration Profiles

Station 80 exhibits a similar pattern to that taken October 29. Stratification is evident, as the depth-averaged sample is lower than the surface sample concentrations. The maximum concentration is lower than October 29; about 2000 ppt compared to 2700 ppt.

Station 320 also exhibits a similar pattern to that taken October 29 with a lower maximum concentration; approximately 1700 ppt compared to 2200 ppt. There is a depth-averaged sample that is lower than the surface concentration approximately 10 metres from the south bank. On this date at this discharge a dilution of 60% is achieved over the first 320 metres.

Station 640 shows a similar pattern to that at 320. There is one depth averaged sample that is suspect of error as it is unusually low. There is very little reduction in the maximum concentration from station 320 to 640 with the maximum concentration roughly 1650 ppt.

Station 1000 shows a slight reduction in the maximum concentration to 1400 ppt and shows a tightening of the plume as no concentration is read past 20 metres from the bank.

Station 1500 shows a spreading of the plume and a significant reduction of the peak concentration to approximately 850 ppt. The surface sample in this case is lower at the bank than the depth averaged sample. This was expected as immediately upstream of station 1500 there is a tributary coming in as a surface discharge just upstream of the from the oil refinery which would dilute the surface concentration.

Station END exhibits a maximum concentration of approximately 700 ppt which is a dilution from the outfall of about 1:4. The surface concentration at the bank remains low due to the surface discharge upstream of the oil refinery plant.

5.4 TRANSVERSE MIXING COEFFICIENT

In order to analyze the transverse mixing of the study reach, the recovery ratio corrected depth averaged sample concentrations were plotted with the modeled cumulative discharge values for cross sections downstream of Station 40 shown in Figures 5.18 and 5.19. The analysis started at Station 40 since upstream of this station the concentration and flow field is rather complicated as momentum effects from the outfall are dominant and therefore the method of moments cannot be applied. The mass flux input at the outfall can be calculated as the average concentration at the outfall times the average effluent flow over the dye test. It was known to be approximately 9114 m^3/s ppt and if no dye is lost between sections then this value of mass flux is expected at each

cross section. The mass flux at each cross section was calculated by numerical integration of the C-q distributions. The target mass flux was used as a guide to adjust the numerical integration where the linear assumption between widely spaced sample points added too much mass or too little mass. Adjustments were made, based on upstream and downstream cross sections and judgment, to October 29 distributions as follows:

Station 40: The high concentration block likely extends past the measured point before decreasing to about zero. A point was added to extend this block to a q = 2 m^3/s to increase the mass flux at this station.

Station 160: The concentration likely reaches zero before q = 17 m^3/s as too much mass is at this station. A point was added to reach a concentration of zero at q = 12 m^3/s based on the previous station reaching zero at a q = 10 m^3/s.

Station 320: Based on Station 80 and 160, the linear assumption along the decrease from a concentration of about 1080 ppt to 285 ppt is not adding enough mass. The concentration likely stays around 1000 ppt before decreasing. A point was added at a concentration of 900 ppt at q = 4 m^3/s.

Adjustments were made to the November 7 distributions as follows:

Station 80: A point was omitted because it was not in line with the rest of the cross section when plotted in plan view so it was not a true concentration distribution at that location.

Station 320: The second point, the surface concentration was used rather than the depth averaged concentration as error was suspected. A point was also omitted because it was not in line with the cross section.

Station 640: Similar to 320, error was suspected on one of the depth averaged concentrations so it was replaced with the surface concentration. Again a point was not in line with the cross section so it was omitted.

Station 1000: A point was added because the concentration likely does not decrease from 1320 to 48 in a linear manner, too much mass was being added. A point was added at a concentration of 475 ppt at q = 5.5 m^3/s based on previous cross sections.

Station 1500: A point was added because the concentration likely reaches zero before q = 23 m^3/s as too much mass was being added. Based on the previous Stations, it is likely that the concentration reaches zero around q = 15 m^3/s.

Station End: The concentration likely reaches zero before q = 27 m^3/s. A point was added to reach zero at q = 15 m^3/s.

The adjusted distributions are illustrated in Figures 5.20 and 5.21. From the adjusted mass flux values, it was evident that approximately 9100 m^3/s ppt mass flux was achieved at Stations 40 through 160. From Station 320 to the end of the study area a mass flux of approximately 7200 m^3/s ppt was achieved. This indicates that between Stations 160 and 320, mass is being lost in the river so only a portion of the mass is being recovered. The concentrations at Stations 320 through to the end were scaled by 1.25 in order to achieve the target 9100 m^3/s ppt mass flux. The scaled adjusted distributions are illustrated in Figures 5.22 and 5.23. All cumulative discharge-concentration profiles are summarized in Tables 5.18 and 5.19 with the italicized entries indicating adjusted points. The corresponding mass flux values are summarized in Table 5.20.

The variance of the adjusted scaled C-q distributions was then calculated by numerical integration using a manner similar to that of the mass flux calculations. The variance is plotted with longitudinal distance, x, shown in Figure 5.24 and summarized in Table 5.21. From this figure the transverse factor of diffusion, D, can be determined as

half the slope of a straight line fitted to the data points. It is evident that the results can be broken down into three main sections. A rather steep slope characterizes the first section from Station 40 to Station 160; a relatively flat slope characterizes the second section spanning from Station 160 to Station 1000; the third section exhibits a steep slope from Station 1000 to the end of the study area.

Linear trendlines were fit to each section and the factor of diffusion calculated shown in Figure 5.25. A transverse factor of diffusion was not calculated for the first section. It is suspected that buoyancy effects are evident based on the separation of the depth averaged and surface concentrations that were observed at Station 80. The depth, velocity magnitude, and shear velocity for each concentration point were determined from the hydrodynamic model. These values were then averaged for the three sections in order to compute the transverse mixing coefficient and the dimensionless transverse mixing coefficient and are summarized in Table 5.22.

These values can be explained in combination with a plot of the cumulative discharge shown in Figure 3.27. The first section occurs between Stations 40 and 160 and is represented by the initial transverse spreading. It is suspected that buoyancy effects are still predominant in this section which is causing the rapid mixing of the plume. The effluent water coming out of the outfall is at a temperature of about 16.5 °C, which is significantly warmer than the ambient river temperature of about 0 °C. The cumulative discharge distribution between these stations shows a spreading of the distribution.

The second relatively flat portion of Figure 5.25 occurs between Stations 160 and 1000. A best-fit line to the data predicted a slope of -0.0004. As can be seen in Figure 3.27, between Station 160 and just before Station 1000 the cumulative discharge distribution shows straight rather widely separated streamtubes with approximately 16% of the flow taking up about 30% of the flow width. This would indicate that very little mixing is being induced in the flow and that spreading of the plume is occurring rather slowly.

The third section occurs downstream of Station 1000. Referring to Figure 3.27, it is evident that the cumulative discharge distribution in this section shows a number of expansions and contractions or curvature in the flow. The first contraction occurs right at the pedestrian bridge where the internal flow curvature is analogous to a very tight bend before hitting an alluvial deposit, which causes the distribution to expand. This flow pattern would cause a significant amount of turbulence as eddies would form at this location thereby enhancing the transverse mixing. After the flow expands, it is forced to contract again as it enters the bend. The bend would also enhance the mixing of the effluent with the presence of strong secondary currents.

These mixing coefficients fall within the range of transverse mixing coefficients cited in the literature for the North Saskatchewan River at Edmonton.

5.5 SENSITIVITY ANALYSIS

A sensitivity analysis was performed to test the effect of the error of the velocity profiles on the cumulative discharge distributions and in turn the effect of the cumulative discharge distribution on the calculated transverse mixing coefficients. In other words, evaluate how well the velocity needs to be known in order to evaluate the mixing characteristics of the reach.

Modeling of November 7 was chosen to evaluate the sensitivity to velocity error as much of the mixing occurred within the section of the reach that was sampled on that date. A total of ten cases were compared, including the final case described above. The files referred to as "step_" involved mesh refinement while the files referred to as "case_" involved bed roughness changes. Table 5.23 summarizes the roughness configurations used for each case. The files were as follows:

I. Step 1: Mesh with 5077 nodes , Roughness 1
II. Step 2: Mesh with 6407 nodes, Roughness 1

III. Step 3: Mesh with 14787 nodes, Roughness 1
IV. Step 4: Mesh with 22211 nodes, Roughness 1
V. Case 1: Mesh with 37553 nodes, Roughness 1, and bank roughness of 0.01
VI. Case 2: Mesh same as Case 1, Roughness 1, and bank roughness of 0.05 m
VII. Case 3: Mesh same as Case 1, Roughness 1, and bank roughness of 0.07 m
VIII. Case 4: Mesh same as Case 1, Roughness 2, and bank roughness of 0.07 m
IX. Case 5: Mesh same as Case 1, Roughness 2, and a bank roughness of 0.15 m
X. Final model: Mesh with 63424 nodes, Roughness 1 with a varied bank roughness along south bank of 0.45 m for the first 100 m downstream of the outfall, 0.01 m from 200 m downstream of the outfall to the end of the study area and a roughness along the north bank of 0.05 m from 850 m downstream of the outfall to the end.

First the velocity profiles were compared for all the stations taken on November 7: 80, 320, 1000, 1500, and the end station shown in Figures 5.26 to 5.30. The error of the modeled velocity profiles were calculated and are summarized in Table 5.24. The error for Station 80 ranged between 23% and 36%, Station 320 between 13% and 24%, Station 1000 between 16% and 21%, Station 1500 between 30% and 46%, and the end Station between 9% and 34%. Overall the average error for "step 2" modeling was the worst and the "final model" the best. The profiles generated from each case generally followed a similar pattern with the greatest difference being noticed in the bank areas.

The concentration-cumulative discharge distributions were then compared for the ten cases. No adjustments were made to any of the distributions so that a true comparison could be made. Figures 5.31 to 5.36 illustrate the distributions for the different cases. Stations 80, 320, 640 and 1000 saw the greatest change in cumulative discharge distribution with little to no effect on Stations 1500 and the end station. At each station, the spread of the cumulative discharge was ranked from the most compact to the most wide-spread and was compared to the error in the modeled velocity profile as shown in Figure 5.37. Linear trendlines were fitted to the data in order to determine the slope of the relationship. With the exception of Station 80, it was observed that the spread of the

cumulative discharge distribution increased with a decrease in the error of the velocity profile. As buoyancy effects are suspected to be dominant at station 80, it was neglected for the remainder of the sensitivity analysis. An indication of the spread of the cumulative discharge distribution is the computed mass flux. The greater the spread, the higher the mass flux would be. The mass flux was ranked from lowest to highest and was correlated with the error of the velocity profiles shown in Figure 5.38. Linear trendlines were fit to the data to get an idea of the slope of the trend. Again, it was found that lower errors in velocity profiles were correlated with higher mass fluxes.

The variances of the C-q distributions were calculated with no adjustments similar to the mass flux. The variances were correlated with the mass flux shown in Figure 5.39. As would be expected, a higher mass flux resulted in a higher variance. This indicates that a lower error in velocity profile would result in a higher variance calculation. Table 5.25 summarizes the velocity, mass flux and variance data for all cases tested.

The variances were plotted as function of longitudinal distance as shown in Figure 5.40. All cases followed a similar pattern and the study area was broken into two sections as in the analysis in the previous section; the first section between Station 320 and 1000 and the second section from Station 1000 to the end. Linear trendlines were fitted to each case in order to determine the transverse factors of diffusion as shown in Figures 5.41 and 5.43. The equations of each trendline are displayed in the same order that the data appears in the tables. The transverse factors of diffusion were calculated as half the slope of the best fit line. The first section the calculated transverse factors of diffusion ranged between -0.026 and 0.0002 with –0.0009 on average. The second section the calculated transverse factors of diffusion ranged between 0.0502 and 0.0581 with 0.0546 on average.

The transverse mixing coefficient and dimensionless transverse mixing coefficient were calculated for each case using plume averaged local hydraulic conditions from each modeled case. The transverse mixing coefficient for the first section ranged between -0.019 and 0.001 with -0.005 on average. The range for the second section was 0.141 to

0.164 with 0.149 on average. Table 5.26 and 5.27 summarizes the calculated transverse factors of diffusion and transverse mixing coefficients.

The value of the transverse mixing coefficient is not highly correlated with the overall error as shown in Figures 5.43 and 5.44. In the first section, the minimum transverse mixing coefficient is associated with the highest overall error in step 2. Conversely in the second section, the maximum transverse mixing coefficient is associated with the highest overall error in step 2. The transverse mixing coefficient was also compared to the average error over the section of interest. Again, there was little correlation between the two. This would suggest that the error in the velocity profile has little effect on the calculated transverse mixing coefficient.

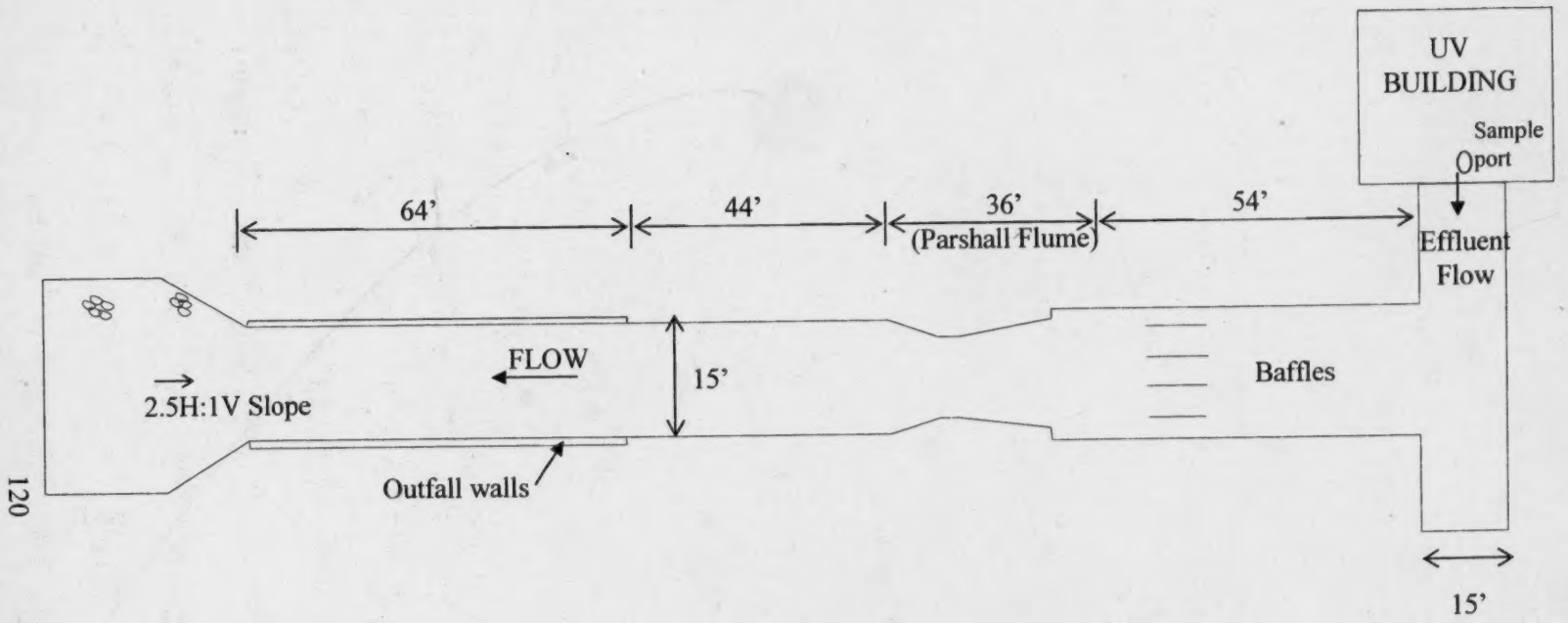

Figure 5.1: Input location in plan view.

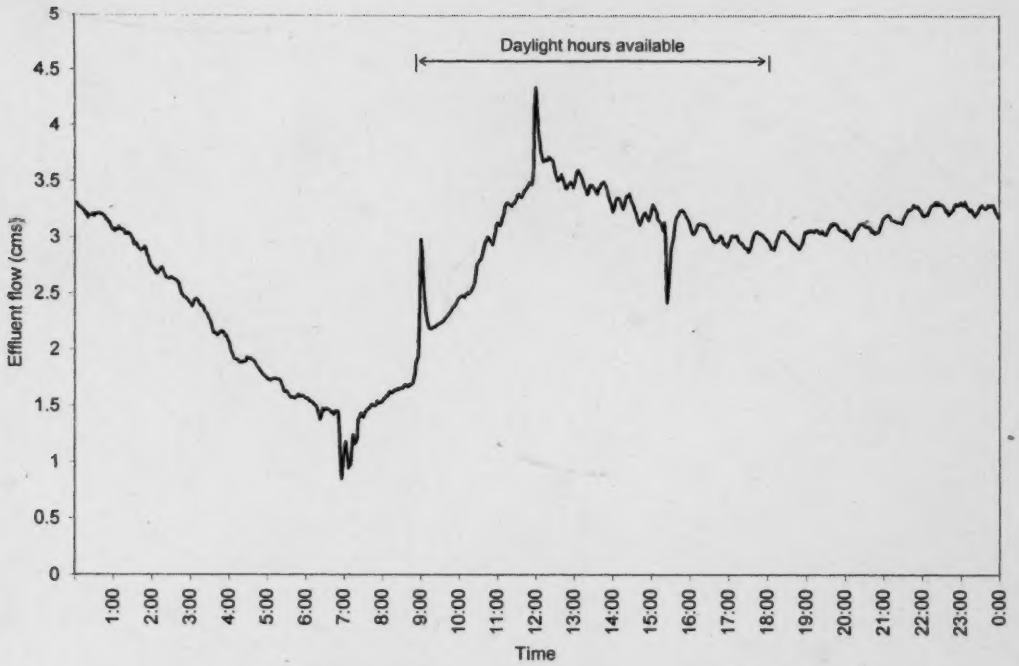

Figure 5.2: Typical effluent flow for weekday in October.

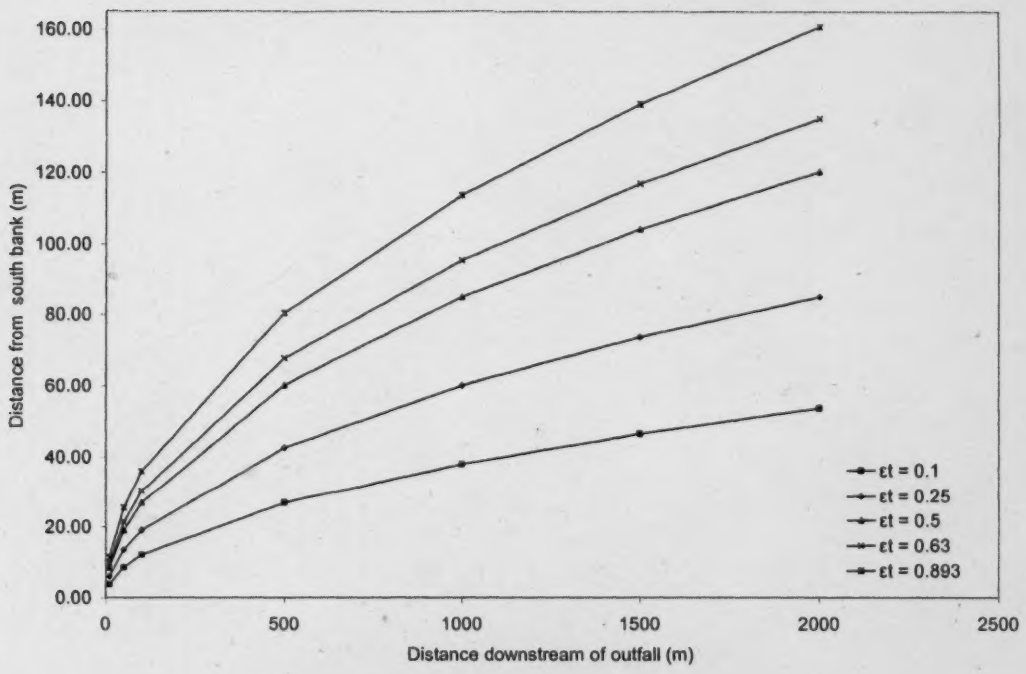

Figure 5.3: Preliminary Plume estimates.

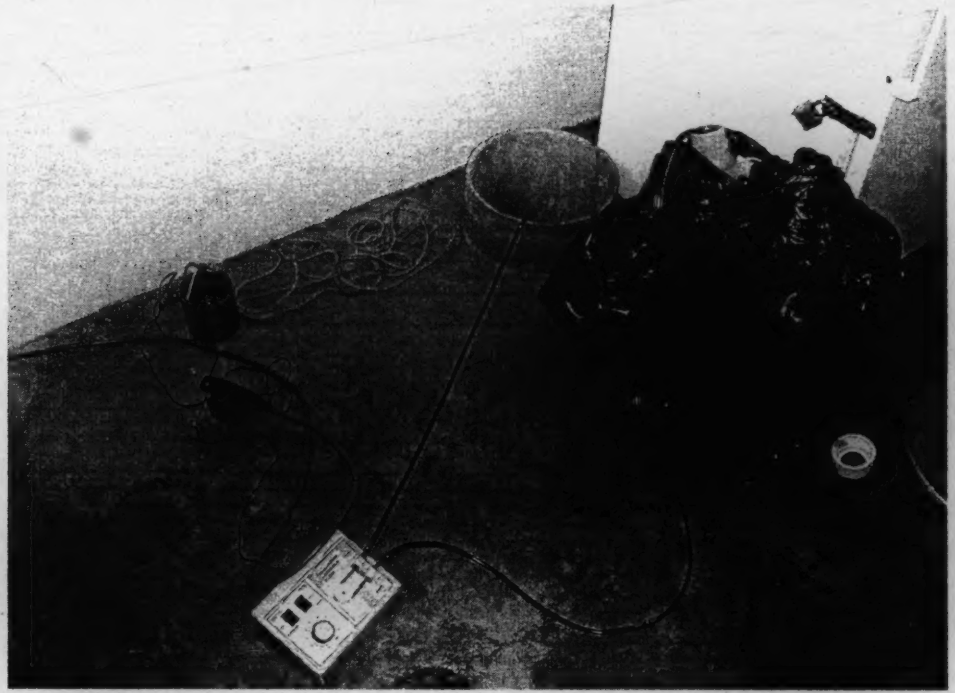

Figure 5.4: Dye injection set up.

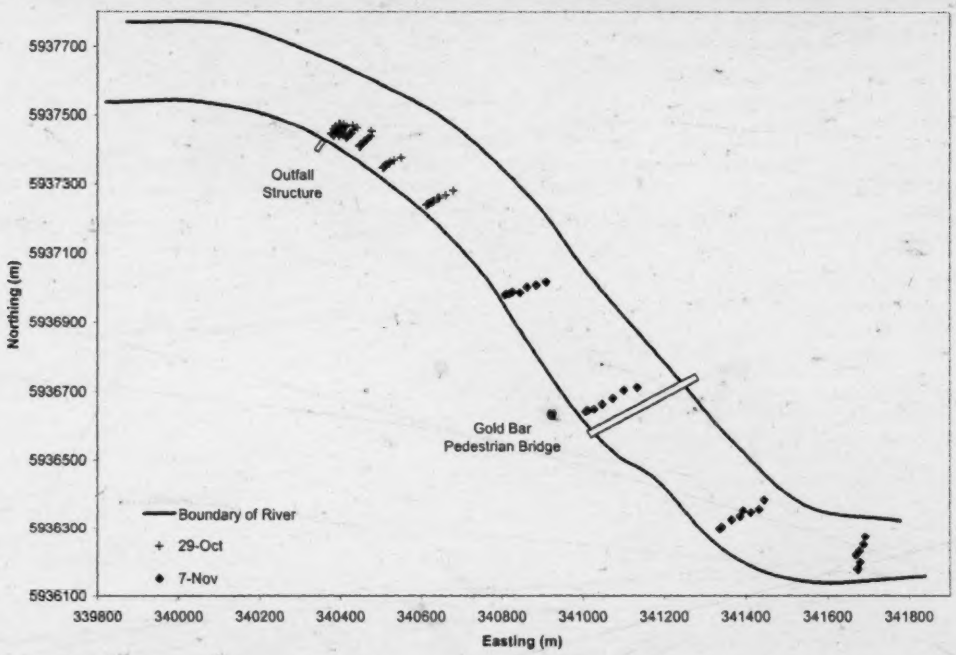

Figure 5.5: Locations of samples collected October 29 and November 7, 2002.

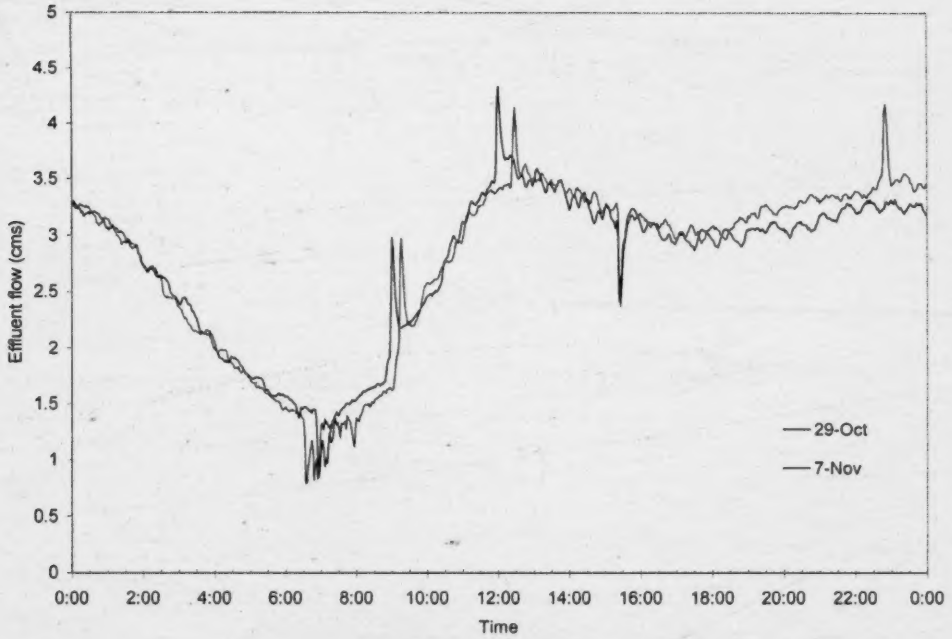

Figure 5.6: Effluent flow on test days.

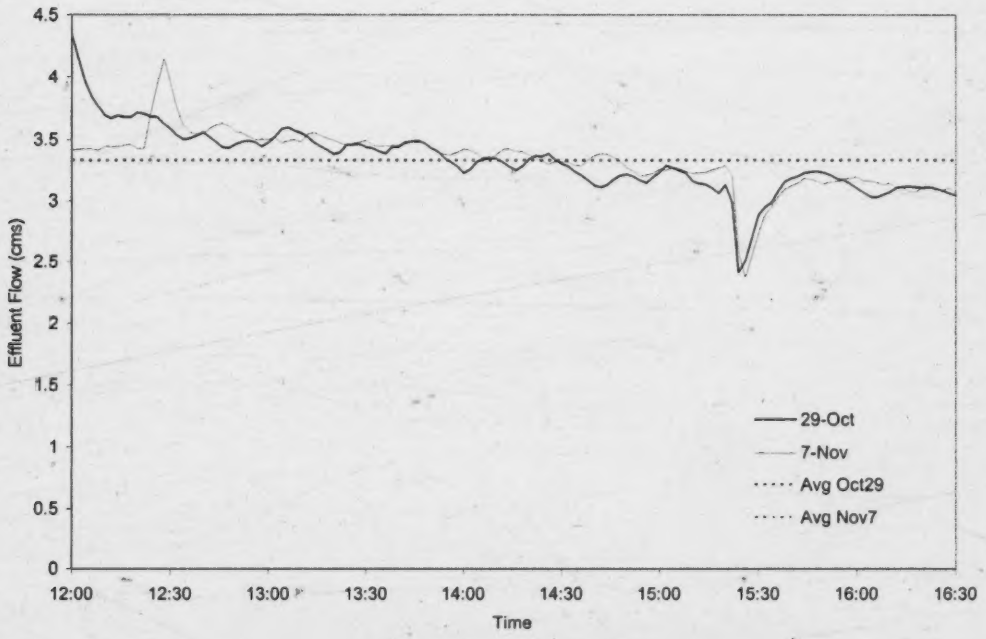

Figure 5.7: Effluent flow during dye tests.

Table 5.1: Summary of calibration curve investigation.

	5 point Calibration using 5000, 2500, 1000, 500, 100 plus blank		3 point Calibration using 5000, 500, 100 plus blank		2 point Calibration using 5000, 100 plus blank	
Actual Concentration (ppt)	**Concentration (ppt)**	**Error (%)**	**Concentration (ppt)**	**Error (%)**	**Concentration (ppt)**	**Error (%)**
5000	4921.54	-1.57	4982.71	-0.35	5235.28	4.71
2500	2225.51	-10.98	2230.19	-10.79	2450.77	-1.97
1000	936.18	-6.38	906.11	-9.39	985.89	-1.41
750	776.29	3.51	737	-1.73	785.39	4.72
500	538.15	7.63	488.74	-2.25	523.51	4.70
250	300.02	20.01	251.26	0.50	259.58	3.83
100	163.94	63.94	107.34	7.34	104.09	4.09
50	123.11	146.22	62.37	24.74	57.04	14.08
0	82.29		19.19		5.89	
Average Absolute Error		***32.53***		***7.14***		***4.94***

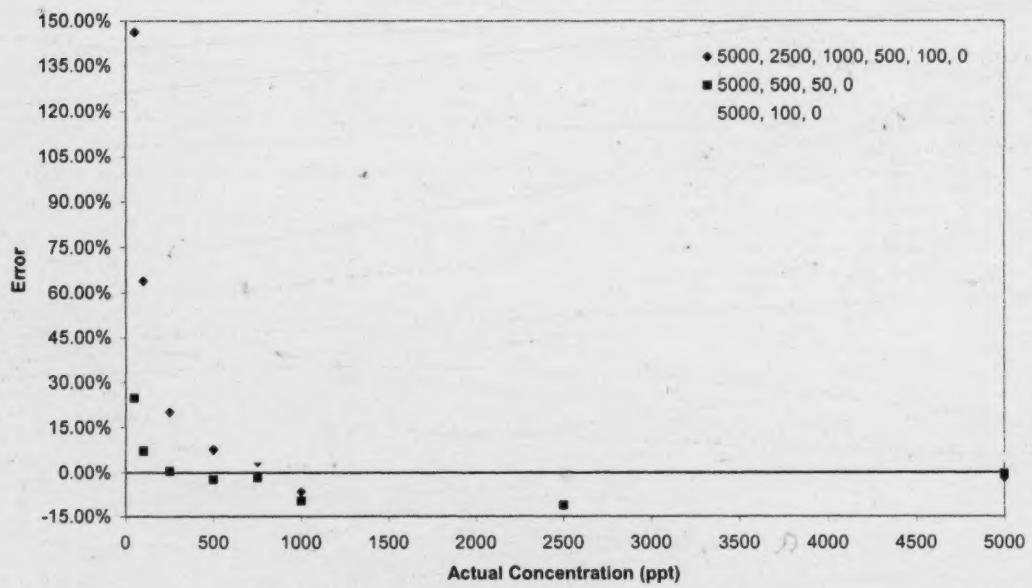

Figure 5.8: Error of calibration curves.

Table 5.2: Calibration standards used for sample analysis.

Initial Concentration (ppt)	Mass of Initial Concentration (g)	Final Mass of Solution (g)	Final Concentration (ppt)
100 000	4.9999	100.0088	**4999.46**
100 000	0.4997	19.9995	**2498.56**
100 000	1.0044	99.9954	**1004.45**
4999.46	3.0023	20.0017	**750.43**
4999.46	2.0018	19.9947	**500.53**
1000.45	4.9967	20.0069	**250.86**
1000.45	2.0029	20.0251	**100.46**
500.53	1.9994	19.9906	**50.06**

Table 5.3: Error from cuvet selection procedure.

Actual Concentration (ppt)	3 point Calibration Curve using 5000, 500, 50, 0				2 point Calibration Curve using 5000, 100, and 0			
	Standard Concentration (ppt)	Error (%)	Clear Concentration (ppt)	Error (%)	Standard Concentration (ppt)	Error (%)	Clear Concentration (ppt)	Error (%)
5000	4982.71	*-0.35*	4364.43	*-12.71*	5235.28	4.71	5048.23	0.96
2500	2230.19	*-10.79*	2240.03	*-10.40*	2450.77	-1.97	2529.17	1.17
1000	906.11	*-9.39*	927	*-7.30*	985.89	-1.41	939.69	-6.03
750	737	*-1.73*	753.13	*0.42*	785.39	4.72	823.49	9.80
500	488.74	*-2.25*	476.04	*-4.79*	523.51	4.70	536.29	7.26
250	251.26	*0.50*	191.7	*-23.32*	259.58	3.83	183.31	-26.68
100	107.34	*7.34*	43.19	*-56.81*	104.09	4.09	100	0.00
50	62.37	*24.74*	-2.09	*-104.18*	57.04	14.08	-31.54	-163.08
0	19.19		26.89		5.89		-20.58	
Average Absolute Error		***7.14***		***27.49***		***4.94***		***26.87***

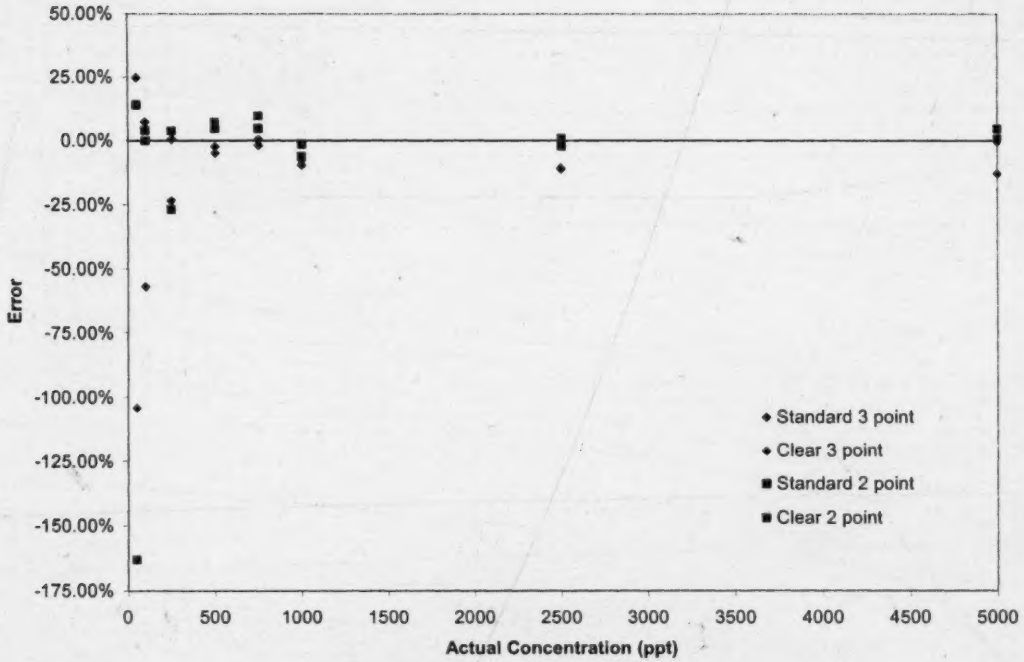

Figure 5.9: Cuvet Selection.

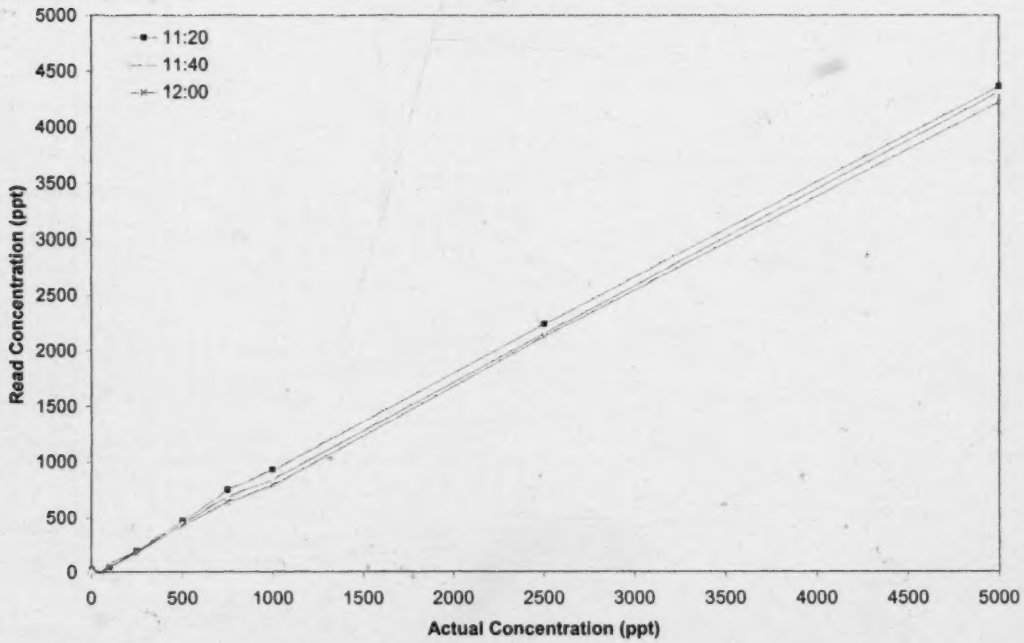

Figure 5.10: Decreasing fluorescence with consecutive readings.

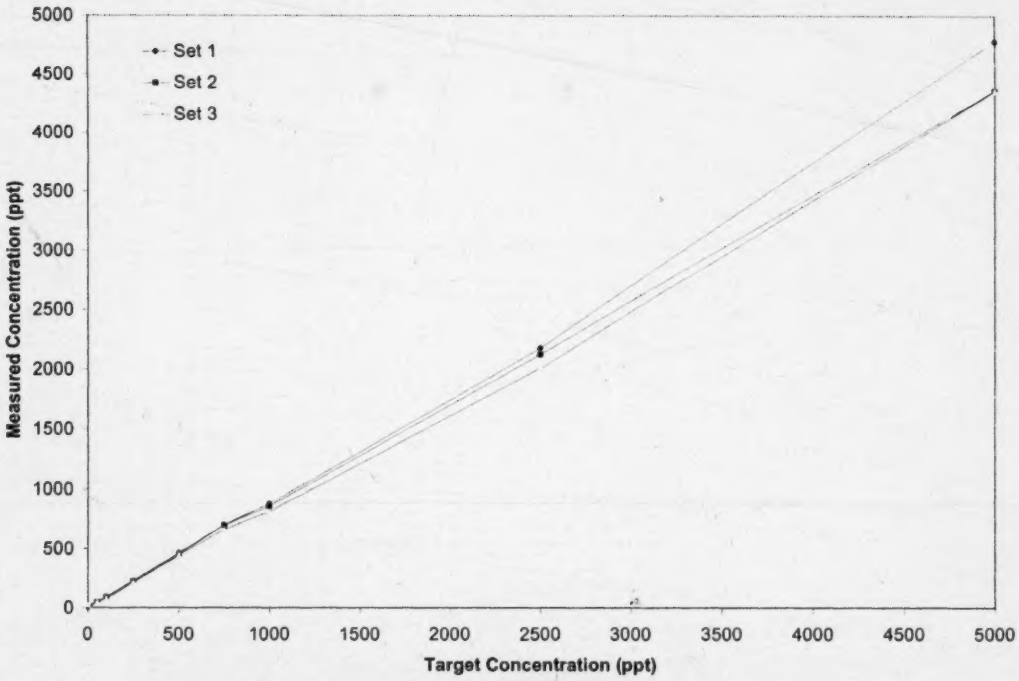

Figure 5.11: Decreasing fluorescence with subsequent sets.

Table 5.4: Accuracy check.

Actual Concentration (ppt)	Read Concentration (ppt)	Error (%)
2498.56	2457.77	-1.63
1004.45	962.93	-4.13
750.43	772.45	2.93
500.53	478.36	-4.43
250.86	251.32	0.18
50.06	56.27	12.40
Average Absolute Error		**4.29**

Table 5.5: Blank samples.

BLANK RIVER 1 (ppt)	47.13	34.59	38.24	33.48	31.5	31.1	27.57
BLANK RIVER 2 (ppt)	42.56	34.59	35.28	26.51	24.01	29.69	28.97
BLANK EFFLUENT 1 (ppt)	598.74	576.14	510.69	520.2	492.55	494.53	
BLANK EFFLUENT 2 (ppt)	589.6	586.41	523.24	526.2	508.12	501.35	

Table 5.6: Effluent samples.

October 29, 2002		November 7, 2002	
Time taken	Concentration (ppt)	Time taken	Concentration (ppt)
13:30	2537.01	13:00	2800.62
14:00	2756.43	13:30	2535.48
14:30	2870.72	14:10	2604.05
15:00	2564.44	14:40	2838.72
15:30	2661.96	15:20	3202.91
16:00	2527.86	16:00	2946.91
16:30	2573.58	16:30	2899.67
Average	**2641.71**	**Average**	**2832.62**

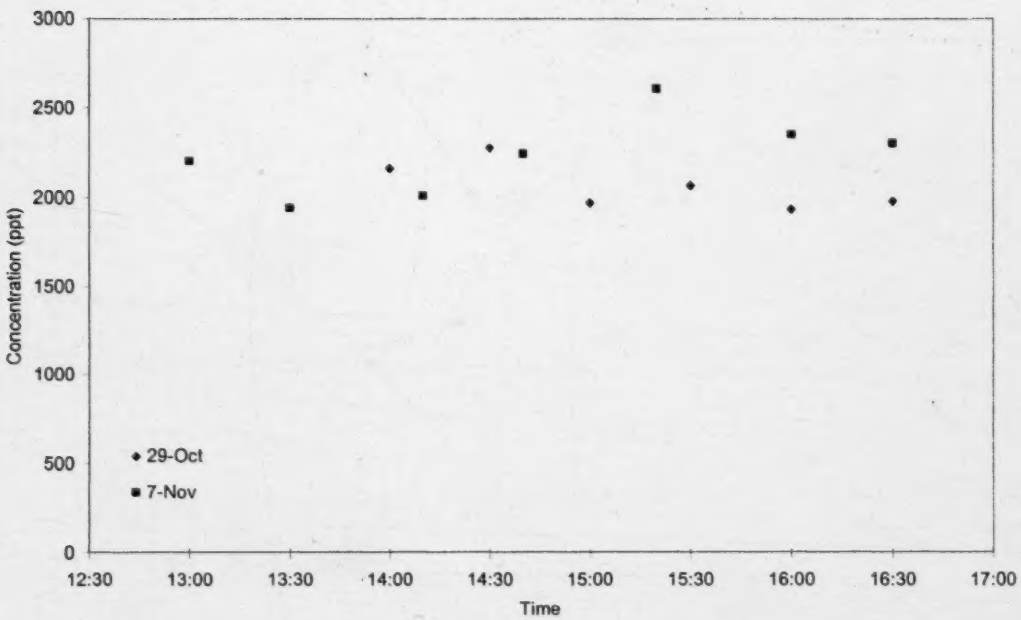

Figure 5.12: Effluent samples collected throughout dye tests.

Table 5.7: River samples collected October 29, 2002.

Depth Sample Number	Concentration (ppt)	Surface Sample Number	Concentration (ppt)
D5	2614.72	S2	2271.87
D7	2416.63	S3	2779.29
D9	1898.54	S4	2226.15
D12	2188.06	S5	2572.05
D14	2683.29	S8	2515.67
D15	2585.77	S9	2559.86
D18	1666.92	S11	2268.82
D19	2418.15	S13	2637.58
D21	2626.91	S14	2473.01
D22	2657.39	S15	2223.11
D23	2556.82	S16	2634.53
D24	2793.01	S18	2146.92
D27	1930.54	S20	2492.82
D28	2521.77	S23	2221.58
D29	1179.31	S24	2259.68
D30	2250.53	S27	1087.88
D41	2590.34	S28	2572.05
D42	2264.25	S33	1947.3
D43	1404.83	S34	2348.06
D44	2613.2	S35	1381.97
D46	1092.45	S36	2134.73
D47	2626.91	S38	1586.16
D48	2226.15	S40	2299.3
D50	2704.63	S41	2547.67
D53	121.79	S42	1138.16
D54	83.7	S44	1878.73
D55	39.51	S45	2730.53
D56	48.65	S47	2157.58
D57	1979.3	S49	2602.53
D58	2601.01	S50	2509.58
D61	1752.25	S51	152.27
D63	2341.96	S53	24.27
D66	1627.3	S54	28.84
D68	2587.29	S58	2524.82
D69	42.56	S59	1308.83
D70	2488.25	S60	24.27
D75	946.17	S64	27.32
D76	59.32	S68	1119.88
D77	33.41	S69	27.32
D78	36.46	S70	1461.21
D79	39.51	S71	27.32
D80	2372.44	S72	2294.72
D82	536.27	S73	30.37
D83	2715.29	S75	25.79
D84	2556.82	S76	24.27
D85	1007.12	S77	86.75
D86	805.98	S78	489.03
D87	34.94	S79	24.27

Depth Sample Number	Concentration (ppt)	Surface Sample Number	Concentration (ppt)
D88	956.83	S80	1115.31
D89	271.13	S84	2520.25
D90	45.6	S85	2544.63
D92	31.89	S86	2690.91
D93	1014.74	S87	22.75
D94	28.84	S89	47.13
D95	2451.68	S90	2189.58
D96	33.41	S91	2505.01
D97	2605.58	S92	2593.39
D99	2233.77	S93	265.03
D100	289.41	S95	25.79
		S96	2681.77
		S97	2608.63
		S98	1886.35
		S99	2881.39
		S100	2532.44

Table 5.8: River samples collected November 7, 2002.

Depth Sample Number	Concentration (ppt)	Surface Sample Number	Concentration (ppt)
D2	21.22	S1	28.84
D3	18.18	S6	62.37
D4	24.27	S7	19.7
D6	25.79	S12	27.32
D8	22.75	S17	444.84
D10	27.32	S19	22.75
D11	700.84	S22	27.32
D13	27.32	S25	19.7
D20	837.98	S26	22.75
D25	27.32	S29	21.22
D31	27.32	S30	1295.11
D33	25.79	S31	24.27
D34	22.75	S32	24.27
D35	21.22	S39	24.27
D36	21.22	S43	21.22
D37	25.79	S52	1578.54
D38	47.13	S55	1811.68
D39	30.37	S56	1420.07
D40	421.98	S57	1752.25
D45	1334.73	S62	1874.16
D51	18.18	S63	862.36
D52	92.84	S65	1587.68
D59	694.74	S67	31.89
D62	868.45	S74	269.6
D64	1406.35	S81	187.32
D65	1328.64	S82	706.93
D67	1729.4	S83	1276.83
D68	1659.3	S88	1037.59

Depth Sample Number	Concentration (ppt)	Surface Sample Number	Concentration (ppt)
D71	191.89	S94	649.03
D72	1607.49	S101	18.18
D73	673.41	S102	62.37
D74	1854.35	S104	833.41
D81	1403.3	S105	74.56
D98	1176.26	S106	22.75
D102	324.46	S107	1302.73
D103	1545.02	S108	22.75
D104	528.65	S109	1645.59
D105	101.98	S110	1587.68
D106	22.75	S111	1700.44
D108	329.03	S112	1247.88
D109	1737.02	S113	22.75
D110	22.75	S114	246.74
D113	24.27	S115	804.45
D114	554.55	S116	1860.44
D116	830.83	S117	21.22
D119	1563.3	S118	543.88
D120	59.32	S119	25.79
		S122	1689.78
		S123	1738.54
		S124	158.36
		S124	716.07
		S125	1967.11

Table 5.9: Dilution Set One.

Initial Concentration	Mass of Final Concentration (g)	Total Mass (g)	Final Concentration
890.86	2.01	20.09	8.91 ppb
8.91	1.00	19.97	178.23 ppb
178.23	1.00	20.02	3564.06 ppb
3564.06	1.00	19.98	71.28 ppm
71.28	1.01	20.10	1.43 g/L
1.43	1.00	19.97	**28.51 g/L**

Table 5.10: Dilution Set Two.

Initial Concentration	Mass of Final Concentration (g)	Total Mass (g)	Final Concentration
1450.02	1.00	99.81	145.31 ppb
145.31	1.00	99.64	14.53 ppm
14.53	1.02	101.49	1452.55 ppm
1452.55	1.00	20.00	**29.03 g/L**

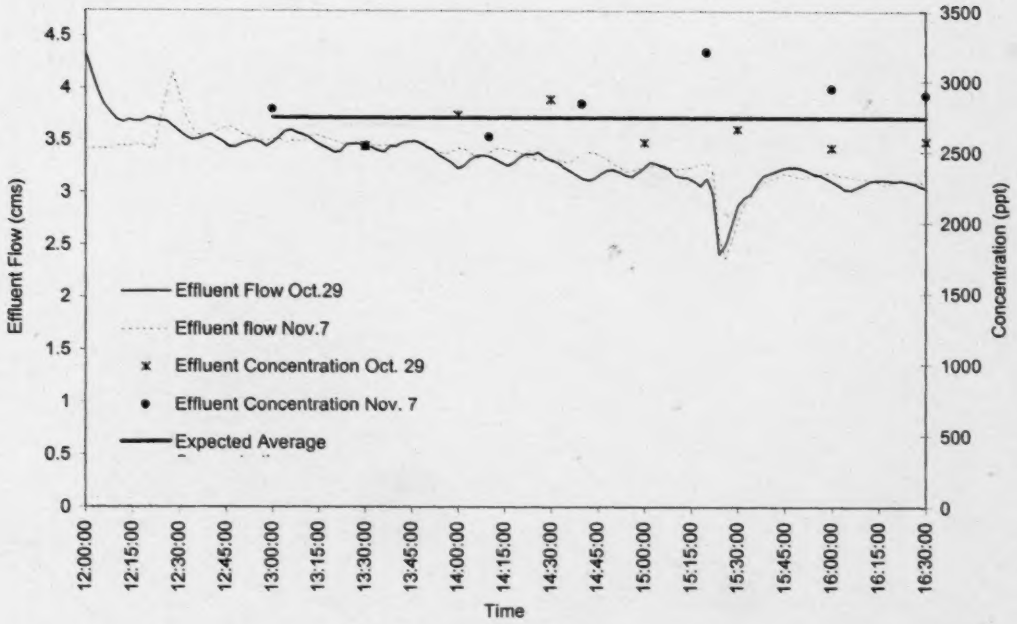

Figure 5.13: Expected average effluent concentration with measured effluent concentrations.

Table 5.11: Recovery ratio summary.

SAMPLE	AVERAGE CONCENTRATION (ppt)	RECOVERY RATIO (%)
Blank River	34.59	-
Blank Effluent	581.28	-
2500 River	1646.86	66.01
1000 River	683.75	67.44
500 River	361.73	66.99
2500 Effluent	3095.92	102.96
1000 Effluent	1570.02	102.72
500 Effluent	1060.65	98.16

Table 5.12: River water recovery check.

SAMPLE	AVERAGE CONCENTRATION (ppt)	RECOVERY RATIO (%)
Blank River	36.76	-
2500 River	1821.85	72.60
1000 River	731.54	69.71
Blank River	30.00	-
2500 River	1811.13	72.16
2500 River using pure dye	1733.7	69.02

Table 5.13: 2500 ppt Standard Recovery Ratio Combinations.

SAMPLE	River water (%)	Average Concentration (ppt)	Average Background Concentration (ppt)	Recovery (%)
Blank River	0	30.00	-	-
Blank Effluent	0	516.97	-	-
River	100	1811.13	30.00	72.16
75% River / 25% Effluent	75	2434.15	151.74	92.47
50% River / 50% Effluent	50	2728.57	273.48	99.46
25% River / 75% Effluent	25	2893.91	395.22	101.23
87.5% River / 12.5% Effluent	87.5	2130.22	90.87	81.80
95% River / 5% Effluent	95	1971.32	54.34	76.97
Effluent	0	3095.92	516.97	102.96
75% River / 25% Distilled	75	1855.89	22.50	73.56
50% River / 50% Distilled	50	1957.82	15.00	77.93
25% River / 75% Distilled	25	2063.51	7.50	82.49
100% DISTILLED	0	2431.54	0.00	97.53
River added to Effluent (5% E)	95	1732.99	54.34	67.87
River added to Effluent (5% E)	95	2449.95	54.34	96.64
Effluent added to River (5% E)	95	1711.86	54.34	67.02
Effluent added to River (5% E)	95	1718.9	54.34	67.31

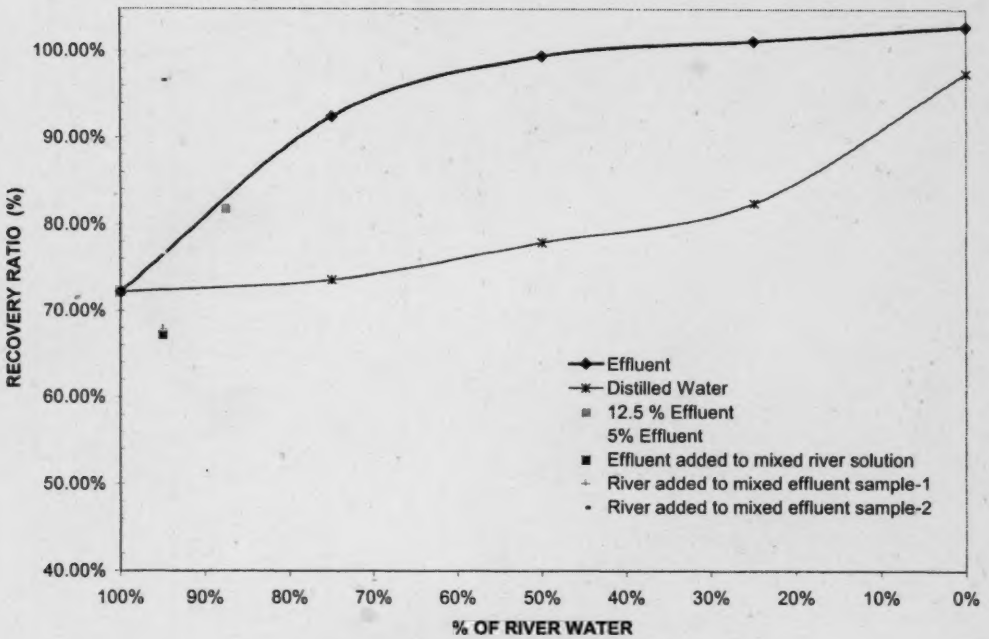

Figure 5.14: Recovery ratio plot.

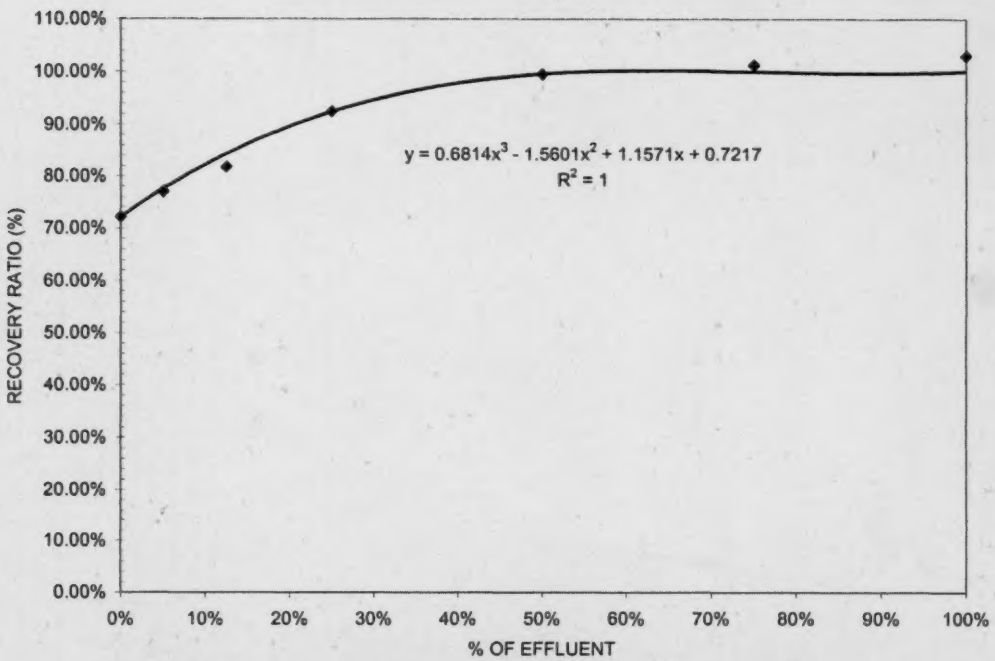

Figure 5.15: Recovery ratio with third order polynomial fit.

Table 5.14: October 29, 2002 Recovery Ratio Corrected Depth Averaged Samples.

Depth Sample Number	East	North	Transverse Distance (m)	Depth Concentration less river background (ppt)	Recovery Ratio (%)	Recovery Ratio Adjusted Depth Concentration less background (ppt)
Station 0						
D83	340377	5937446	0.00	2680.35	100	2683.85
D80	340382	5937459	13.43	2337.50	100	2345.93
D66	340387	5937468	23.76	1592.36	100	1590.79
D100	340397	5937475	34.71	254.47	83	305.70
D55	340399	5937475	36.41	4.57	72	6.31
Station 10						
D47	340383	5937442	1.26	2591.97	100	2599.36
D41	340384	5937444	2.97	2555.40	100	2563.78
D14	340384	5937444	3.43	2648.35	100	2653.52
D97	340385	5937446	5.45	2570.64	100	2578.65
D58	340389	5937452	12.81	2566.07	100	2574.20
D70	340391	5937458	18.33	2453.31	100	2462.80
D99	340398	5937461	25.62	2198.83	100	2204.05
D99	340398	5937461	25.83	2198.83	100	2204.05
D54	340408	5937474	41.36	48.76	75	65.16
Station 20						
D15	340397	5937442	1.77	2550.83	100	2559.31
D7	340397	5937443	3.68	2381.69	100	2390.76
D22	340398	5937445	5.59	2622.45	100	2628.75
D84	340403	5937450	11.78	2521.88	100	2530.88
D57	340406	5937457	19.31	1944.36	100	1943.04
D75	340411	5937464	28.50	911.23	96	945.88
D90	340415	5937468	33.88	10.66	73	14.65
D78	340430	5937471	46.58	0.00	72	0.00
Station 40						
D23	340416	5937436	3.57	2521.88	100	2530.88
D21	340418	5937438	6.45	2591.97	100	2599.36
D5	340419	5937440	8.08	2579.78	100	2587.54
D28	340420	5937441	10.15	2486.83	100	2496.20
D63	340425	5937446	16.56	2307.02	100	2314.87
D95	340426	5937448	18.39	2416.74	100	2426.12
D76	340432	5937457	29.50	24.38	74	33.15
D92	340441	5937462	39.95	0.00	72	0.00
Station 80						
D50	340448	5937411	2.87	2669.69	100	2673.78
D24	340450	5937412	4.89	2758.07	100	2757.80
D44	340452	5937414	7.65	2578.26	100	2586.06
D42	340453	5937416	9.88	2229.31	100	2235.34
D61	340458	5937423	18.42	1717.31	100	1714.16
D88	340460	5937425	21.40	921.89	96	955.79
D86	340464	5937427	25.91	771.04	95	815.12
D56	340469	5937433	33.05	13.71	73	18.80
D96	340474	5937440	41.60	0.00	72	0.00
D87	340477	5937453	53.92	0.00	72	0.00

Depth Sample Number	East	North	Transverse Distance (m)	Depth Concentration less river background (ppt)	Recovery Ratio (%)	Recovery Ratio Adjusted Depth Concentration less background (ppt)
Station 160						
D19	340507	5937349	2.52	2383.21	100	2392.29
D48	340509	5937351	5.56	2191.21	100	2196.22
D9	340511	5937353	7.86	1863.60	100	1861.01
D18	340513	5937355	11.25	1631.98	100	1629.70
D93	340521	5937360	19.86	979.80	97	1009.65
D85	340522	5937364	23.86	972.18	97	1002.56
D82	340533	5937369	34.78	501.33	90	557.96
D69	340550	5937377	53.51	7.62	73	10.50
Station 320						
D30	340614	5937241	2.45	2215.59	100	2221.26
D12	340616	5937242	5.22	2153.12	100	2157.07
D27	340620	5937244	8.93	1895.60	100	1893.44
D43	340624	5937247	13.97	1369.89	100	1375.83
D29	340627	5937249	17.89	1144.37	98	1163.03
D46	340630	5937250	21.39	1057.51	98	1081.96
D89	340641	5937259	34.73	236.19	83	285.84
D53	340644	5937260	38.79	86.85	77	113.25
D79	340660	5937268	56.18	4.57	72	6.31
D77	340679	5937282	80.11	0.00	72	0.00

Table 5.15: October 29, 2002 Recovery Ratio Corrected Surface Samples.

Surface Sample Number	East	North	Transverse Distance (m)	Surface Concentration less river background (ppt)	Recovery Ratio (%)	Recovery Ratio Adjusted Surface Concentration less background (ppt)
Station 0						
S99	340377	5937446	0	2852.33	100	2852.04
S86	340382	5937459	13.43	2661.85	100	2666.34
S70	340387	5937468	23.76	1432.15	100	1435.41
S51	340397	5937475	34.71	123.21	78	157.32
S89	340399	5937475	36.41	18.07	73	24.68
Station 10						
S40	340382	5937441	0	2270.24	100	2277.28
S49	340383	5937442	1.26	2573.47	100	2581.40
S8	340384	5937444	2.97	2486.61	100	2495.98
S41	340384	5937444	3.43	2518.61	100	2527.65
S85	340385	5937446	5.45	2515.57	100	2524.65
S96	340389	5937452	12.81	2652.71	100	2657.66
S58	340391	5937458	18.33	2495.76	100	2505.06
S90	340398	5937461	25.62	2160.52	100	2164.67
S90	340398	5937461	25.83	2160.52	100	2164.67
S73	340408	5937474	41.36	1.31	72	1.81
Station 20						
S24	340396	5937440	0	2230.62	100	2236.68
S14	340397	5937442	1.77	2443.95	100	2453.43

Surface Sample Number	East	North	Transverse Distance (m)	Surface Concentration less river background (ppt)	Recovery Ratio (%)	Recovery Ratio Adjusted Surface Concentration less background (ppt)
S20	340397	5937443	3.68	2463.76	100	2473.23
S16	340398	5937445	5.59	2605.47	100	2612.41
S97	340403	5937450	11.78	2579.57	100	2587.33
S84	340406	5937457	19.31	2491.19	100	2500.52
S59	340411	5937464	28.50	1279.77	99	1290.28
S64	340415	5937468	33.88	0.00	72	0.00
S69	340430	5937471	46.58	0.00	72	0.00
Station 40						
S2	340414	5937433	0	2242.81	100	2249.18
S50	340416	5937436	3.57	2480.52	100	2489.93
S5	340418	5937438	6.45	2542.99	100	2551.63
S9	340419	5937440	8.08	2530.80	100	2539.66
S28	340420	5937441	10.15	2542.99	100	2551.63
S100	340425	5937446	16.56	2503.38	100	2512.60
S91	340426	5937448	18.39	2475.95	100	2485.38
S60	340432	5937457	29.50	0.00	72	0.00
S71	340441	5937462	39.95	0.00	72	0.00
Station 80						
S4	340447	5937409	0	2197.09	100	2202.26
S45	340448	5937411	2.87	2701.47	100	2703.69
S3	340450	5937412	4.89	2750.23	100	2749.95
S13	340452	5937414	7.65	2608.52	100	2615.35
S11	340453	5937416	9.88	2239.76	100	2246.05
S72	340458	5937423	18.42	2265.66	100	2272.59
S92	340460	5937425	21.40	2564.33	100	2572.50
S98	340464	5937427	25.91	1857.29	100	1854.62
S53	340469	5937433	33.05	0.00	72	0.00
S76	340474	5937440	41.60	0.00	72	0.00
S95	340477	5937453	53.92	0.00	72	0.00
Station 160						
S15	340505	5937348	0	2194.05	100	2199.13
S34	340507	5937349	2.52	2319.00	100	2327.09
S47	340509	5937351	5.56	2128.52	100	2131.78
S33	340511	5937353	7.86	1918.24	100	1916.44
S38	340513	5937355	11.25	1557.10	100	1556.32
S80	340521	5937360	19.86	1086.25	98	1108.74
S68	340522	5937364	23.86	1090.82	98	1113.01
S78	340533	5937369	34.78	459.97	89	517.26
S79	340550	5937377	53.51	0.00	72	0.00
Station 320						
S36	340612	5937239	0	2105.67	100	2108.29
S23	340614	5937241	2.45	2192.52	100	2197.56
S18	340616	5937242	5.22	2117.86	100	2120.82
S44	340620	5937244	8.93	1849.67	100	1846.92
S35	340624	5937247	13.97	1352.91	100	1359.65
S42	340627	5937249	17.89	1109.10	98	1130.06
S27	340630	5937250	21.39	1058.82	98	1083.18
S93	340641	5937259	34.73	235.97	83	285.60
S77	340644	5937260	38.79	57.69	75	76.62
S54	340660	5937268	56.18	0.00	72	0.00
S87	340679	5937282	80.11	0.00	72	0.00

Table 5.16: November 7, 2002 Recovery Ratio Corrected Depth Averaged Samples.

Depth Sample Number	East	North	Transverse Distance (m)	Depth Concentration less river background (ppt)	Recovery Ratio (%)	Recovery Ratio Adjusted Depth Concentration less background (ppt)
Station 80						
D109	340447	5937409	2.72	1713.51	100	1710.38
D67	340449	5937412	6.17	1705.89	100	1702.80
D74	340451	5937415	9.61	1830.84	100	1827.91
D64	340455	5937417	13.96	1382.84	100	1388.19
D103	340454	5937420	15.42	1521.51	100	1521.69
D102	340462	5937425	24.51	300.95	85	355.27
D52	340469	5937429	32.45	69.33	76	91.39
D51	340488	5937436	51.38	0.00	72	0.00
Station 320						
D68	340614	5937240	3.13	1635.79	100%	1633.45
D98	340618	5937244	8.48	1152.75	98%	1170.86
D81	340621	5937246	12.35	1379.79	100%	1385.28
D62	340627	5937251	19.72	844.94	96%	884.16
D116	340625	5937253	19.77	807.32	95%	849.05
D71	340636	5937256	29.87	168.38	80%	210.05
D106	340647	5937265	44.19	0.00	72%	0.00
D110	340665	5937279	67.12	0.00	72%	0.00
Station 640						
D72	340809	5936981	1.78	1583.98	100%	1582.58
D119	340811	5936982	4.14	1539.79	100%	1539.46
D108	340818	5936983	11.46	305.52	85%	360.08
D104	340826	5936988	20.84	505.14	90%	561.68
D105	340844	5936987	37.85	78.47	76%	102.84
D8	340862	5937002	59.63	0.00	72%	0.00
D4	340885	5937009	82.88	0.76	72%	1.05
D3	340909	5937017	108.73	0.00	72%	0.00
Station 1000						
D65	341008	5936645	2.51	1305.13	99	1314.28
D45	341012	5936646	6.47	1311.22	99	1320.05
D120	341028	5936650	22.25	35.81	74	48.29
D34	341047	5936665	46.00	0.00	72	0.00
D113	341073	5936681	76.94	0.76	72	1.05
D31	341100	5936705	112.36	3.81	72	5.26
D33	341133	5936713	144.57	2.28	72	3.16
Station 1500						
D114	341337	5936300	2.28	531.04	90	586.92
D59	341339	5936303	5.41	671.23	93	721.19
D20	341341	5936306	9.31	814.47	95	855.73
D40	341365	5936327	40.08	398.47	87	455.78
D39	341386	5936337	63.00	6.86	73	9.45
D35	341393	5936355	80.32	0.00	72	0.00
D6	341412	5936349	91.33	2.28	72	3.16
D25	341432	5936358	113.19	3.81	72	5.26
D2	341445	5936385	139.22	0.00	72	0.00
Station END						
D73	341674	5936178	1.29	649.90	93	700.97

Depth Sample Number	East	North	Transverse Distance (m)	Depth Concentration less river background (ppt)	Recovery Ratio (%)	Recovery Ratio Adjusted Depth Concentration less background (ppt)
D11	341674	5936180	3.18	677.33	93	726.96
D38	341680	5936199	22.89	23.62	74	32.13
D10	341670	5936220	43.77	3.81	72	5.26
D13	341678	5936232	55.96	3.81	72	5.26
D36	341688	5936251	76.14	0.00	72	0.00
D37	341692	5936275	100.20	2.28	72	3.16

Table 5.17: November 7, 2002 Recovery Ratio Corrected Surface Samples.

Surface Sample Number	East	North	Transverse Distance (m)	Surface Concentration less river background (ppt)	Recovery Ratio (%)	Recovery Ratio Adjusted Surface Concentration less background (ppt)
Station 80						
S123	340446	5937407	0	1715.51	100	1712.37
S57	340447	5937409	2.72	1729.22	100	1726.02
S125	340449	5937412	6.17	1944.08	100	1942.75
S116	340451	5937415	9.61	1837.41	100	1834.54
S55	340455	5937417	13.96	1788.65	100	1785.46
S62	340454	5937420	15.42	1851.13	100	1848.39
S112	340462	5937425	24.51	1224.85	99	1238.50
S67	340469	5937429	32.45	8.86	73	12.19
S113	340488	5937436	51.38	0.00	72	0.00
Station 320						
S109	340612	5937238	0	1622.56	100	1620.42
S122	340614	5937240	3.13	1666.75	100	1664.00
S65	340618	5937244	8.48	1564.65	100	1563.69
S83	340621	5937246	12.35	1253.80	99	1265.76
S63	340627	5937251	19.72	839.33	95	878.92
S115	340625	5937253	19.77	781.42	95	824.83
S114	340636	5937256	29.87	223.71	82	272.15
S117	340665	5937279	67.12	0.00	72	0.00
Station 640						
S110	340807	5936980	0	1564.65	100	1563.69
S111	340809	5936981	1.78	1677.41	100	1674.55
S52	340811	5936982	4.14	1555.51	100	1554.77
S88	340818	5936983	11.46	1014.56	97	1041.97
S118	340826	5936988	20.84	520.85	90	577.00
S105	340844	5936987	37.85	51.53	75	68.72
S106	340862	5937002	59.63	0.00	72	0.00
S101	340885	5937009	82.88	0.00	72	0.00
S7	340909	5937017	108.73	0.00	72	0.00
Station 1000						
S30	341007	5936643	0	1272.08	99	1283.01
S56	341008	5936645	2.51	1397.04	100	1401.76
S107	341012	5936646	6.47	1279.70	99	1290.21
S102	341028	5936650	22.25	39.34	74	52.91

Surface Sample Number	East	North	Transverse Distance (m)	Surface Concentration less river background (ppt)	Recovery Ratio (%)	Recovery Ratio Adjusted Surface Concentration less background (ppt)
S39	341047	5936665	46.00	0.00	72	0.00
S25	341073	5936681	76.94	0.00	72	0.00
S119	341100	5936705	112.36	0.00	72	0.00
S22	341133	5936713	144.57	0.00	72	0.00
Station 1500						
S124	341335	5936299	0	135.33	79	171.67
S81	341337	5936300	2.28	164.29	80	205.35
S74	341339	5936303	5.41	246.57	83	297.14
S104	341341	5936306	9.31	810.38	95	851.91
S17	341365	5936327	40.08	421.81	88	479.26
S32	341386	5936337	63.00	0.00	72	0.00
S12	341393	5936355	80.32	0.00	72	0.00
S43	341412	5936349	91.33	0.00	72	0.00
S108	341432	5936358	113.19	0.00	72	0.00
S1	341445	5936385	139.22	0.00	72	0.00
Station END						
S124	341674	5936176	0	135.33	79	171.67
S82	341674	5936178	1.29	683.90	93	733.17
S94	341674	5936180	3.18	626.00	92	678.23
S6	341680	5936199	22.89	39.34	74	52.91
S31	341670	5936220	43.77	0.00	72	0.00
S19	341678	5936232	55.96	0.00	72	0.00
S26	341688	5936251	76.14	0.00	72	0.00
S29	341692	5936275	100.20	0.00	72	0.00

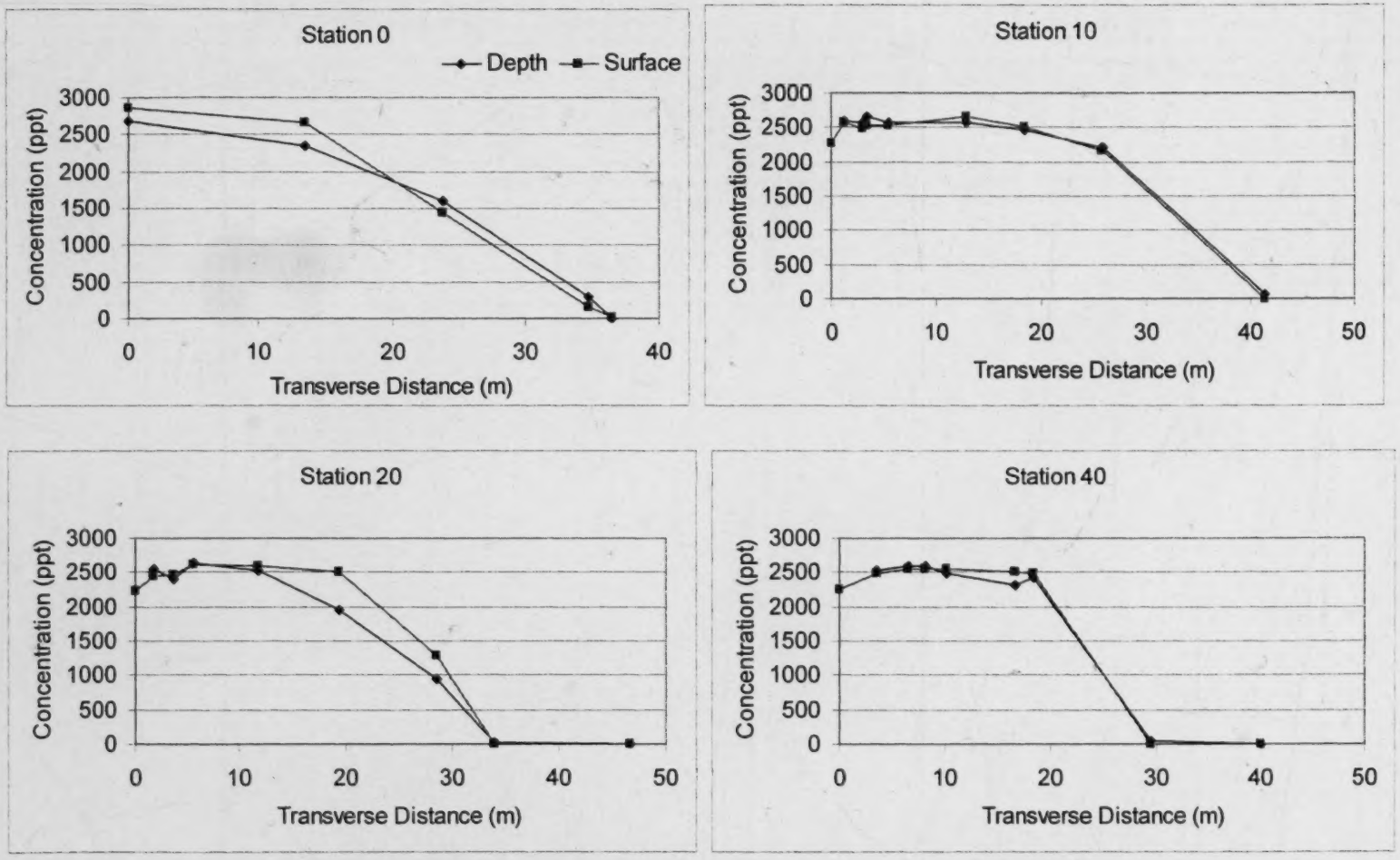

Figure 5.16: Concentration plots for cross sections taken October 29, 2002.

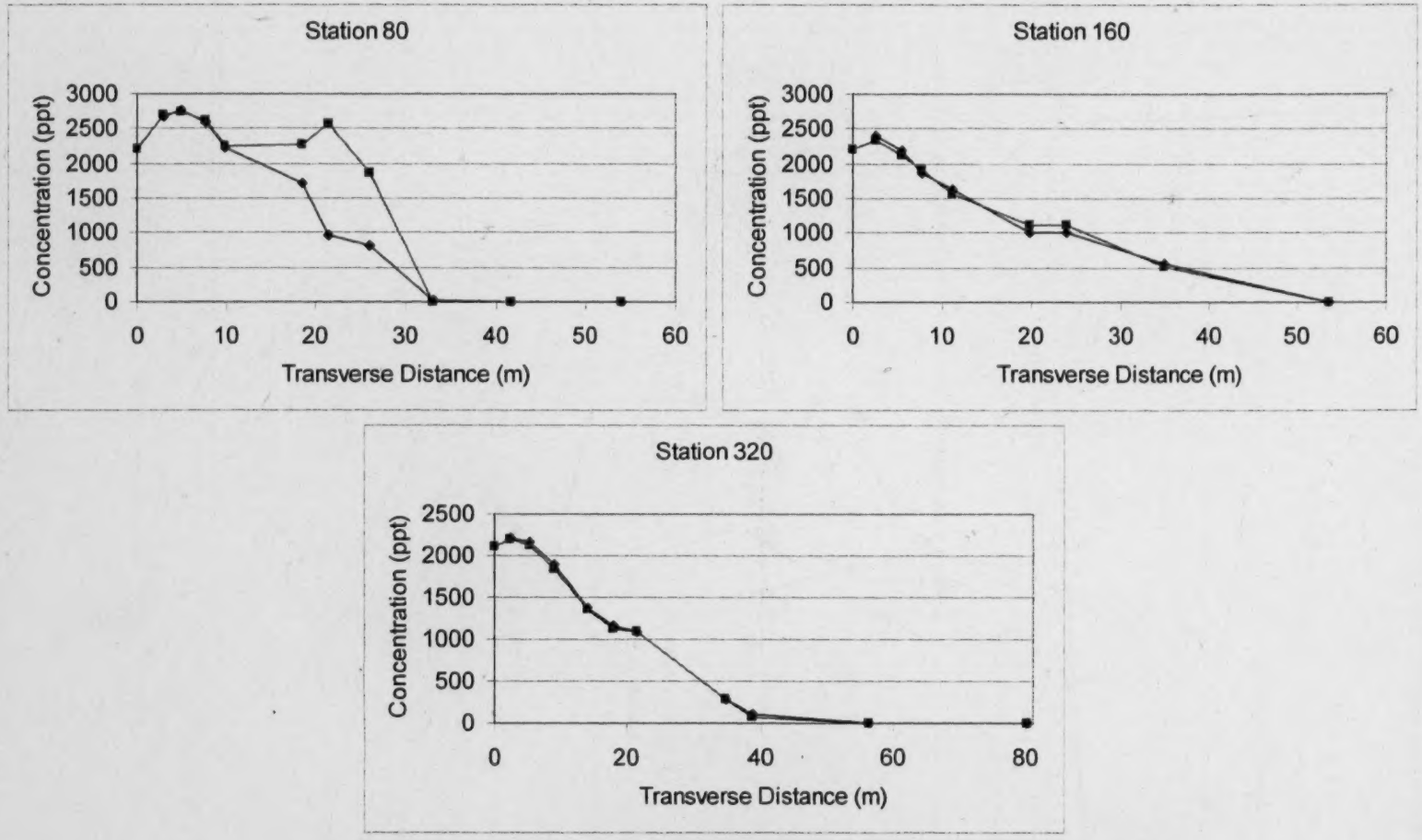

Figure 5.16 (cont'd): Concentration plots for cross sections taken October 29, 2002.

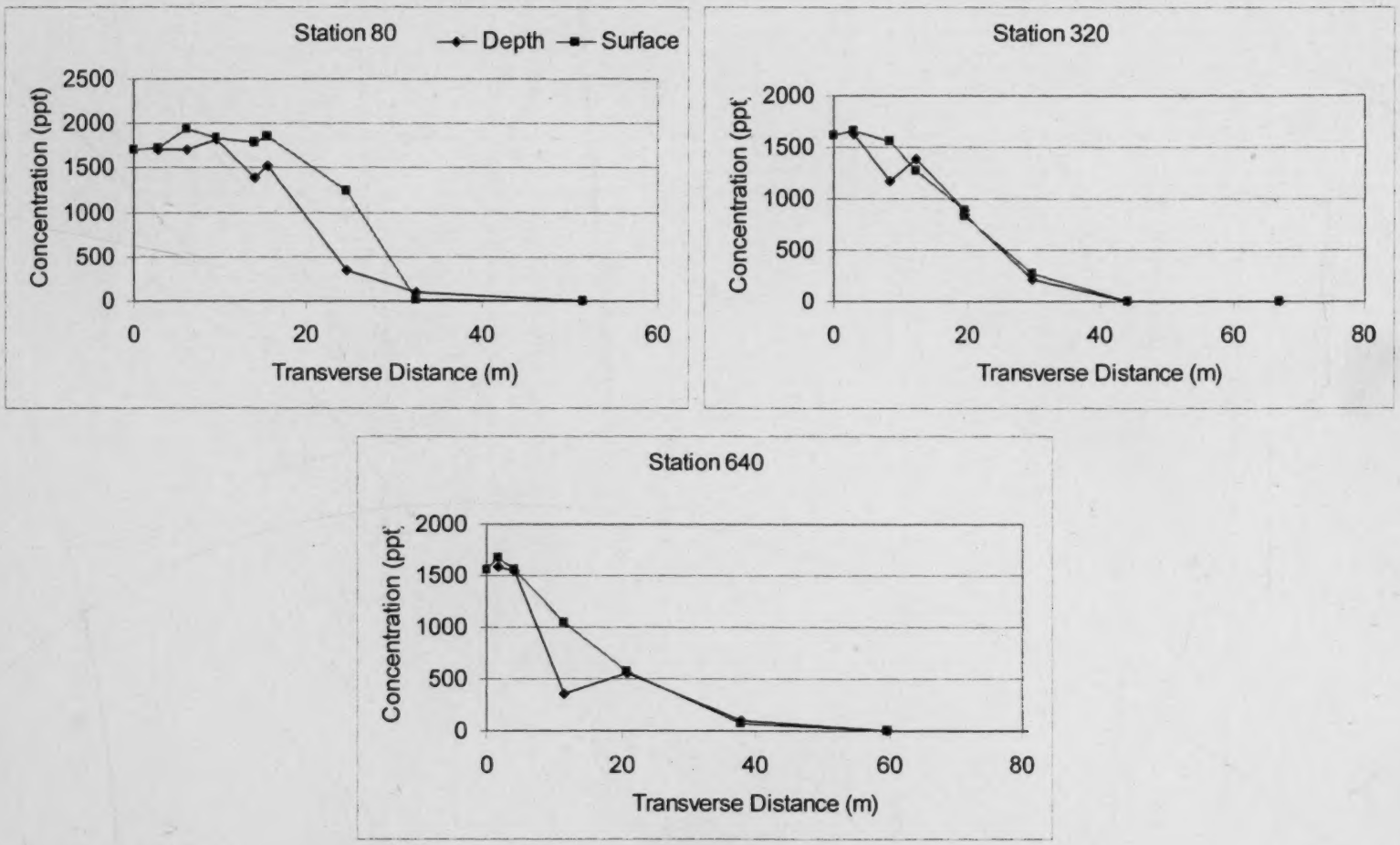

Figure 5.17: Concentration plots for cross sections taken November 7, 2002.

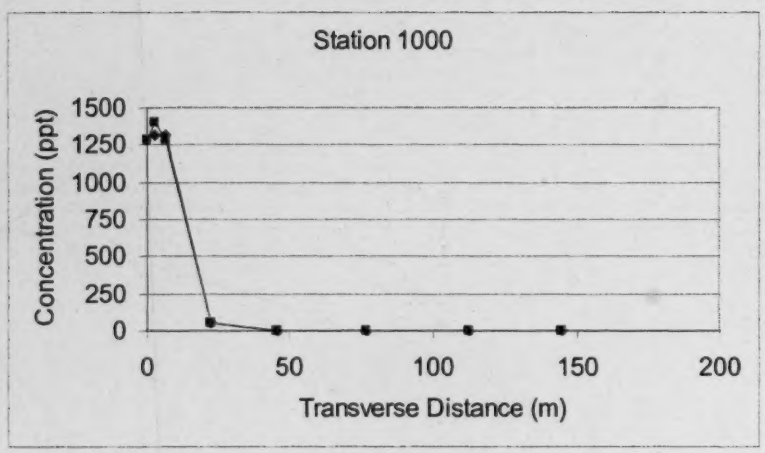

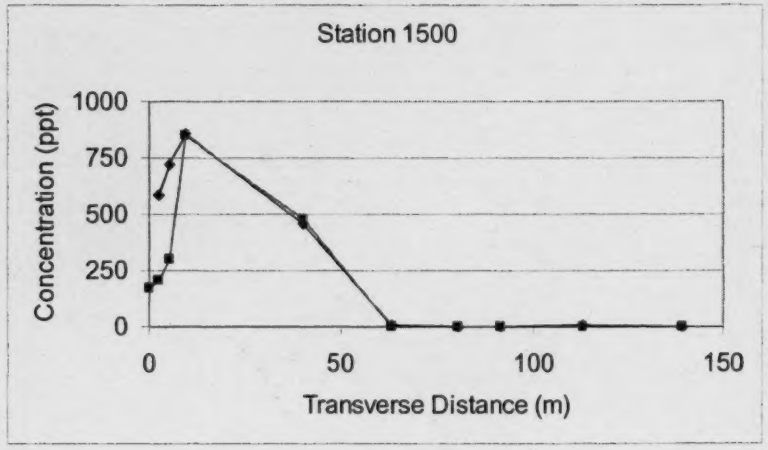

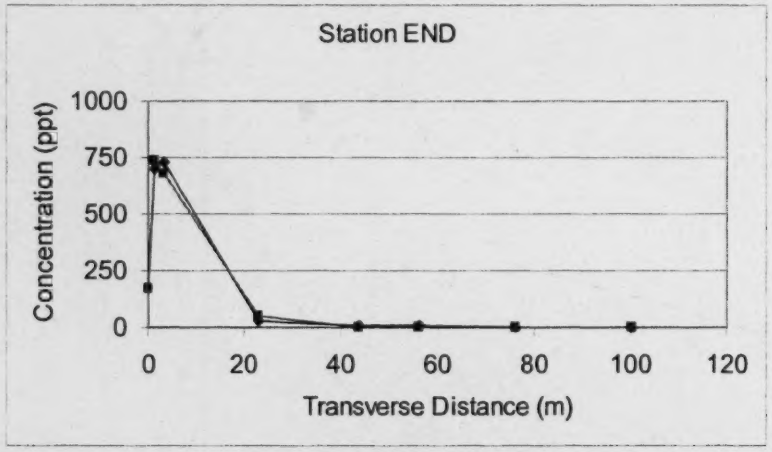

Figure 5.17 (cont'd): Concentration plots for cross sections taken November 7, 2002.

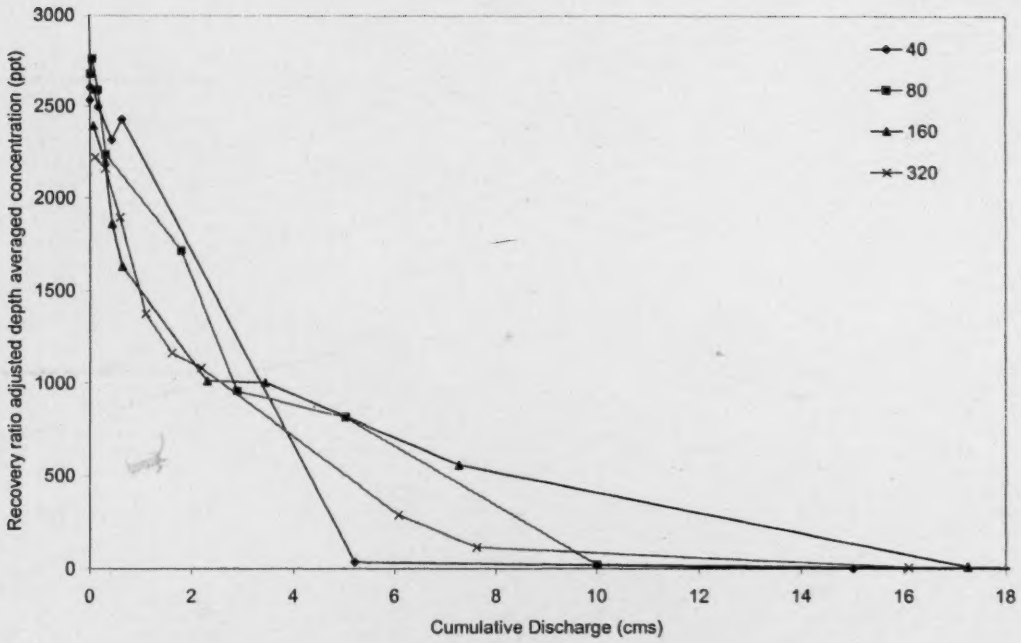

Figure 5.18: Original C-q distributions for October 29, 2002.

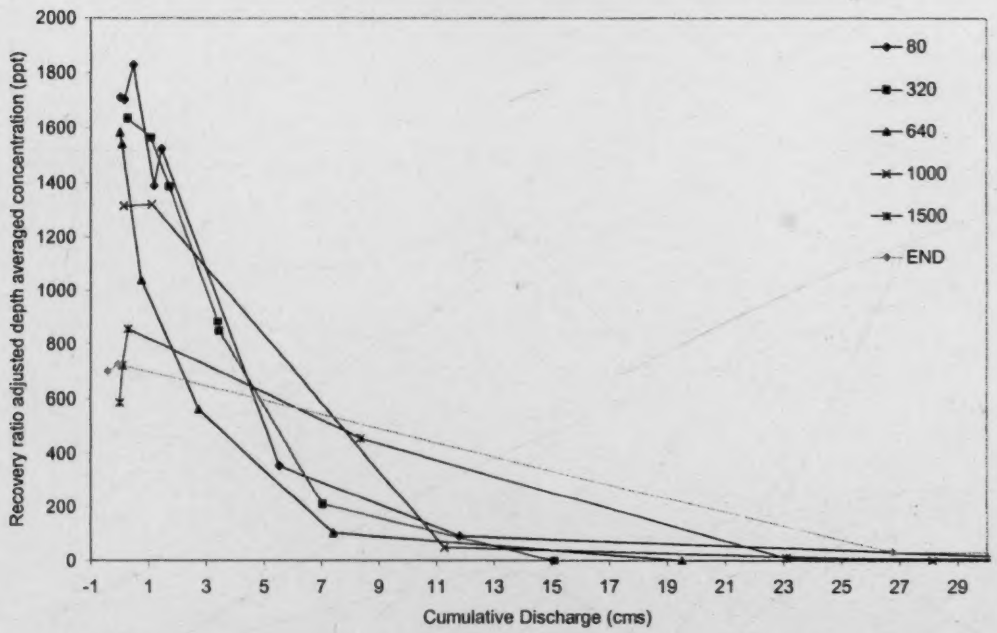

Figure 5.19: Original C-q distributions for November 7, 2002.

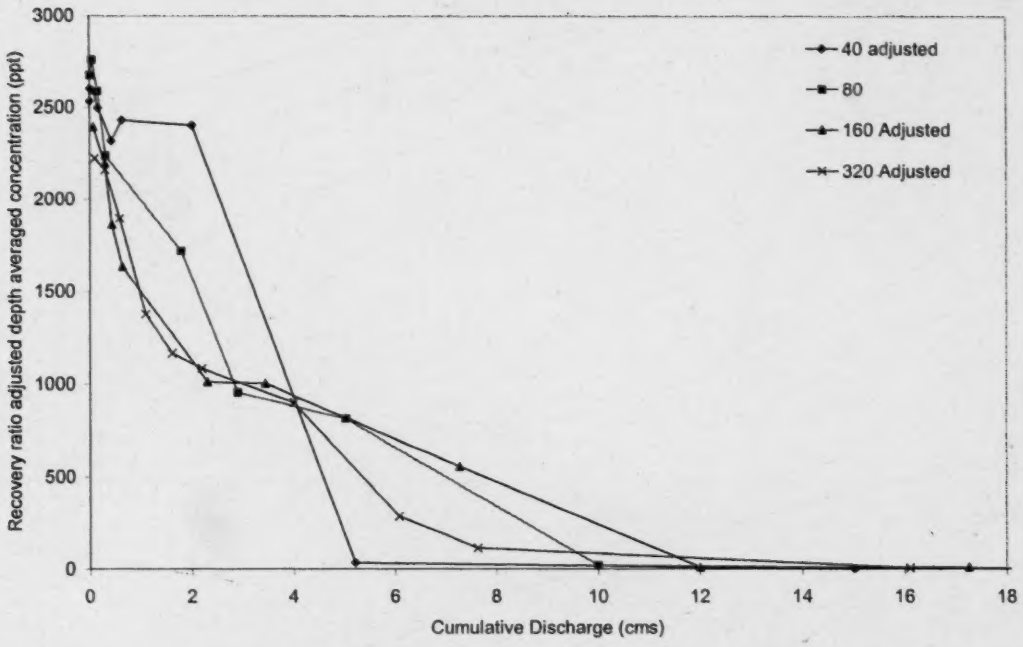

Figure 5.20: Adjusted C-q distributions for October 29, 2002.

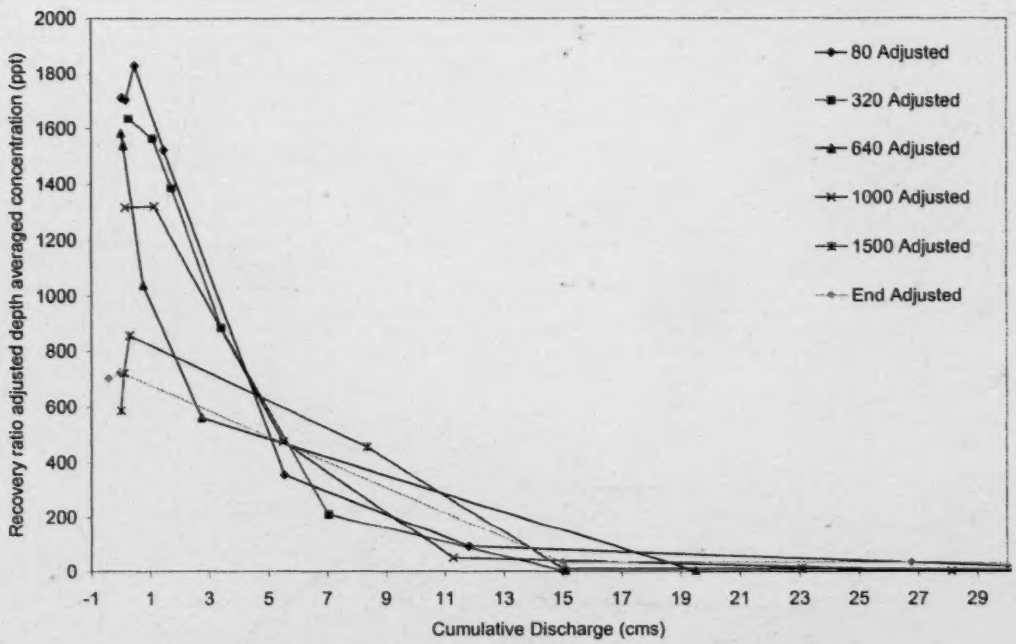

Figure 5.21: Adjusted C-q distributions for November 7, 2002.

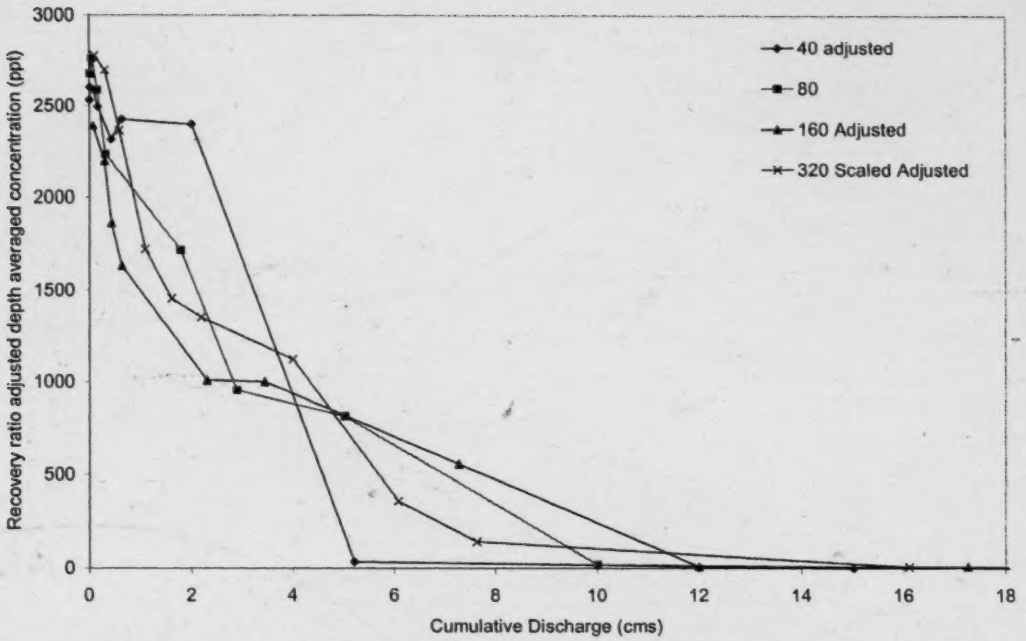

Figure 5.22: Scaled adjusted C-q distributions for October 29, 2002.

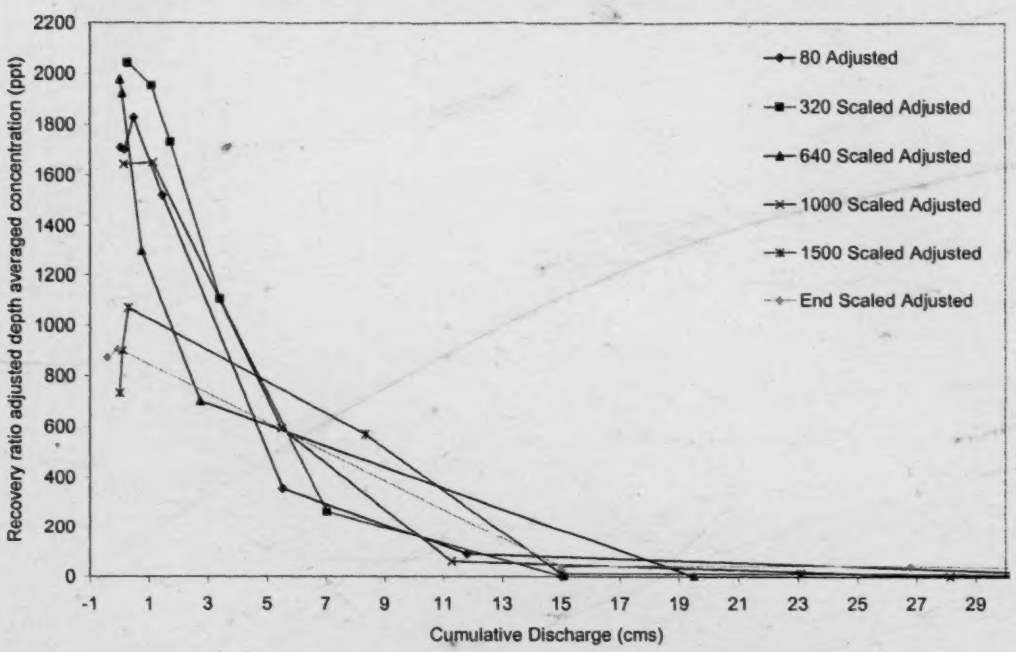

Figure 5.23: Scaled adjusted C-q distributions for November 7, 2002.

Table 5.18: Cumulative discharge summary for October 29, 2002.

East	North	Cumulative Discharge, qc (cms)	Cactual less river background (ppt)	Scaled Concentration (ppt)
Station 0				
340376.798	5937446.289	0	2683.85	
340382.124	5937458.619	0.9521	2345.93	
340387.442	5937467.534	0.8777	1590.79	
340396.864	5937474.617	0.3121	305.70	
340399.420	5937474.822	0.5253	6.31	
Station 10				
340382.222	5937441.223	0.0031		
340382.903	5937442.287	0.0192	2599.36	
340384.098	5937443.528	0.0943	2563.78	
340384.384	5937443.889	0.1401	2653.52	
340385.396	5937445.652	0.5673	2578.65	
340389.181	5937451.981	0.9369	2574.20	
340390.624	5937457.517	0.9451	2462.80	
340398.079	5937461.340	0.7639	2204.05	
340398.291	5937461.442	0.7476	2204.05	
340407.739	5937473.770	2.2251	65.16	
Station 20				
340395.925	5937439.944	0.0108		
340396.681	5937441.546	0.1219	2559.31	
340397.336	5937443.342	0.3751	2390.76	
340398.397	5937444.961	0.5931	2628.75	
340402.796	5937449.509	0.704	2530.88	
340405.827	5937456.519	0.5788	1943.04	
340411.439	5937463.849	0.4791	945.88	
340415.402	5937467.671	2.6861	14.65	
340430.286	5937471.392	14.7463	0.00	
Station 40				
340414.178	5937433.188	0		
340416.176	5937436.144	0.0005	2530.88	
340418.256	5937438.184	0.0053	2599.36	
340418.986	5937439.677	0.0758	2587.54	
340420.035	5937441.483	0.1606	2496.20	
340424.524	5937446.118	0.4237	2314.87	
340425.726	5937447.501	0.6284	2426.12	
		2	***2400.00***	
340432.024	5937456.681	5.2075	33.15	
340441.384	5937462.441	15.0136	0.00	
Station 80				
340446.528	5937408.541	0.0004		
340448.329	5937410.772	0.0143	2673.78	
340449.608	5937412.344	0.0539	2757.80	
340451.690	5937414.189	0.1526	2586.06	
340453.385	5937415.656	0.3028	2235.34	
340457.906	5937423.024	1.7937	1714.16	
340459.722	5937425.393	2.8909	955.79	
340464.442	5937427.259	5.0253	815.12	
340468.531	5937433.200	10.0037	18.80	
340474.168	5937439.632	18.4263	0.00	
340477.393	5937452.756	34.7506	0.00	

East	North	Cumulative Discharge, qc (cms)	Cactual less river background (ppt)	Scaled Concentration (ppt)
Station 160				
340504.762	5937347.76	0.0021		
340506.884	5937349.123	0.0676	2392.29	
340508.901	5937351.476	0.2938	2196.22	
340510.830	5937352.756	0.432	1861.01	
340513.443	5937354.908	0.6325	1629.70	
340520.581	5937359.771	2.3034	1009.65	
340522.135	5937364.107	3.4395	1002.56	
340532.648	5937368.552	7.2685	557.96	
		12	***10.50***	
340549.847	5937376.580	17.2552	10.50	
Station 320				
340612.131	5937238.993	0.0086		
340614.058	5937240.501	0.0961	2221.26	2776.57
340616.469	5937241.898	0.2998	2157.07	2696.34
340619.647	5937243.806	0.5815	1893.44	2366.80
340623.722	5937246.797	1.0943	1375.83	1719.79
340627.214	5937248.618	1.6134	1163.03	1453.78
340630.276	5937250.313	2.1894	1081.96	1352.45
		4	***900.00***	1125.00
340640.666	5937258.781	6.0781	285.84	357.31
340644.487	5937260.388	7.6236	113.25	141.56
340660.217	5937268.038	16.0969	6.31	7.89
340679.457	5937282.413	35.759	0.00	0.00

Table 5.19: Cumulative discharge summary for November 7, 2002.

East	North	Cumulative Discharge, qc (m^3/s)	Cactual less river background (ppt)	Scaled Concentration (ppt)
Station 80				
340445.71	5937406.76	0.0012		
340447.235	5937409.012	0.0269	1710.38	
340449.184	5937411.855	0.1708	1702.80	
340451.347	5937414.542	0.4672	1827.91	
340455.422	5937416.791	***1.1908***	***1388.19***	
340454.082	5937419.713	1.4523	1521.69	
340461.847	5937425.203	5.5364	355.27	
340468.902	5937429.463	11.7996	91.39	
340487.964	5937435.997	34.5175	0.00	
Station 320				
340611.81	5937238.06	0.0189		
340613.898	5937240.393	0.2749	1633.45	2041.81
340617.762	5937244.108	1.0769	***1562.71***	1953.39
340620.875	5937246.453	1.7154	1385.28	1731.60
340626.809	5937250.859	3.4019	884.16	1105.19
340624.925	5937252.849	***3.4441***	***849.05***	1061.32
340635.638	5937256.068	7.0408	210.05	262.57
340646.827	5937265.014	15.0934	0.00	0.00
340664.821	5937279.239	33.7419	0.00	0.00
Station 640				
340806.99	5936979.79	0.0013		
340808.501	5936980.715	0.0082	1582.58	1978.23
340810.508	5936981.969	0.0766	1539.46	1924.33
340817.950	5936983.134	0.7516	***1039.31***	1299.14
340826.078	5936988.137	2.7295	561.68	702.10
340844.176	5936986.839	***7.4064***	***102.84***	128.56
340862.200	5937002.322	19.5018	0.00	0.00
340884.699	5937008.583	38.1835	1.05	1.32
340909.123	5937017.062	68.2856	0.00	0.00
Station 1000				
341006.65	5936643.08	0.0343		
341008.138	5936645.089	0.1472	1314.28	1642.85
341012.194	5936646.406	1.1234	1320.05	1650.06
		5.5	***475.00***	593.75
341027.657	5936650.388	11.2673	48.29	60.36
341047.211	5936664.773	28.1176	0.00	0.00
341073.439	5936681.263	40.96	1.05	1.32
341100.341	5936705.082	65.6582	5.26	6.58
341133.239	5936712.892	93.9756	3.16	3.94
Station 1500				
341335.46	5936299.05	-0.0082		
341337.226	5936300.488	0.0053	586.92	733.65
341339.261	5936302.899	0.0958	721.19	901.48
341341.250	5936306.340	0.2996	855.73	1069.66
341364.599	5936326.563	8.3442	455.78	569.72
		15	***9.45***	11.81
341386.045	5936336.593	23.0905	9.45	11.82
341393.270	5936354.803	43.4601	0.00	0.00

East	North	Cumulative Discharge, qc (m^3/s)	Cactual less river background (ppt)	Scaled Concentration (ppt)
Station 1500 (cont'd)				
341412.160	5936348.634	56.518	3.16	3.94
341432.328	5936357.601	89.0041	5.26	6.58
341445.161	5936384.760	134.3819	0.00	0.00
End Station				
341674.32	5936176.47	-0.4309		
341674.170	5936177.749	-0.4137	700.97	876.21
341674.246	5936179.647	-0.0456	726.96	908.70
		15	***32.13***	40.16
341679.972	5936198.651	26.7569	32.13	40.17
341669.563	5936219.972	67.6273	5.26	6.58
341678.251	5936232.284	90.608	5.26	6.58
341688.356	5936251.298	120.1072	0.00	0.00
341691.903	5936275.107	145.8573	3.16	3.94

Table 5.20: Summary of calculated Mass flux.

Station	Original Mass Flux	Adjusted Mass Flux	Scaled Mass Flux
October 29, 2002			
Station 40	7323.28	8904.57	
Station 80	9224.29	9224.29	
Station 160	10480.14	9041.64	
Station 320	6891.06	7257.98	9072.48
November 7, 2002			
Station 80	8626.59	8732.39	
Station 320	7341.61	7391.26	9239.07
Station 640	4747.27	7281.69	9102.11
Station 1000	8781.17	7278.11	9097.64
Station 1500	9029.63	7224.10	9030.12
Station END	11211.94	7127.38	8909.23

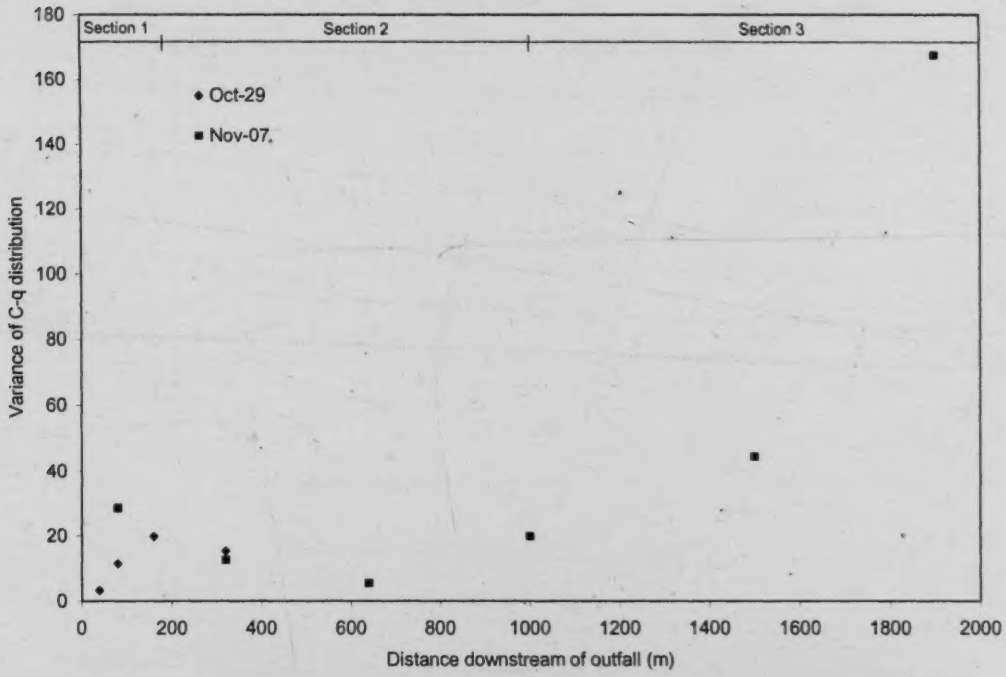

Figure 5.24: Variance of scaled adjusted C-q distributions.

Table 5.21: Summary of calculated variances based on scaled adjusted C-q profiles.

x	σ
October 29, 2002	
40	3.22
80	11.49
160	19.85
320	15.40
November 7, 2002	
80	28.52
320	12.64
640	5.49
1000	19.93
1500	44.43
1900	167.57

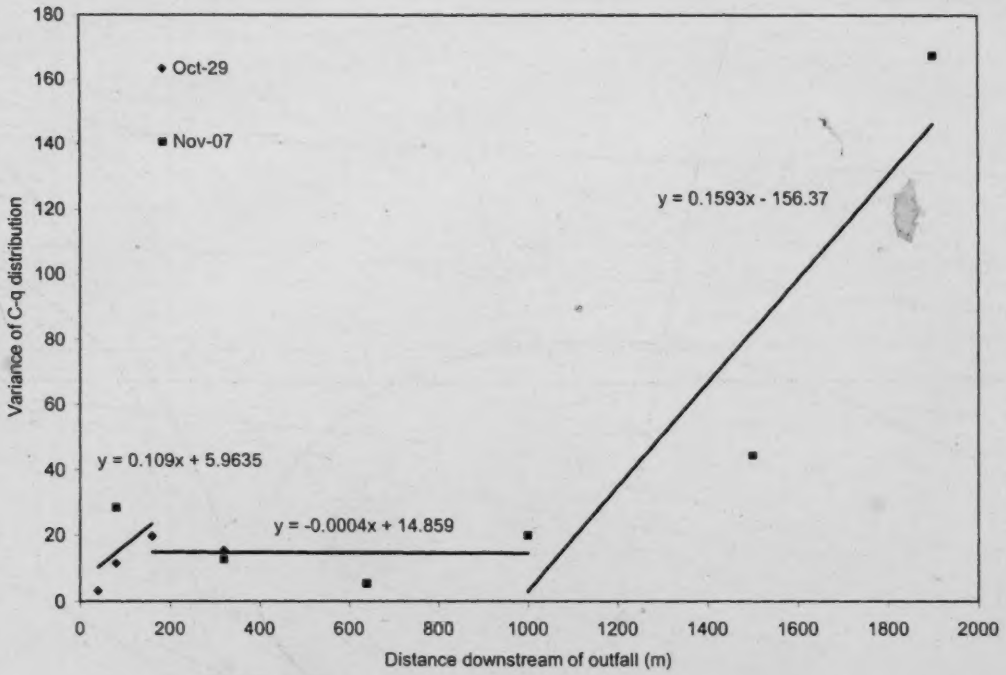

Figure 5.25: Linear trendlines fit to variance distribution.

Table 5.22: Calculated transverse factor of diffusion and transverse mixing coefficients.

Stations	Slope from best fit	D (m^5/s^2)	Average Modeled Depth (m)	Average Modeled Velocity (m/s)	Average Modeled Shear Velocity (m/s)	εt (m^2/s)	εt/hu*
40-160	0.109	N/A	1.056	0.209	0.023	N/A	N/A
160-1000	-0.0004	-0.0002	0.794	0.276	0.029	-0.001	-0.050
1000-End	0.1593	0.0797	1.239	0.257	0.018	0.202	9.124

Table 5.23: Roughness definition for sensitivity analysis.

	Roughness, k	start	end
Roughness 1	0.35	beginning	350 m
	0.1	350 m	750m
	0.3	750 m	1000 m
	0.1	1000 m	1200 m
	0.07	1200 m	END
Roughness 2	0.35	Beginning	just before outfall
	0.1	just before outfall	750 m
	0.3	750m	1000m
	0.1	1000m	1200m
	0.07	1200m	END

Note: All distances approximate from outfall structure.

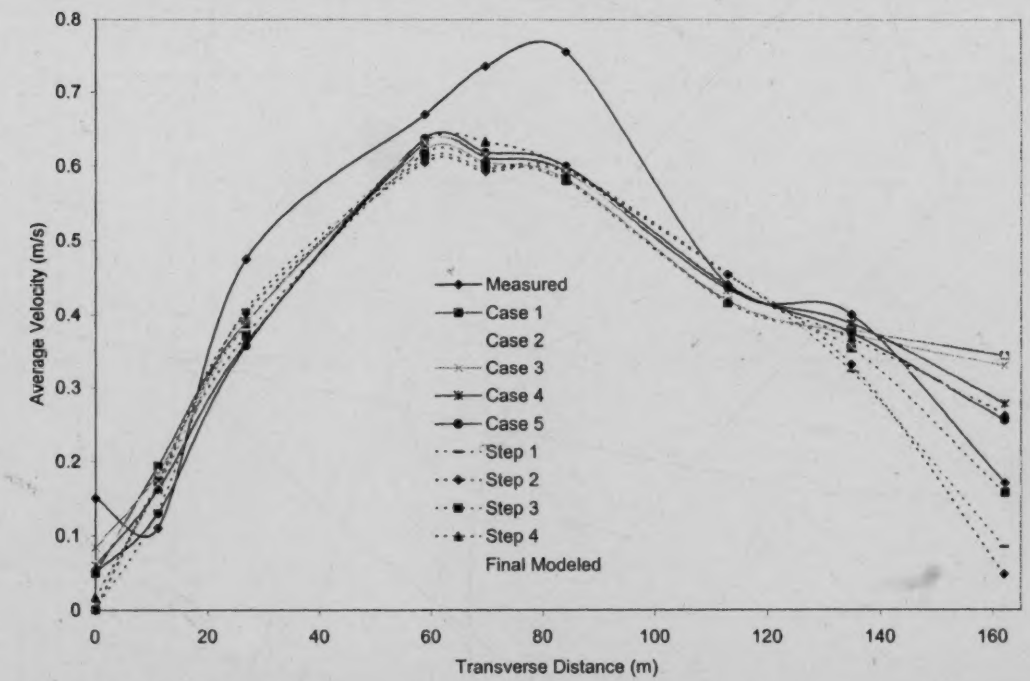

Figure 5.26: Sensitivity analysis of velocity profile: Station 80, November 7, 2002.

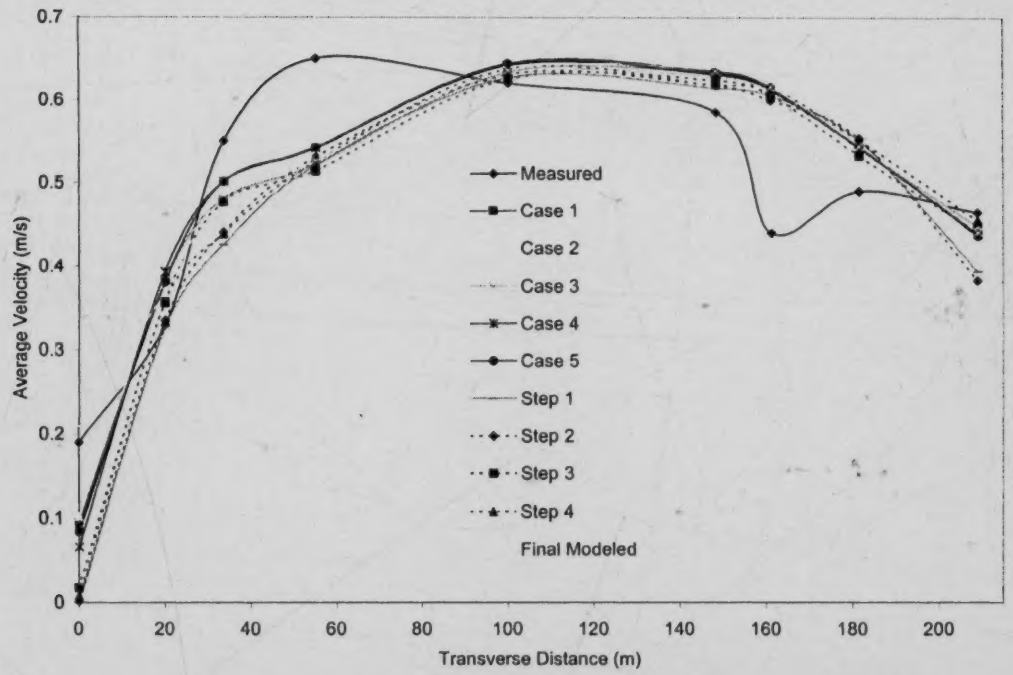

Figure 5.27: Sensitivity analysis of velocity profile: Station 320, November 7, 2002.

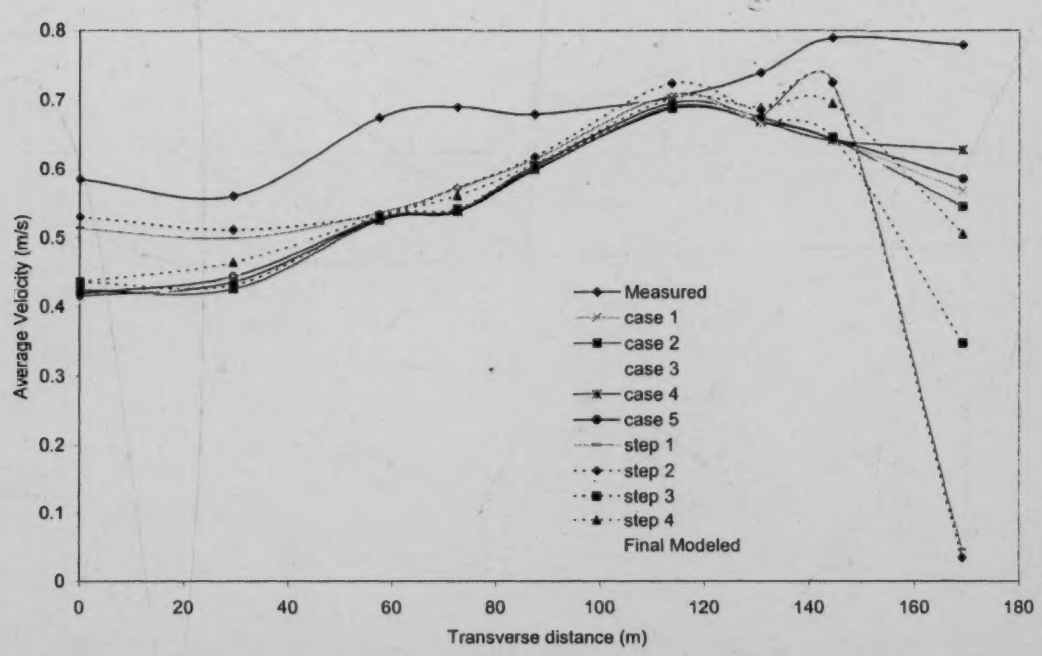

Figure 5.28: Sensitivity analysis of velocity profile: Station 1000, November 7, 2002.

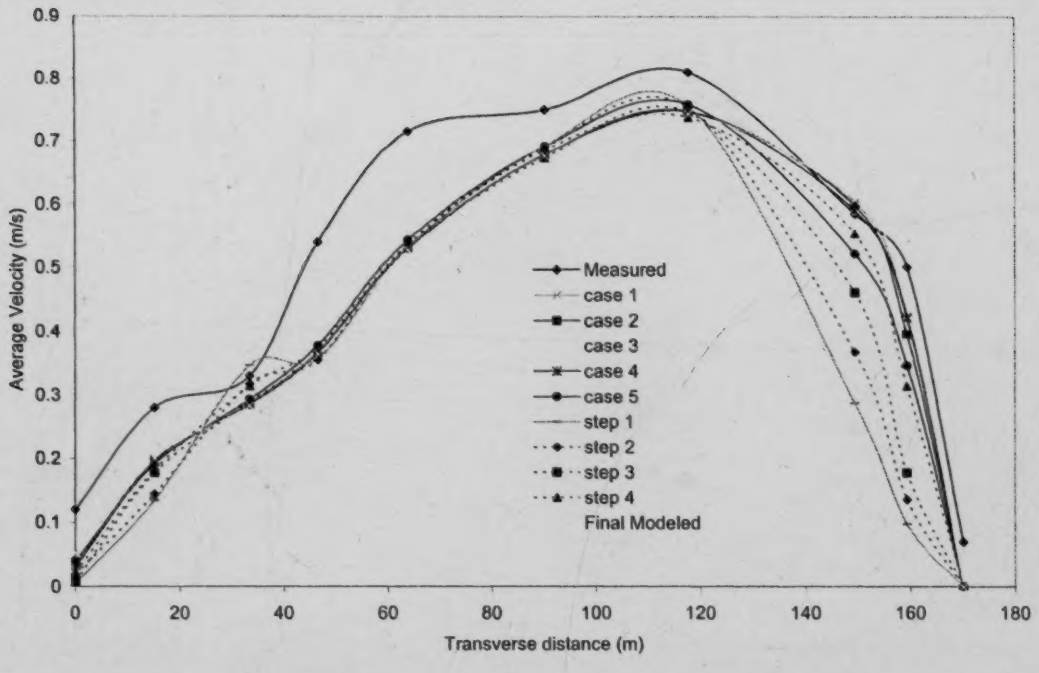

Figure 5.29: Sensitivity analysis of velocity profile: Station 1500, November 7, 2002.

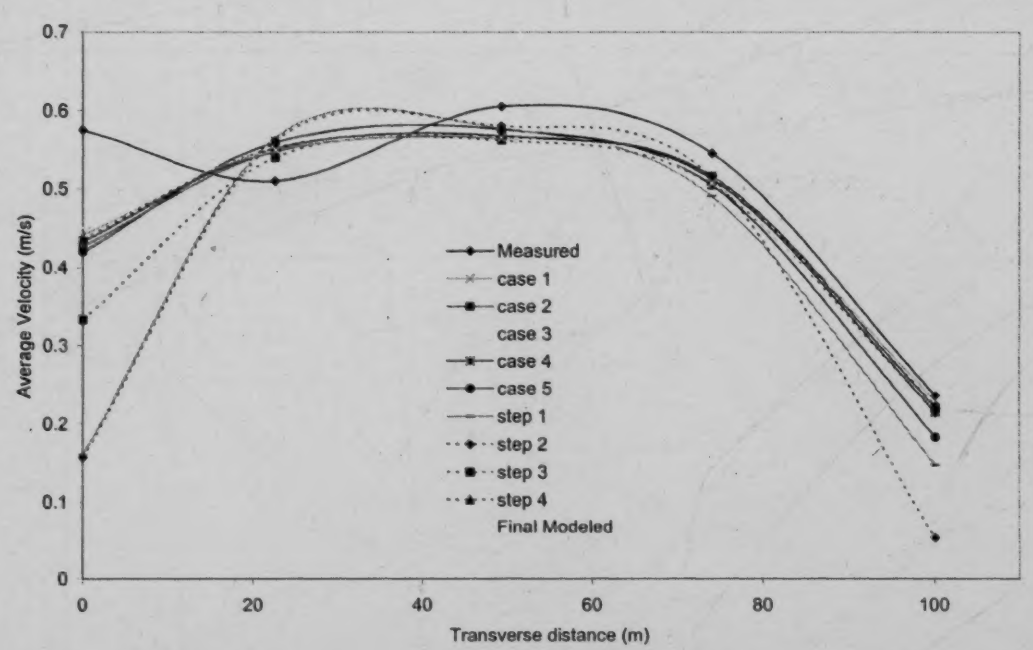

Figure 5.30: Sensitivity analysis of velocity profile: Station End, November 7, 2002.

Table 5.24: Sensitivity analysis: Absolute error in modeled velocities.

POINT ID	case 1	case 2	case 3	case 4	case 5	step 1	step 2	step 3	step 4
V80-1	102%	103%	94%	64%	50%	50%	72%	7%	55%
V80-2	5%	5%	7%	3%	6%	19%	17%	11%	8%
V80-3	5%	5%	5%	1%	0%	4%	3%	5%	0%
V80-04	23%	23%	23%	21%	21%	21%	22%	23%	21%
V80-05	18%	18%	18%	17%	16%	19%	19%	18%	14%
V80-07	8%	8%	7%	6%	5%	9%	10%	8%	6%
V80-08	18%	18%	18%	24%	25%	14%	15%	22%	18%
V80-09	76%	69%	68%	47%	18%	22%	56%	57%	51%
V80-10	67%	64%	44%	60%	66%	99%	100%	100%	89%
Average	**36%**	**35%**	**31%**	**27%**	**23%**	**29%**	**35%**	**28%**	**29%**
V320-01	51%	46%	55%	65%	56%	100%	99%	91%	97%
V320-02	16%	15%	16%	19%	15%	1%	1%	8%	8%
V320-03	13%	13%	13%	9%	9%	23%	20%	13%	20%
V320-04	20%	20%	20%	17%	17%	20%	18%	21%	19%
V320-05	2%	2%	2%	3%	4%	1%	2%	1%	3%
V320-06	7%	7%	8%	8%	8%	5%	6%	7%	6%
V320-07	39%	39%	39%	39%	40%	38%	36%	38%	40%
V320-8	10%	10%	11%	11%	11%	12%	13%	9%	12%
V320-09	4%	4%	4%	6%	6%	15%	17%	5%	2%
Average	**18%**	**17%**	**19%**	**20%**	**18%**	**24%**	**24%**	**21%**	**23%**
V1000-2	28%	28%	29%	29%	28%	12%	9%	25%	25%
V1000-3	24%	24%	22%	22%	21%	11%	9%	23%	17%
V1000-4	22%	22%	22%	22%	22%	21%	21%	21%	21%
V1000-5	22%	22%	22%	22%	22%	17%	17%	22%	19%
V1000-6	12%	12%	12%	12%	11%	10%	9%	11%	11%
V1000-7	2%	2%	2%	2%	1%	1%	3%	2%	0%
V1000-8	9%	9%	10%	10%	9%	8%	7%	9%	7%
V1000-9	18%	19%	19%	19%	18%	8%	8%	18%	12%
V1000-10	27%	30%	19%	19%	25%	94%	96%	55%	35%
Average	**18%**	**19%**	**17%**	**17%**	**17%**	**20%**	**20%**	**21%**	**16%**

POINT ID	case 1	case 2	case 3	case 4	case 5	step 1	step 2	step 3	step 4
V1500-1	73%	73%	74%	74%	67%	96%	85%	94%	82%
V1500-2	29%	30%	31%	31%	31%	52%	48%	37%	35%
V1500-3	13%	14%	13%	13%	11%	5%	4%	12%	5%
V1500-4	32%	32%	32%	32%	30%	34%	34%	32%	31%
V1500-5	26%	26%	26%	26%	24%	26%	25%	26%	25%
V1500-6	10%	10%	9%	9%	8%	8%	8%	10%	9%
V1500-7	8%	8%	8%	8%	6%	7%	7%	8%	9%
V1500-8	3%	2%	1%	1%	11%	51%	37%	21%	5%
V1500-9	15%	21%	16%	16%	31%	80%	73%	64%	37%
V1500-10	100%	100%	100%	100%	100%	100%	100%	100%	100%
Average	**31%**	**32%**	**31%**	**31%**	**32%**	**46%**	**42%**	**40%**	**34%**
VE-1	23%	26%	25%	25%	27%	72%	73%	42%	24%
VE-2	7%	7%	8%	8%	10%	11%	10%	6%	8%
VE-3	7%	7%	6%	6%	5%	5%	4%	7%	6%
VE-4	5%	5%	6%	6%	7%	10%	6%	7%	6%
VE-5	3%	6%	9%	9%	22%	37%	77%	9%	5%
Average	**9%**	**10%**	**11%**	**11%**	**14%**	**27%**	**34%**	**14%**	**10%**
Overall Average	**23.9%**	**23.9%**	**23.1%**	**22.4%**	**21.9%**	**29.6%**	**30.9%**	**26.4%**	**23.9%**

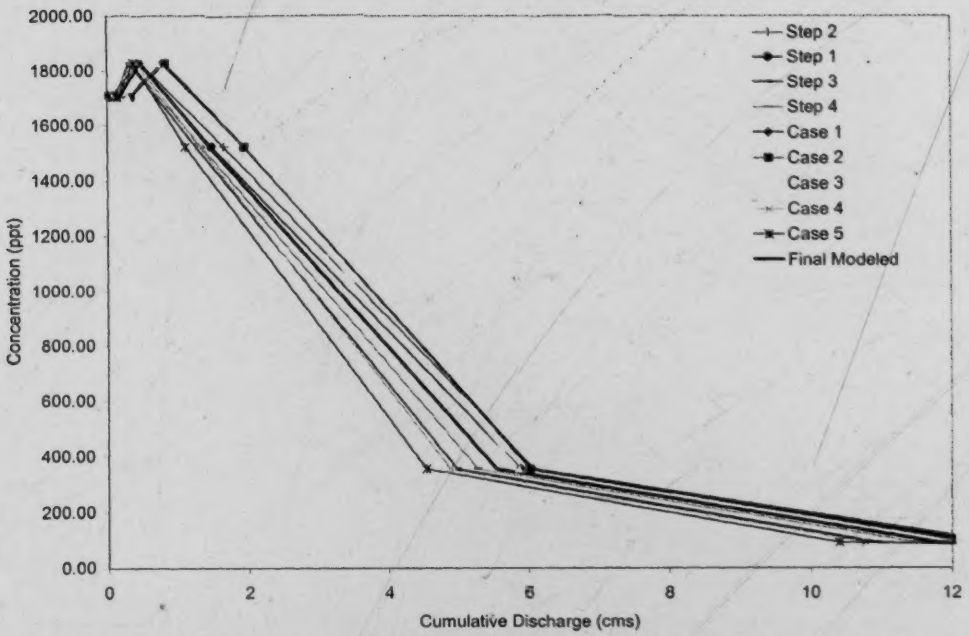

Figure 5.31: Sensitivity analysis: Concentration – Cumulative Discharge distribution, Station 80, November 7, 2002.

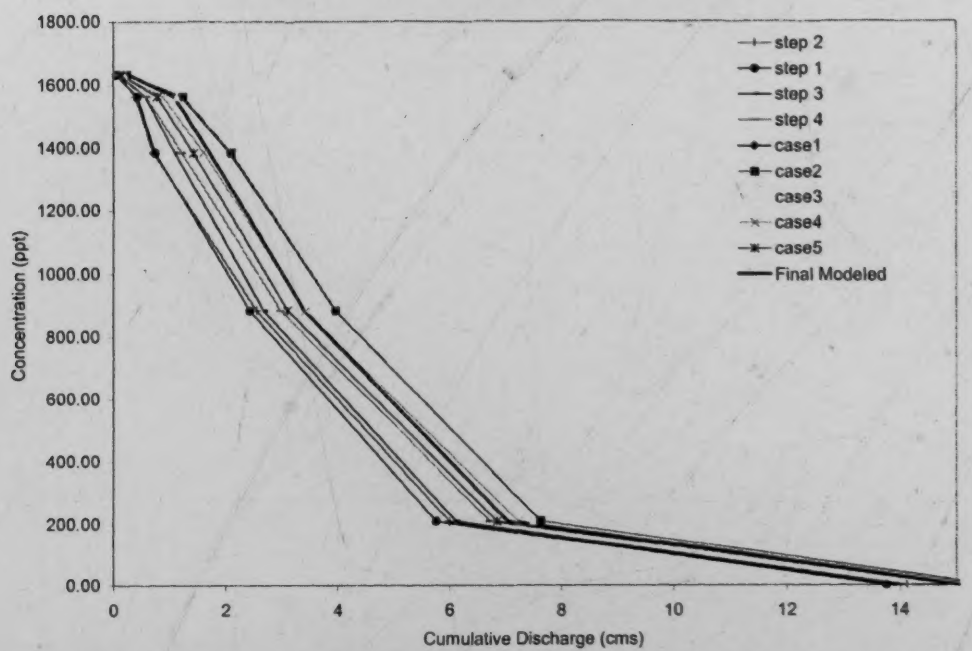

Figure 5.32: Sensitivity analysis: Concentration – Cumulative Discharge distribution, Station 320, November 7, 2002.

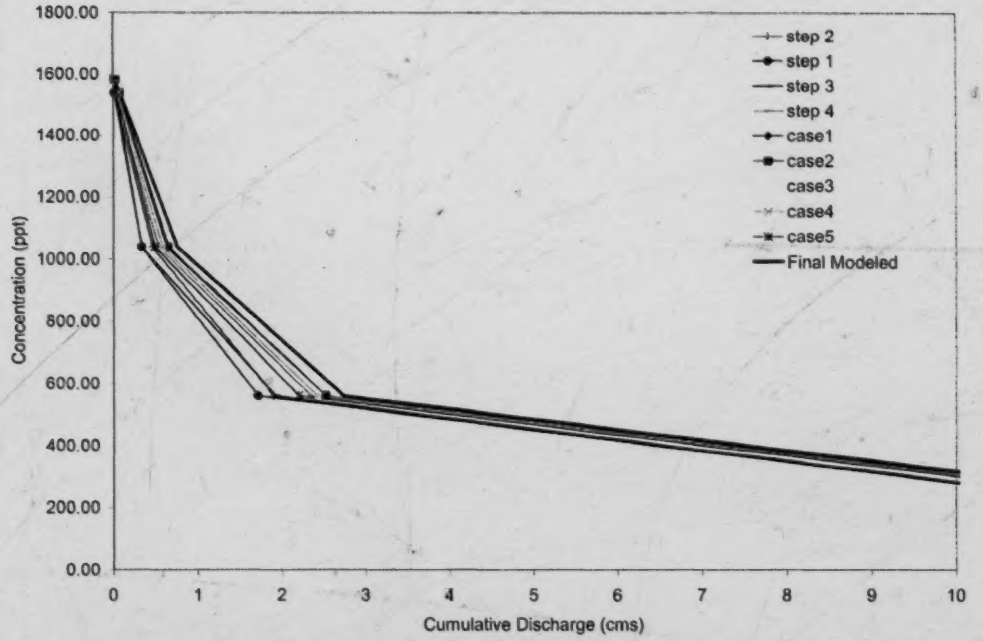

Figure 5.33: Sensitivity analysis: Concentration – Cumulative Discharge distribution, Station 640, November 7, 2002.

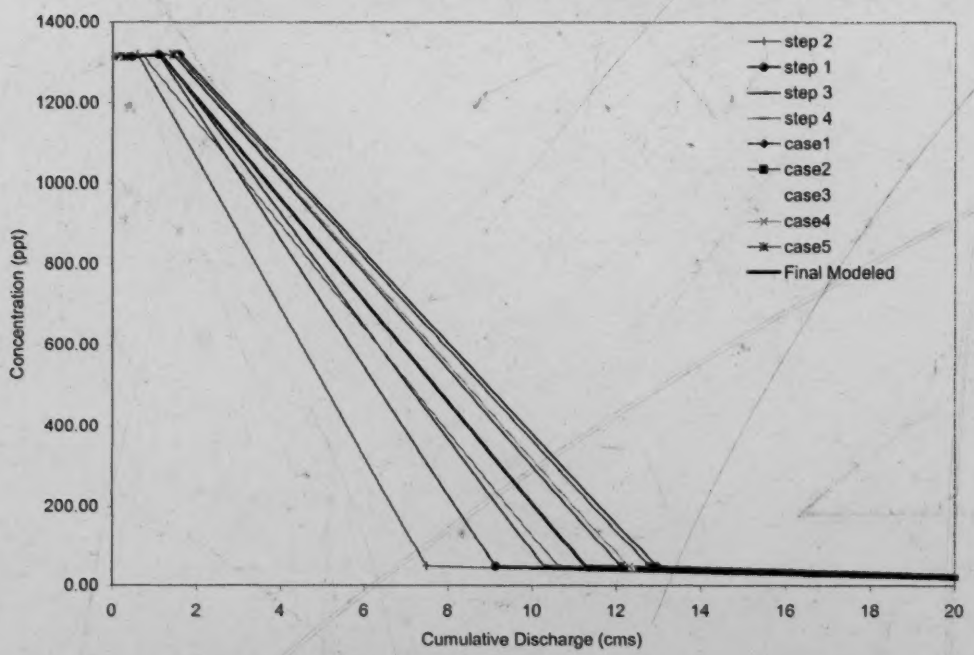

Figure 5.34: Sensitivity analysis: Concentration – Cumulative Discharge distribution, Station 1000, November 7, 2002.

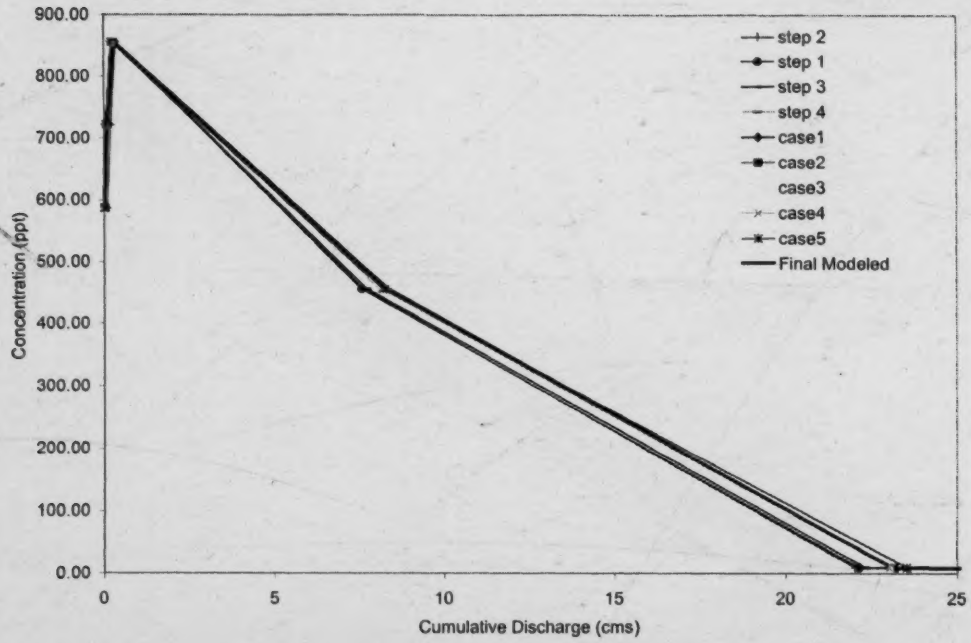

Figure 5.35: Sensitivity analysis: Concentration – Cumulative Discharge distribution, Station 1500, November 7, 2002.

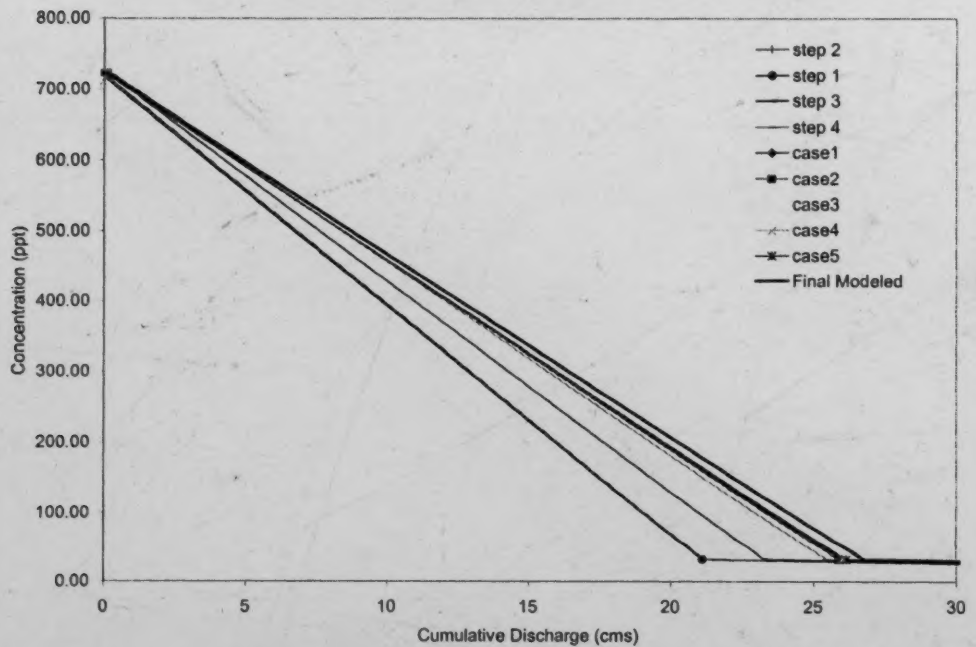

Figure 5.36: Sensitivity analysis: Concentration – Cumulative Discharge distribution, Station End, November 7, 2002.

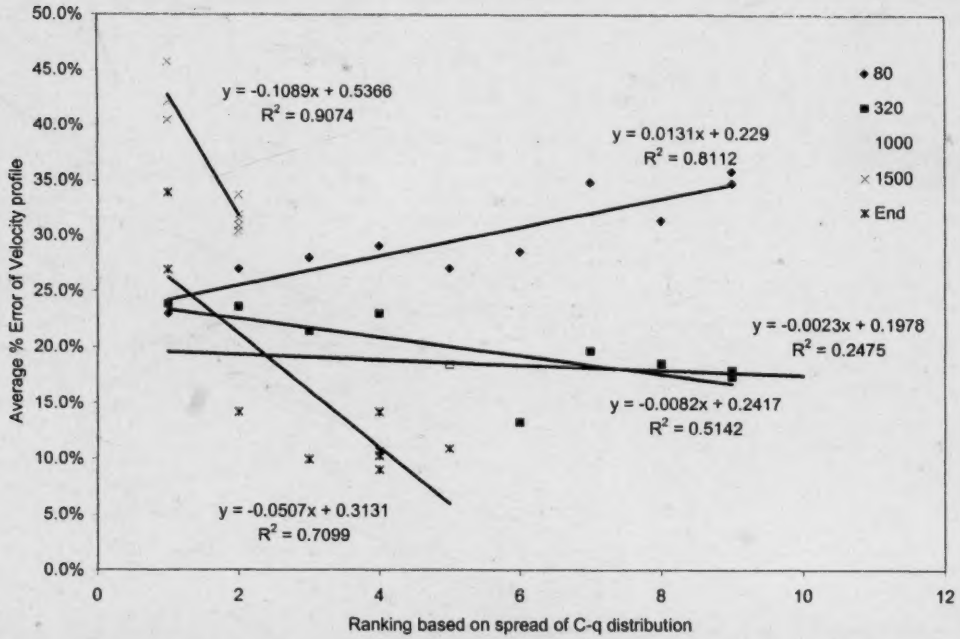

Figure 5.37: Sensitivity analysis: Ranking based on spread of C-q distribution compared with the average modeled velocity error of stations.

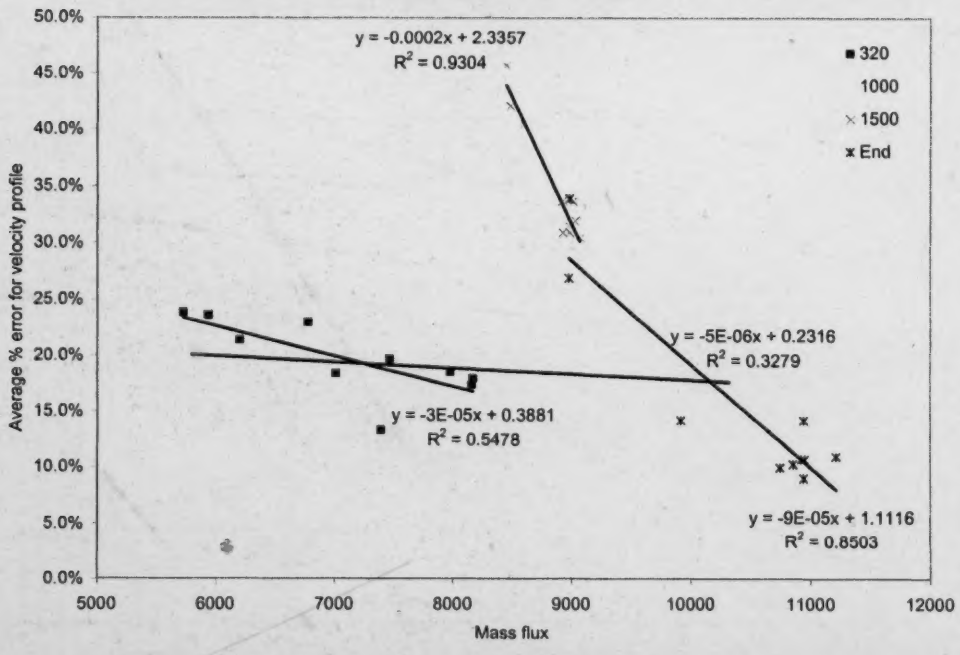

Figure 5.38: Sensitivity analysis: Mass flux from C-q distribution compared with the average modeled velocity error.

Table 5.25: Sensitivity analysis: Summary of modeled velocity error, calculated mass flux, and calculated variance.

VELOCITY										
Station	**step 2**	**step 1**	**step 3**	**step 4**	**case 1**	**case 2**	**case 3**	**case 4**	**case 5**	**FINAL CASE**
80	35%	29%	28%	29%	36%	35%	31%	27%	23%	27%
320	24%	24%	21%	23%	18%	17%	19%	20%	18%	13%
1000	20%	20%	21%	16%	18%	19%	17%	17%	17%	19%
1500	42%	46%	40%	34%	31%	32%	31%	31%	32%	30%
END	34%	27%	14%	10%	9%	10%	11%	11%	14%	11%
Average	**30.9%**	**29.6%**	**26.4%**	**23.9%**	**23.9%**	**23.9%**	**23.1%**	**22.4%**	**21.9%**	**21.2%**
MASS FLUX										
Station	**step 2**	**step 1**	**step 3**	**step 4**	**Case 1**	**Case 2**	**Case 3**	**Case 4**	**Case 5**	**FINAL CASE**
80	9379.828	9055.183	7976.270	8381.701	9555.972	9480.195	9283.987	7924.664	7443.093	8732.389
320	5935.680	5722.443	6199.891	6774.781	8168.103	8154.865	7974.024	7465.137	7012.628	7391.257
640	6362.457	6160.147	6280.351	6898.240	7034.141	7033.945	6943.007	6944.918	6738.947	7281.687
1000	5794.793	6844.304	7852.345	8231.578	10317.664	10186.221	9787.419	9757.300	9498.543	8781.167
1500	8452.844	8481.471	8594.881	9010.924	8975.868	8983.000	8921.515	8921.540	9067.369	9029.626
END	8979.898	8975.087	9916.330	10744.509	10922.292	10853.556	10941.136	10940.844	10948.996	11211.935
VARIANCE										
Station	**step 2**	**step 1**	**step 3**	**step 4**	**Case 1**	**Case 2**	**Case 3**	**Case 4**	**Case 5**	**FINAL CASE**
80	30.50	30.40	25.15	27.55	29.30	29.32	28.86	24.81	24.01	28.52
320	9.96	9.25	9.88	11.85	14.59	14.63	14.09	13.33	12.18	12.64
640	2.86	2.38	2.93	4.25	4.77	4.77	4.43	4.44	3.75	5.49
1000	6.20	8.85	9.80	9.58	13.30	12.92	12.35	12.17	12.10	10.36
1500	43.48	43.28	44.40	50.08	49.17	49.48	48.48	48.48	49.95	49.97
END	100.46	101.56	101.34	112.59	113.34	113.18	114.35	114.35	117.27	116.26

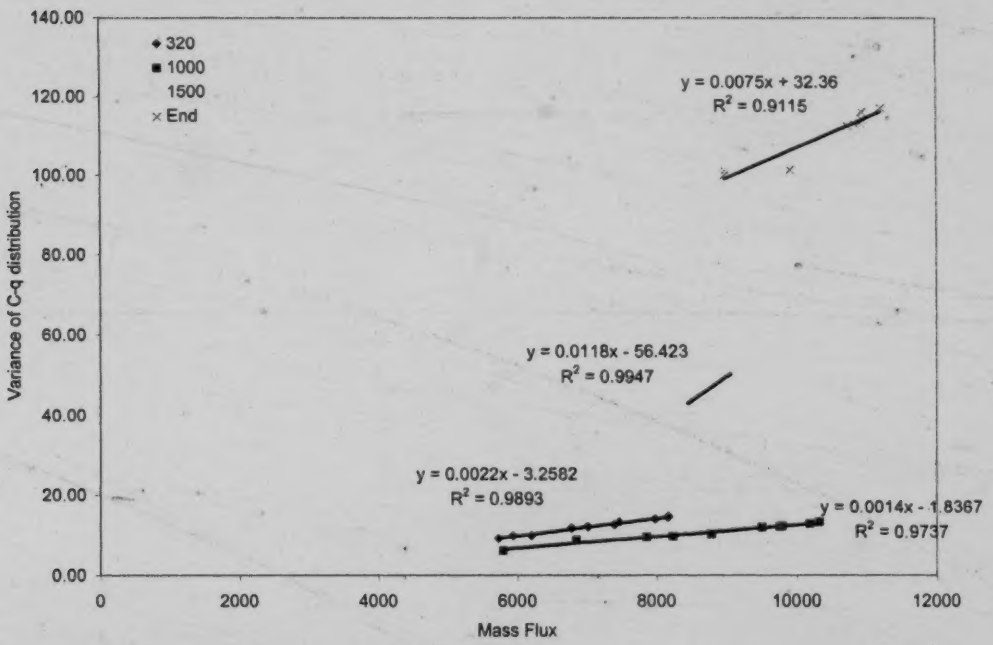

Figure 5.39: Sensitivity analysis: Calculated mass flux compared with calculated variance.

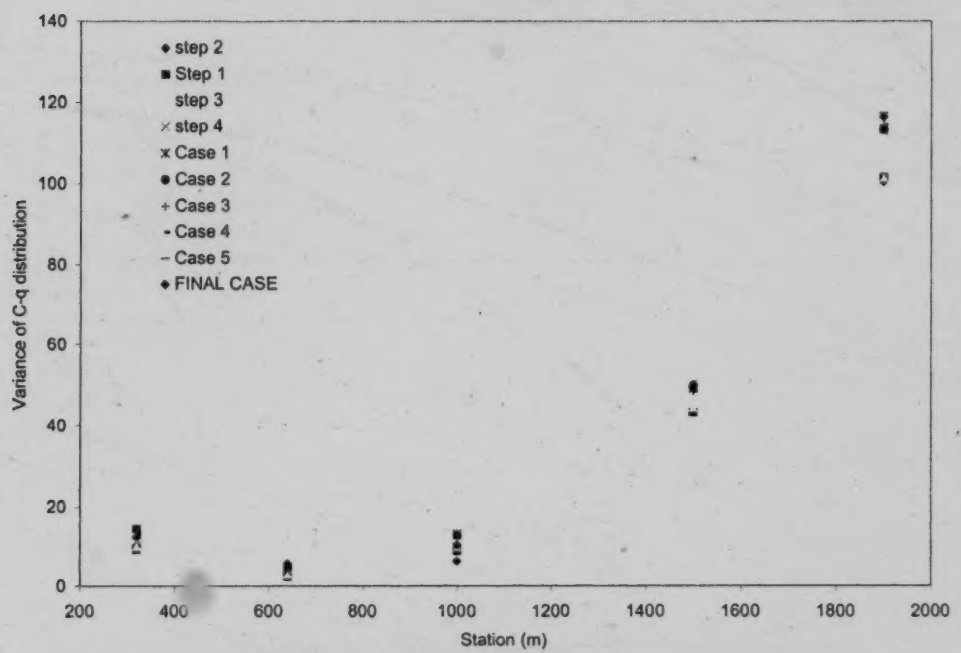

Figure 5.40: Variance of cases along the study area.

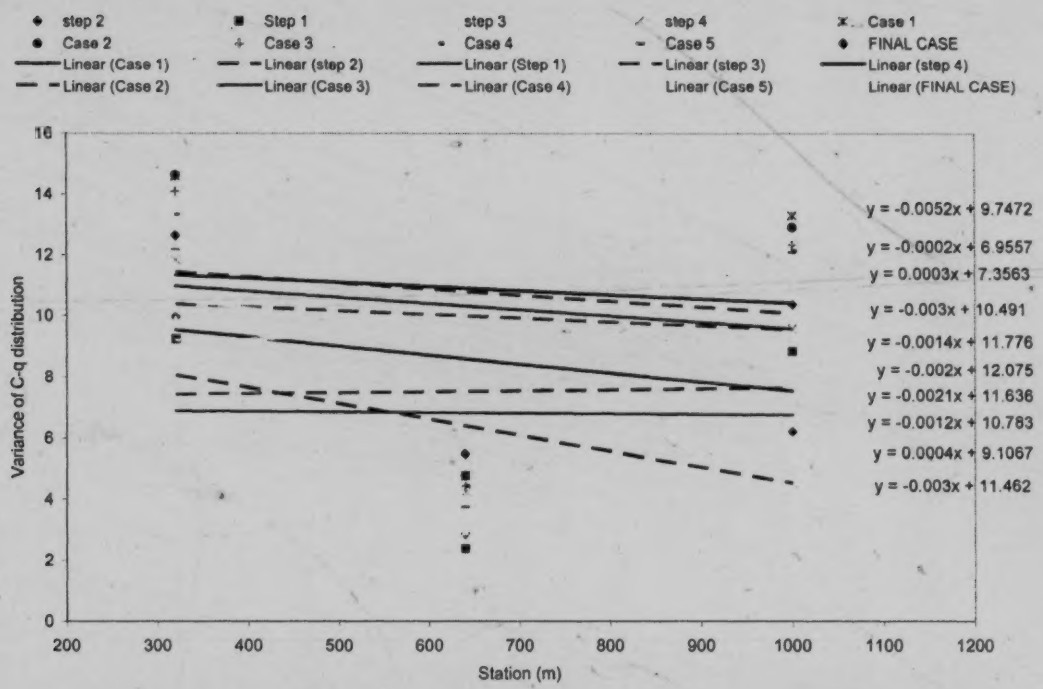

Figure 5.41: Linear trendlines fit to variances between stations 320 and 1000.

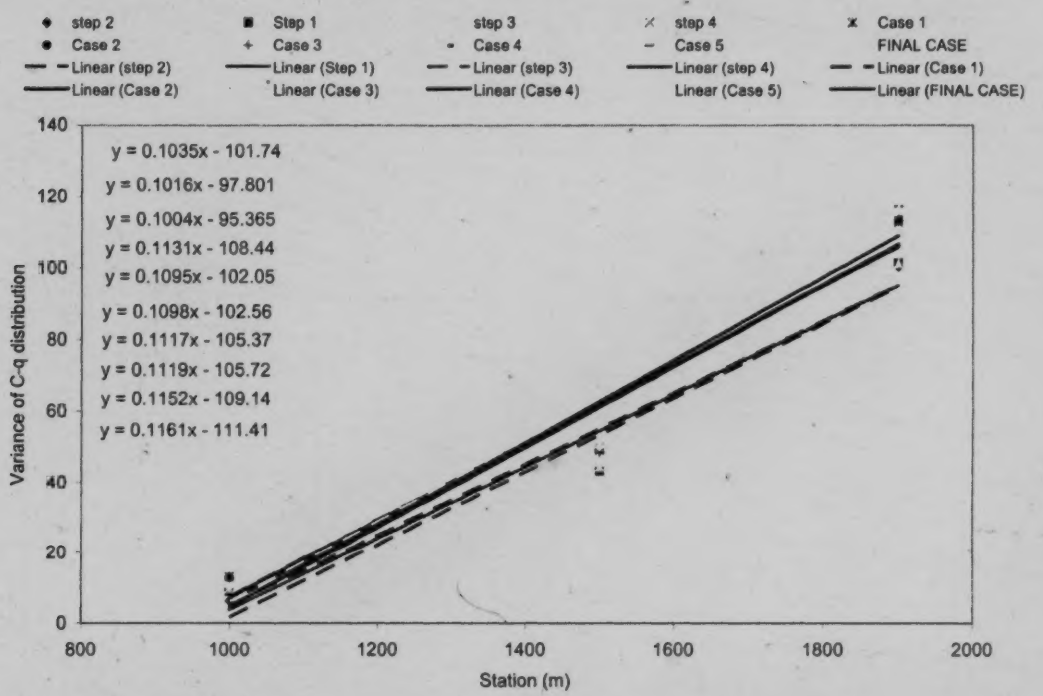

Figure 5.42: Linear trendlines fit to variances between stations 1000 and the end.

Table 5.26: Sensitivity analysis: Calculated transverse factors of diffusion and mixing coefficients for section between Station 320 and 1000.

Case	Slope From best fit line	D (m^5/s^2)	Average Modeled Depth (m)	Average Modeled Velocity (m/s)	Average Modeled Shear Velocity (m/s)	εt (m^2/s)	εt/hu*	Overall Velocity Error	Average section
Step 2	-0.0052	-0.0026	0.782	0.227	0.023	-0.019	-1.044	**30.9%**	**26.1%**
Step 1	-0.0002	-0.0001	0.778	0.220	0.022	-0.001	-0.044	**29.6%**	**24.2%**
Step 3	0.0003	0.0002	0.801	0.245	0.025	0.001	0.047	**26.4%**	**24.1%**
Step 4	-0.003	-0.0015	0.794	0.260	0.027	-0.009	-0.434	**23.9%**	**23.6%**
Case 1	-0.0014	-0.0007	0.831	0.295	0.027	-0.003	-0.153	**23.9%**	**23.4%**
Case 2	-0.002	-0.0010	0.830	0.294	0.027	-0.005	-0.221	**23.9%**	**22.8%**
Case 3	-0.0021	-0.0011	0.828	0.289	0.027	-0.005	-0.237	**23.1%**	**22.5%**
Case 4	-0.0012	-0.0006	0.827	0.285	0.024	-0.003	-0.158	**22.4%**	**21.4%**
Case 5	0.0004	0.0002	0.831	0.276	0.024	0.001	0.053	**21.9%**	**19.6%**
FINAL CASE	-0.003	-0.0015	0.826	0.292	0.027	-0.008	-0.332	**21.2%**	**19.6%**
Average		-0.0009				-0.005	-0.252		
Maximum		0.0002				0.001	0.053		
Minimum		-0.0026				-0.019	-1.044		

Table 5.27: Sensitivity analysis: Calculated transverse factors of diffusion and mixing coefficients for section between Station 1000 and the End.

Case	Slope From best fit line	D (m^5/s^2)	Average Modeled Depth (m)	Average Modeled Velocity (m/s)	Average Modeled Shear Velocity (m/s)	εt (m^2/s)	εt/hu*	Overall Velocity Error	Average section
step 2	0.1035	0.0518	1.207	0.217	0.016	0.164	8.447	**30.9%**	**32.2%**
Step 1	0.1016	0.0508	1.232	0.218	0.016	0.154	7.831	**29.6%**	**32.1%**
step 3	0.1004	0.0502	1.208	0.226	0.017	0.152	7.471	**26.4%**	**27.6%**
step 4	0.1131	0.0566	1.251	0.256	0.020	0.141	5.769	**23.9%**	**22.8%**
Case 1	0.1095	0.0548	1.246	0.250	0.018	0.141	6.442	**23.9%**	**22.3%**
Case 2	0.1098	0.0549	1.246	0.247	0.017	0.143	6.605	**23.9%**	**22.3%**
Case 3	0.1117	0.0559	1.246	0.246	0.018	0.147	6.722	**23.1%**	**21.9%**
Case 4	0.1119	0.0560	1.246	0.246	0.018	0.147	6.734	**22.4%**	**21.7%**
Case 5	0.1152	0.0576	1.241	0.249	0.019	0.150	6.534	**21.9%**	**21.7%**
FINAL CASE	0.1161	0.0581	1.239	0.257	0.018	0.147	6.650	**21.2%**	**21.6%**
Average		0.0546				0.149	6.920		
Maximum		0.0581				0.164	8.447		
Minimum		0.0502				0.141	5.769		

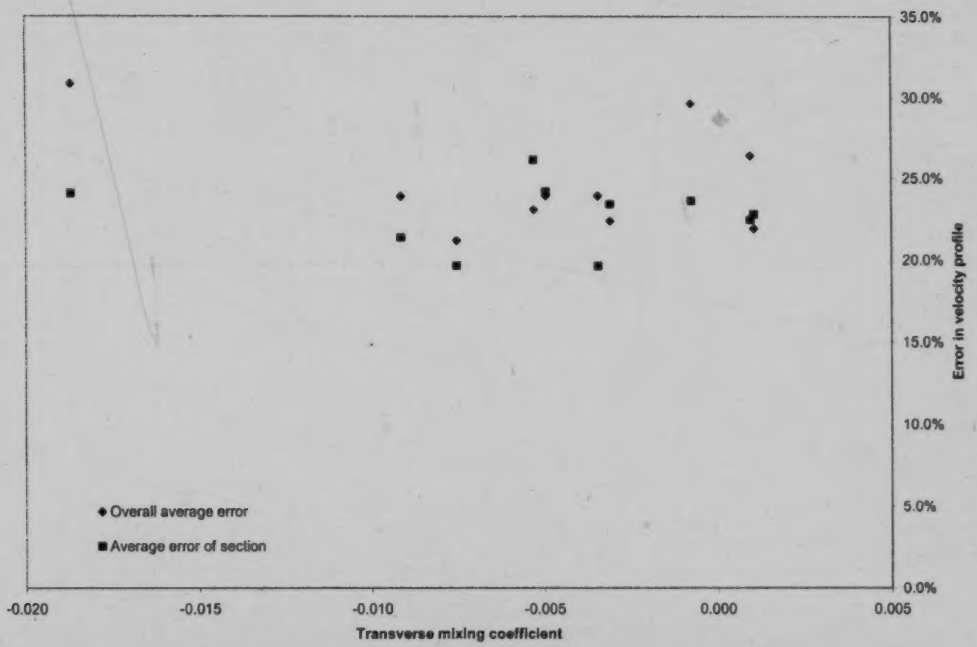

Figure 5.43: Comparison of error in velocity profiles with calculated transverse mixing coefficient for Stations 320 to 1000.

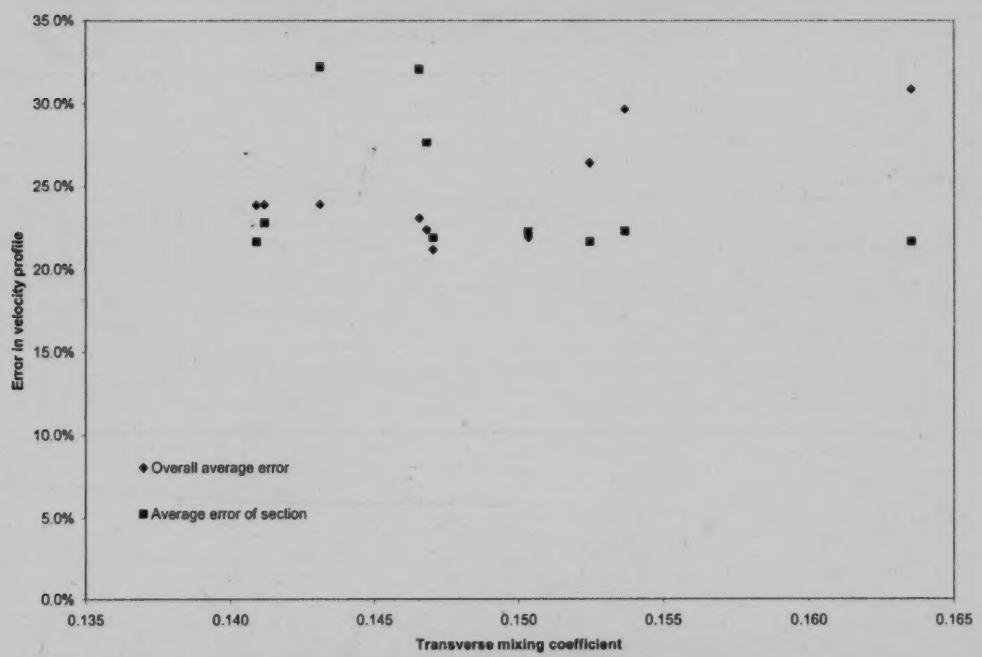

Figure 5.44: Comparison of error in velocity profiles with calculated transverse mixing coefficient for Stations 1000 to End.

CHAPTER 6 CONCLUSIONS AND RECOMMENDATIONS

This chapter will first present a summary of the field data established and the results obtained from this research. Recommendations will then be discussed.

6.1 SUMMARY

In order to understand the mixing characteristics of the North Saskatchewan River at Edmonton, a detailed field study was undertaken. The bathymetry of the river was mapped from a point 0.5 kilometers upstream of the GBWWTP outfall structure to a point 2 kilometers downstream of the outfall structure. The bathymetry around and immediately downstream of the outfall has a direct effect on mixing processes through the hydrodynamic interaction of the receiving and effluent waters so a great knowledge of the actual bathymetry is critical to the understanding of the mixing characteristics. The topography data and limited water surface elevations and velocity data were used to create and validate a two dimensional hydrodynamic model of the study area.

The hydrodynamic modeling assisted in understanding the flow patterns in the river. The sloped rip rap blanket at the outfall structure actually splits the effluent flow and causes a portion of the effluent flow to be directed upstream around the rip rap barrier. This splitting is dependent on the ambient discharge in the river. At a lower discharge, approximately 2/3 of the effluent flow is directed upstream around the exposed rip rap. At a higher discharge, the effluent flow simply flow downstream and the rip rap remains unexposed.

Through the first 1000 metres downstream of the outfall, the south bank remains quite shallow. In this region approximately 16% of the total discharge is being carried by 1/3 of the river width. The majority of the flow is being carried in the deeper portion of the channel near the north bank. Just before the Gold Bar Pedestrian Bridge, the flow tightens up as the south bank becomes steep before hitting an alluvial fan-like deposit

which causes the flow to expand. From here the flow tightens up again as it heads into a bend at the end of the study area.

Dye tests are the most common method of studying mixing characteristics in rivers. In order to understand the mixing characteristics, a steady state dye test for the low flow conditions was conducted over two days: October 29, 2002 and November 7, 2002. Rhodamine WT was premixed with the effluent and pumped into the river at a constant rate. Water samples at pre-determined near field locations as well as downstream cross-sections were collected and dye concentrations analyzed. It was found that only 70% of the dye was being recovered in the river water while 100% of the dye was being recovered in effluent water with a third order polynomial curve followed for combinations of river water and effluent water in between. Sample concentrations were corrected to account for this.

On October 29, 2002 the river discharge was approximately 116 m^3/s and November 7, 2002 the river discharge was approximately 152 m^3/s. On October 29, the concentration did not begin to degrade until a point approximately 80 metres downstream of the outfall. Buoyancy effects were dominant until a point approximately 160 metres downstream of the outfall as station 80 remained stratified indicated by the difference in depth averaged concentration and surface concentration. At a point 320 metres downstream of the outfall structure, a dilution of 75% was achieved. On November 7, buoyancy effects were still dominant at station 80 as stratification was observed. At a point approximately 320 metres downstream of the outfall, a dilution of 60% is achieved. A dilution of 1:4 is achieved at a point roughly 2 kilometers downstream of the outfall structure.

The dye test results were combined with the two dimensional hydrodynamic modeling results. From these results a good understanding of the mixing characteristics of the study reach were achieved. Mass conservation was realized up to a point approximately 320 metres downstream of the outfall. From this point to the end of the study area, approximately 25% of the mass was lost. Concentrations were scaled to

reflect this loss. It was evident that the study area could be broken down into three sections: the first exhibited rapid mixing, the second section exhibited little to no mixing, while the third section exhibited considerable mixing. These results could be correlated well with local hydraulic conditions from the hydrodynamic model.

6.2 CONCLUSIONS

This analysis suggests that the mixing coefficients could be selected based on an interpretation of the cumulative discharge distribution. Areas that exhibit a relatively flat distribution with little change would be assigned a small mixing coefficient while areas of local flow and channel curvature would be assigned a high mixing coefficient.

It is evident that the use of modeled velocities rather than measured field velocities has many benefits. Using a depth averaged hydrodynamic model to predict velocities assists engineers in two ways; (i) it produces the cumulative discharge distribution which can be used analyze the transverse mixing coefficients in combination with measured concentration profiles and (ii) it provides an understanding of the flow patterns in the study reach that help interpret the derived mixing coefficients. This will allow a reduction in the amount of field velocity data collection necessary as only a few velocity measurements are required in order to calibrate a hydrodynamic model.

Finally, the results of the transverse mixing analysis did not appear to be very highly correlated with the error in the modeled velocity profile. This suggests that the extra effort taken to improve the modeling solution had very little affect on the final mixing analysis.

6.3 RECOMMENDATIONS

The following recommendations are presented on the basis of the work presented herein:

1. Use the results of the two dimensional hydrodynamic model and concentration profiles to validate a two dimensional contaminant transport model of the wastewater effluent.

2. Use the results of the bathymetry and dye test to validate a near field mixing model such as CORMIX to study the near field mixing characteristics in detail.

3. Evaluate other wastewater effluent input alternatives at GBWWTP such as retrofitting the existing outfall structure or using an alternative method such as diffusers.

4. Use the results of the two dimensional hydrodynamic to assist in an analysis of fish habitat availability in the reach.

CHAPTER 7 REFERENCES

Allan, J.H., (1984). *An Overview of the Fish and Fisheries of the North Saskatchewan River Basin.* Prepared for Alberta Environment - Planning Division, Pisces Environmental Consulting Services, Red Deer, AB.

Barber, D.G. (2001). *53.373 Geographic Information Systems Course Notes.* Centre for Earth Observation Science (CEOS), The University of Manitoba.

Beltaos, S. (1979). Transverse mixing in natural streams. *Canadian Journal of Civil Engineering*, 6, 275-591.

Bencala, K.E., Rathbun, R.E., Jackman, A.P., Kennedy, V.C., Zellweger, G.W., & Avanzino, R.J. (1983). Rhodamine WT Dye Losses in a mountain stream environment. *Water Resources Bulletin*, 19(6), 943-950.

Bouthillier, P.H. (1984). *A History of Stream Pollution Assessment and Control – North Saskatchewan River 1950s-1980s*. Alberta Environment, Edmonton, AB.

Buchanan, T.J. (1964). Time of Travel of Soluble Contaminants in Streams, Journal Sanitation Engineering Division, ASCE:90:SA3, 1-12.

Cochrane Engineering Inc. (1997). *Near Field Mixing of Outfall Discharges in the North Saskatchewan River.* Prepared for the City of Edmonton, Cochrane Engineering Inc, Edmonton, Alberta.

Deaner, D.G. (1973) Effect of Chlorine on Fluorescent Dyes. Journal of Water Pollution Control Fed., 45:3, 507-514.

Demetracopoulos, A.C. and Stefan, H.G. (1983). Transverse mixing in wide and shallow river: Case Study. *Journal of Environmental Engineering,* 109(3), 685-699.

Digital Wizaeds (Ontario) Inc. (2003). *North Saskatchewan River*. Retrieved August 14, 2003, from http://greatcanadianrivers.com.

Elhadi, N., Harrington, A., Hill, I., Lau, L., and Krishnappan, B.G. (1984). River Mixing – A State of the Art Report. *Canadian Journal of Civil Engineering*, 11, 585-609.

Everts, C.J. & Kanwar, R.S. (1994). Evaluation of Rhodamine WT as an adsorbed tracer in an agricultural soil. *Journal of Hydrology*, 153, 53-70.

Fischer, H.B., List, E.J., Koh, R.C.Y., Imberger, J. and Brooks, N.H. (1979) Mixing in Rivers. In *Mixing and Inland and Coastal Waters* (pp.104-147). London: Academic Press.

GARMIN Corporation (2000). *Garmin GPS GUIDE for beginners*. Retrieved August 12, 2002, from http://www.garmin.com/aboutGPS/manual.html

Ghanem, A., Steffler, P., Hicks, F. and Katopodis, C. (1995). *Two Dimensional Finite Element Model for Aquatic Habitats.* Water Resources Engineering Report 95-S1, Department of Civil Engineering, University of Alberta, 189 pp.

Golder Associates Ltd. (1994). *Modelling of Mixing of wet weather discharges in the North Saskatchewan River, Edmonton to the Saskatchewan Border*. Prepared for the City of Edmonton, Golder Associates Ltd., Calgary, AB.

Golder Associates Ltd. (1995). *Joint Industry – Municipal North Saskatchewan River Study.* Prepared for City of Edmonton, Golder Associates Ltd., Calgary, AB.

Gowda, T.P.H. & Post, L.E. (1984b). Mixing Zone Studies in the Grand River Basin. *Canadian Journal of Civil Engineering*, 11, 204-216.

Gowda, T.P.H. (1984a). Critical Point Method for Mixing Zones in Rivers. *Journal of Environmental Engineering*, Vol. 110, No. 1, pp. 244-262.

Holley, E.R., Siemons, J., and Abraham, G. (1972). Some aspects of analyzing transverse dispersion in rivers. *Journal of Hydraulic Research*, 10(1): 27-57.

Kasnavia, T., Vu, D., Sabatini, D.A. (1999). Fluorescent Dye and Media Properties Affecting Sorption and Tracer Selection. *Ground Water*, 37(3), 376-381.

Milne, G.D., Stanley, S.J., Smith, D.W. (1993). Residual Chlorine Decay in a Broad, Shallow River. *Water Resources*, Vol. 27, No. 6, pp. 993-1001.

Montes, S. 1998. *Hydraulics of Open Channel Flow*. Reston, VA: ASCE Press.

Rutherford, J.C. (1994). *River mixing*. John Wiley & Sons, West Sussex, England.

Sabatini, D.A. & Austin, T.A. (1991). Characteristics of Rhodamine WT and Fluorescein as Adsorbing Ground-water tracers. *Ground Water*, 29(3), 341-349.

Smart, P.L. & Laidlaw, I.M.S. (1977). An Evaluation of Some Fluorescent Dyes for Water Tracing. *Water Resources Research*, 13(1), 15-33.

Trimble Tutorial. Retrieved August 12, 2002, from http://www.trimble.com/gps/index.html

Turner Designs. *A Practical Guide to Flow Measurement.* Retrieved September 2, 2002, from http://www.turnerdesigns.com/t2/doc/appnotes/998_5000.html

Turner Designs. *Bulletin 104 Fluorescent Tracer Dyes*. Retrieved September 3, 2002, from http://www.turnerdesigns.com/t2/doc/appnotes/998_5104.html

Turner Designs. *Flow Measurements in Sanitary Sewers by Dye Dilution.* Retrieved September 3, 2002, from http://www.turnerdesigns.com/t2/doc/appnotes/998_5107.html

Turner Designs. *Fluorescent Tracer Studies.* Retrieved August 28, 2002, from http://www.turnerdesigns.com/t2/doc/appnotes/998_5121.html

Turner Designs. *Preparation of Standards for Dye Studies using Rhodamine WT.* Retrieved August 29, 2002, from http://www.turnerdesigns.com/t2/doc/appnotes/998_5111.html

Van der Vinne, G. (1991) *Low Flow, Open Water Tracer Dye Studies on the North Saskatchewan River, Edmonton to Saskatchewan Border.* Report No. SWE-02. Prepared for Alberta Environment, Environmental Research and Engineering Department, Alberta Research Council, Edmonton, AB.

Webel, G. and Schatzmann, M. (1984). Transverse mixing in open channel flow. *Journal of Hydraulic Engineering*, 110(4), 423-435.

Wilson, J.F., Jr., Cobb, E.D., & Kilpatrick, F.A. (1986) "Fluorometric Procedures for Dye Tracing" Techniques of Water-Resources Investigations of the United States Geological Survey, Book 3, Applications of Hydraulics, Chapter A12, U.S. Government Printing Office, Washington, D.C.

Wolf, P.R. & Brinker, R.C. (1994). *Elementary Surveying.* New York: HarperCollins College Publishers.

World Health Organization. (1986). *Environmental Health Criteria 54 Ammonia.* Geneva: Author.

Yotsukura, N. & Sayre, W.W. (1976). Transverse mixing in natural channels. *Water Resources Research* 12(4), 695-704.

APPENDIX: Rhodamine WT as a Tracer

Information provided in this section was modified from Turner Designs recommendations for use of Rhodamine WT as a Tracer.

The Rhodamine WT dye should be mixed prior to injection in order to achieve concentration values within the target range. In order to achieve proper mixing, at least 20% of the reservoir should be left as air space. The container should be one that can easily be picked up and should be mixed by swirling the solution in a rotary motion, turning upside and swirling again. This should be repeated ten times in order to achieve proper mixing. It is important to know that when Rhodamine WT is mixed with water, it initially acts like detergent and foams. Adding more water to an already mixed solution can cause it to foam over.

Injection of the dye must be at a constant rate and a constant concentration without surging or splashing. Injection rates below 10 mL/minute are difficult to handle. When injecting the dye should not free fall for more than one or two feet because splashing or erratic results will occur and the dye should not be injected using a long tube as flexible vinyl tubing does adsorb dye reversibly. This is not a problem if the tubing is a couple metres, but it will be if the length of the tubing is on the order of 30 metres. Flow rates should be check before and after dye injection. The accuracy of the final result is strongly dependent upon the knowledge of the rate of flow of dye into the water. The dye should be injected at a point to ensure complete mixing has occurred before sampling takes place.

When conducting a field test, samples of the natural water should be collected immediately prior to injecting the dye. This water will be used to determine the background concentration and to determine the behavior of the natural water with the dye to ensure an appropriate recovery is achieved. A sample of the dye being injected should

also be collected to determine the actual concentration being injected. The highest background fluorescence encountered by Turner Designs was 2 ppb in raw sewage. Background in pure water of natural unpolluted streams is around 20 ppt and typical values of raw sewage of about 1 ppb.

Samples and standards are generally very stable can be kept for months if stored away from strong sunlight but must be stored in the appropriate container. The best materials known to be safe for sample collection include borosilicate glass such as Pyrex® or Kimax®, polyethylene, polypropylene, and polystyrene. Polyseal® screw caps are also safe to use as well as Parafilm®. Kimble glass scintillation vials with Polyseal® caps are safe to use also.

The fluorometer should be warmed up 10 minutes prior to making any readings. Cuvets must be wiped off before being placed in the fluorometer for reading. The reading should be made rapidly due to the high temperature of the fluorometer.

The fluorometer must be calibrated using a standard: a known concentration of the dye that is injected that can be prepared by weighing or measuring a sample of dye and accurately diluting it. Rhodamine WT readings are linear to 0.5 ppm or in terms of active ingredient (the 20% solution) it is linear to 0.1 ppm so the fluorometer can be calibrated using a single standard within the linear range of the dye. Calibration can be achieved by preparing a range of standards within the linear range or duplicate the one to ensure accuracy. Smart & Laidlaw (1977) suggested that it is best to use distilled water to prepare the general calibration curves. The concentration in the natural water can then be calculated by subtracting the natural background values. This way the absolute fluorescence is always measured and there is no chance of encountering negative fluorescence values.

A recovery ratio test should always be conducted as the physical and chemical properties of the water of interest could interfere with the fluorescence of the Rhodamine dye. Two identical standards are prepared: one using distilled water and the other using

study water. The ratio is calculated by dividing the fluorescence reading of the study water standard (subtracting the background fluorescence) by the fluorescence reading of the distilled water standard. All cases encountered by Turner Designs had a recovery ratio less than one. A recovery ratio of 0.9 indicates an expected accuracy of ±5%. A low recovery ratio can be caused by a number of factors, but in most cases is caused by suspended sediments. In order to improve the recovery ratio, filtration is required. The recovery ratio could also be low due to pH extremes or dye adsorption. Dye adsorption has never been encountered by Turner Designs, but could happen if the solids contained partially burned coal or similar materials. It can be checked by filtering the sample before adding the dye when preparing the standard and rechecking the recovery ratio. If it is notably higher then adsorption is indicated. Since the dye is truly removed from the system accurate measurements are not possible, corrections must be applied to the fluorescence readings.